A STUDY ON HYDROXYL TERMINATED POLYETHER BASED COMPOSITE PROPELLANTS

A THESIS SUBMITTED TO
THE GRADUATE SCHOOL OF NATURAL AND APPLIED SCIENCES OF
MIDDLE EAST TECHNICAL UNIVERSITY

BY

HACI EŞİYOK

IN PARTIAL FULFILLMENT OF THE REQUIREMENTS
FOR
THE DEGREE OF DOCTOR OF PHILOSOPHY
IN
CHEMICAL ENGINEERING

NOVEMBER 2016

Approval of the thesis:

A STUDY ON HYDROXYL TERMINATED POLYETHER BASED COMPOSITE PROPELLANTS

submitted by **Hacı EŞİYOK** in partial fulfillment of the requirements for the degree of **Doctor of Philosophy in Chemical Engineering Department, Middle East Technical University** by,

Prof. Dr. Gülbin Dural Ünver
Dean, Graduate School of **Natural and Applied Sciences** _____

Prof. Dr. Halil Kalıpçılar
Head of Department, **Chemical Engineering** _____

Prof. Dr. Ülkü Yılmazer
Supervisor, **Chemical Engineering Dept., METU** _____

Examining Committee Members:

Prof. Dr. Göknur BAYRAM
Chemical Engineering Dept., METU _____

Prof. Dr. Ülkü YILMAZER
Chemical Engineering Dept., METU _____

Prof. Dr. Teoman TİNÇER
Chemistry Dept., METU _____

Prof. Dr. Halil İbrahim ÜNAL
Chemistry Dept., Gazi Uni. _____

Doç. Dr. Özcan KÖYSÜREN
Energy&Materials Engineering Dept., Ankara Uni. _____

Date: **01.11.2016**

I hereby declare that all information in this document has been obtained and presented in accordance with academic rules and ethical conduct. I also declare that, as required by these rules and conduct, I have fully cited and referenced all material and results that are not original to this work.

Name, Last name: **Hacı EŞİYOK**

Signature :

ABSTRACT

A STUDY ON HYDROXYL TERMINATED POLYETHER BASED COMPOSITE PROPELLANTS

Eşiyok, Hacı
Ph.D., Department of Chemical Engineering
Supervisor: Prof. Dr. Ülkü YILMAZER

November 2016, 206 pages

The present study was aimed at investigating the effects of isocyanate, chain extender and curing catalyst types on the mechanical, structural and thermal properties of Hydroxyl Terminated Polyether (HTPE) based gumstock samples and the effects of oxidizer, energetic plasticizer, and ballistic modifier types on the ballistic and thermal properties of propellant samples. HTPE based polyurethane networks were synthesized by hand mixing and applying vacuum for degassing of resulting mixtures. After curing, they were characterized in terms of mechanical (Uniaxial tensile test, hardness test), structural (Swelling test, X-ray diffraction) and thermal (Differential scanning calorimeter (DSC), thermal gravimetric analysis (TGA), vacuum stability) properties. Propellant samples were prepared by incorporating energetic components like oxidizer, energetic plasticizer, burning rate catalyst to HTPE based elastomers in a 1-pint size vertical mixer. The linear burning rates of the propellant samples were measured by a Crawford bomb with respect to pressure. They were also characterized by DSC, TGA, and vacuum stability tester for thermal properties. Hazard classifications were made by impact and friction sensitivity tests. The smoke classification of propellants was carried out according to the STANAG 6016. A larger scale candidate propellant namely propellant 091 was prepared in an APV BAKER 1 galon mixer. The mechanical, ballistic, thermal and safety properties were determined by procedures as in the case of polyurethane and propellant samples. The ultimate tensile strength, elongation at break and Young's modulus were obtained as 0.80 MPa, 41.2% and 0.76 MPa, respectively, at 25^{o}C.

Glass transition temperature was determined as about -61^{o}C. The propellant showed two stages decomposition pattern with exothermic peaks at about 240 ^{o}C and 320^{o}C. The burning rate was calculated as 15 mm/s at 6.89 MPa with a pressure exponent below 0.5 between the 6.9-13.8 MPa pressure range. The shelf life of propellant developed was estimated by means of a microcalorimeter. It was said to be chemically stable for 10 years at 25^{o}C.

Keywords: HTPE, rocket propellant, insensitive munition, specific impulse, high performance

ÖZ

HİDROKSİL SONLU POLİETER BAZLI KOMPOZİT YAKITLAR ÜZERİNE BİR ÇALIŞMA

Eşiyok, Hacı
Doktora, Kimya Mühendisliği
Tez Yöneticisi: Prof. Dr. Ülkü YILMAZER

Kasım 2016, 206 sayfa

Bu çalışmada, kür ajanı, zincir uzatıcı ve kür katalizörü tiplerinin, hidroksil sonlu polieter (HTPE) bazlı polimerik yapıların mekanik, yapısal ve termal özelliklerine olan etkileri ile oksitleyici, enerjik plastikleştirici ve balistik düzenleyici tiplerinin, yakıt numunelerinin balistik ve termal özelliklerine olan etkilerinin incelenmesi amaçlandı. HTPE bazlı poliüretan yapılar el karışımı ve elde edilen karışımlara vakum uygulanarak elde edildi. Kürleşmeden sonra, bu yapılar, mekanik (Tek eksenli çekme testi, sertlik testi), yapısal (Şişme testi, X-ışını kırınımı) ve termal (DSC, TGA ve vakum kararlılık) özellikler açısından karakterize edildi. Yakıt numuneleri, oksitleyici, enerjik plastikleştirici ve yanma hızı katalizörü gibi enerjik bileşenlerin HTPE bazlı elastomer yapılara 1-pint boyutlu dikey mikserde eklenmesi ile hazırlandı. Yakıt numunelerinin basınca bağlı doğrusal yanma hızları Crawford bomb cihazıyla ölçüldü. Yakıt numunelerinin termal özellikleri ayrıca DSC, TGA ve vakum stabilite test cihazı yardımıyla karakterize edildi. Darbe ve sürtünme hassasiyeti testleri ile yakıtların tehlike sınıflandırması yapıldı. STANAG 6016'a göre yakıtların duman sınıflandırması gerçekleştirildi. Yakıt 091 adlı büyük ölçekli aday yakıt formülasyonu, APV BAKER 1 galon karıştırıcıda hazırlandı. Mekanik, balistik, termal ve güvenlik özellikleri, yakıt ve poliüretan numuneler için uygulanan metotlarla belirlendi. 25^{o}C'de maksimum çekme kuvveti, kopma anında uzama ve Young's modülüs değerleri sırasıyla 0.80 MPa, 41.2% ve 0.76 MPa olarak elde edildi. Camsı geçiş sıcaklığı -61^{o}C olarak belirlendi. Yakıt iki kademeli olarak 240 ^{o}C ve 320^{o}C'de ekzotermik tepkime vererek bozunmuştur. 6.89 MPa'da yakıt yanma

hızı 15 mm/s, 6.9-13.8 MPa basınç aralığında basınç üssü ise 0.5'den düşük olarak hesaplandı. Yakıt raf ömrü, mikrokalorimetre ile tahmin edildi. 25^{o}C'de 10 yıl boyunca yakıtın kararlı olduğu söylenebilir.

Anahtar Sözcükler: HTPE, roket yakıtı, duyarsız mühimmat, özgül darbe, yüksek performans

To My Wife Peruze & My Son Atilla

ACKNOWLEDGMENTS

I would like to express my gratitude to my thesis supervisor Prof. Dr. Ülkü Yılmazer for his guidance, valuable suggestions and kind support throughout my research. It was a great pleasure to work with him as a leader and benefit from his experience.

I am greatly indebted to Prof. Dr. Göknur Bayram and Prof. Dr. Erdal Bayramlı for serving as committee members, their criticisms and valuable discussion.

I would like to thank ROKETSAN's various departments especially to the test laboratory department for mechanical analysis, to the static test engineering department for firing tests, to the ballistic modelling unit for ballistic analysis, and to the material technologies laboratory for thermal analysis.

I also express my sincere appreciation to all of the member's of ROKETSAN Propellant and Explosive Technologies Department for their friendship.

My sincerest gratitude goes to my family. My dearest wife Peruze Ayhan Eşiyok was always with me and my lovely thanks extend to her for love and endless support. My dearest son Atilla Eşiyok was the source of my energy and motivation.

Special thanks to the ROKETSAN as a company for their financial support during my study.

TABLE OF CONTENTS

LIST OF TABLES

TABLES

LIST OF FIGURES

FIGURES

NOMENCLATURE

A_{cr}	Integral intensity of crystalline phase
A_m	Integral intensity of amorphous phase
A_e	Nozzle exit area, m^2
a	Coefficient of Saint Robert law
A^*	Throat area, m^2
c^*	Characteristic velocity, m/s
C_p	Specific heat at constant pressure, J/mol.K
C_r	The degree of crystallinity
d_1	The density of solvent, g/cm^3
d_2	The density of polymer, g/cm^3
E_{cryst}	Energy released from crystallization, J/g
E_{melt}	Energy required for melting, J/g
g	Gravitational constant, m^2/s
H_c	Specific enthalpy of combustion chamber, J/mol.K
H_{exit}	Specific enthalpy of nozzle exit, J/mol.K
HS	Hard segment
I_{sp}	Specific impulse, s
m	Mass flow rate, kg/s
L_c	Crystallite size, nm
M_{ave}	Average molecular weight, g/mol
M_c	Average molecular weight between crosslinks, g/mol
$M_{isocyanate}$	Mass of isocyanate
$M_{chain\ extender}$	Mass of chain extender
M_{polyol}	Mass of polyol
n	Pressure index of Saint Robert law
N_i	Optical property constant of i_{th} component
P_c	Combustion chamber pressure , Pa
P_e	Nozzle exit pressure, Pa
P_a	Surrounding atmospheric pressure, Pa
Q	Swelling ratio

OB	Oxygen balance, %
r	Linear burning rate, mm/s
R	Gas constant, J/mol.K
RH_{amb}	Ambient relative humidity, %
SG_i	Specific gravity of i_{th} component
SS	Soft segment
T_c	Adiabatic chamber temperature, K
T_g	Glass transition temperature, ^oC
T_{cryst}	Microcrystallization temperature, ^oC
T_{melt}	Melting temperature, ^oC
u_{exit}	Exhaust jet velocity, m/s
ΔH	Decomposition enthalpy, J/g
v_2	Volume fraction of the polymer
V_e	Velocity of the gases at nozzle exit, m/s
w_s	Weight of swollen elastomer specimen, g
w_{us}	Weight of unswollen elastomer specimen, g
w_2	Weight fraction of the polymer
w_1	Weight fraction of the solvent

Greek Symbols

γ	The ratio of specific heats of combustion gases at constant pressure and constant volume
δ	Solubility parameter, $(cal.cm^3)^{1/2}$
λ	Polymer-solvent interaction parameter and instrument constant in Scherrer equation
κ	Thermal diffusivity, in^2/h
α	Coefficient of linear thermal expansion, $in/in.^oF$
λ	Principal extension ratio
σ	Tensile stress, Pa
k	Thermal conductivity, $Btu/in.h.^oF$
ν_e	Crosslink density, mol/m^3
ρ	Density, g/cm^3
θ	Angle of reflection

Abbreviations

Al	Aluminum
AP	Ammonium Perchlorate
Al_2O_3	Aluminum Oxide
AGARDP	Primary Smoke Classification
AGARDS	Secondary Smoke Classification
AN	Ammonium Nitrate
BDO	1,4-Butanediol
BuNENA	N-n-Butyl-N-(2-Nitroxy-Ethyl)Nitramine
BoM	Bureau of Mines
BDNPA-F	Bis (2,2-Dinitropropyl)Acetal/Bis (2,2-Dinitropropyl)Formal
Cr_2O_3	Chromium(III) Oxide
CTPB	Carboxy Terminated Polybutadiene
DABCO	1,4-Diazabicyclo[2.2.2]Octane
DBTDL	Dibutyltindilaurate
DesmodurW	Dicyclohexylmethane-4,4’-diisocyanate
DTA	Differential Thermal Analysis
DDI	Dimeryldiisocyanate
DSC	Differential Scanning Calorimeter
DB	Double-base Propellants
Fe_2O_3	Iron(III) Oxide
FeAA	Ferric Acetyl Acetonate
GAP	Glycidyl Azide Polymer
HTPB	Hydroxy Terminated Polybutadiene
HMX	Cyclotetramethylene Tetranitramine
HTPE	Hydroxy Terminated Polyether
HFC	Heat Flow Calorimeter
HCI	Hydrochloric Acid
HF	Hydrogen Floride
HDI	Hexamethylenediisocyanate
IPDI	Isophoronediisocyanate
IM	Insensitive Munitions

KNO_3	Potassium Nitrate
LH_2	Liquid Hydrogen
LO_2	Liquid Oxygen
MAPO	Tris[1-(2-Methylaziridinyl)Phosphine Oxide]
MMH	Monomethyl Hydrazine
MNA	N-methyl-p-nitroaniline
NC	Nitrocellulose
NG	Nitroglycerine
SiO_2	Silicon Dioxide
STA	Simultaneous Thermal Analyzer
PPG	Polypropylene Glycol
PSAN	Phase Stabilized Ammonium Nitrate
RDX	Cyclotrimethylene Trinitramine
TPEG	Terathane-Polyethyleneglycol
TMETN	Methyltrimethylolmethane
TGA	Thermogravimetric Analysis
TEPAN	Tetraethylene-Pentaamineacrylonitrile
TDI	Toluene-2,4-Diisocyanate
TPB	Triphenylbismuth
TMP	1,1,1-Tris(hydroxymethyl)Propane
UDMH	Unsymmetrical Dimethyl Hydrazine
XRD	X-ray Diffraction
ZrC	Zirconium Carbide
$ZrSiO_4$	Zirconium Silicate

CHAPTER 1

INTRODUCTION

Solid rocket propellants can be defined as a polymeric mixture of oxidizer, fuel, and other ingredients which are processed and construct the end grain. Modern propellants can be classified in many ways as described below. The classification is not straight forward and simple. The same propellant can be match with more than one of the classifications.

Propellants are often classified by their specific uses, for instance, space booster propellants, the propellants of ballistic and tactical missiles. They have particular chemical ingredients, different burning rates, physical properties and performances [1].

The early propellants were used to be categorized into two classes namely: double base propellants that were the first class of propellants and composite propellants that became feasible after the development of polymers as binders in formulations. Double-base propellants (DB) form a homogeneous propellant structure. They are made of usually nitrocellulose (NC) which is a solid ingredient that absorbs liquid nitroglycerine (NG), and minor amount of additives. Both are the major ingredients of explosives and function as a fuel and oxidizer in formulation. Composite propellants form a heterogeneous structure. The oxidizer crystals (usually ammonium perchlorate (AP)) and a powdered fuel (usually aluminum or other metals) are sticked together in a polymeric matrix structure, such as polybutadiene (HTPB). They are cast in a vacuum from a mixture of solid (AP crystals, Al powder) and liquid (HTPB, CTPB) contents. The propellant is stiffened by crosslinking reaction or curing the polymeric binder with a small amount of curing chemical agent. Then, the propellant was cured at high temperatures in an oven, where it becomes solid [2].

Propellants can also be assorted by the smoke density in the exhaust as minimum smoke, reduced smoke, or smoky propellants. It is known that aluminum powder is oxidized to aluminum oxide forming visible solid particles in the exhaust plume. The amount of smoke is reduced by reducing the aluminum content in composite propellant, however carbon particles and metal oxides, such as iron oxide or zirconium oxide, can also be visible if they are in high concentration [3].

The propellants can be distinguished according to their safety properties as a detonable material (Class 1.1) or as a nondetonable material (Class 1.3). The double-base propellants and composite propellants containing a significant amount of solid explosive such as HMX or RDX can be given as examples of Class 1.1 propellants.

Propellants can be classified by their manufacturing processes. Cast propellants are produced by mechanical mixing which is followed by casting into rocket motor and curing at high temperature. The propellant curing is accomplished by the chemical reaction between the polymer and the curing agent at elevated temperature such as 45 to 150°C. However, some propellants can be cured at ambient temperatures from 20 to 25°C. The solvation process in which a plasticizer is dissolved in solid pelletized structure is another manufacturing tool. Extruded propellants are made by mechanical mixing which is followed by extrusion at high pressure. Solvation and extrusion processes are mainly applied to double-base propellants [4].

Many catastrophic incidents have taken place during the history of energetic materials, because of thermal and mechanical sensitiveness of munitions such as impact and shock, and these have brought about the development of the concept of Insensitive Munition (IM). Insensitive Munitions can be defined as munitions that meet their performance, readiness, and operational requirements. However, the violence of a reaction as subjected to unplanned situation were minimized [5].

The requirements stated in STANAG 4439 that gives a policy for IM tests and their assessment should be fulfilled. IM will reduce the threat to personnel and minimize the effect of adverse motor response on operations specifically in rocket propellants. The criteria for IM are less violent responses to fast and slow cook-off, bullet impact and fragment impact tests [6].

Many rocket motors are composed of a metal case which is loaded with propellant based on ammonium perchlorate (AP) as an oxidizer, aluminum (Al) as a fuel, and a hydroxy terminated polybutadiene (HTPB) as a polymeric binder. These optimized propellants have been studied over the past 30 years in terms of performance, mechanical properties, manufacturing, and signal properties for the needs of tactical missiles [7].

The company Alliant Techsystems (ATK) developed a newly propellants based on a polymeric system containing hydroxy terminated polyether (HTPE) [8]. It is claimed that these propellants can be as a less sensitive alternative for HTPB/AP based propellants that were used in many tactical rocket motors in order to meet IM requirements [9]. HTPE based copolymer consists of a block copolymer of polybutanediol and polyethyleneglycol in a molar ratio of approximately 1 to 1 [10]. This propellant type was developed in order to lower solid loading by using an energetic plasticizer that is compatible with HTPE binder i.e. N-n-Butyl-N-(2-Nitroxy-Ethyl)Nitramine (BuNENA). By this way, the sensitivity is diminished by replacing an AP by less sensitive AN and the energy of propellant is maintained at of above of the HTPB based propellant [11].

The objective of the present study is aimed to get access to understand of the behaviour of HTPE based propellants. In order to achieve this objective, several HTPE based polyurethane structures (gumstocks) were prepared and characterized. Samples were tested by Instron test machine for uniaxial tensile properties. The effects of isocyanate (mono or mixed type) and stoichiometric ratio of curative to binder (NCO/OH) on the mechanical properties such as rupture stress, rupture strain and tensile modulus of gumstocks were investigated. Morphologies of non-energetic parts of the propellants were characterized by swelling tests to determine the crosslink density and by XRD to investigate the crystalline structure. Thermal properties of gumstocks were analyzed by DSC and TGA. Some of the energetic components like Ammonium Perchlorate (AP), Cyclotetramethylene Tetranitramine (HMX), Aluminum (Al), and Phase Stabilized Ammonium Nitrate (PSAN) were incorporated into selected network formulations together with some additives such as energetic plasticizer, curing catalyst, burning rate catalyst, combustion stabilizer to improve general properties. Ballistic properties like linear burning rate, pressure

exponent, temperature and pressure sensitivity of burning rate were identified by a chimney type strand burner test machine. Thermal characterization of the propellant samples were done again by DSC and TGA. Characterization included the glass transition temperature, auto ignition temperature, crystallization and melting point determination, and also investigation of the decomposition behaviour. Mechanical sensitivity, safety and stability properties of propellant samples were investigated by impact tests, friction tests and vacuum stability tests. Signature classification of propellants were done theoretically, according to STANAG 6016 standard by using ICT thermochemical code. Based on the results mentioned, a candidate propellant was manufactured in a 5 liter propellant mixer. Complete characterization of the propellant was made in terms of mechanical, thermal and ballistic properties.

CHAPTER 2

LITERATURE SURVEY AND BACKGROUND INFORMATION

2.1 Propellants

Propellants can be defined as materials that generate a large number of gaseous molecules at high temperature during combustion and can sustain combustion without the presence of oxidizers. Both oxidizers and fuels are required to form a propellant, because combustion is a self-sustaining exothermic reaction. Propellants can be mainly classified according to their physical state as solid and liquid propellants [12].

2.1.1 Liquid Propellants

The oxidizer and fuel are stored in separate tanks in a liquid propellant. A combination of pipes, valves, and turbopumps were used in order to fed the propellants to a combustion chamber in which the thrust is produced by the reaction. Liquid propellants have several advantages as compared to solid propellants. By controlling the flow rate of the oxidizer and fuel, the engine can be throttled, stopped, or restarted. A proper liquid propellant provides a high specific impulse with a combustion reaction producing exhaust gas with high velocities. This means a high combustion temperature and exhaust gases with small molecular masses. However, the high density of the propellant is another important factor to decrease the volume of storage tanks. Liquid propellants can be mainly grouped into three types [13]:

i. Petroleum,
ii. Cryogenic,
iii. Hypergolics.

Petroleum-based propellants are usually composed of a mixture of high-purity refined kerosene which is denoted by RP-1. The chemical purity of the petroleum is an important parameter, since combustion residues must be maintained at a minimum level to prevent clogging phenomena. The liquid oxygen is a typical oxidizer used with kerosene. They deliver a lower specific impulse than cryogenic fuels, whereas they perform better than hypergolic propellants [14].

Cryogenic propellants are liquefied gases stored at very low temperatures. The proper thermal insulation of the propellant tanks is needed in order to store for a long time. The most commonly used cryogenic fuel-oxidizer system is the liquid hydrogen (LH_2)-liquid oxygen (LO_2). The maximum specific impulse that can be attained is around 370 second which is the highest among the liquid propellants used in operation [15].

The fuels and oxidizers igniting spontaneously as they contact are called hypergolic propellants. Any external ignition source are not required. They do not have the storage problems as in the case of cryogenic propellants, since hypergolic propellant are in liquid state at room temperature. On the other hand, they are highly hazardous due to their chemical reactivity. Hydrazine, monomethyl hydrazine (MMH), and unsymmetrical dimethyl hydrazine (UDMH) are the common hypergolic fuels used in spacecrafts and fuming nitric acid, nitrogen tetroxide, and hydrogen peroxide are the common hypergolic oxidizers [15].

A typical liquid propellant rocket engine is illustrated in Figure 1.

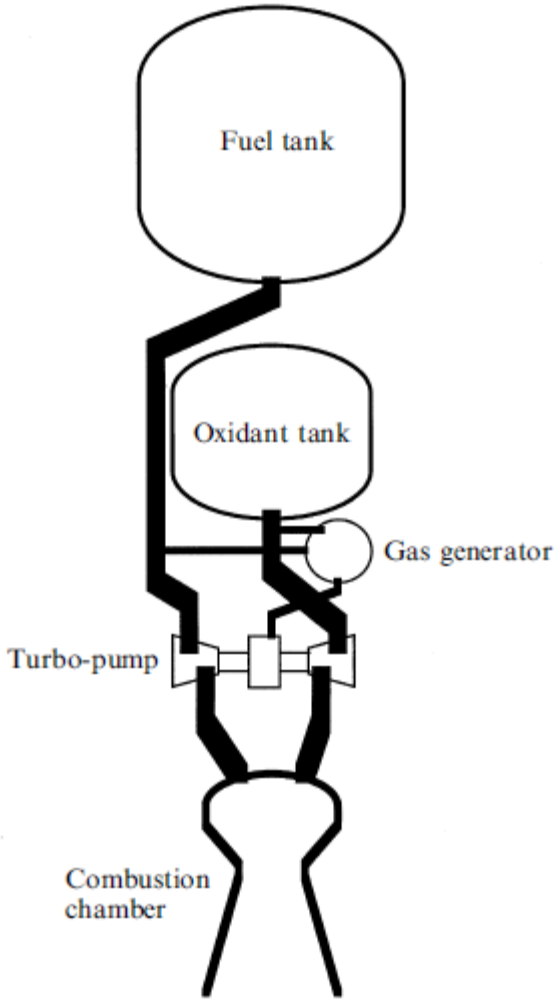

Figure 1 Schematic of a liquid-propellant engine [16].

2.1.2 Solid Propellants

In comparison to the complexities of liquid rocket engines, the design and development of solid rocket engines are much simpler. Solid propellants have a range of applications such as the small and medium launchers' main propulsion system, the third stage for orbital injection, booster for heavy launchers. A solid propellant is storable and safe to handle. The solid propellants are reliable and cost effective, because of the fact that a propellant delivery system is not needed. However, there exist mainly two disadvantages: the rocket motor can not be controlled as ignited and the specific impulse is lower as compared to a liquid propellant due to lower chemical energy [17].

Figure 2 shows a configuration of typical solid motor. It is very simple as compared to the liquid rocket combustion chamber. It is mainly composed of a casing for the propellant that is joined to a nozzle of identical geometry. When the propellant grain's inner surface is ignited, the motor continuously generates a thrust.

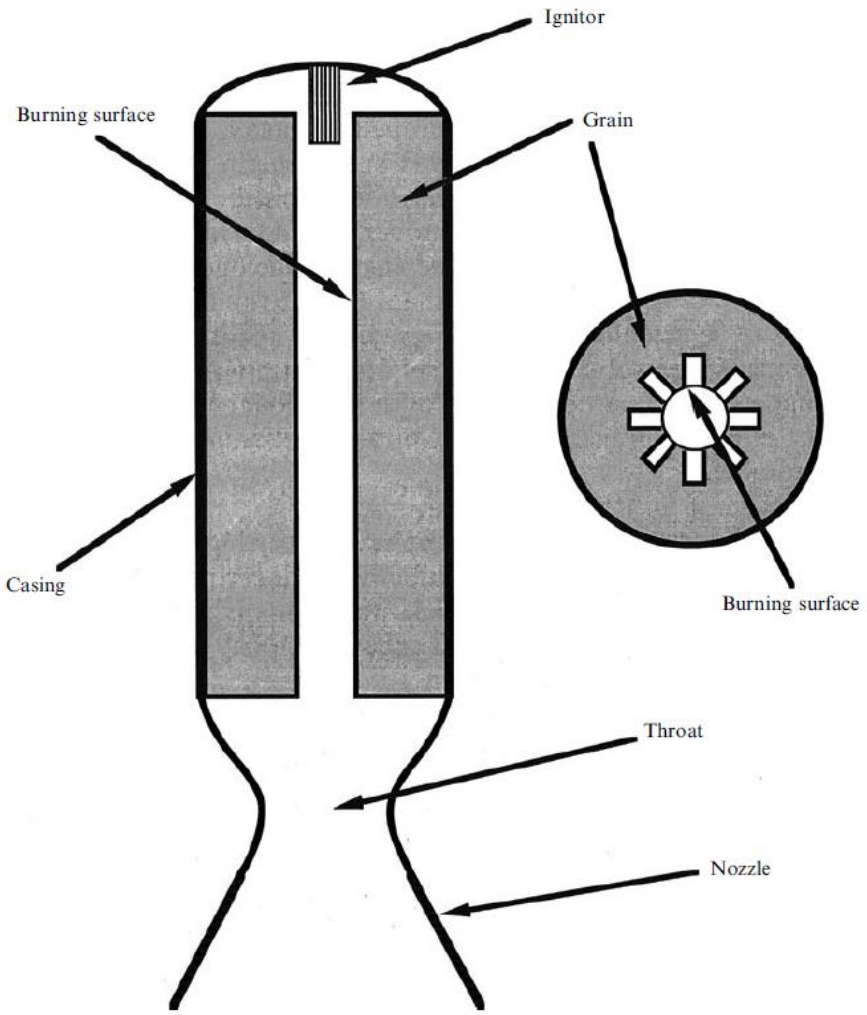

Figure 2 Schematic of a solid rocket motor [17].

Solid propellants are mainly classified into two types [18]:

i. Homogeneous propellant,
ii. Heterogeneous propellant.

Homogeneous propellants contain nitrocellulose (NC) and nitroglycerine (NG) as main ingredients. The stabilizer, burning rate modifier, plasticizer, opacifier, coolant

and lubricant can be used as additives [18]. These propellants can be manufactured by two ways: extrusion and casting. They are frequently used in anti-tank missiles.

Heterogeneous propellants are mainly composed of a binder, metallic fuel, and an oxidizer. The binder forms the matrix structure that contains a solid oxidizer such as ammonium perchlorate (AP) or ammonium nitrate (AN), and metallic fuel such as aluminum (Al) or magnesium (Mg). The oxidizer acts as a filler and provides the oxygen needed for combustion [17]. Hydroxy-terminated polybutadiene (HTPB) and carboxy-terminated polybutadiene (CTPB) can be given as examples of binders. The availability, processing, cost and performance are the critical requirements for the choice.

2.2 Performance of Rocket Propellants

Propellant characteristics are critical to fulfil the rocket motor design requirements of various missions in terms of performance and specific impulse (I_{sp}), wide range of burning rate with low burning rate pressure index. The other essential requirements of propellants are the high density and low temperature sensitivity [19]. The details about these performance parameters are mentioned below.

2.2.1 Burn Rate

The efficiency of a propellant strongly depends on its burn rate for a specific application. Burning starts from the propellant surface and as it goes on, the burning surface draws off through the web of the grain which is the web thickness that is defined as the minimum thickness of the propellant that must be consumed during combustion. This is known as Piobert's Law [20]:

$$\text{Linear burning rate } (r) = \text{Web thickness} / \text{Time of burning} \quad (1)$$

Burn rate is generally influenced by the temperature and the pressure. It tends to increase with the increase in temperature and pressure, and decreases as the pressure and temperature are lowered. Calorific value of the propellant is another factor that

affects the burn rate. If it is higher, then the higher propellant burn rate was obtained [21].

The Vieille or de Saint Robert law describes the burning rate dependence on pressure [22]:

$$r = aP_c^n \qquad (2)$$

where r = burn rate
P_c = chamber pressure
a = a coefficient
n = pressure index

Strand burner (Crawford bomb) is used to determine the burning rate of propellants at various pressures using an inert gas, generally nitrogen, for pressurization at constant initial temperature [23]. The pressure index "n" and the coefficient "a" can be easily calculated when the data are fitted with the empirical de Saint Robert law. The burn rates at different pressures are also determined by static test motor firings [24].

The pressure exponent (n) depends on the chamber pressure range and it is peculiar to specific propellant. It is typically range from 0.2 to 0.5 for double base propellants. However, AP-based composite propellants give relatively low values like from 0.1 to 0.4. A value that is close to zero is preferred from safety considerations [25].

2.2.2 Thrust

A rocket motor can be given as an example of an energy transfer system which can be explained by Newton's second law. When a pressurized high-temperature gas which is generated during combustion is expanded adiabatically, the energy of the gas is converted to kinetic energy by producing a reaction force. The aim is to get high-pressure and high-temperature gas in combustion chamber and to convert

effectively the sensible energy into kinetic energy in thermodynamic point of view [26].

The thrust can be defined as the reaction force (F) exerted by the ejection of combustion gases from the nozzle and expressed by the following equation [27]:

$$F = mV_e + A_e (P_e - P_a) \quad (3)$$

where
- m = mass flow rate
- V_e = velocity of the gases at nozzle exit
- A_e = nozzle exit area
- P_e = nozzle exit pressure
- P_a = surrounding atmospheric pressure

2.2.3 Specific Impulse

I_{sp} can be interpreted as the thrust delivered per unit weight flow of propellant or the enthalpy release converted into kinetic energy of the exhaust jet, that is more important to the propellant chemist. The relationship given by Eq. 4 is obtained by the energy balance by assuming adiabatic conditions. The jet velocity divided by the gravity constant is equal to the I_{sp} as seen in Eq. 5 [28].

$$u_{exit} = (2(H_c - H_{exit})^{1/2} = (-2\Delta H)^{1/2}) \quad (4)$$

$$I_{sp} = u_{exit} / g \quad (5)$$

Eq. 6 is resulted as it is also assumed that the expansion process from the chamber to the nozzle exit is isentropic. It tells us that the specific impulse is proportional to the square root of the adiabatic chamber temperature T_c and inversely proportional to the square root of the molecular weight (MW) [28]:

$$I_{sp} = 1 / g\{2\gamma / (\gamma - 1)\, RT_c / MW\, [1 - (P_e - P_c)^{\gamma / \gamma - 1}]\}^{1/2} \quad (6)$$

Because the I_{sp} is also sensitive to the pressure ratio (P_e / P_c), comparison of I_{sp} values must be made at standard conditions that are defined as the optimum expansion from 1000 psia (6.895 MPa) to 14.7 psia (0.1 MPa) [29]. The I_{sp} of propellant can be improved by increasing the enthalpy release and by lowering the average molecular weight of gases product [30].

2.2.4 Characteristic Velocity

The efficiency of conversion of thermal energy into high velocity exhaust gas is defined by the characteristic velocity (c^*). This is given by the pressure in the combustion chamber (P_c), integrated over the throat area (A^*), divided by the mass flow rate [31]:

$$c^* = P_c A^* / m \qquad (7)$$

The thermodynamic form of c^* is given by Eq.8. [31]:

$$c^* = (\gamma (2 / \gamma+1)^{(\gamma+1)/(\gamma-1)} (M_{ave} / RT_c))^{-1/2} \qquad (8)$$

The characteristic velocity depends on the temperature and, inversely, on the molecular weight. Again, the comparison between the expected and actual values can be used to assess the performance of the motor; or c^* can be used to estimate the expected performance of a new motor design.

2.2.5 Theoretical Calculations

The performance parameters of propellant such as specific impulse and characteristic velocity can be computed by a method that uses the thermodynamics based computer programs based on the main algorithms developed by the Lewis Research Center of NASA [32]. The ICT-Thermodynamic Code is one of the methods that developed by the Fraunhofer Institute for Chemical Technology [33]. The program computes chemical equilibria by solving the non-linear equations formed from the mass action and mass balance expressions. The NASA method uses gaseous atoms as independent variables. They are called components. The dependent

variables are then either gaseous molecular compounds or condensed compounds or elements. The program uses both the ideal equation of state (EOS), and Virial EOS, especially for the high pressure conditions of closed vessels. The pressures can be calculated which are close to experimental values by applying the Virial EOS (including the second and third virial coefficients) pressures [34].

2.3 Solid Rocket Propellants Ingredients

Composite propellants are generally used in modern solid rockets and missiles. They consist of three basic components. One of them is an organic polymer that uses as both the polymeric binder and combustible fuel. The other one is an oxygen-rich solid oxidizer which is the source of oxygen for combustion purposes. The last one is the metal additive used as the primary source of additional thermal energy leading to an increase in the propellant performance. Some other minor components such as plasticizers, bonding agents, stabilizers or anti-oxidants, and burn rate modifiers are also utilized in formulations.

2.3.1 Oxidizers

The major ingredient of a composite propellant is the oxidizer which forms more than 70% (by weight) of the propellant. It should be compatible with other ingredients. It should have high oxygen content, low heat of formation, high density and high thermal stability. It should also be low hygroscopic. Long shelf-life, safe handling and non-metalic nature are other characteristics that are required.

2.3.1.1 Ammonium Perchlorate

Ammonium Perchlorate is the most commonly used inorganic oxidizer in composite propellants. It satisfies most of the requirements. The advantages of AP are the great experience and a lot of informations on AP-based propellants that is available over several decades [35]. On the other hand, it is not environmentally friendly and brings about acid rain which is resulted in ozone depletion. Furthermore, the detection and tracking of rockets or missiles are the problems of its exhaust signature [36].

2.3.1.2 Nitramines

Nitramines are white crystalline solids such as HMX or RDX which can react or burn by themselves as initiated with activating energy. They can be detonated under certain conditions. They are quite similar in structure and properties. They can be produced in different particle sizes [37]. As compared to RDX, HMX has a higher density, a higher detonation rate by yielding more energy per unit volume. They are also used in military and commercial explosives and can be incorporated in double base or composite propellants in order to get higher performance. However, processing of propellants with these ingredients can be hazardous and needs extra safety precautions which is led to more expensive processing [38].

2.3.1.3 Ammonium Nitrate

Ammonium nitrate is frequently used in the area of nitrogen fertilizers and explosives [39]. It acts as a source of nitrate ion which is the source of oxygen and finds its application as an oxidizer in explosives and propellants especially for low burning rate and low performance applications [40]. AP is the main oxidizer in most of solid rocket motors currently used. In addition to its low energetic value, AN is hygroscopic, and it undergoes a room temperature phase transformation involving a significant volume change. These adverse properties make it even less attractive as an alternative oxidizer [41].

2.3.1.4 Phase Stabilized Ammonium Nitrate

Ammonium nitrate crystallizes in five phases. The phases I, II, IV, and V appear on cooling dry ammonium nitrate from the melt after passing through order-disorder transitions. The phase III which is the structurally not related phase appears only in the presence of water helping to nucleate the phase [42]. The transition paths are represented in Figure 3.

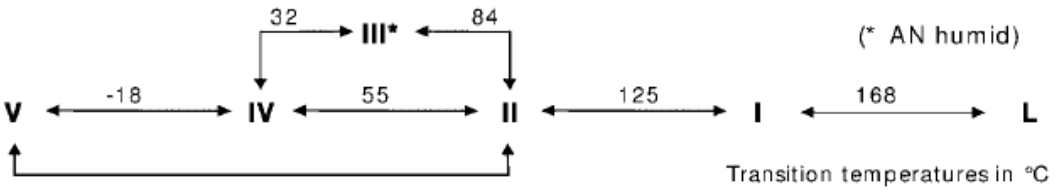

Figure 3 Ammonium nitrate transition paths

Many of the methods have been employed to improve the phase transition behavior of ammonium nitrate. Potassium nitrate has been used as a solid additive to suppress undesirable transitions and stabilized Phase III [43, 44]. The stability ranges of the related phases II and V can be extended by incorporating cesium into the ammonium nitrate lattice [45]. Another method was developed in ICT by incorporating diamine complexes of nickel, copper or zinc into the ammonium nitrate lattice for stabilizing ammonium nitrate [46].

2.3.2 Binders

Most of the advanced missiles use composite propellants mainly because of higher I_{sp} leading to higher range or payload. In the initial stages of composite propellant development, many fuel-binders like polyethylene, polyester, polyisobutylene, polyvinylchloride, polyacrylonitrile, and polysulfide were used. The use of these polymers as binders for composite propellants is not desired because of poor performance and mechanical properties. The recent trends are research and development on polybutadiene, polyether and energetic binders in the field of binders for composite propellants [47].

2.3.2.1 Hydroxy Terminated Polybutadiene

The HTPB polyurethane binder system gives the highest specific impulse with AP oxidizer. HTPB is the only pre-polymer which is specifically synthesized for its use as a propellant binder. It is usually produced by the free radical solution polymerization of 1,3-butadiene using hydrogen peroxide initiator. The pre-polymer has molecular weight in the range of 2500 to 2800; average functionality 2.2 to 2.4 and viscosity 65 P at 30^{o}C. Many favourable properties of the polyurethane system, like high density, rapid burning rate, high tensile strength, excellent fuel value, etc.,

make it a binder of choice. As a matter of the fact, currently the most widely used binder system is based on HTPB polyurethane [48].

2.3.2.2 Hydroxy Terminated Polyether

Hydroxy-terminated polyether (HTPE) is a new kind of polymeric binder that is thought to be as an alternative to HTPB which is widely used in many tactical motor systems. It is stated that HTPE based propellants are more insensitive than HTPB propellants such that they can meet the insensitive munitions requirements mentioned in STANAG 4439. HTPE is in non-crystalline form and has a polar structure. For this reason, it is compatible with energetic plasticizers in contrast to HTPB. In this way, the same thrust levels can be obtained with less amount of solid fillers in proportion to HTPB. Electrical conductivity of HTPE propellants is higher than HTPB ones. Thus, the probability of accidents that can result from electrostatic discharges is lower [49]. Especially in tactical and strategic missile systems, it is expected that percent elongation values should be higher than %40 at -30^{o}C, and it is known that mechanical properties of HTPE based propellants are superior than HTPB based ones at low temperature conditions [50].

2.3.2.3 Carboxy Terminated Polybutadienes

Carboxyl groups condense easily with epoxides and aziridines without liberating any small molecules. This reaction has been the basis of evolving pre-polymers based on carboxyl terminated polybutadiene. Liquid polybutadiene pre-polymers and its copolymers with acrylic acid and acrylonitrile having carboxyl groups have been synthesized and used extensively in producing very large size propellant grains. Being composed of almost a pure hydrocarbon chain, polybutadienes have high calorimetric values and are preferred fuels. As binders they provide high solid loadings and satisfactory mechanical properties over a wide range of temperatures. The curing of CTPB is achieved by reacting it with trifunctional epoxides or aziridines. These attributes of CTPB helped in achieving substantially improved mechanical behavior of highly loaded solid propellants, particularly at low temperatures. The CTPB based propellants provide very high specific impulse, just about 1s less than the HTPB/polyurethane system [51].

2.3.2.4 Energetic Binders

Maximizing the specific impulse has been the major criterion of many issues relating to the rocket performance. This can be achieved by opting for more energetic oxidizers and binders. Approaches to improve the energetics of the binder involves the introduction of explosophore groups, like $–NO_2$, $-ONO_2$, $-NF_2$ and N_3 in the polymeric chain. These groups contribute to increase in the heat of formation, and hence enhance the overall heat of combustion. The density of polymer is also increased which means higher amount of the oxidizer can be loaded per unit volume. The presence of oxidizing elements in the binder could be advantageous as it reduces the amount of loading of the powder inorganic oxidizer required for complete combustion making the mixing process easier [52]. The most prominent among the energetic polymers are the ones containing the azido groups. The hydroxyl terminated polymers of azidomethyl-oxirane (epoxide) and oxetane have been prepared for their use as binders. The most widely studied binder of this class is the glycidyl azide polymer (GAP) of the oxirane family. It is an uncrosslinked polyol and is a viscous liquid at room temperature. It has an average functionality of 2.7 hydroxyl groups and molecular weight of 700. GAP can be cured with a diisocyanate and by itself sustains combustion. Hence, it has been examined as a fuel for integrated ram rockets [53].

2.3.3 Metal Fuels

Aluminum is the most commonly used metallic element used to increase the impulse of propellants because of its highly exothermic reaction with the oxidizer. There exists other materials such as beryllium, beryllium hydride, aluminum hydride, and boron. They provide increased impulse, however, they are not frequently used because of cost, toxicity and instability. Increasing the aluminum content of a propellant leads to increase in its density. The combustion instability caused by the formation of pressure waves in the motor chamber can be reduced or eliminated by the presence of aluminum. The two-phase flow losses in the nozzle caused by aluminum oxide particles are observed in aluminum containing propellants and this led to delivering less than the calculated impulse. The solid reaction products also show a velocity lag during nozzle expansion, and may fail to attain thermal

equilibrium with the gas exhaust. These phenomena may brought about an overall efficiency loss of 5 to 8% from theoretical results [54, 55].

2.3.4 Plasticizers

Plasticizers are used to improve the processability and flexibility especially at low temperatures. They must have a very low melting point and dissolve in the polymer. If it is possible, they should provide oxygen in the combustion process in order to minimize any reduction in the specific impulse of the propellant. Typical plasticizers which are used with polybutadiene binders are isodecyl pelargonate and diisooctyl adipate. Apart from these nonenergetic plasticizers, the energy level of the propellant are increased by high energy plasticizers. Nitroglycerin, butanetriol trinitrate, trimethylethane trinitrate, bis(dinitropropylethyl)formal, and 1:1 mixture of bis(dinitropropyl) acetol and formal are typical examples. In addition, propellant solids loading can be improved by the use of plasticizers by leading to better performance. However, propellant sensitivity are tended to increase by many of the high energy plasticizers [56].

2.3.5 Bonding Agents

Modern rockets and missiles need high energy composite propellants having acceptable mechanical properties in order to sustain stress and strain during flight. The adhesion between the filler particles and binder structure is one of the major factors which improves the mechanical properties of propellants. The bonding agents improved the binder-filler adhesion of propellants. They promote the interaction between the solid particles and the binder [57]. They help to incorporate solid oxidizer particles into the binder system by improving the mechanical properties, aging characteristics, resistance to moisture, brittleness of propellants [58]. Common bonding agents used in composite propellants are tris[1-(2-methylaziridinyl) phosphine oxide] (MAPO), tetraethylene-pentaamineacrylonitrile (TEPAN).

2.3.6 Stabilizers

Propellants have a limited shelf-life. There exists some chemicals that were added during their production delay their deterioration reactions and therefore, increase their lifetime without adversely affecting their manufacturing processes and properties. Such chemicals or additives are known as stabilizers. Most commonly used stabilizers for double base and composite modified double base propellants are diphenylamines(diphenylamine, 2-nitrodiphenylamine) and centralites (methyl centralite, ethyl centralite), whereas phenolics (2,5-Di-t-butylhydroquinone, 2,2-methylene bis(4-methyl-6-t-butylphenol)) and amines (N-phenyl-β-naphthylamine, dioctyldiphenylamine) compounds are preferred for composite propellants [59].

2.3.7 Burn Rate Modifiers

The thermal decomposition and combustion of propellants is ended up with heat releasing or energy releasing. Burning rate modifiers or catalysts always play a key role in heat releasing of a propellant [60]. By this way, they enable to change the inherently high dependence of the burn rate on chamber pressure. It is known that various lead compounds have high catalyzing effect on the burning rate of double base propellants. The oxides and metal salts with variable valence like iron(III) oxide, copper (II) oxide, copper chromite, copper chromate, and solid or liquid organometallic compounds such as ferrocene and its various derivatives like iron(III) acetyl acetonate and metal chelates are typical burn rate modifiers used in composite propellants [61].

2.3.8 Isocyanates

The application of the polyurethane polymeric system widely used as fibers and foams provides an excellent base for the development of propellants. It provides a wide selection of starting chemicals that produces the required high energy and the rubbery structural characteristics of case bonding, through the reproducible isocyanate cure system [62]. Polyurethanes can be formed by the reaction of isocyanates (diisocyanates or polyisocyanates) with macroglycol or polyol and possibly with a combination of chain extenders that is shown in Figure 4.

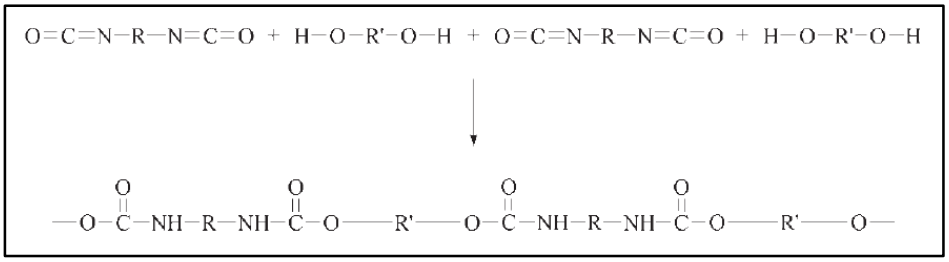

Figure 4 The formation of linear, branched or crosslinked polyurethanes by polyaddition reaction [63].

The most commonly used isocyanates in the propellant formulations with hydroxy prepolymers can be illustrated in Table 1.

Table 1 Typical isocyanates used in propellant formulations

Material	
Diisocyanate	**Polyisocyanate**
Toluene-2,4-diisocyanate (TDI)	Desmodur N-100
Methylenediisocyanate (MDI)	Desmodur N-3200
Hexamethylenediisocyanate (HDI)	
Isophoronediisocyanate (IPDI)	
Dimeryldiisocyanate (DDI)	

2.3.9 Combustion Stabilizers

Combustion stabilizers have been proven to be very effective in reducing and/or eliminating combustion instability in many solid rocket systems. It is known that the additives like zirconium carbide (ZrC), aluminum oxide (Al_2O_3) and zirconium-silicate ($ZrSiO_4$) suppress combustion instability especially in reduced smoke solid rocket systems. Even 0.5% additive can stabilize an unstable rocket motor [64]. The additives show effects on both linear and non-linear pulsed instabilities. Figure 5 illustrates effect of stability additive on the pulsed rocket motor. It shows that the use

of 1% ZrC as a stabilizer enabled to damp the large scale pressure oscillation. Even, it provided to prevent the motor failure resulted from non-linear oscillations.

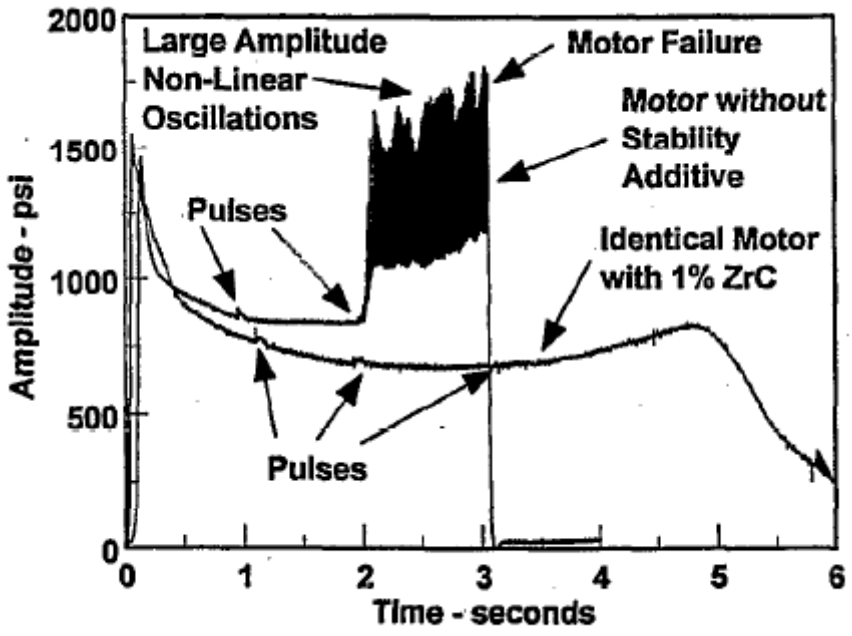

Figure 5 Stability additive effect on combustion instability of pulsed rocket motor [65].

2.3.10 Curing Catalysts

Polyurethane gel formation reaction between polyol and isocyanate groups can be activated by various kinds of catalysts. The reactions of the isocyanate group are extraordinarily sensitive to many different kinds of catalyst such as Lewis bases (1,4-diazabicyclo[2.2.2]octane (DABCO), dimethylbenzylamine, triethylamine, bis (2 (dimethylamino)ethyl]ether), Lewis acids (bis(ethylhexanoyloxy)tin(tin dioctanoate), bis(dodecanoyloxy) dibutyltin, dichlorodimethyltin [63]. Each catalyst has a specific activity profile. The situation is complicated, since the urethane group exerts a catalytic effect itself such that metal catalysts activate the isocyanate groups by making them more electrophilic, while bases make the hydroxyl groups more nucleophilic [66].

2.4 Solid Propellant Characterization Methods

2.4.1 Performance Characterization

The estimates of the theoretical specific impulse, I_{sp}, and density are needed in the early stage of motor design effort. These estimates not only influence the grain design itself, but also influence hardware weight and thus the mass ratio of the motor. If the chamber and exit pressures are specified, I_{sp} may be calculated by determining chamber temperature, average molecular weight of the gas and the specific heat ratio. Figure 6 illustrates the iterative approach used in the computer programs for the calculation of I_{sp} [67]. The estimate of delivered specific impulse is based on a theoretical impulse reduced by efficiency and heat losses, however, the prediction of a delivered specific impulse in a particular motor configuration is more difficult and less reliable than calculation of I_{sp}.

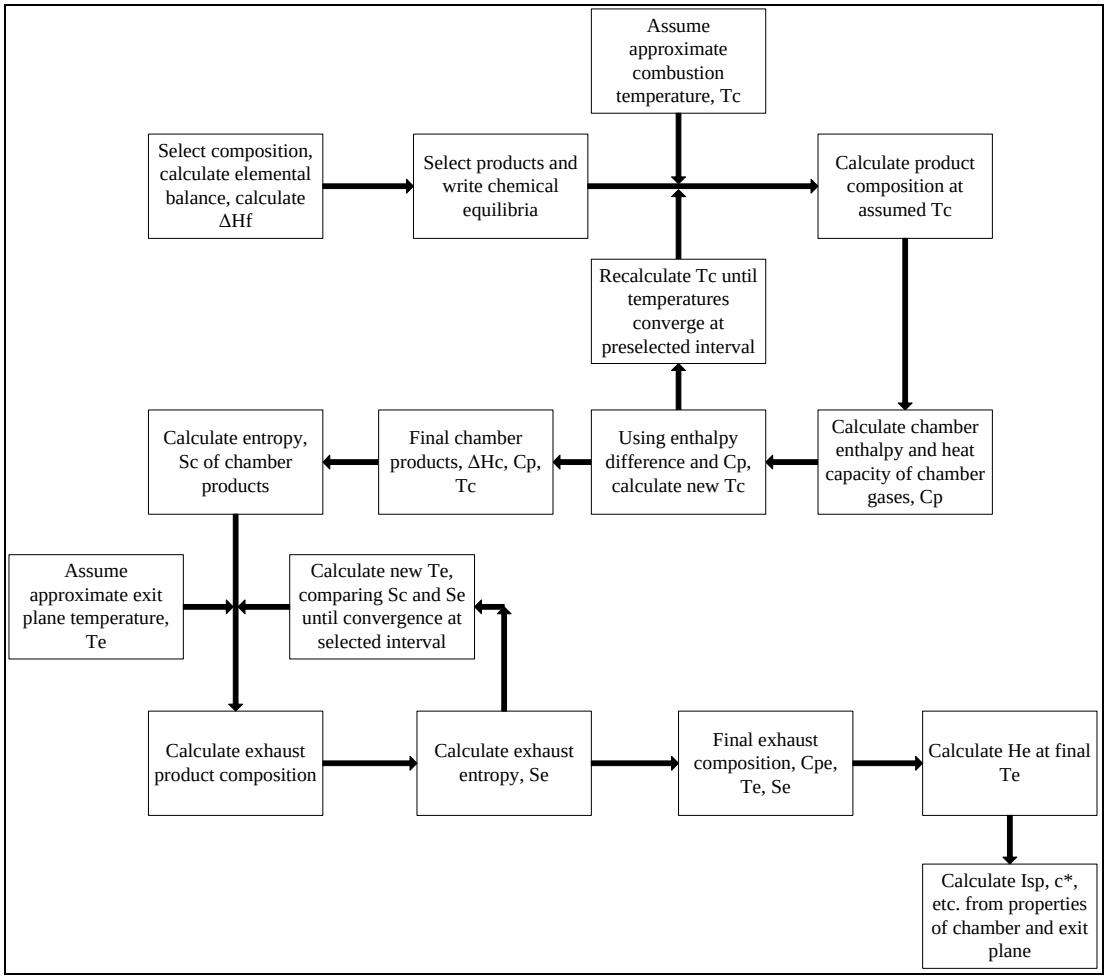

Figure 6 Flow diagram for calculation of propellant theoretical performance [68].

2.4.2 Internal Ballistics and Combustion Characterization

Internal geometry design enables the determination of free volume of the motor. Then, the type of propellant and igniter are determined. Subsequently, propellant modifications are made to give the required burning rate and any other needed internal ballistic properties. These modifications can be understood better in terms of treatments, in which different types of propellant combustions are modelled [69].

The primary heat generating reactions occur among gaseous pyrolysis products and gaseous metals in both composite and double base propellants. As a result, the burning rates of solid propellants show a strong pressure dependence that may be defined generally by the empirical Saint Robert law. Burning rates are usually plotted as the ordinate against pressure on the abscissa on log-log scale. In the region of 500 to 1500 psi, this usually yields a straight line whose slope gives the pressure exponent [22].

2.4.3 Mechanical Characterization

It is necessary to understand the grain materials used in rocket motor and obtain data on their properties before structural analysis can be performed. Propellant constitutes the most critical part of grain structure. Propellant is an incompressible rubber-like material. It has generally a bulk modulus about 1500 MPa in its original undamaged state. Its compression strain is low because of the presence of very few voids, much less than 1%, in a properly made propellant. However, the propellant can be damaged by applied forces. A propellant is a viscoelastic material that shows a nonlinear viscoelastic behavior. This reveals that the maximum stress and elongation decrease each time as a significant load is applied. In order to determine the physical properties of propellant, several kinds of laboratory tests are routinely performed on small samples [70]. The uniaxial tensile test is the most common test at a constant strain rate. Figure 7 shows the results of one set sample.

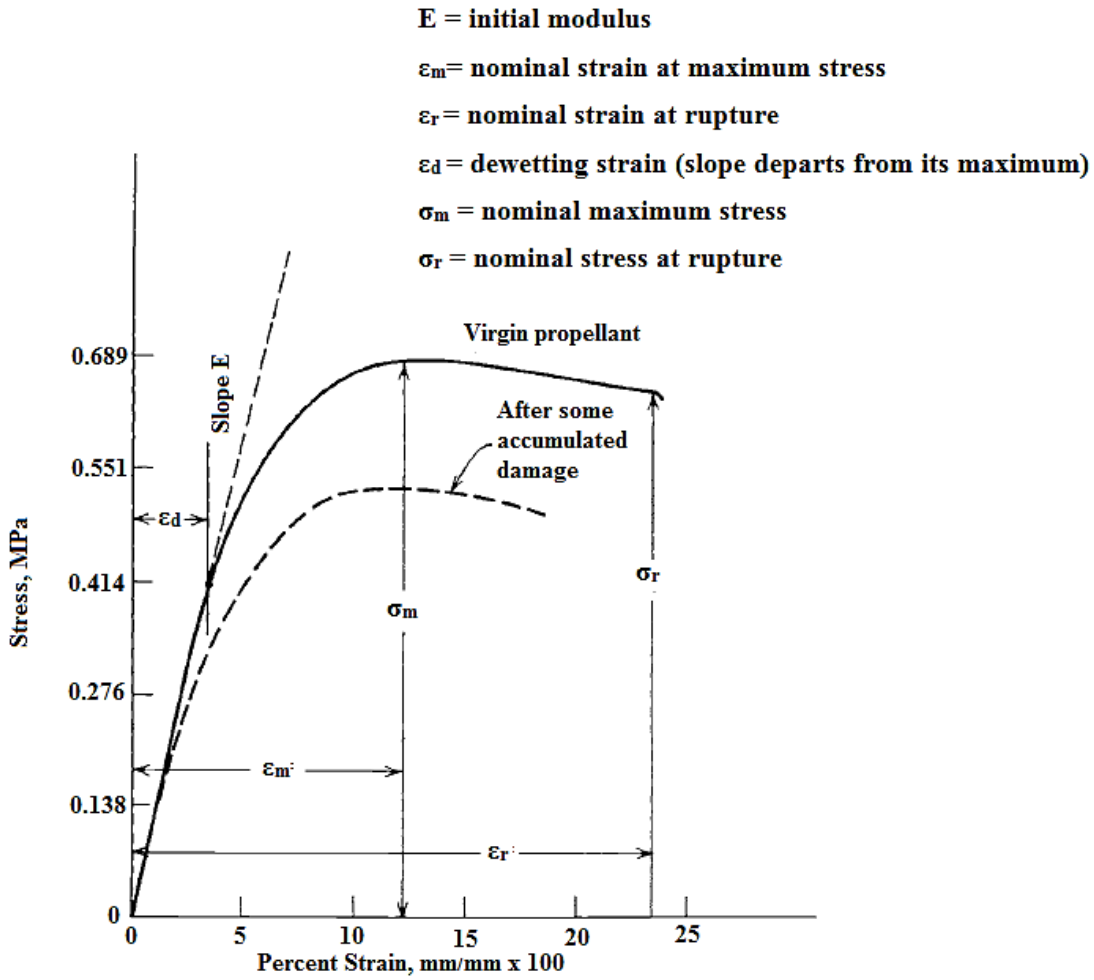

Figure 7 Stress-strain curves for a typical composite rocket propellant [70].

The test is commonly carried out for quality control, propellant development and determining failure criteria. When the sample has been loaded or unloaded and restressed several times, the damage to the material changes its response and properties as shown by the dashed curve. Figure 8 shows the standart specimen dimensions with varying thickness of 0.635 to 1.016 cm.

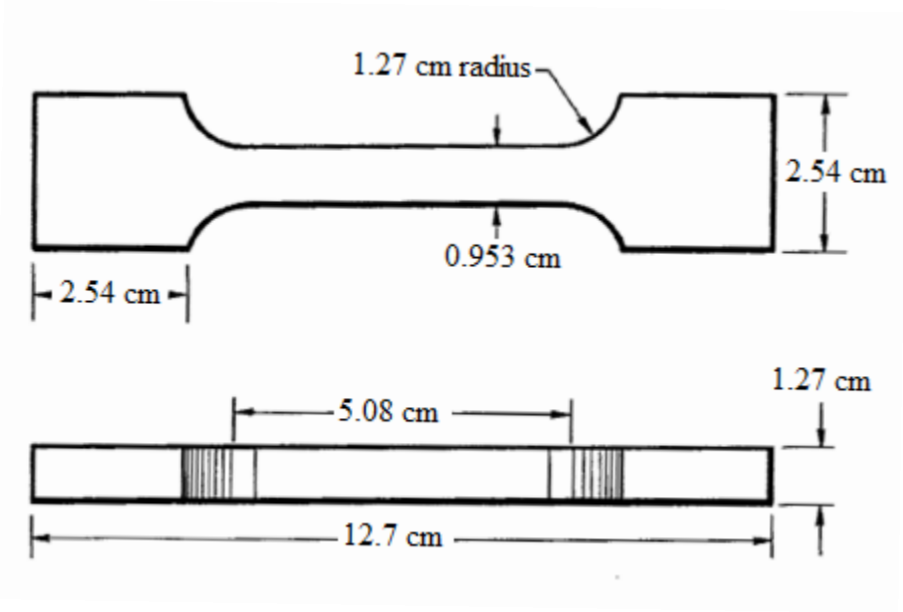

Figure 8 JANAF Test Specimen [71].

2.4.4 Stability Characterization

Mechanical property requirement of a solid propellant is prescribed by the structural loads during combustion, flight, and transportation. Different applications require different mechanical properties. For example, rocket motors for launch vehicles need low moduli grains, while sounding rockets and missiles require stiff propellant grains. The structural integrity of the propellant is mainly determined by the binder characteristics. Thus, the mechanical strength of solid propellant grain can be altered by tailoring binder characteristics [73]. The integrity of the solid propellant is the deciding factor in determining the motor storage life. Therefore, it is necessary to predict the propellant lifetime to be sure about a motor's service lifetime. This involves determining both the type and relative rates of ageing mechanisms [74].

2.4.4.1 Binder Stability

The evaluation of the mechanical properties is the most common method of binder characterization. Further, an evaluation of the crosslink density is essential since it is the most important structural property determining mechanical, swelling and damping characteristics of the binder network [75].

The crosslink density of the composite propellant binder is determined periodically during storage if degradation of the binder is suspected. These data show any change in crosslinking affecting the mechanical properties of the binder structure. The number of moles of effective chains per unit volume (crosslink density) for polymeric materials can be calculated from the theory of rubber-like elasticity in the form

$$\sigma = \nu_e RT (\lambda - \lambda^{-2}) \qquad (9)$$

where

λ = principal extension ratio = $(1 + \varepsilon)$
T = absolute temperature, K
R = gas constant
ν_e = crosslink density, moles of effective chains/cm^3

Swelling the binder structure in a nondegrading solvent provides a method for determining equilibrium properties. The effect of the imbibed liquid on Eq. 10 is accounted by

$$\sigma = \nu_e RT (\nu_2)^{1/3} (\lambda - \lambda^{-2}) \qquad (10)$$

where ν_2 is the volume fraction of the gel in the swollen gumstock. Tensile stress is based on the unstrained unswollen area corrected for sol fraction, and λ is the extension ratio based on the swollen, unstrained gage length [76].

2.4.4.2 Shelf Life

The service life or useful shelf life of a propellant can best be determined by an actual storage-surveillance program under the service conditions of temperature and humidity. Since the propellant ingredients rarely degrade sufficiently on storage to affect the total energy of the propellant, deterioration of the propellant usually can not be detected by measurement of thrust of a stored motor unless cracks are present or volatile burning-rate catalyst has been lost. The most reliable method of following the stability of a propellant during a storage program is to measure changes in

uniaxial properties during storage that often signal the deterioration of the motor. The appearance of gassing voids or cracks can be detected by X-ray during the program [77]. In addition, thermal stability of a propellant can be tested by the proposed HFC method [78]. The heat generation rate of decomposition of propellants is determined as a function of time at isothermal conditions. The upper limit of heat flow obtained is compared with the values calculated for 10 years of service life at 25ºC storage condition. If it is below the upper limit, the propellant is said to be thermally stable and has a minimum 10 years of service life at 25ºC. A typical heat flow curve of a double base propellant at 89 ºC is depicted in Figure 9 in which the y axis represents the heat flow per unit mass of propellant while x axis shows the time domain.

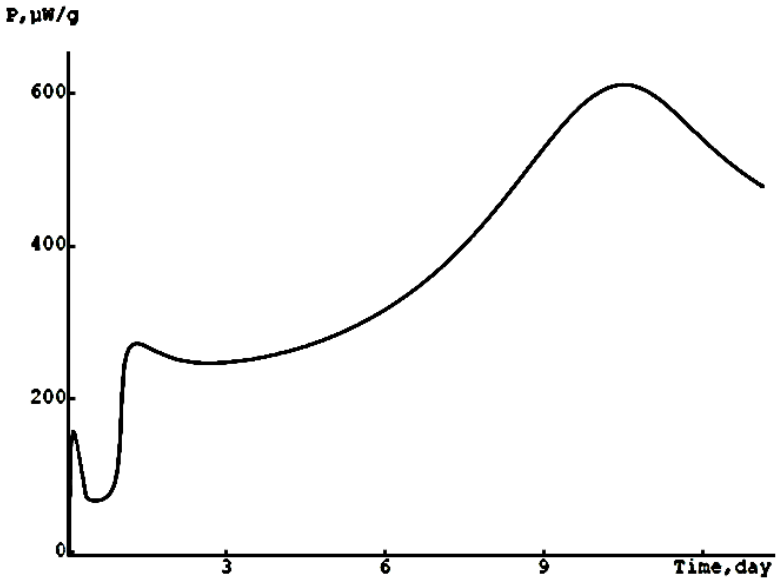

Figure 9 Heat flow curve of a double base propellant at 89ºC [78].

2.4.5 Thermal Characterization

Thermal properties of a propellant are inherent to the binder/filler system and not easily changed. The following thermal properties normally are evaluated for solid propellants even though only three are really required for thermal stress analysis of grains:

Coefficient of linear thermal expansion, α, m/m.K

Glass transition temperature, T_g, K

Thermal conductivity, k, W/m.K

Specific heat, C_p, J/kg.K

Thermal diffusivity, κ, m^2/s

Grain thermal analysis can be conducted with only α and κ, but the usual method for obtaining κ is to calculate it from k, C_p, and density data for the propellant. T_g is required to decide whether the propellant retains its structural integrity and is usable in the operational conditions of missile which is generally between -40°C and +60°C. The value of α is the most important of all of the thermal properties in structural analysis. Grain thermal strains are directly proportional to α, so uncertainity in this parameter would affect the structural safety factors [79].

2.4.6 Hazard Characterization

The results of hazard tests determine the degree of care to be exercised during the motor's manufacture, transportation and storage. The propellant's relative sensitivity to initiation by impact, friction or spark and its relative susceptibility to detonation can be coded by different colors that would be different for various companies. No single area of propellant characterization is more controversial than that of propellant hazard characterization. No single impact or friction tester is universally accepted by the industry, and no clear rules exist for interpreting the data from any of the available apparatus. The interpretation of hazard data is often semi-intuitive [80]. Explosives are generally exposed to various external stimuli such as heat, impact, friction during production, handling, storage and transport. The hazard property of explosives is considered a crucial factor in order to determine practical applications of a given explosive.

2.4.6.1 Heat Sensitivity

The thermal behavior of propellants can be determined by thermal analytical techniques as a function of temperature and time. Differential thermal analysis (DTA), thermogravimetric analysis (TGA) and differential scanning calorimetry (DSC) are the most common methods of thermal analysis that are as listed in Table 2 [81].

Table 2 Thermal analysis techniques for propellant

Technique	**Parameter measured**	**Apparatus**
TG	Weight change	Thermobalance
Derivative TG	Rate of weight change	Thermobalance or derivative thermobalance
DTA	Temperature difference between sample and reference material	DTA apparatus
Derivative DTA	Derivative of temperature difference between sample and reference material	DTA apparatus
DSC	Heat necessary to form zero temperature difference between sample and reference material	Differential scanning calorimeter
STA	DTA, TGA, DSC and derivatives of DTA/TGA	Simultaneous thermal analyzer
Evolved gas analysis	Gas liberated during thermal analysis and its composition	Gas analyzer

The endothermic and exothermic heat transitions due to vaporization, decomposition, melting and crystallization are recorded by comparing the heat exchanges with reference material upon heating in the differential thermal analysis (DTA) method. The thermal transitions are then used to characterize the system under study [82]. A typical DTA thermogram is shown in Figure 10. Points A, B, C, D, and E represent the start of heating, onset of endothermic heat change, peak of endothermic heat change, endset of endothermic reaction and onset of exothermic heat change, respectively.

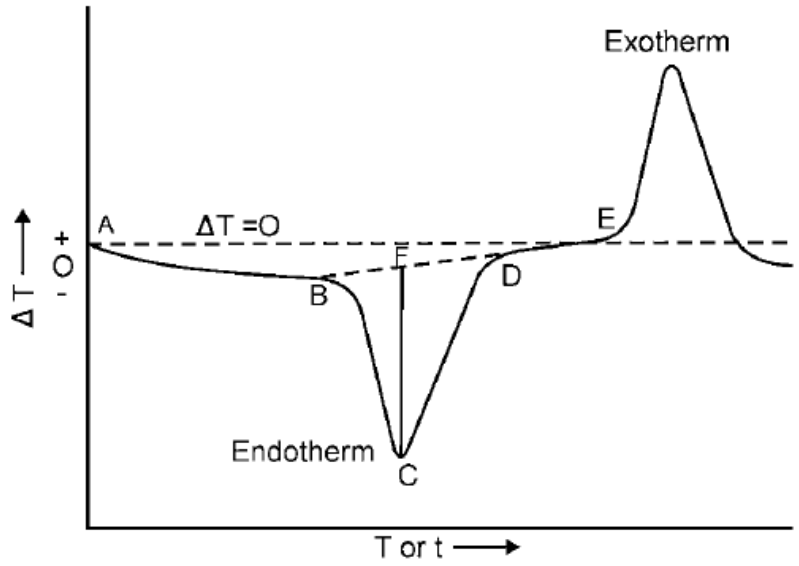

Figure 10 A typical DTA curve (thermogram) [82].

TGA describes the tool of the weight change of a sample at constant temperature by time or the weight change of a sample as a function of temperature. Thermogravimetric curves are often used as supplementary information derived from DTA in terms of chemical and physical changes. The rate of weight change is often shown by taking the first derivative with time in order to show sharply the details of the original curve which is called derivative thermogravimetric analysis (DTG) [83]. An idealistic weight loss vs temperature/time curve is shown in the Figure 11.

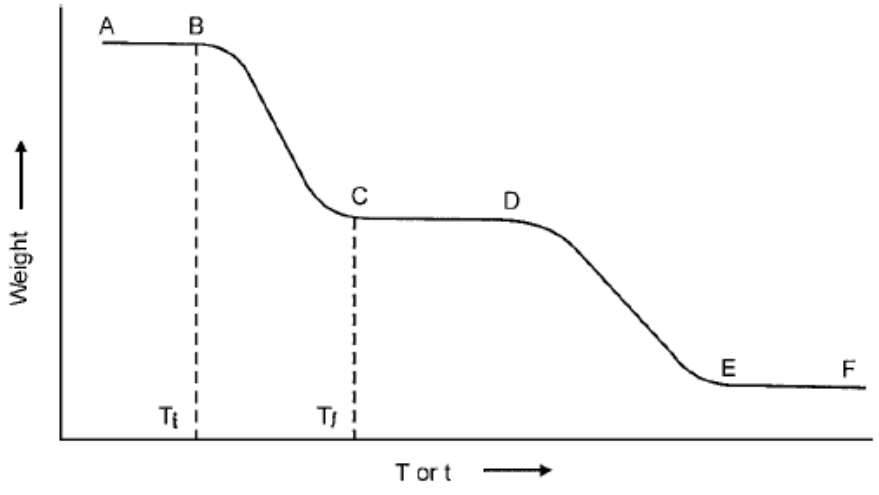

AB, CD and EF : Plateaus; T_i : Initial Temperature, T_f : Final Temperature; $T_f - T_i$: Reaction interval.

Figure 11 A typical TGA curve [83].

DSC measures the energy necessary to establish zero temperature difference between the sample and reference material against time/temperature. The output signal is measured in terms of heat capacity as a function of time/temperature [84]. The typical DSC curves are shown in Figure 12 [85]. It represents the DSC curves with various heating rates (DSC 10, DSC 20, DSC 30...etc.) and TGA curve with 30°C/min. heating rate.

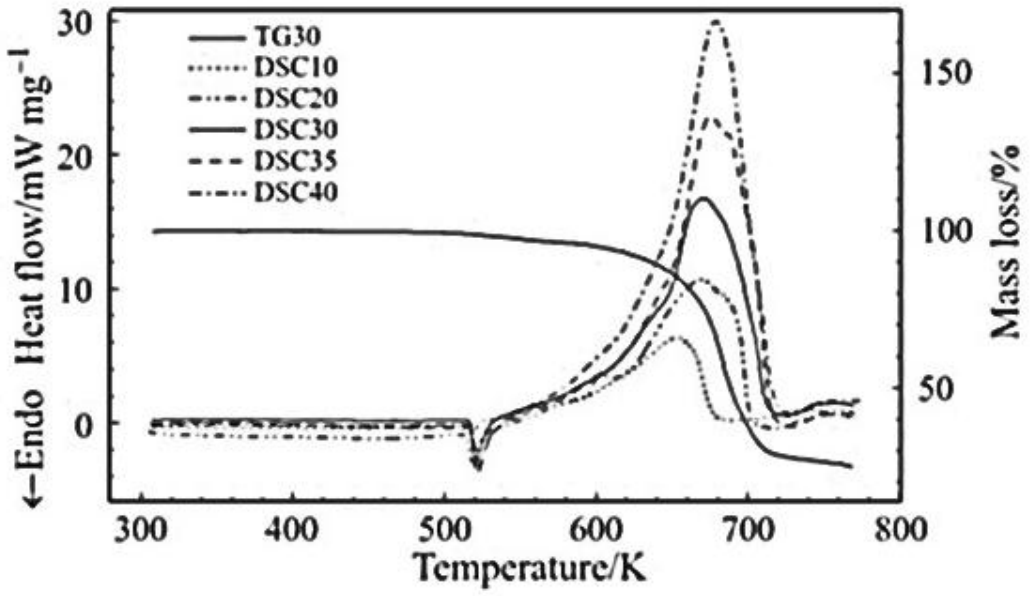

Figure 12 DSC curves of thermal decomposition of AP/HTPB based propellants at various heating rates [85].

2.4.6.2 Impact Sensitivity

Many propellants can be ignited or detonated by impact, thus it is crucial that the impact hazard of a propellant be characterized. A wide variety of impact devices are utilized to characterize the impact hazards of propellant ingredients, uncured propellant mixes and cured propellant mixes. The most common principle for such a device involves calibrated weight falling on a propellant sample. Two types of impact devices are most commonly used within the industry. The Olin-Mathieson impact apparatus uses a 2 kg weight and the impact test results generally are reported in kg-cm. The Bureau of Mines (BoM) test apparatus uses a 1-lb weight; the impact test results generally are reported in inches. Impact data frequently are given on the basis of a 50 percent impact point, the height at which 50 percent of the samples

tested deflagrated or detonated. Figure 13 represents the schematic of the BoM impact sensitivity apparatus [86].

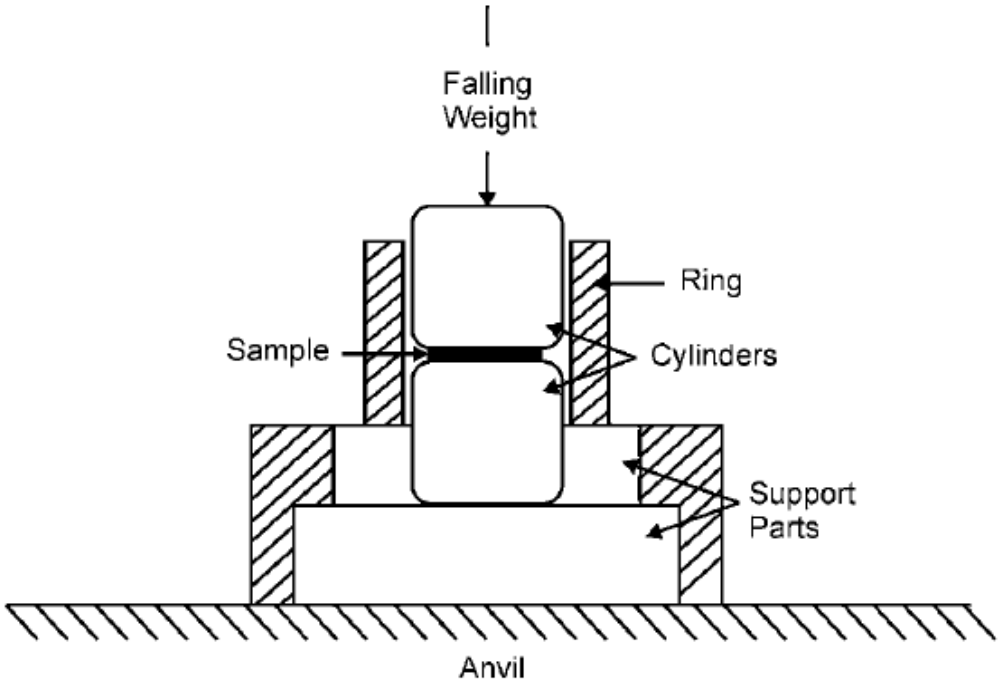

Figure 13 BoM impact apparatus [87].

The impact test is generally run on propellant ingredients, the uncured propellant mix, and the cured propellant. The values obtained are useful in assessing the degree to which the ingredients, uncured propellant, and cured propellant should be protected from the common mechanical shocks encountered in processing and handling. An impact sensitivity on the order of 5 kg-cm represents an extremely low value in most devices, and such a propellant properly may be judged as hazardous to handle. Many of the common composite propellants such as the aluminized polybutadiene propellants are relatively insensitive. The impact sensitivities of composite double-base propellants, however, are sufficiently low that greater care must be taken in processing and handling [88].

2.4.6.3 Friction Sensitivity

The cured propellant often is subjected to friction during normal handling operations such as mold disassembly, mandrel removal, machining and trimming and motor

assembly. Many propellants are particularly sensitive to friction. Metal containing composite propellants that are oxidized by AP, are more friction-sensitive than classical double-base propellants. There is no widely accepted standard friction test. Two common friction sensitivity tests are the pendulum friction test and the ESSO screw friction test that can be found in literature [89]. The pendulum friction test machines use the swing of a pendulum to impart energy to a sliding bar that abrades the test specimen. Several variations of this device have been developed. In the Bureau of Mines (BoM) device, the pendulum is fitted with shoes of various composition (fiber, steel, etc.) and allowed to swing directly across the propellant sample [90]. Other variations within the industry include spring-loaded devices and other techniques for imparting mechanical energy to an abrading slide.

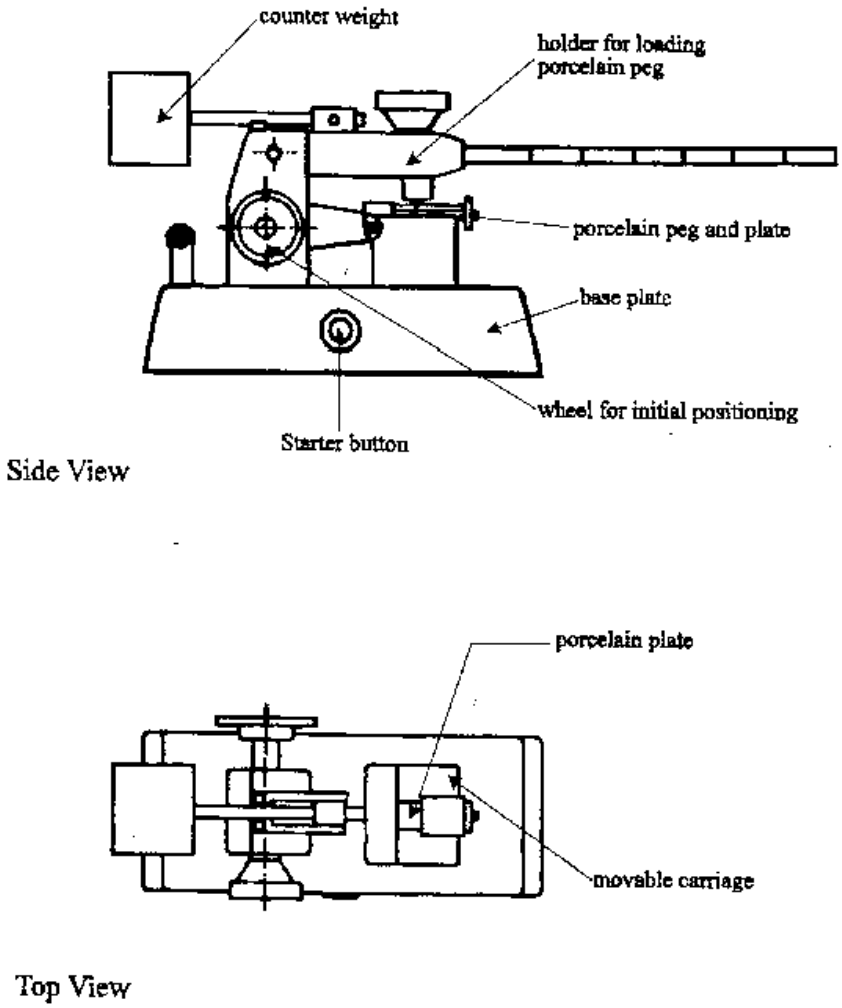

Figure 14 A schematic of the BAM friction tester [91].

Today, the most commonly used method is the BAM friction test. The apparatus of the method is shown in Figure 14. It is composed of a fixed porcelain peg and a moving porcelain plate. A forward and a backward motion of the plate determine the point at which explosive shows a positive reaction due to friction under the porcelain peg of 10 mm in each direction. Counterweight is used for balancing the system [91].

2.4.7 Solid Propellant Smoke Classification

The smoke classification of solid propellant is proceeded according to the STANAG 6016 which is the standardization agreement ratified by NATO nations [92]. The exhaust plume smoke characteristics associated with a solid propellant are specified by two letters, the first refers to primary smoke and the second to secondary smoke as illustrated in Table 3.

Table 3 Solid propellant smoke classification

Increasing Primary Smoke ↓	**Increasing Secondary Smoke** →		
	AA	AB	AC
	BA	BB	BC
	CA	CB	CC

In this table, AA solid propellant would be close to the general concept of a Minimum Smoke propellant. AC would correspond approximately to a Reduced Smoke propellant and CC to a Smokey propellant. Primary and secondary smoke classifications are made separately. AGARDP or primary smoke classification is to be determined by the following procedure. First of all, propellant ingredients are input into a chemical equilibrium, adiabatic combustion code with a chamber pressure of 70 atm and an exit pressure of 1 atm specification. The mass percentages of each of the condensable metallics are recorded for shifting equilibrium nozzle exit conditions. Then, AGARDP is calculated by the following relation [93].

$$AGARDP = 1 - e^{[-\sum i\ (\%MpixNi)\ /\ SGi]} \qquad (11)$$

where $\%M_{pi}$, SG_i and N_i are the mass percentage, specific gravity and optical property constant (currently taken as 1.0) of species i, respectively. Primary smoke is assigned as follows.

If $AGARDP \leq 0.35$	assign an A classification
If $0.35 \leq AGARDP \leq 0.9$	assign a B classification
If $AGARDP > 0.9$	assign a C classification

The AGARDS or secondary smoke classification is based on the condensation of water vapor and/or water/acid vapor by exhaust gases in the presence of ambient humidity. The ambient relative humidity (RH_{amb}) required for the onset of condensation is calculated by a given mole fraction (f) of condensable species (i.e., HCI, HF, and H_2O) in the exhaust products using the following equation.

$$AGARDS = RH_{amb} = 100x(K - f_{total} \text{ x } 0.16589) \qquad (12)$$

where K is the P/P_0. Figure 15 shows the variation of K as a function of the partial pressure of diluted concentration for HCI and HF at 0^oC [95].

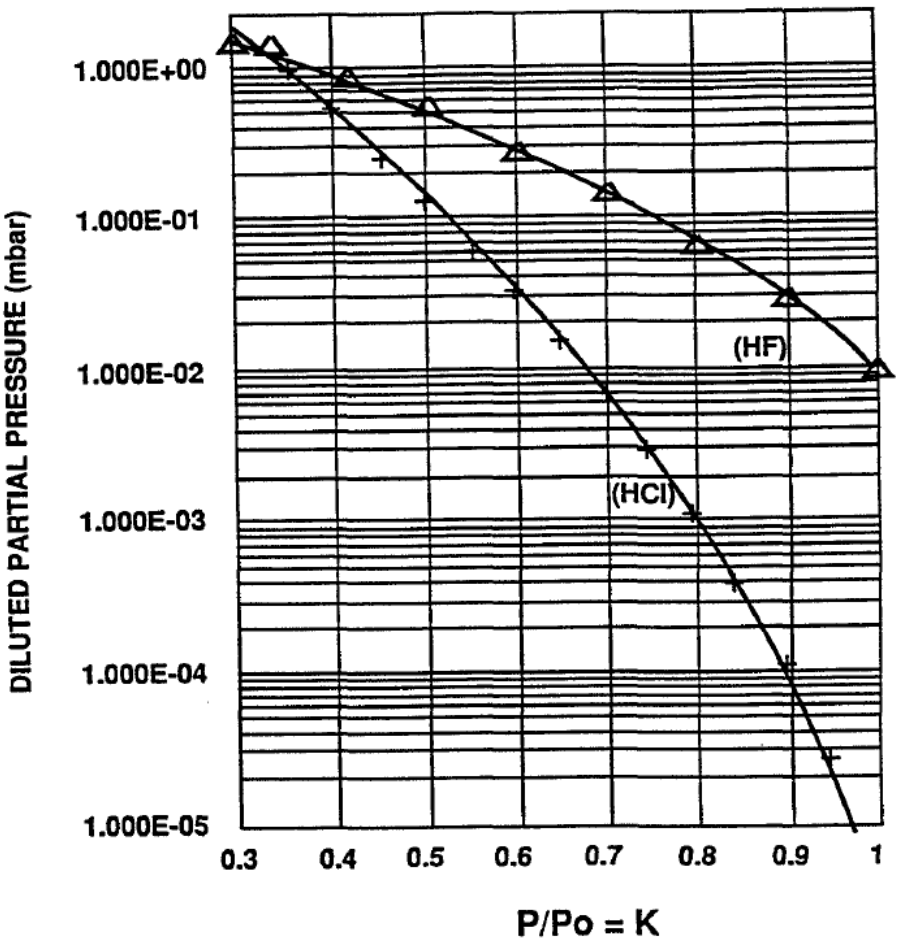

Figure 15 Oliver depression factor for acid/water vapor equilibrium at 0°C [95].

Secondary smoke, AGARDS, is assigned by the following criteria.

If $AGARDS \geq 90\%$	assign an A classification
If $90\% > AGARDS \geq 55\%$	assign a B classification
If $AGARDS < 55\%$	assign a C classification

2.5 Insensitive Propellant Concept

Despite the fact that the rocket propellant is only one aspect of a munition system, there are specific characteristics that have been identified as contributing factors to the achievement of IM status [95]. There are various ways of categorizing these characteristics. Categorizing propellant characteristics might lead us to three general approaches to reducing sensitivity [96]:

- Changing the friability or “toughness” of the propellant

Propellants with good elongation properties (particularly at low temperatures), those that absorb energy and deform with minimum damage, tend to perform well against shock and impact threats.

- Managing the partitioning of energy

That can be achieved in many ways. First, the solid loading of propellant can be reduced. In general, decreasing the total solids level improves the mechanical properties and decreases detonability of the propellant. This can be accomplished in several ways by increasing the density of crystalline oxidizers, by using an energetic binder system, which allows a corresponding decrease in solids loading without decreasing total energy, by using high-density additives to maintain or increase propellant density-impulse while decreasing the total level of solids.

Next, the particle size and distribution in propellant formulation can be controlled. The particle distributions should be optimum for binder wetting and particle to particle bond strength.

Then, the less sensitive solid ingredients can be used. This is accomplished by reducing the level of nitramines, reducing or changing ballistic modifiers and reducing the amount of ammonium perchlorate (AP). This may also involve the development of new ingredients, or the use of new combinations of existing propellant ingredients, such as energetic plasticizers.
Finally, low ignition temperature binder materials can be used. They melt at temperatures below the melting temperatures of the solid additives.

- Developing extinguishable propellants–propellants that extinguish at atmospheric pressure

Obviously, choosing the best propellant from an IM perspective is not a simple process. Besides considering the influence of other system components and factoring in a scientific evaluation of the hazard/munition interaction, the designer must also

weigh the IM requirements against other system constraints when tailoring propellants for specific applications. Performing the appropriate trade-offs between hazard reduction and the other considerations as shown in
Figure 16 involves understanding of the interaction of the normal (i.e. non-IM) propellant selection criteria with their influence on desensitizing the propellant to the hazard threats [97].

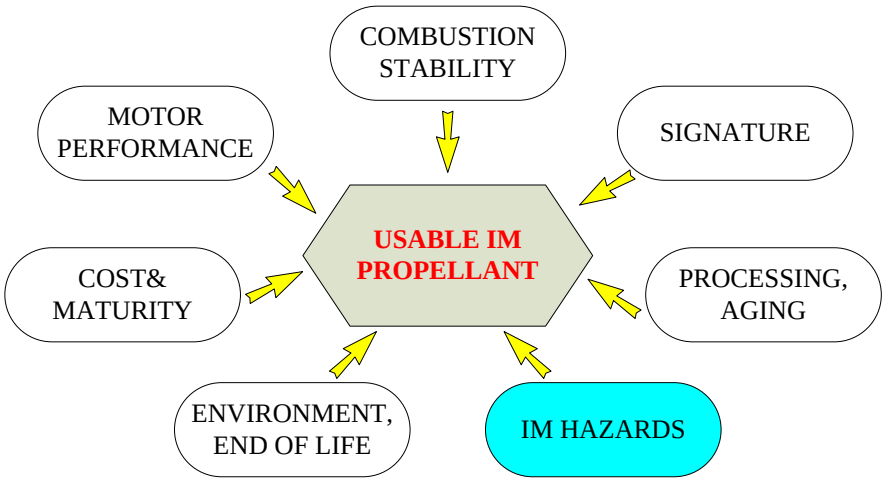

Figure 16 Rocket motor design tradeoffs [97].

2.6 HTPE Propellants

Hydroxy Terminated Polyether (HTPE) binders are developed and are being used in certain composite rocket propellant formulations as less sensitive alternatives to HTPB which is the most common polymer used in propellant formulations. Polyether binders have been used in formulations since the mid-1950s [47] before the development of HTPB propellants, although, HTPE is described as a new type of binder [10]. They are also called HTPE propellants which is developed as less sensitive replacements for HTPB/AP propellants [98]. It is claimed that HTPE propellants give a less severe response than HTPB propellants in IM tests especially in slow cook-off and bullect impact [99].

The basic approach to IM-ness employed is the reduction in solids loading accomplished by using an energetic plasticizer that is compatible with the HTPE polymer. This permits the HTPE propellant to maintain a theoretical specific impulse

at or above that of a comparable HTPB propellant while significantly reducing the level of solids, as shown in Figure 17. Sensitivity of the propellant is further reduced by the replacement of a portion of the AP with ammonium nitrate (AN) [100].

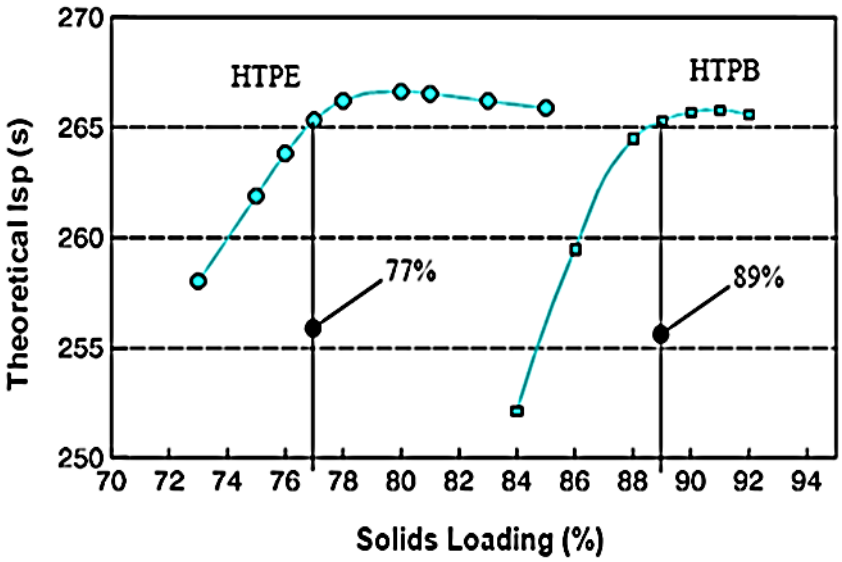

Figure 17 HTPE's advantage: Reduced solid loading at the same level of energy [100].

The comparison of the properties of HTPE and HTPB propellants in critical design tradeoff areas can be noted as in Table 4.

Table 4 Comparison of properties, HTPB vs HTPE [100].

Characteristic	**HTPB**	**HTPE**
Isp.ρ (gr.s/cm^3) reduced smoke	≥415	≥415
Burn rate at 6.89 MPa (mm/s)	7.6-38.1	7.6-30.5
Pressure exponent	~0.5	~0.5
Failure stress at 25^{o}C (MPa)	0.83	1.17
Failure strain at 25^{o}C (%)	40	50
Modulus at 25^{o}C (MPa)	4.14	3.45
Pot life (hours)	10	20
Shock sensitivity	0 cards	0 cards

HTPE propellant formulations have been tested in a variety of configurations, at the sub-scale or generic level, as well as in full-scale prototype rocket motors, from 5-inch diameter to the 10-inch diameter. Several of these configurations have undergone the full range of IM tests, and have generally performed quite well, especially when combined with graphite composite motor cases. Table 5 illustrates the results of a series of IM tests conducted on 10-inch diameter analog test motors, and offers a comparison between the IM-ness of similar configurations using HTPB and HTPE propellants. As can be seen from IM test results, HTPE propellants give less response proving their more IM character than HTPB's [101].

Table 5 Comparison of IM test results: HTPB vs. HTPE [101].

IM Test	**Configuration (10 inch analog motors with graphite composite cases)**	
	HTPB	**HTPE**
Slow Cookoff	Explosion	Burn
Fast Cookoff	Burn	Burn
Bullet Impact	Deflagration	Burn
Fragment Impact	Explosion	Extinguish

CHAPTER 3

EXPERIMENTAL

3.1 Materials

3.1.1 Binder

3.1.1.1 Terathane-Polyethyleneglycol (TPEG)

In this study, a novel type of hydroxy terminated polyether binder which is the Terathane-Polyethyleneglycol (TPEG) block co-polymer was used. It was purchased from the ATK Missile Subsystems and Components Division in 100 kg drum with end-use certificate, since it is subjected to Missile Technology Control Regime. Figure 18 shows the chemical structure of TPEG. The properties provided by the supplier are given in
Table 6.

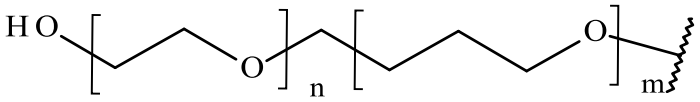

Figure 18 The chemical structure of TPEG polymer

Table 6 Technical properties of TPEG

Characteristics	Requirements		Actual Values
	Min.	Max.	
Viscosity at 120^{o}F (Poise)	-	15	12.0, 10.0
Hydroxyl value (grams/equiv)	1300	1700	1597, 1591
Moisture (%)	-	0.05	0.047, 0.046
BHT Antioxidant Content (%)	0.05	0.2	0.08, 0.08

3.1.2 Oxidizer

3.1.2.1 Ammonium Perchlorate

Ammonium perchlorate, AP, were used in three different particle sizes as 400 μm, 200 μm, and 20 μm. AP 400 μm was purchased from American Pacific (AMPAC), Western Electrochemical Co. USA and AP 200 μm was purchased from China Precision Machinery Import-Export Corporation (CPMIEC) since they are commercially available. AP 20 μm was obtained by crushing of AP 200 μm by a hammer mill. The physical and chemical properties are shown in Table 7.

Table 7 The physical and chemical properties of ammonium perchlorate

Properties	**Values**
Chemical formula	NH_4ClO_4
Appearance	White crystal
Physical state	Solid
Molecular weight (g/mol)	117.5
Solubility in water (wt%)	20.8 g/100 mL at 20°C
Density (g/cm^3)	1.95
Mean particle sizes (μm)	400, 200, 20

3.1.2.2 Cyclotetramethylene Tetranitramine

Cyclotetramethylene Tetranitramine, HMX, was procured from Chemring Nobel AS, Norway, as Grade B (higher purity than Grade A) in two different classes, Class I and Class III. Figure 19 shows the chemical structure of HMX. Table 8 summarizes its chemical and physical properties.

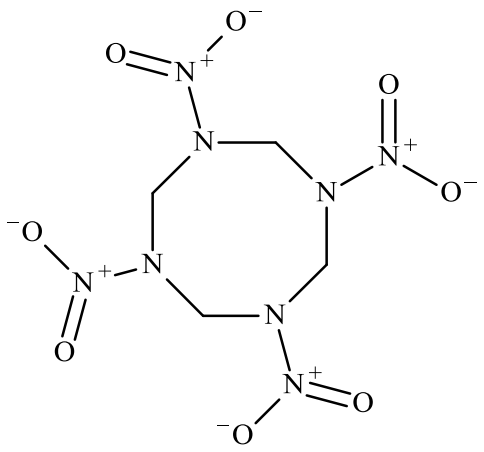

Figure 19 The chemical structure of HMX

Table 8 The chemical and physical properties of HMX

Test	**Values**
HMX content (%)	98
Melting point (^{o}C), min.	277
Acetone insoluble material (wt%), max.	0.05
Inorganic insoluble (wt%), max.	0.03
Acidity (wt%), max.	0.02
Granulation	Class I (D50: 150 μm), Class III (D50: 460 μm)

3.1.2.3 Phase Stabilized Ammonium Nitrate

Phase Stabilized Ammonium Nitrate, PSAN, is a type of ammonium nitrate that is stabilized for preventing the Phase III to Phase IV transition of ammonium nitrate at about 30^{o}C. In this study, the PSAN stabilized with KNO_3 was used. It was purchased from YANXA International Industrial Co., China. The specification of PSAN is tabulated in Table 9.

Table 9 The product specification of PSAN

Properties	**Values**
Chemical formula	NH_4NO_3-KNO_3
Appearance	White powder, free flowing without impurities
Ammonium Nitrate content (%)	89
Potassium Nitrate content (%)	10
Moisture (%)	0.1
Water insoluble material (%)	0.7
Anti-caking agent content (%)	0.6
pH value	5.0
D50 value (μm)	200
Phase stability	Shall exhibit no crystalline phase changes below -55°C~100°C

3.1.3 Metallic Fuel

3.1.3.1 Aluminum

Aluminum, Al, powder was manufactured by ROKETSAN and stored in 25 kg drum. The specifications are shown in Table 10.

Table 10 The technical properties of Al powder

Properties	**Values**
Active Al content (%)	≥98
Iron content (%)	≤0.2
Particle size (μm)	Min: 12 Max: 18

3.1.4 Energetic Plasticizer

3.1.4.1 N-n-Butyl-N-(2-Nitroxyethyl)Nitramine

N-n-Butyl-N-(2-Nitroxyethyl)Nitramine, BuNENA, is one type of NENA plasticizer used in propellant formulation in order to increase performance and processability of

a propellant. It was purchased from Chemring Nobel AS, Norway, in 60 kg drum. The chemical structure of BuNENA is presented in Figure 20. The physical and chemical properties are tabulated in Table 11.

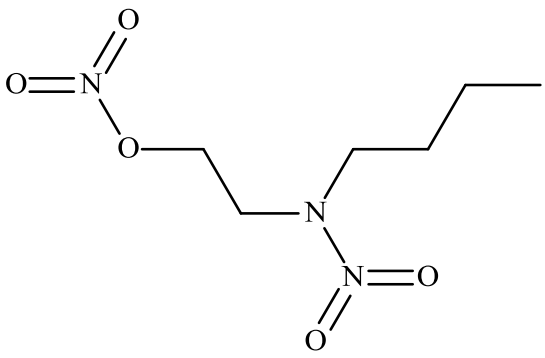

Figure 20 The chemical structure of BuNENA

Table 11 The physical and chemical properties of BuNENA

Properties	**Values**
Purity (%)	≥99
Physical state	Fluid
Colour	Yellow
Odour	Sweetish
Melting point	-27^{o}C
Stabilizer (MNA) content (%)	0.5
Specific gravity (g/cm^{3})	1.2
Solubility in water	Insoluble
Decomposition temperature	210^{o}C

3.1.4.2 Methyltrimethylolmethane

Methyltrimethylolmethane, TMETN, is a nitrate ester used in formulations as an energetic plasticizer. ROKETSAN produces TMETN batchwise in 5 gallon drums for its own needs. The chemical structure is shown in Figure 21. The chemical and physical properties are shown in Table 12.

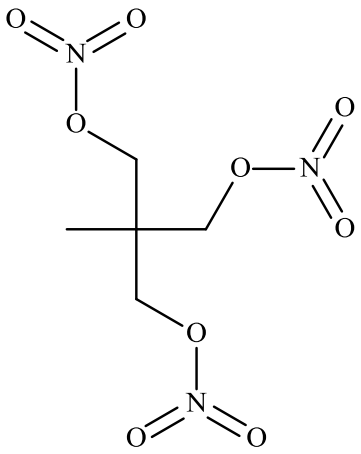

Figure 21 The chemical structure of TMETN

Table 12 The physical and chemical properties of TMETN

Properties	**Values**
Purity (%)	98 min.
Acidity/Alkalinity (%)	0.002 max.
Moisture (%)	0.2 max.
Physical state	Oily liquid
Color	Colorless
Molecular weight	255.15
Specific gravity (20^{o}C)	1.47
Freezing point	-3^{o}C
Oxygen balance as CO_2 (%)	-34.5
Viscosity (20^{o}C)	156 cP

3.1.4.3 Bis (2,2-Dinitropropyl)Acetal / Bis (2,2-Dinitropropyl)Formal

Bis (2,2-Dinitropropyl)Acetal/Bis (2,2-Dinitropropyl)Formal, BDNPA-F, is a high energy two component nitroplasticizer, composed of a 50/50 wt% eutectic mixture of bis(2,2-dinitropropyl)acetal (BDNPA) and bis (2,2-dinitropropyl)formal (BDNPF). It was procured from Mach I Chemicals, USA, in 100 kg drum. The chemical structure and specifications are shown in Figure 22 and Table 13.

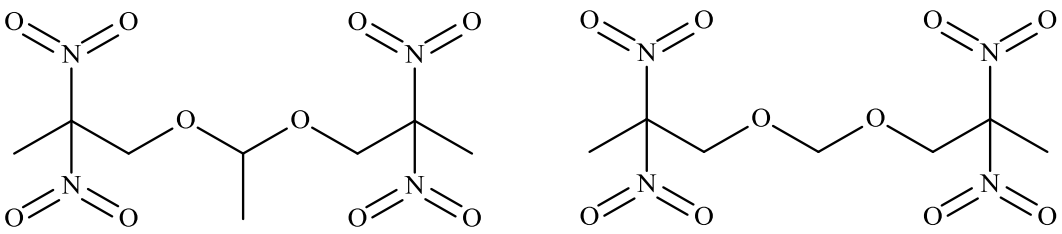

50% 50%

Figure 22 The chemical structure of BDNPA-F

Table 13 The specification of BDNPA-F

Properties	**Value**
BDNPA content (wt%)	45.0-55.0
BDNPF content (wt%)	45.0-55.0
PBNA content (wt%)	0.08-0.18
Density g/mL @25°C	1.383-1.397
Acid number (mg KOH/g)	0.5 max.
Water content (%)	0.05 max.

3.1.5 Stabilizer

3.1.5.1 N-methyl-p-Nitroaniline

N-methyl-p-Nitroaniline, MNA, is a yellow crystalline powder used as a stabilizer in the formulations. It was purchased from Mach I Chemicals, USA in 25 kg bucket. The chemical structure of MNA is shown in Figure 23. The product specifications are listed in Table 14.

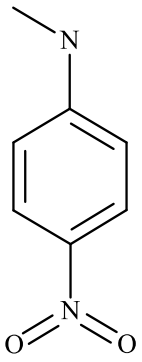

Figure 23 The chemical structure of MNA

Table 14 The product specifications of MNA

Properties	**Values**
Purity (%)	≥98
Moisture content (%)	0.5≥
pH of water extract (%)	5-7
Acid number (mg KOH/g)	0.3≥
Acetone insolubles (%)	0.15≥
Iron content (%)	0.005≥
Calcium content (%)	0.003≥
Chloride content (%)	0.005≥

3.1.6 Isocyanate

3.1.6.1 Toluene-2,4-Diisocyanate

Toluene-2,4-Diisocyanate, TDI, was used as an aromatic diisocyanate type isocyanate that reacts to give crosslinked polyurethane matrix with TPEG binder. It was purchased from Sigma-Aldrich Co.LLC. in 500 mL glass bottle. The chemical structure of TDI is presented in Figure 24. The product specifications of TDI are shown in Table 15.

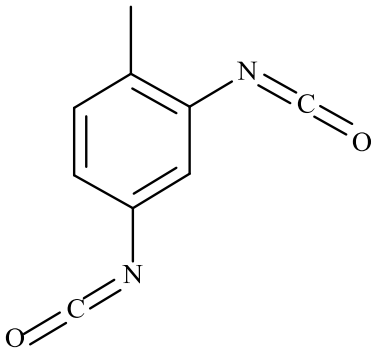

Figure 24 The chemical structure of TDI

Table 15 The product specifications of TDI

Properties	**Values**
Purity (%)	≥98
Hydrolyzed chlorine (%)	0.01≥
Total chlorine content (%)	0.04≥
Density at 20°C (g/cm^3)	1.21
Boiling point (°C)	251
Melting point (°C)	19.5-21.5

3.1.6.2 Isophoronediisocyanate

Isophoronediisocyanate, IPDI, is a diisocyanate having a ring structure that is used as a isocyanate. It was purchased from KİMETSAN Kimya, Turkey, in a 25 kg bottle. IPDI's chemical structure is as shown in Figure 25. The product specifications are given in Table 16.

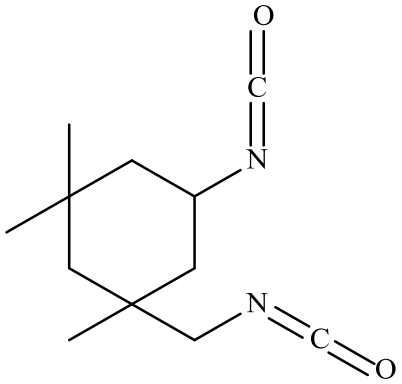

Figure 25 The chemical structure of IPDI

Table 16 The product specification of IPDI

Properties	**Values**
Purity (%)	≥99.5
NCO content (%)	37.5-37.8
Density at 20°C (g/cm^3)	1.06
Viscosity at 23°C (mPa.s)	13-15
Total chlorine (ppm)	10≥

3.1.6.3 Dimeryldiisocyanate

Dimeryldiisocyanate, DDI, has a long linear diisocyanate structure with high molecular weight. It was used as an alternate isocyanate and purchased from BASF Corporation, US, in a 25 kg bottle. DDI's chemical structure is shown in Figure 26. The product specifications are listed in Table 17.

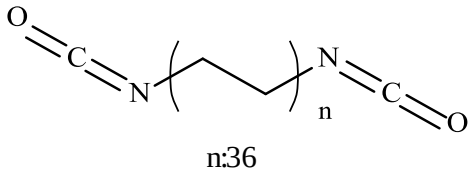

n:36

Figure 26 The chemical structure of DDI

Table 17 The technical details of DDI

Properties	**Values**
NCO content (%)	13.6-14.4
Specific gravity at 25^{o}C	0.924
Viscosity at 25^{o}C (cps)	130
Hydrolyzable chloride (%)	0.05≥
Molecular weight	600
Equivalent weight	300

3.1.6.4 Hexamethylenediisocyanate

Hexamethylenediisocyanate, HDI, is an organic compound in the class of isocyanates. More specifically, it is an aliphatic diisocyanate. It is a symmetric molecule and thus has two isocyanate groups of equal reactivity. It was purchased from Sigma Aldrich Co.LLC. in a 1 L glass bottle. The chemical structure is shown in Figure 27. The product properties are tabulated in Table 18.

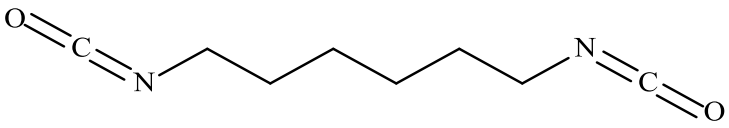

Figure 27 The chemical structure of HDI

Table 18 The properties of HDI

Properties	**Values**
Purity (%)	≥98.0
Molecular weight (g/mol)	478.6
Density at 20°C (g/mL)	1.047
Melting point (°C)	-70
Boiling point (°C)	240

3.1.6.5 Desmodur W

Dicyclohexylmethane-4,4'-Diisocyanate, H_{12}MDI-Desmodur W, is an cycloaliphatic diisocyanate having a molecular weight of 262 and equivalent weight of 131. It was obtained from Bayer MaterialScience AG, Germany . Its structure is shown in Figure 28. The specifications of product are listed in Table 19.

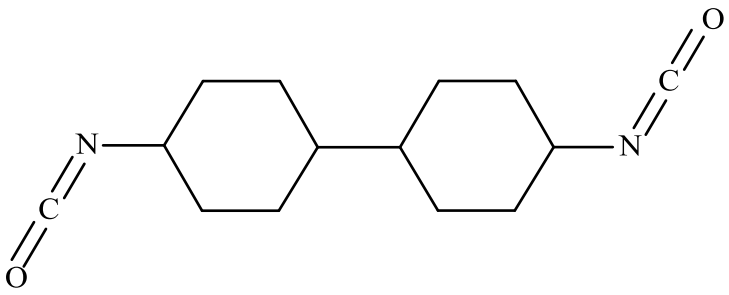

Figure 28 The chemical structure of Desmodur W

Table 19 The product specifications of Desmodur W

Properties	**Value**
NCO Content (%)	≥31.8
Assay (%)	≥99.5
Hydrolyzable chlorides (mg/kg)	≤10
Acidity (mg/kg)	≤10
Density at 20^{o}C (g/mL)	1.07
Viscosity at 25 ^{o}C (mPa.s)	30

3.1.6.6 Desmodur N-100

Desmodur N-100 is an aliphatic polyisocyanate whose structure is given in Figure 29. It was obtained from Bayer MaterialScience AG, Germany. The specifications of the product are illustrated in Table 20.

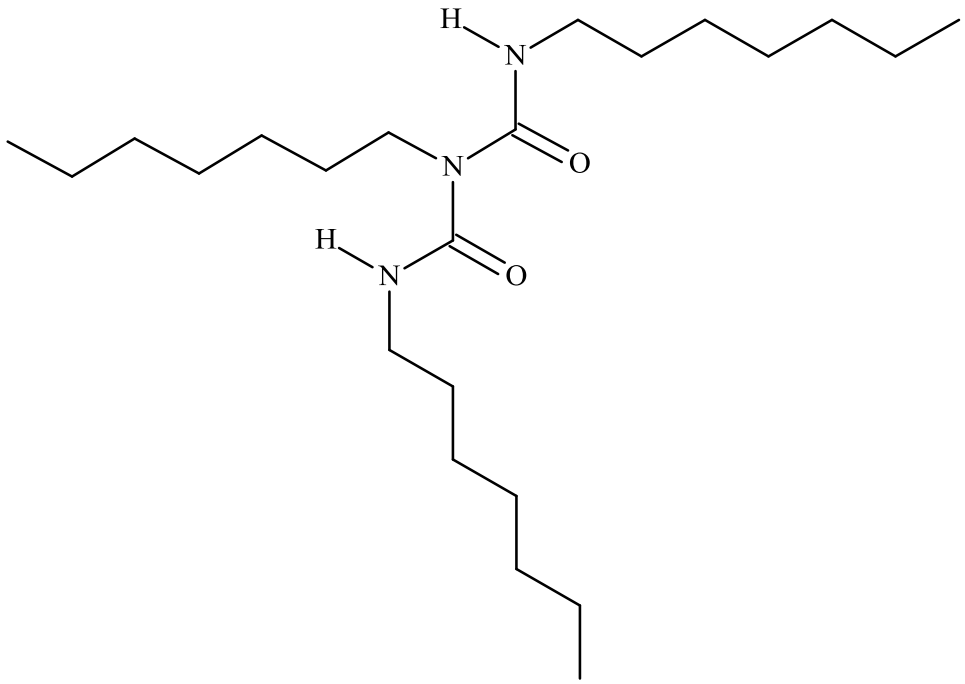

Figure 29 The chemical structure of Desmodur N-100

Table 20 The product specifications of Desmodur N-100

Properties	**Values**
NCO Content (%)	22.0±0.3
Equivalent weight	191
Density at 20^{o}C (g/mL)	1.14
Viscosity at 25 ^{o}C (mPa.s)	8000

3.1.6.7 Desmodur N-3200

Desmodur N-3200 is an aliphatic polyisocyanate whose structure is the same as Desmodur N-100. However, it has a lower viscosity and equivalent weight than Desmodur N-100. It was obtained from Bayer MaterialScience AG, Germany. The specifications of the product are given in Table 21.

Table 21 The product specification of Desmodur N-3200

Properties	**Values**
NCO Content (%)	23.0±0.5
Equivalent weight	183
Density at 20^{o}C (g/mL)	1.13
Viscosity at 23 ^{o}C (mPa.s)	2500±1000

3.1.7 Burning Rate Catalyst

3.1.7.1 Iron(III)Oxide

Iron(III) Oxide, Fe_2O_3, is a commonly used transition metal catalyst, especially in AP based propellant formulations. It was purchased from Mil-Spec Industries Corp. USA in a 5 kg Al container. It was in a accordance to the standard MIL-F-82655, Class I (Fine). The product specifications of iron(III) oxide are shown in Table 22.

Table 22 The product specification of Iron(III) Oxide

Properties	**Values**
Moisture (wt%)	≤0.5
Calcination loss (dry basis) (wt%)	≤2.0
Iron, as Fe_2O_3 (calcined bases) (wt%)	≥98.0
Acidity as H_2SO_4 (wt%)	≤0.02
Weight mean diameter, particle size (μm)	4.5-6.0

3.1.7.2 Chromium(III) Oxide

Chromium(III) Oxide, Cr_2O_3, is an inorganic compound used as burning rate catalyst. It is a green powder and one of the principal oxides of chromium. It is generally used as a pigment. It was provided by Sigma Aldrich Co.LLC in a 500 g glass bottle. The product specifications are shown in Table 23.

Table 23 The properties of Chromium(III) Oxide

Properties	**Values**
Chemical formula	Cr_2O_3
Assay (%)	≥98.0
Appearance	Green powder
Density (g/cm^3)	5.22

3.1.7.3 Silicon Dioxide

Silicon Dioxide, SiO_2, is a chemical compound that is an oxide of silicon. It was used as a burning rate catalyst in the formulations. It was purchased from Sigma Aldrich Co.LLC in a 500 g polymeric bottle. The product specifications are shown in Table 24.

Table 24 The properties of Silicon Dioxide

Properties	**Values**
Chemical formula	SiO_2
Assay (%)	~99.0
Particle size (μm)	0.5-10
Appearance	White to off-white powder

3.1.8 Curing Catalyst

3.1.8.1 Triphenylbismuth

Triphenylbismuth, TPB, is a white powder used as a curing catalyst. It was procured from Boulder Scientific Company, USA, in a 5 kg bag and it meets the requirements of military specification MIL-T-82825. The chemical structure is shown in Figure 30. The product specifications are stated in Table 25.

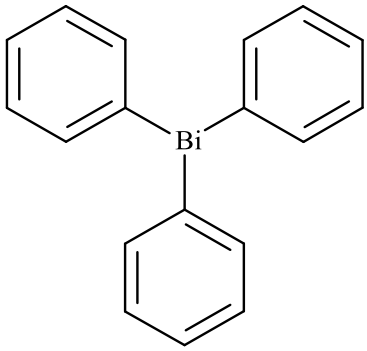

Figure 30 The chemical structure of TPB

Table 25 The product specifications of TPB

Properties	**Values**
Purity (%)	≥97.0
Melting point (^oC)	76.0
Acetone insoluble matter (%)	≤0.1
Magnesium (%)	≤0.003
Total halides as Chlorides (%)	≤0.05

3.1.8.2 Ferric Acetyl Acetonate

Ferric Acetyl Acetonate, FeAA, is used as curing catalyst. It was provided by Sigma Aldrich Co.LLC. in a 500 g plastic bottle. The chemical structure is given in Figure 31. The properties of the product are tabulated in Table 26.

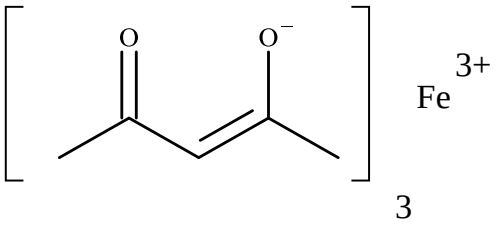

Figure 31 The chemical structure of FeAA

Table 26 The product specifications of Ferric Acetyl Acetonate

Properties	**Values**
Appearance	Red crystalline powder
Iron content (%)	15.5-16.2
Methylene Chloride Insolubles (%)	≤1.0
Water (%)	≤0.5

3.1.8.3 Dibutyl Tin Dilaurate

Dibutyltindilaurate, DBTDL, is an organotin compound that is used as a curing catalyst. It is a colourless oily liquid. It was purchased from Sigma Aldrich Co.LLC. in a 25 g glass bottle. The chemical structure is given in Figure 32. The product specifications are shown in Table 27.

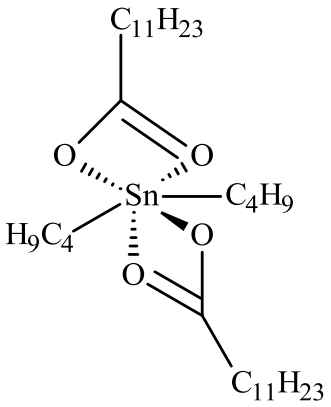

Figure 32 The chemical structure of DBTDL.

Table 27 The product specifications of Dibutyltindilaurate

Properties	**Values**
Appearance	Colorless to Pale Yellow Liquid
Sn content (%)	17.7-19.9
Density (g/mL)	1.066

3.1.9 Chain Extender

3.1.9.1 1,4-Butanediol

1,4-Butandiol, BDO, is a colorless viscous liquid used as a chain extender. It is a bifunctional alcohol. It was provided by Sigma Aldrich Co.LLC. in a 1 lt glass bottle. The chemical structure is given in Figure 33. The product specifications are listed in Table 28.

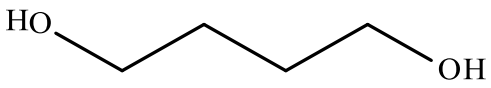

Figure 33 The chemical structure of BDO

Table 28 The product specifications of BDO

Properties	**Values**
Purity (%)	99
Density (g/mL)	1.017
Boiling point (^{o}C)	230
Melting point (^{o}C)	16
Refractive Index (n20/D)	1.445

3.1.9.2 1,1,1-Tris(hydroxymethyl)propane

1,1,1-Tris(hydroxymethyl)propane, TMP, is a colorless solid used as triol chain extender. It contains three hydroxy functional groups. It was purchased from Sigma Aldrich Co.LLC in a 1 kg polymeric bottle. The chemical structure is given in Figure 34. The product specifications are given in Table 29.

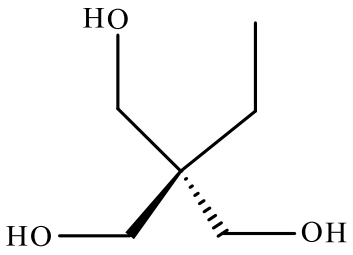

Figure 34 The chemical structure of TMP

Table 29 The product specifications of TMP

Properties	**Values**
Purity (%)	≥98
Boiling point (^{o}C)	159-161
Melting point (^{o}C)	56-58

3.2 Experimental Procedure

3.2.1 Preparation of HTPE Networks

HTPE based networks were synthesized in order to understand the structure-property relationships in segmented polyurethane structures. HTPE networks were obtained by the end-linking process of the HTPE chains via its terminal OH groups with isocyanate containing molecules. The properties of networks can be changed by using different types of isocyanate, curing catalysts and chain extenders with the corresponding TPEG binder. In addition, by manipulating the curative/binder equivalent ratio (NCO/OH ratio-R value) and weights of the network's ingredients, various kinds of polymeric structures were obtained.

The general procedure can be stated as follows: TPEG binder was degassed under 250 mmHg vacuum at 60^{o}C for 1h. If required, chain extenders were added and mixed for 10 min at 60^{o}C. Then, the isocyanates were added and mixed for 5 min. more. The resultant mixtures were degassed under 550-600 mmHg vacuum for 10 min. and then poured into Al molds in which epoxy-based mold release agents were used. Samples were prepared as 150 g weight and cured at between 50-60^{o}C for 7 days.

The calculation of R-value is based on the equivalent weight, which is a measure of the effective grams per reactive group of OH or NCO, of each compound, the binder and isocyanate. The ratio of the equivalent weight of isocyanate to binder gives the R-value.

The equivalent weight (EW) for polymeric binder can be calculated as shown below:

EW = 56100 / Hydroxyl number = 1000 / Hydroxyl value = 1700 / %OH (13)

Similarly, the equivalent weight (EW) for isocyanate can be calculated as shown below:

EW = 4200 / %NCO (14)

Table 30 shows the samples prepared for investigating the effects of isocyanate and R-value on the mechanical, structural and thermal properties of polyurethane structures. TPB was used as a curing catalyst in negligible amount in these samples. The composition column was coded so that it represents the ingredients of the samples prepared as polyol-isocyanate-R value for example, TP-TDI-R0.8 which is sample no 1 shows that TPEG and TDI were used as polyol and isocyanate, respectively, with R value of 0.8.

Table 30 Samples prepared to study the effects of isocyanate, mixed isocyanate and R-value on the polyurethane structure properties

		Concentration wt%		
Sample No	**Composition**	**TPEG**	**Isocyanate I**	**Isocyanate II-IPDI**
1	TP-TDI-R0.8	95.9	4.1	-
2	TP-TDI-R1.0	94.9	5.1	-
3	TP-TDI-R1.2	94.0	6.0	-
4	TP-IPDI-R0.8	94.8	5.2	-
5	TP-IPDI-R1.0	93.6	6.4	-
6	TP-IPDI-R1.2	92.4	7.6	-
7	TP-DDI-R0.8	87.2	12.8	-
8	TP-DDI-R1.0	84.5	15.5	-
9	TP-DDI-R1.2	81.9	18.1	-
10	TP-N100-R0.8	91.4	8.6	-
11	TP-N100-R1.0	89.5	10.5	-
12	TP-N100-R1.2	87.7	12.3	-
13	TP-N3200-R0.8	91.8	8.2	-
14	TP-N3200-R1.0	89.9	10.1	-
15	TP-N3200-R1.2	88.1	11.9	-
16	TP-W-R0.8	94.0	6.0	-
17	TP-W-R1.0	92.6	7.4	-
18	TP-W-R1.2	91.2	8.8	-
19	TP-HDI-R0.8	96.0	4.0	-
20	TP-HDI-R1.0	95.1	4.9	-
21	TP-HDI-R1.2	94.1	5.9	-
22	TP-N100/IPDI(1:2)-R1.0	92.7	2.4	4.9
23	TP-N100/IPDI(1:1)-R1.0	92.1	4.0	4.0
24	TP-N100/IPDI(2:1)-R1.0	91.4	5.8	2.9
25	TP-N3200/IPDI(1:2)-R1.0	92.7	2.4	4.9
26	TP-N3200/IPDI(1:1)-R1.0	92.2	3.9	3.9
27	TP-N3200/IPDI(2:1)-R1.0	91.6	5.6	2.8

In addition, the effects of chain extenders such as 1,4-butanediol (BDO) and trimethylolpropane (TMP) as difunctional and trifunctional hydroxyl compounds, respectively, were investigated by preparing samples shown in Table 31. Desmodur N-3200 was utilized as isocyanate. The R-value was kept constant as 1.0, and TPB was used as the curing catalyst in very small amounts. The composition column was coded so that it represents the ingredients of the sample prepared as polyol-isocyanate-chain extender for example, TP-N3200-0.2BDO which is sample no 28 shows that TPEG, Desmodur N-3200, and 1,4-butandiol were used as polyol, isocyanate, and chain extender, respectively. The coefficient (equivalence ratio) of chain extender represents the hydroxyl content of corresponding chain extender to the total hydroxyl content of chain extender plus prepolymer structure as illustrated in Eq. 15.

$$\text{Equivalence ratio} = OH_{BDO \text{ or } TMP} / (OH_{BDO \text{ or } TMP} + OH_{TPEG}) \qquad (15)$$

Table 31 Samples prepared to study the effects of chain extender and equivalence ratio on the polyurethane structure properties

		Concentration wt%		
Sample No	**Composition**	**TPEG**	**BDO or TMP**	**N3200**
28	TP-N3200-0.2BDO	87.2	0.6	12.2
29	TP-N3200-0.2TMP	87.2	0.6	12.2
30	TP-N3200-0.4BDO	83.0	1.5	15.5
31	TP-N3200-0.4TMP	83.0	1.5	15.5
32	TP-N3200-0.8BDO	59.8	6.6	33.6
33	TP-N3200-0.8TMP	59.8	6.6	33.6

One of the critical additives affecting the structural properties of polyurethane networks is the curing catalyst. Table 32 shows the samples prepared in order to understand the effects of type and amount of the curing catalyst. Desmodur N-3200 was again the preferred isocyanate. BDO was used as the chain extender with 0.4 equivalence ratio. The R-value in all the samples was kept constant as 1.0. The coefficient of curing catalyst represents the weight of the corresponding catalyst in gram required for 150 gr of sample.

Table 32 Samples prepared to study the effects of curing catalyst on the polyurethane structure and properties

		Concentration wt%		
Sample No	**Composition**	**TPEG**	**BDO**	**N3200**
34	TP-N3200-BDO-0.01TPB	83.0	1.5	15.5
35	TP-N3200-BDO-0.02TPB	83.0	1.5	15.5
36	TP-N3200-BDO-0.04TPB	83.0	1.5	15.5
37	TP-N3200-BDO-0.01FeAA	83.0	1.5	15.5
38	TP-N3200-BDO-0.02FeAA	83.0	1.5	15.5
39	TP-N3200-BDO-0.04FeAA	83.0	1.5	15.5
40	TP-N3200-BDO-0.01DBTDL	83.0	1.5	15.5
41	TP-N3200-BDO-0.02DBTDL	83.0	1.5	15.5
42	TP-N3200-BDO-0.04DBTDL	83.0	1.5	15.5

3.2.2 Preparation of Propellant Samples

Propellant samples were prepared by incorporating energetic components to HTPE based elastomers. The main ingredients of any propellant formulations are composed of polymeric binder, oxidizer, energetic as well as non energetic plasticizer, burning rate catalyst, curing catalyst or catalyst system, and some additives like combustion stabilizer and antioxidant stabilizer. The propellant formulations shown in Table 33 and Table 34 were prepared in order to characterize the propellant samples in terms of thermochemical and ballistic properties. The type and weight percents of propellant ingredients were adjusted to get the desired propellant properties. The propellant samples were coded such that TPAP samples represent that the propellant was based on TPEG and AP. The coding at the end of TPAP such as X, L and SN shows that the propellant samples were additionally composed of HMX, Al and PSAN.

Table 33 Samples prepared for evaluation of the ballistic properties of HTPE based propellants

		Concentration wt%			
Material	**Function**	**TPAP-1**	**TPAP-2**	**TPAP-3**	**TPAP-4**
AP-400 µm	Oxidizer	70	-	-	-
AP-200 µm		-	70	-	35
AP-20 µm		-	-	70	35
TPEG	Polyol	17	17	17	17
BuNENA	Energetic plasticizer	10	10	10	10
TMETN		-	-	-	-
BDNPA-F		-	-	-	-
Fe_2O_3	Burning rate catalyst	0.5	0.5	0.5	0.5
Cr_2O_3		-	-	-	-
SiO_2		-	-	-	-
N-3200	Isocyanate	2.0	2.0	2.0	2.0
Additives	-	0.5	0.5	0.5	0.5
		Concentration wt%			
Material	**Function**	**TPAP-5**	**TPAP-6**	**TPAP-7**	**TPAP-8**
AP-400 µm	Oxidizer	35	23.3	-	-
AP-200 µm		-	23.3	70	70
AP-20 µm		35	23.3	-	-
TPEG	Polyol	17	17	17	17
BuNENA	Energetic plasticizer	10	10	-	-
TMETN		-	-	10	-
BDNPA-F		-	-	-	10
Fe_2O_3	Burning rate catalyst	0.5	0.5	0.5	0.5
Cr_2O_3		-	-	-	-
SiO_2		-	-	-	-
N-3200	Isocyanate	2.0	2.0	2.0	2.0
Additives	-	0.5	0.5	0.5	0.5

Table 33 Samples prepared for evaluation of the ballistic properties of HTPE based propellants (Cont'd)

		Concentration wt%			
Material	**Function**	**TPAP-9**	**TPAP-10**	**TPAP-11**	**TPAP-12**
AP-400 µm	Oxidizer	-	-	-	-
AP-200 µm		70	70	60	60
AP-20 µm		-	-	-	-
TPEG	Polyol	17	17	17	17
BuNENA	Energetic plasticizer	10	10	20	20
TMETN		-	-	-	-
BDNPA-F		-	-	-	-
Fe_2O_3	Burning rate catalyst	-	-	0.5	0.25
Cr_2O_3		0.5	-	-	0.25
SiO_2		-	0.5	-	-
N-3200	Isocyanate	2.0	2.0	2.0	2.0
Additives	-	0.5	0.5	0.5	0.5
		Concentration wt%			
Material	**Function**	**TPAP-13**			
AP-400 µm	Oxidizer	-			
AP-200 µm		60			
AP-20 µm		-			
TPEG	Polyol	17			
BuNENA	Energetic plasticizer	20			
TMETN		-			
BDNPA-F		-			
Fe_2O_3	Burning rate catalyst	0.25			
Cr_2O_3		-			
SiO_2		0.25			
N-3200	Isocyanate	2.0			
Additives	-	0.5			

Table 34 Propellant samples containing different kinds of oxidizer and fuel

		Concentration wt%		
Material	**Function**	**TPAPX-1**	**TPAPX-2**	**TPAPXL-1**
AP(200 μm)	Oxidizer	50	50	40
HMX(Class I)	Energetic nitramine	20	-	20
HMX(Class III)		-	20	-
Al(12-18 μm)	Metal fuel	-	-	10
PSAN(200 μm)	Oxidizer	-	-	-
TPEG	Polyol	17	17	17
BuNENA	Energetic plasticizer	10	10	10
Fe_2O_3	Burning rate catalyst	0.5	0.5	0.5
N-3200	Isocyanate	2.0	2.0	2.0
Additives	-	0.5	0.5	0.5
		Concentration wt%		
Material	**Function**	**TPAPXL-2**	**TPAPXL-3**	**TPAPSN-1**
AP(200 μm)	Oxidizer	30	40	50
HMX(Class I)	Energetic nitramine	20	10	-
HMX(Class III)		-	-	-
Al(12-18 μm)	Metal fuel	20	20	-
PSAN(200 μm)	Oxidizer	-	-	20
TPEG	Polyol	17	17	17
BuNENA	Energetic plasticizer	10	10	10
Fe_2O_3	Burning rate catalyst	0.5	0.5	0.5
N-3200	Isocyanate	2.0	2.0	2.0
Additives	-	0.5	0.5	0.5

A 1-pint size vertical mixer that is shown in Figure 35 was utilized in the batchwise propellant production. The order of addition was mainly such that binder, energetic solids and isocyanate were added, respectively. The mixing times and temperatures were optimized by following viscosity variation during operation. The general procedure can be stated as follows. All of the solid components like AP, HMX, Al, PSAN, and burning rate catalysts such as Fe_2O_3 were dried in an oven at 50-60^oC for about 24 hrs. Then, they were sieved through 18-mesh screen. First, the polymeric binder TPEG and the energetic plasticizer were mixed for 10 min at 500-600 mmHg vacuum conditions. Then, the burning rate catalyst and additives were added to the mixture, and mixed for 30 min. at 500-600 mmHg vacuum. After that, the solid energetic ingredients like oxidizer, and if necessary, nitramine and metal fuel were added separately. They were first mixed for 10 min. at atmospheric pressure then 30 min at 500-600 mmHg vacuum conditions. Finally, the isocyanate was added to the resulting mixture, followed by mixing for 10 min at atmospheric condition. Then, the concentrated slurry was additionally mixed for 30 min at 500-600 mmHg vacuum. All of the mixing procedures were carried out at 50-60^oC. The resulting propellant was vacuum cast to the proper paperboard mould. The propellants were prepared as 750 g. Then, they were cured at 50-60^oC for about 6-7 days.

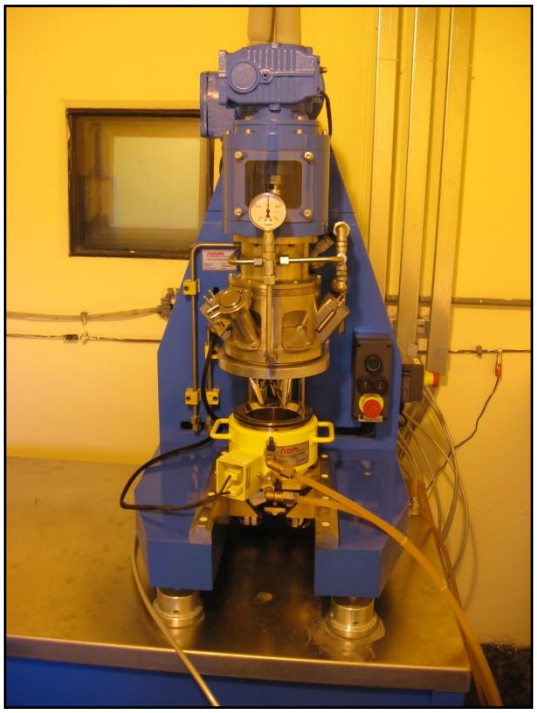

Figure 35 1 pint vertical mixer used in preparation of propellant samples

3.2.3 A Candidate Propellant Production

The same procedure stated in section 3.2.2 was followed. However, the amount of the propellant was increased to 4500 g in this case. In addition, the propellant was prepared in an APV BAKER 1 galon mixer that is shown in Figure 36. Both the paperboard moulds and rocket test motors having 127 mm diameter were cast under vacuum. They were cured again at 50-60^{o}C for about 6-7 days. The typical propellant formulation is given in Table 35.

Figure 36 APV Baker 1 galon mixer used in production of candidate propellant

Table 35 A typical HTPE based propellant formulation

Material	**Function**	**Propellant 091**
AP	Oxidizer	75-80%
TPEG	Polyol	5-10%
BuNENA	Energetic plasticizer	5-10%
Fe_2O_3	Burning rate catalyst	0.5-1.0%
N-3200	Isocyanate	1.0-2.0%
Additives	-	0.5-1.0%

3.3 Characterization Experiments

In order to investigate the effects of propellant ingredients on the inert polyurethane matrix structure, mechanical, morphological and thermal analyses were performed. Furthermore, propellant samples prepared during the development phase were characterized in terms of ballistic and thermal properties. A candidate propellant whose formulation was finalized after these analyses was subjected to mechanical, ballistic, thermal, hazard, propellant smoke and accelerated aging characterization.

Mechanical behavior such as stress-strain curves of gumstocks and propellant samples were obtained by a tensile test machine. Morphologies of polyurethane networks were investigated by swelling experiments and XRD measurements. Thermal characterization was performed by DSC, TGA and vacuum stability tester. Ballistic properties of propellants were determined by Crawford burner and static test motor firings. The impact and friction sensitivity of the propellants were measured by BAM fall hammer tester and BAM friction tester, respectively. Propellant's smoke was classified theoretically by using mass percentages of exhaust combustion products which were calculated by the ICT thermochemical code. Accelerated aging of propellant was performed by HFC (microcalorimetry). The details of characterization experiments are explained in the following sections.

3.3.1 Mechanical Characterization

3.3.1.1 Tensile Tests

Uniaxial tensile tests were performed using Instron 4481. Specimens were carefully prepared, load and strain ranges were selected so that the test would fit within the range. The specimens were placed in the grips and were secured by closing the grips. Stress at rupture (MPa), strain at rupture (%) and tangent modulus (MPa) were measured and recorded. These mechanical properties were reported as the average results on three specimens and standard deviations were also calculated. Test specimen shape is shown in Figure 37, and its corresponding dimensions are tabulated in Table 36. The tests were performed with 50 mm/min. crosshead speed at 25^{o}C.

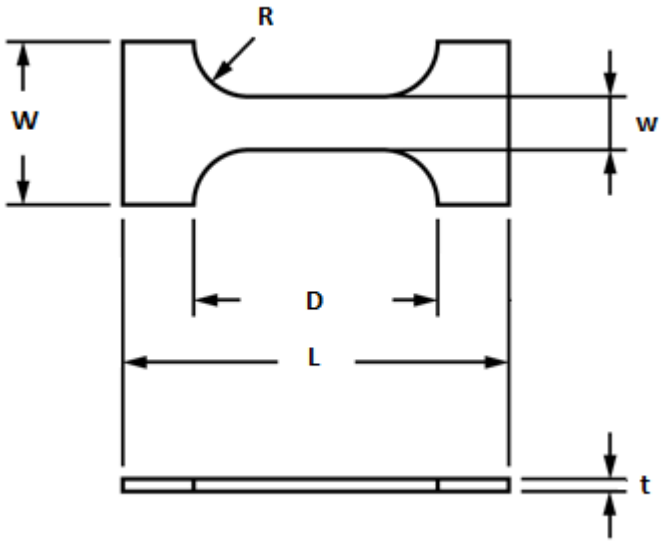

Figure 37 Dog bone shape microtensile test specimen

Table 36 Dimensions of the tensile test specimen

Definition	**Dimensions (mm)**
Overall length-L	38.0
Distance between grips-D	22.0
Radius of curvature on grips-R	5.0
Narrow section width-w	5.0
Test specimen width-W	15.0
Thickness-t	3.0

3.3.1.2 Hardness Tests

Hardness tests were performed by PTC-Instrument ergo style durometer Type A, according to the ASTM D 2240-05(2010) standard. Durometer measures the depth of an indentation in the material created by a given force on a standardized presser foot. The force was applied for 10 sec., and the shore-A scale hardness value was determined as the average results on three specimens and standard deviations were also calculated. Figure 38 shows the durometer used in the tests.

Figure 38 Type A Durometer used for hardness test

3.3.2 Structural Characterization

3.3.2.1 Swelling Tests

The swelling behavior of HTPE based polyurethanes was investigated in aniline and THF solvents to determine the crosslink density (ν_s) and chain length between crosslinks or average molecular weight between crosslinks (M_c), in order to observe the effects of isocyanate, NCO/OH ratio, curing catalyst, and chain extender on ν_s and M_c.

Crosslink density (ν_s) by swelling was determined from the volume fraction of the swollen polymer in a good solvent. The elastomer specimens measuring 10x10x3mm were weighed (w_{us}) and placed in aniline or THF for 48 hrs. Then, the solvent was removed from the swollen specimen, and it was weighed after the solvent was gently wiped off (w_s). From the weight of (w_s) and (w_{us}), the swelling ratio (Q) was determined as:

$$Q = (w_s/w_{us}) - 1 \qquad (16)$$

The weight fraction of the polymer (w_2) and the weight fraction of the solvent (w_1) in the swollen specimen were calculated as follows:

$$w_2 = (1/1+Q) \quad (17)$$

$$w_1 = 1 - w_2 \quad (18)$$

Volume fraction of the polymer (ν_2) in swollen specimen was calculated from the known solvent and polymer densities, (d_1) and (d_2), respectively, where d_2 was used as 1.08 g/cm^3. d_1 was used as 1.02 g/cm^3 for aniline and 0.89 g/cm^3 for THF.

$$\nu_2 = (w_2/d_2) / (w_1/d_1) + (w_2/d_2) \quad (19)$$

Crosslinked density (ν_s) by swelling was obtained from (ν_2) by means of Flory-Rehner equation [102] in mol/m^3.

$$\nu_s = - [\ln(1- \nu_2) + \nu_2 + \lambda\nu_2^2] / V_s(\nu_2^{1/3} - \nu_2/2) \quad (20)$$

where V_s is the molar volume of the solvent and λ is the polymer-solvent interaction parameter. λ values for the HTPE-aniline and the HTPE-THF systems were used as 0.344 and 0.485, respectively. These were calculated from the solubility parameter (δ) in (J/cm^3)$^{1/2}$ using the following relation:

$$\lambda = 0.34 + (V_s/RT)(\delta_{polymer} - \delta_{solvent})^2 \quad (21)$$

where $\delta_{polymer}$ was 10.13 and $\delta_{solvent}$ was 10.3 and 9.1 for aniline and THF, respectively, R is the gas constant in J/mol.K and T is the absolute temperature in K.

Average molecular weight between the crosslinks (M_c) was determined from the following relation in g/mol:

$$M_c = (\rho/\nu_s)10^5 \quad (22)$$

where ρ is the density of network in g/cm^3 and taken as 1.05 as determined experimentally by density meter through liquid displacement.

3.3.2.2 X-ray Diffraction (XRD)

The degree of crystallinity, C_r, of polyurethane network structures was determined by X-ray diffraction analysis using a RIGAKU D/MAX 2200/PC X-Ray diffractometer that generates a voltage of 40kV and current 40 mA from Cu Kα radiation source (λ=1.5418). The diffraction angle 2θ was scanned from 3^o to 80^o with scanning rate of 1^o/min and a step size of 0.01^o at room temperature. The degree of crystallinity was determined from the integral intensities of the amorphous and crystalline contributions according to Hermans and Weidinger [103].

$$C_r = A_{cr} / (A_{cr} + 2.17A_m) \quad (23)$$

where

$$A_{cr} = A_{total} - A_m \quad (24)$$

where

A_{cr} = Integral intensity due to crystalline region

A_m = Integral intensity due to amorphous region

A_{total} = Integral intensity due to both region

The crystallite size L_c of the polyurethanes were calculated by using Scherrer's equation:

$$L_c = K\lambda / \beta\cos\theta \quad (25)$$

where K is the instrument constant taken as 0.9, β is the half value width in radians of the X-ray intensity vs 2θ curve, and θ is the angle of reflection. The analysis was done at ambient temperature 25^oC.

3.3.3 Thermal Characterization

3.3.3.1 Differential Scanning Calorimetry (DSC)

Phase separation and crystallization phenomena of HTPE based polyurethane structures were studied using differential scanning calorimetry (DSC-TA Instruments Q200). The sample weighing 10 mg was used at a heating rate of 10^{o}C/min in the temperature range from -100^{o}C to 500^{o}C under a nitrogen atmosphere with 10mL/min flow rate.

3.3.3.2 Thermal Gravimetric Analysis (TGA)

Thermal degradation of polyurethanes was investigated by using thermogravimetry (TGA-TA Instruments Q500). The sample weighing 10 mg was analyzed at a heating rate of 10^{o}C/min in the temperature range from -100^{o}C to 500^{o}C under a nitrogen atmosphere with 10 mL/min flow rate.

3.3.3.3 Vacuum Stability Tester

The vacuum stability test was used to assess the thermal stability of propellant by measuring the volume of gas evolved on heating the propellant under specified conditions. Propellant samples of 5.0±0.01 g were transferred to the heating tube of 25 cm^3 volume of STABIL vacuum stability tester. The tests were carried out at 100^{o}C for 40 hrs duration under vacuum (appr. 600-700 Pa). Gas evaluations were recorded with respect to time. Thermal stability of the propellants were evaluated on three samples.

3.3.4 Ballistic Characterization

3.3.4.1 Thermochemical Calculations

The thermodynamic properties of the propellants were theoretically calculated by ICT Thermodynamic Code program. The calculations were made by assuming that the expansion ratio was 70:1. This means that the pressure in combustion chamber is 7 MPa and hot gases expand into the medium with 0.1 MPa pressure.

3.3.4.2 Strand Burner Tests

The linear burning rates of propellant samples were determined by Crawford bomb which is shown in Figure 39. Strands of propellant having square cross section, with side of 3 to 6 mm were employed. The overall strand length was about 10 mm. Propellant strands were supported in a suitable holder and inserted into a closed vessel which was pressurized with nitrogen. Two small holes were drilled on the separate square cross section. Fuse wires were passed through each hole and then connected to terminals. The strand was ignited at the top by a hot wire, and the time taken for burning to pass from the first to the second fuse wire was measured. The linear burning rate and pressure exponent of propellants were determined for the pressure range of 6.9 – 13.8 MPa at 20^{o}C according to MIL-STD-286C standart. Three measurements were made at each pressure.

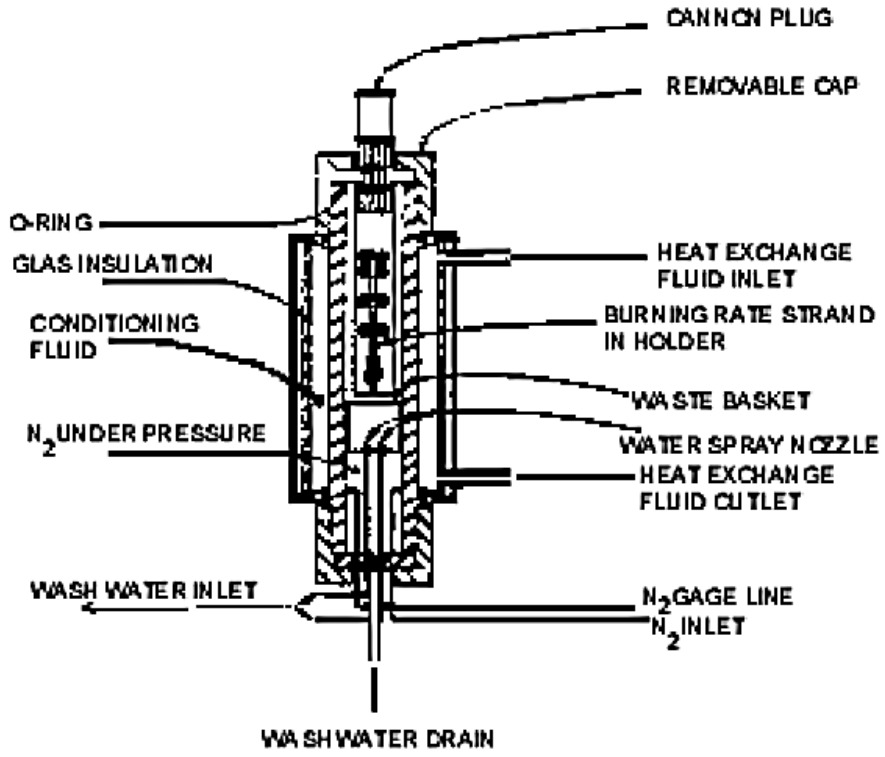

Figure 39 A typical crawford bomb [104].

3.3.4.3 Static Test Firings

The ballistic properties such as delivered specific impulse, burning rate, and burning rate pressure exponent were additionally determined by firing small size rocket test motors which were 12.5 mm in diameter. They were made with a stainless steel case and fitted with nozzles of different sizes in order to provide a number of convenient operating pressures. The static test firings were performed at 6.9, 10.3 and 13.8 MPa pressure and at 20^{o}C temperature.

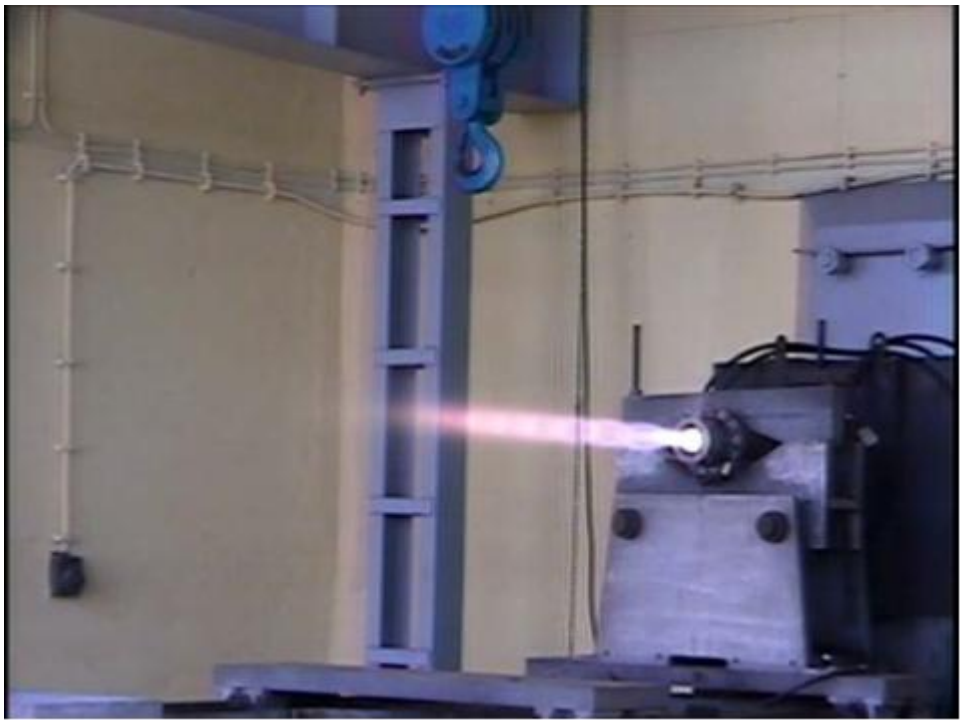

Figure 40 The static test firing of small size rocket motor

3.3.5 Hazard Classification

3.3.5.1 Impact Sensitivity Test

BFH-10 BAM Fall Hammer Impact Sensitivity test device was used for measuring impact sensitivity of the propellant samples. BFH measured the impact energy causing 50% positive reactions with a hammer of 2 kg weight falling from a 1 m height. Flash, flame or explosion, considered as positive reaction, were observed upon sample initiation. Impact energies were recorded in joule. Average of three measurements were taken.

3.3.5.2 Friction Sensitivity Test

The sensitivity of propellant samples to friction was tested by means of the FSKM 50-20K BAM Friction Sensitivity Test. Friction force varying in the range of 0.5-360 N between a moving porcelain plate and a static porcelain peg causing sample initiation was applied, and the corresponding force value in Newton was determined. Sample initiation was visually detected as flash, smoke or cracking. Average of three measurements were taken.

3.3.6 Smoke Classification

The smoke classification of solid propellant was carried out according to the STANAG 6016 which is the standardization agreement ratified by NATO nations. The exhaust plume combustion products were calculated by ICT Thermochemical Code with a chamber pressure of 7 MPa and an exit pressure of 0.1 MPa specification.

3.3.7 Accelerated Ageing of Propellant

The shelf life of propellant developed and manufactured in 1 galon mixer was estimated by means of TA Instruments TAM III Heat Flow Calorimeter. 3-4 gr of propellant samples were transferred to the vessel that had a volume of 4.0 mL. The sum of the heat flows which were produced during the ageing of a propellant by chemical and physical reactions were measured at a constant temperature of 80ºC for 10.6 days which is the time considered to be equivalent to at least a 10 years of storage at 25ºC. The maximum permissible heat flow limit was calculated as 114 µW/g which was derived from Arrhenius equation by assuming activation energy of 105 kJ/mol.

CHAPTER 4

RESULTS AND DISCUSSION

4.1 Mechanical Analysis

The mechanical properties of the rocket propellant are mainly based on the mechanical properties of the polymeric network. The propellant must be able to expand and contract within the rocket shell without cracking or detaching itself from the inner walls of the casing. The fundamental mechanical properties such as tensile strength, percent elongation at break and Young's modulus of both the polymeric network and the propellant should be characterized for use in a rocket motor. Tensile tests were performed in order to determine these properties. Hardness is another static mechanical property which was determined along with tensile tests by a durometer. The mechanical property results are shown in the following sections. The corresponding mechanical test results are tabulated in Appendix A. The stress-strain curves obtained from tensile tests are given in Appendix B.

4.1.1 Tensile Tests

Uniaxial tensile tests were performed to determine the ultimate tensile strength, percent elongation at break and Young's modulus of both the polymeric networks and the propellant developed. The stress-strain curves were obtained and discussed.

4.1.1.1 Tensile Test Results of Polymeric Networks

Polyurethane network structures were prepared mainly by the reaction of HTPE polymer, TPEG, and difunctional or branched polyfunctional isocyanates. A small molecule chain extender diol or triol was added to the resultant mixture if it was required (Figure 41). The resulting polymer may be considered as a copolymer of the macrodiol and diisocyanate chain extender sequences which were termed as the soft segment (SS) and the hard segment (HS) respectively.

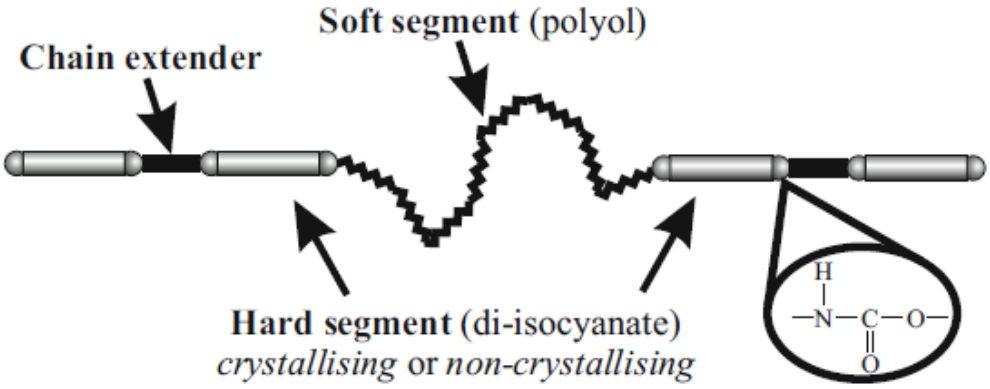

Figure 41 Typical structure of a polyurethane network [105].

The HS are constructed from alternating diisocyanate-chain extender sequences while the SS are originated from the polyol. The HS are grouped into hard domains acting as physical crosslinks and as filler particles within the rubbery SS matrix, as shown in Figure 42.

It is known that the urethane groups conjugate the HS and the flexible SS together by means of both covalent bonds and hydrogen bonds. They are usually arranged at the borderline between the domains and form linear hydrogen bonds in either a parallel or an anti parallel fashion.

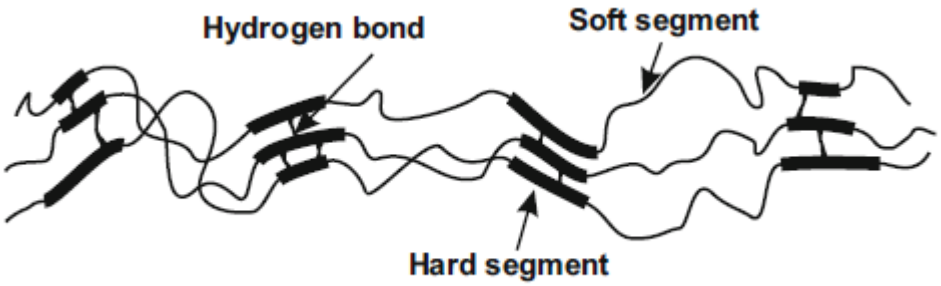

Figure 42 The alternating hard segment (HS)-soft segment (SS) structure of polyurethanes [105].

The three hydrogen bonding interactions in polyether based polyurethanes can be mentioned as illustrated in Figure 43. It is known that the polyether polyurethanes are extensively hydrogen bonded which involves the N-H group as the proton donor

and the urethane carbonyl and ether oxygen in polyether polyurethane as proton acceptor which influences the degree of microphase segregation. The inter-urethane linkages through the N-H and carbonyl of urethane groups are also possible.

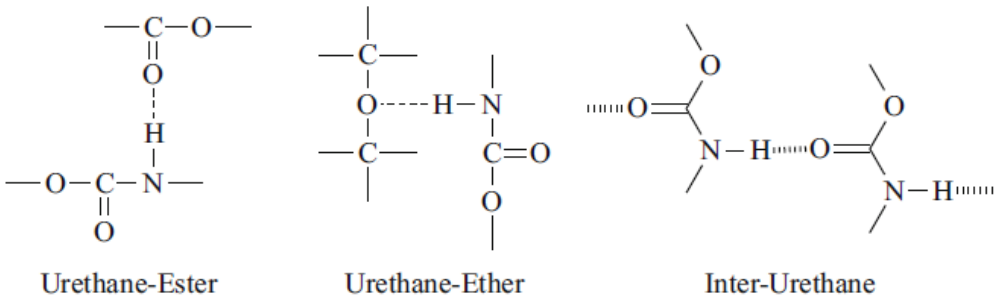

Figure 43 The hydrogen bonding interactions in polyether polyurethanes [105].

The first isocyanate used was 2,4-TDI which has an aromatic benzene structure with difunctional isocyanate with a methyl moiety that is shown in Table 30 (Sample No 1, 2, 3). A cured polymer network was not obtained with TDI as the HS for all NCO/OH ratios, although TDI is an aromatic isocyanate which is generally known to be more reactive than the aliphatic ones. Sample 3 seemed to be partially cured, but it was too sticky, and therefore it was not suitable for characterization. This might have resulted from undesired side reactions such as allophanate and biuret formation reactions which were activated at excess isocyanate contents. The results indicate that there existed phase incompatibility between TDI as the HS and TPEG as the SS. One of the reasons could be the insufficient inter-urethane hydrogen bonding in order to stabilize the HS domains. Another reason for polyurethane phase incompatibility could be the high solubility parameter difference between TPEG and TDI as shown in Table 37. A high solubility parameter difference indicates high thermodynamic incompatibility between the hard and soft segments. High incompatibility gives rise to segregation and uncured polyurethane network. This situation is called phase mixing as shown in Figure 44. The properties of the final bulk material are strongly affected by the extent of microphase separation depending on whether the polyurethane system is well organized or not and by the unsymmetrical isocyanate groups in TDI structure.

Table 37 The solubility parameters[a] of TPEG and some isocyanates used

Substance	Solubility parameter, δ $(cal/cm^3)^{1/2}$
TPEG	10.13
IPDI	8.66
W-H_{12}MDI	8.98
Desmodur Series	11.48
TDI	12.8
DDI	8.95
HDI	11.14
[a] Obtained by estimation method [106]	

Figure 44 Schematic representation of a phase mixed polyurethane system [105].

IPDI was also tried to be used as the isocyanate with TPEG (Sample No 4, 5, 6). It is an aliphatic type isocyanate with a ring structure. It has a lower reactivity of urethane formation than the aromatic ones. This lower reactivity might have resulted in incomplete polyurethane structures formed with IPDI in comparison to the TDI ones. The sample in which IPDI was utilized in excess amount, namely Sample 6, seemed to be cured, but as in the case of TDI, it was too sticky, thus it could not be measurable. The IPDI unsymmetrical structure might have also led to phase mixing and phase segregation. These factors resulted in lower degree of HS crystallization.

DDI was another isocyanate used as the isocyanate (Sample No 7, 8, 9). It has a long linear structure with two isocyanate end groups. The polyurethane samples prepared with DDI could not be cured just like in the case of TDI and IPDI. The DDI is a large molecule with relatively high molecular weight. The low reactivity of DDI to form the polyurethane chains with TPEG might have resulted from structure induced steric effect. The penetration of this large molecule to construct polyurethane structure

through the TPEG polyol was difficult. DDI is a nonpolar molecule, whereas TPEG has a polar structure. The energetically unfavorable polar-nonpolar interactions could have led to low intermolecular interaction between TPEG and DDI. This nonpolarity of the system is also due to insufficient urethane bond structure. The phase segregation resulted from low hydrogen bonding between the urethane linkages.

Desmodur N-100 is a polyisocyanate with three isocyanate functionalities. It has a polar structure which mainly eliminates the incompatibility problem with TPEG polyol. The high reactivity of Desmodur N-100 enabled the formation of complete polyurethane structures at all three NCO/OH ratios (Sample No 10, 11, 12). Similar results were obtained with Desmodur N-3200 which has a similar backbone structure as Desmodur N-100, but with different equivalent weight (Sample No 13, 14, 15). Both isocyanates resulted in formation of organized structures leading to more complete phase segragation as shown in Figure 45. Phase segregation proves the presence of high intermolecular interaction between the urethane linkages. The high interaction might have resulted from high degree of hydrogen bonding through the nitrogen atoms on isocyanate and amide functionalities with TPEG and polar urethane groups.

H_{12}MDI-Desmodur W was another isocyanate that was used with TPEG (Sample No 16, 17, 18). It did not give any successful results. The thermodynamic incompatibility between these two constituents may have arised from the energetically unfavorable polar-nonpolar interactions. The low degree of reaction affinity to form urethane bonds would result from the lack of dipole-dipole interactions that were followed by covalent bond and hydrogen bond formations. The steric effect can be mentioned as another reason for incomplete polyurethane formation. H_{12}MDI-Desmodur W has a cyclohexane structure separated symmetrically on the single bond axes in its backbone. This large cyclohexane structure provides sterical hindrance and rigidity to the molecule. This leads to low degree of polyurethane formation.

HDI was another aliphatic isocyanate used as the isocyanate (Sample No 19, 20, 21). The same situation was encountered as in TDI, IPDI, DDI and H_{12}MDI. The low reactivity of HDI might have resulted in uncured polymeric matrix. It comes from

the fact that the electron delocalization of electron pair on the nitrogen atom is difficult along the long linear hydrocarbon chain. The nonpolar structure of HDI also resulted in degree of low interaction with the polyol giving rise to less HS crystallization.

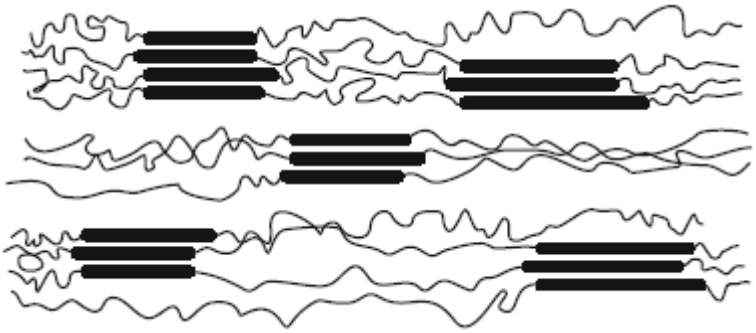

Figure 45 Schematic representation of a well phase segregated polyurethane system [105].

The Desmodurs were also used together with IPDI in various stoichiometric ratios in order to understand the effects of co-isocyanate on the formation of polyurethane structure and its properties. To do that, first Desmodur N-100-IPDI samples (Sample No 22, 23, 24) were prepared. Results showed that samples 23 and 24 in which Desmodur N-100/IPDI equivalent ratios were 1.0 and 2.0, respectively, satisfied the desired formation of polyurethane networks. On the other hand, the HS crystallization and urethane bond formation could not be obtained in sample 22 in which Desmodur N-100/IPDI equivalent ratios were 0.5. IPDI was also employed with Desmodur N-3200 as a second isocyanate (Sample No 25, 26, 27). Only sample 27 was successful indicating that Desmodur N-3200/IPDI equivalent ratio of 2.0 furnished the formation of polyurethane matrix while equivalent ratios of 0.5 and 1.0 did not. It seemed that the increase in the concentration of IPDI gave rise to lower polyurethane bond formation yield, possibly due to the low HS crystallization obtained by Desmodur N-3200-IPDI couple. Results showed similarities with the ones obtained with IPDI used alone which had low intermolecular interaction induced by low hydrogen bonding index. Table 38 shows the general comments on the results of polyurethane sample preparation without a chain extender.

Table 38 Polyurethane samples prepared to study the effects of isocyanate, secondary isocyanate and R-value

Sample No	Composition	Comments
1	TP-TDI-R0.8	Failed to cured
2	TP-TDI-R1.0	Failed to cured
3	TP-TDI-R1.2	Cured but not measurable
4	TP-IPDI-R0.8	Failed to cured
5	TP-IPDI-R1.0	Failed to cured
6	TP-IPDI-R1.2	Cured but not measurable
7	TP-DDI-R0.8	Failed to cured
8	TP-DDI-R1.0	Failed to cured
9	TP-DDI-R1.2	Failed to cured
10	TP-N100-R0.8	Cured
11	TP-N100-R1.0	Cured
12	TP-N100-R1.2	Cured
13	TP-N3200-R0.8	Cured
14	TP-N3200-R1.0	Cured
15	TP-N3200-R1.2	Cured
16	TP-W-R0.8	Failed to cured
17	TP-W-R1.0	Failed to cured
18	TP-W-R1.2	Failed to cured
19	TP-HDI-R0.8	Failed to cured
20	TP-HDI-R1.0	Failed to cured
21	TP-HDI-R1.2	Failed to cured
22	TP-N100/IPDI(1:2)-R1.0	Failed to cured
23	TP-N100/IPDI(1:1)-R1.0	Cured
24	TP-N100/IPDI(2:1)-R1.0	Cured
25	TP-N3200/IPDI(1:2)-R1.0	Failed to cured
26	TP-N3200/IPDI(1:1)-R1.0	Failed to cured
27	TP-N3200/IPDI(2:1)-R1.0	Cured

TPEG-Desmodur N-3200 based polyurethane samples were then prepared by using 1,4-butanediol (BDO), trimethylolpropane (TMP) as difunctional and trifunctional hydroxyl compounds, respectively, in varying amounts to see the effects of these chain extenders on the general characteristics of the network structures. They were all successfully cured and polyurethane structures were obtained as shown in Table 39.

Table 39 Propellant samples prepared to study the effects of chain extender and equivalence ratio

Sample No	Composition	Comments
28	TP-N3200-0.2BDO	Cured
29	TP-N3200-0.2TMP	Cured
30	TP-N3200-0.4BDO	Cured
31	TP-N3200-0.4TMP	Cured
32	TP-N3200-0.8BDO	Cured
33	TP-N3200-0.8TMP	Cured

Last but not least, the effects of curing catalyst type and amount were also explored with the TPEG-Desmodur N-3200-BDO based polymeric matrix. TPB, FeAA and DBDTL were utilized as the curing catalysts. The details of the samples are shown in Table 40. Results showed that TPB should be the choice of cure catalyst at all concentrations. However, FeAA had some solubility problems with TPEG with an increase at high FeAA concentrations. In addition, the polymerization reaction was so fast. DBTDL also gave rise to very fast reaction, even faster than FeAA, and to formation of gas bubbles which is undesired.

Table 40 Polyurethane samples prepared to study the effects of curing catalyst

Sample No	Composition	Comments
34	TP-N3200-BDO-0.01TPB	Cured
35	TP-N3200-BDO-0.02TPB	Cured
36	TP-N3200-BDO-0.04TPB	Cured
37	TP-N3200-BDO-0.01FeAA	Cured
38	TP-N3200-BDO-0.02FeAA	Solubility problem, fast reaction
39	TP-N3200-BDO-0.04FeAA	Solubility problem, fast reaction
40	TP-N3200-BDO-0.01DBTDL	Cured
41	TP-N3200-BDO-0.02DBTDL	Fast reaction, air bubbles
42	TP-N3200-BDO-0.04DBTDL	Fast reaction, air bubbles

Tensile tests were carried out on the polyurethane samples which were successfully cured. Figure 46-48 present the ultimate tensile strength, elongation at break and Young's modulus values, respectively. The corresponding mechanical test results are given in Appendix A, and stress-strain curves are illustrated in Appendix B.

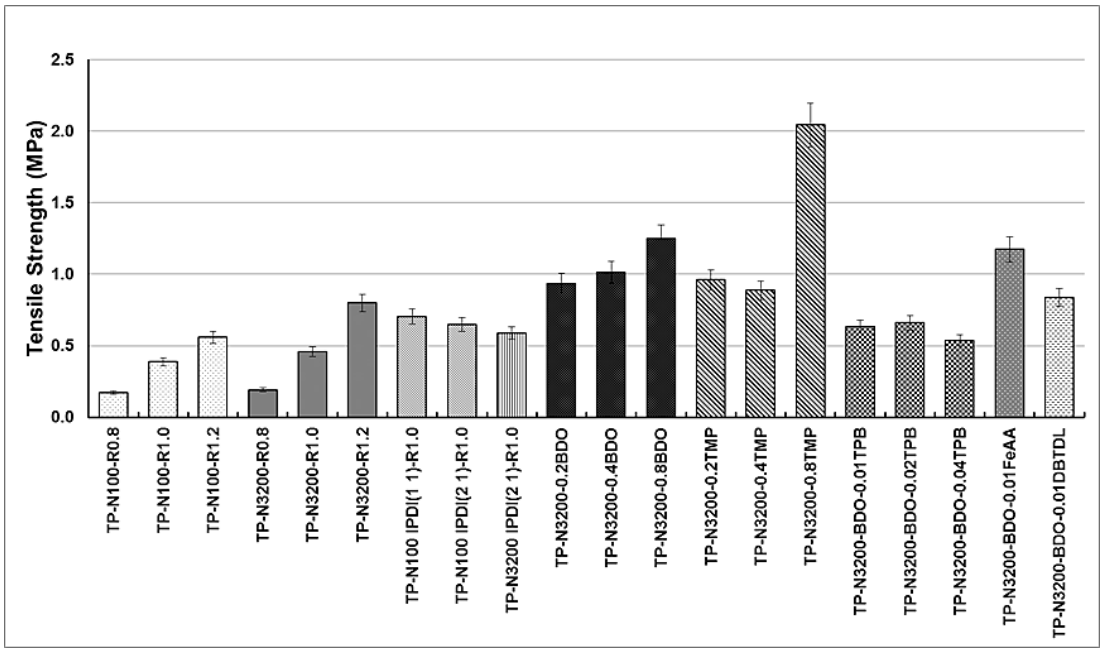

Figure 46 Tensile strength data of non-energetic polyurethane network structures

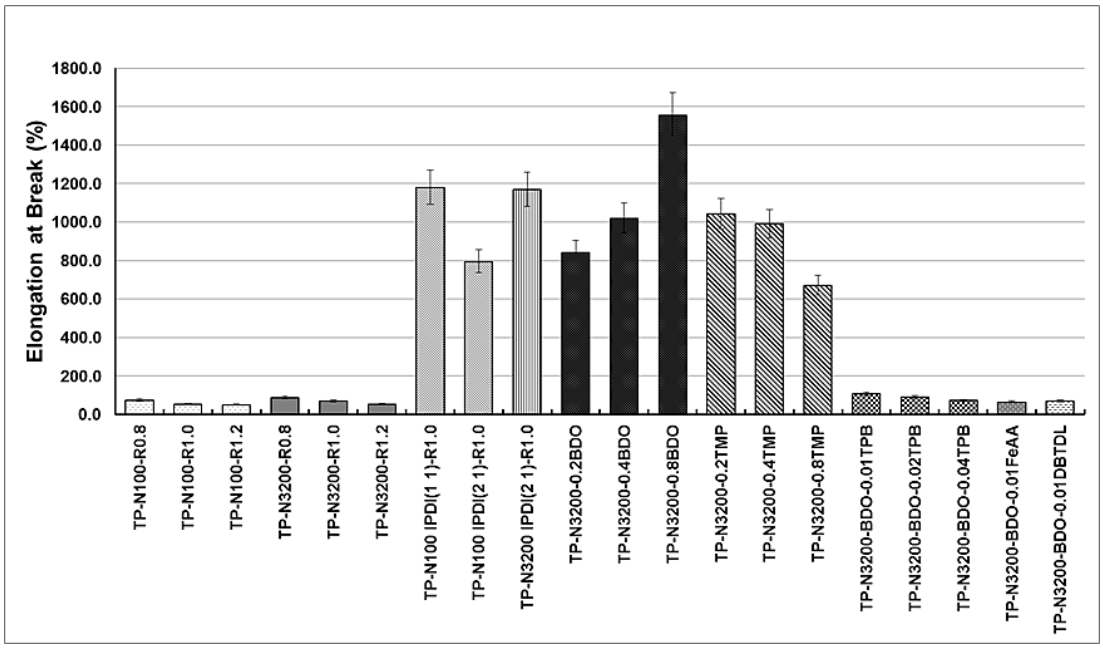

Figure 47 Percent elongation at break data of non-energetic polyurethane network structures

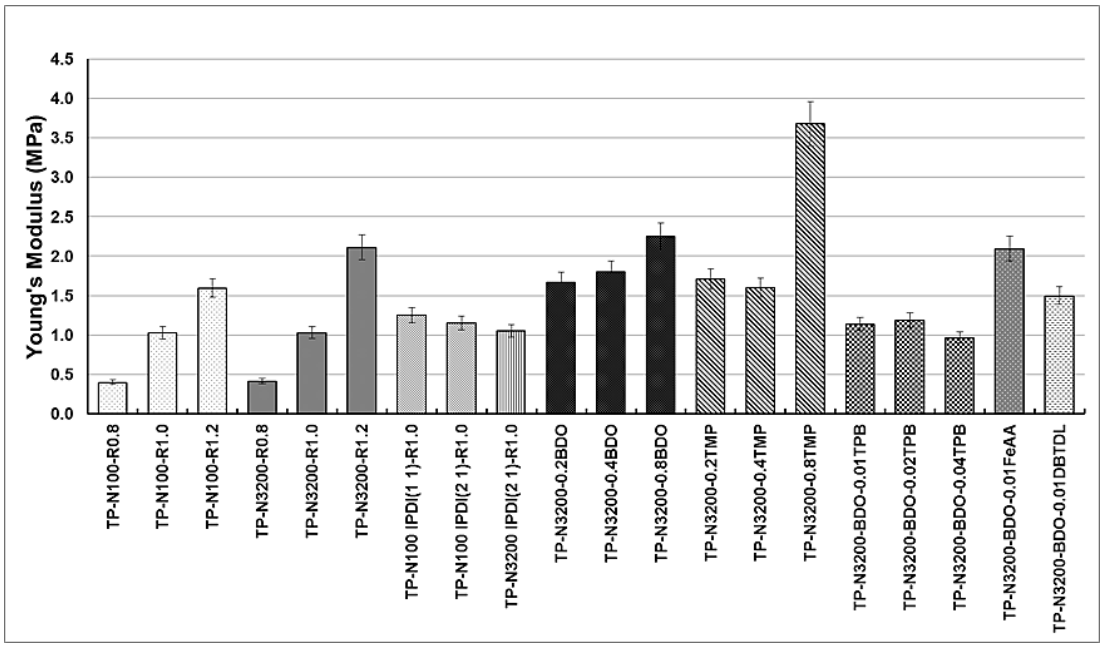

Figure 48 Young's modulus data of non-energetic polyurethane network structures

The hard segment content (HS%) of a polyurethane structure can be approximately calculated from the equation 24 [107].

$$HS\% = (M_{isocyanate} + M_{chain\ extender}) / (M_{isocyanate} + M_{chain\ extender} + M_{polyol})x100 \qquad (26)$$

where

$M_{isocyanate}$: mass of isocyanate that reacts with the chain extender

$M_{chain\ extender}$: mass of chain extender

M_{polyol} : mass of polyol

For the TP-N100 samples prepared, the dependence of tensile strength, elongation at break and Young's modulus with respect to HS content is shown in Figure 49. It is clear that the increase in HS content led to an increase in tensile strength and Young's modulus, whereas the elongation at break decreased. An increase in HS content gives rise to an increase in hydrogen bonding between -NH and -C=O of HS and hence to an increase of stress and decrease of strain property. The HS microdomains act similar to reinforcing fillers and therefore Young's modulus generally increases with HS content as in the case of TP-N100 samples. The HS content increases as $M_{chain\ extender}$ increases as can be interpreted from Equation 24.

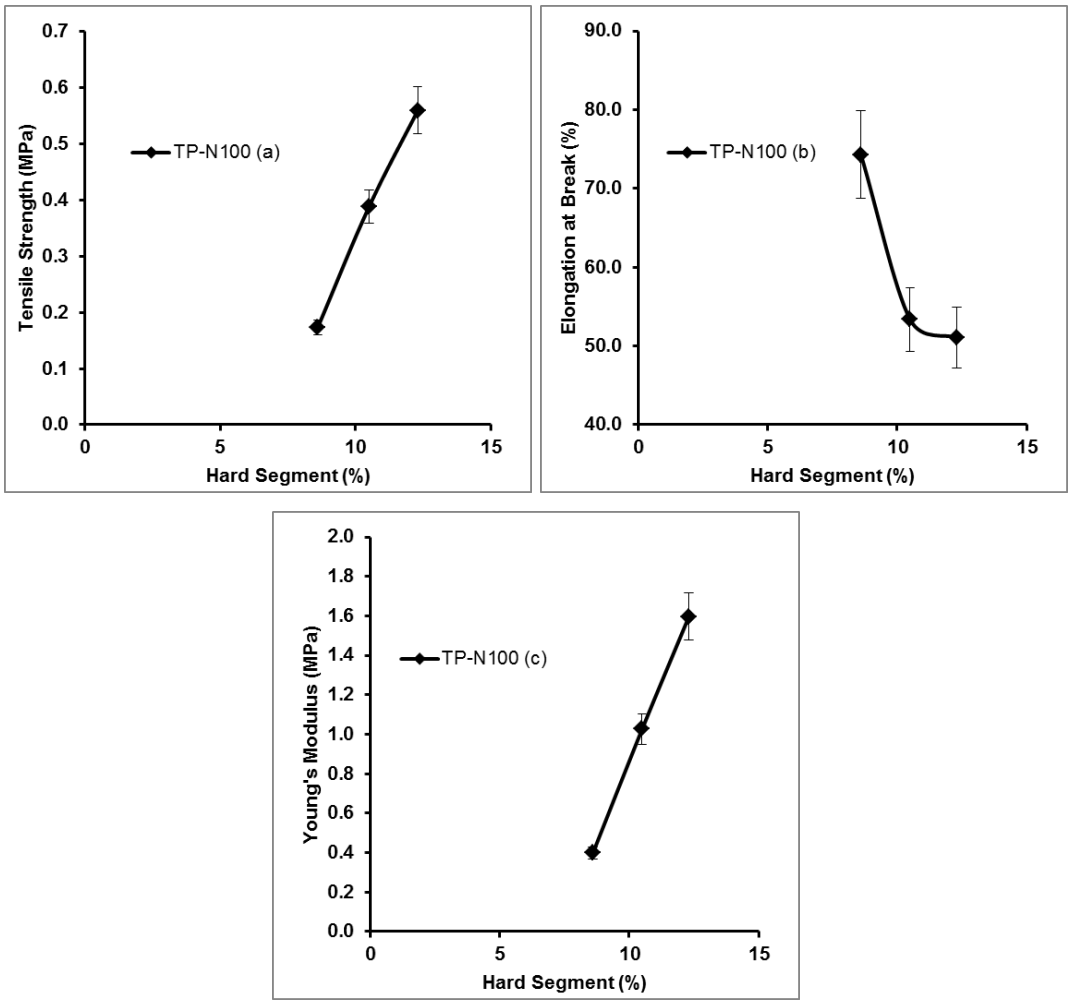

Figure 49 The effects of hard segment content (%) on the (a) Tensile strength (MPa), (b) Elongation at break (%), (c) Young's modulus of TP-N100 based samples

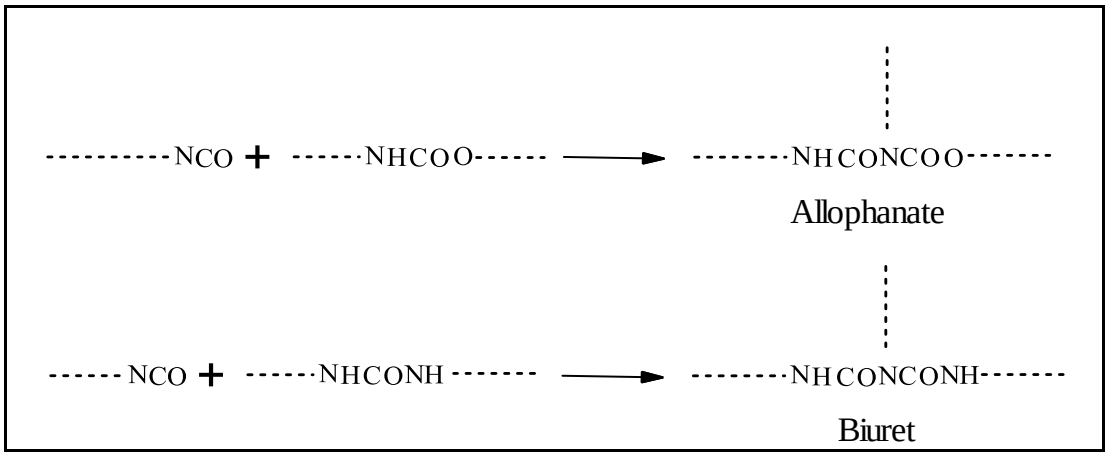

Figure 50 The allophanate and biuret formation reactions by excess isocyanate consumption

It is known that if the NCO/OH ratio is higher than one, the three-dimensional allophanate or biuret crosslinks or urea structures are formed and the number of urethane groups are increased [108]. The reactions mentioned are shown in Figure 50. The existence of three-dimensional allophanate or biuret structure restricts the mobility of the molecular chain. The increase of intermolecular attraction between the hard segments by the increase of NCO/OH ratio tends to increase the stress property and decrease the strain property. By increasing the interchain forces, crystallinity and rigidity of the hard segments will increase but macromolecular slippage will decrease. This variation can be clearly seen in stress-strain curves of TP-N100 based samples with different NCO/OH ratios as shown in Figure 51. The curves show that the polymer structure became hard and brittle by the increase in the NCO/OH ratio.

IPDI was used as the co-isocyanate in the TP-N100 IPDI(1:1)-R1.0 and TP-N100 IPDI(2:1)-R1.0 samples in which N100/IPDI equivalent ratio was equal to 1.0 and 2.0, respectively. The NCO/OH ratio was kept constant as 1.0 in both of them. As the mechanical test results, which are shown in Appendix A, of TP-N100 IPDI(1:1)-R1.0 is compared with TP-N100-R1.0, it is seen that the ultimate tensile strength increased from 0.4 MPa to 0.7 MPa. Percent elongation at break showed an increase from 53% to 1180%. Furthermore, Young's modulus showed again an increase from 1.0 MPa to 1.25 MPa. Similar observations were obtained with the TP-N100 IPDI(2:1)-R1.0 sample. In this case, the ultimate tensile strength increased to 0.65 MPa and elongation at break was obtained as 796%. Young's modulus increased from 1.0 MPa to 1.15 MPa. Results showed that IPDI behaved like a chain extender. The low molecular weight structure of IPDI with respect to N100 might have led to increase in urethane formation. Then, the use of IPDI as the secondary isocyanate resulted in the lowest energy fully extended conformation of polyurethane structure and to an increase in hydrogen bonding. It is apparent that polymer chains prefer to adopt lowest energy staggered conformations, one trans and two gauche, to maximize the entropy. The increase in hydrogen bonding index brought about easier crystallization, thus more complete phase segregation was obtained. This gave rise to better elastomeric properties than TP-N100-R1.0 samples.

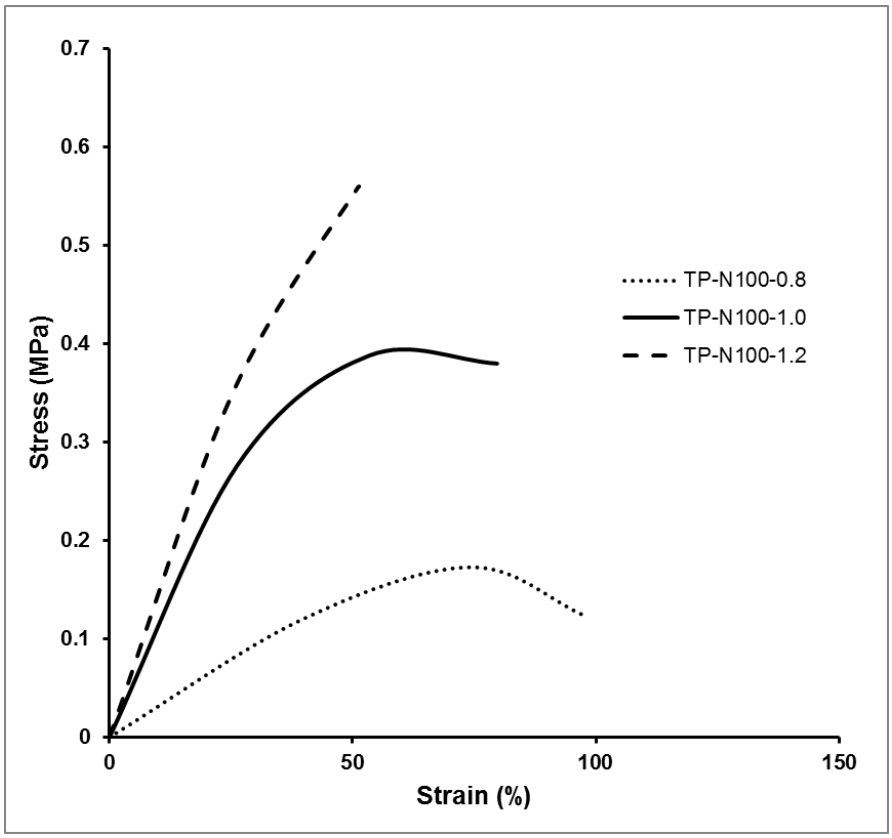

Figure 51 The stress-strain curves of TP-N100 samples

The change of mechanical properties with the HS content of TP-N3200 samples are shown in Figure 52. Results show that the increase in HS content increased both tensile strength and Young's modulus, whereas elongation at break decreased. Similar discussion can be made as in the case of TP-N100. The increase in the molar ratio of the isocyanate to polyol up to NCO/OH ratio of 1.0 gave rise to increase in urethane bond formation. This increase resulted in increase in hydrogen bonding between the hydrogen atom bonded to nitrogen in the urethane structure with the oxygen of carbonyl moiety in the long polyurethane structure. As it is known, more hydrogen bonding means more regular and aligned structure and higher crystallinity. That restricts the mobility of polymer chains increasing the strength and modulus values while the strain at break values decrease. The formation of allophanate and biuret structures when the N3200 was in excess amount (NCO/OH ratio is greater than 1.0) resulted in higher intermolecular interaction by limiting the mobility of molecular chains. This situation led to increase in stress and decrease in elongation properties.

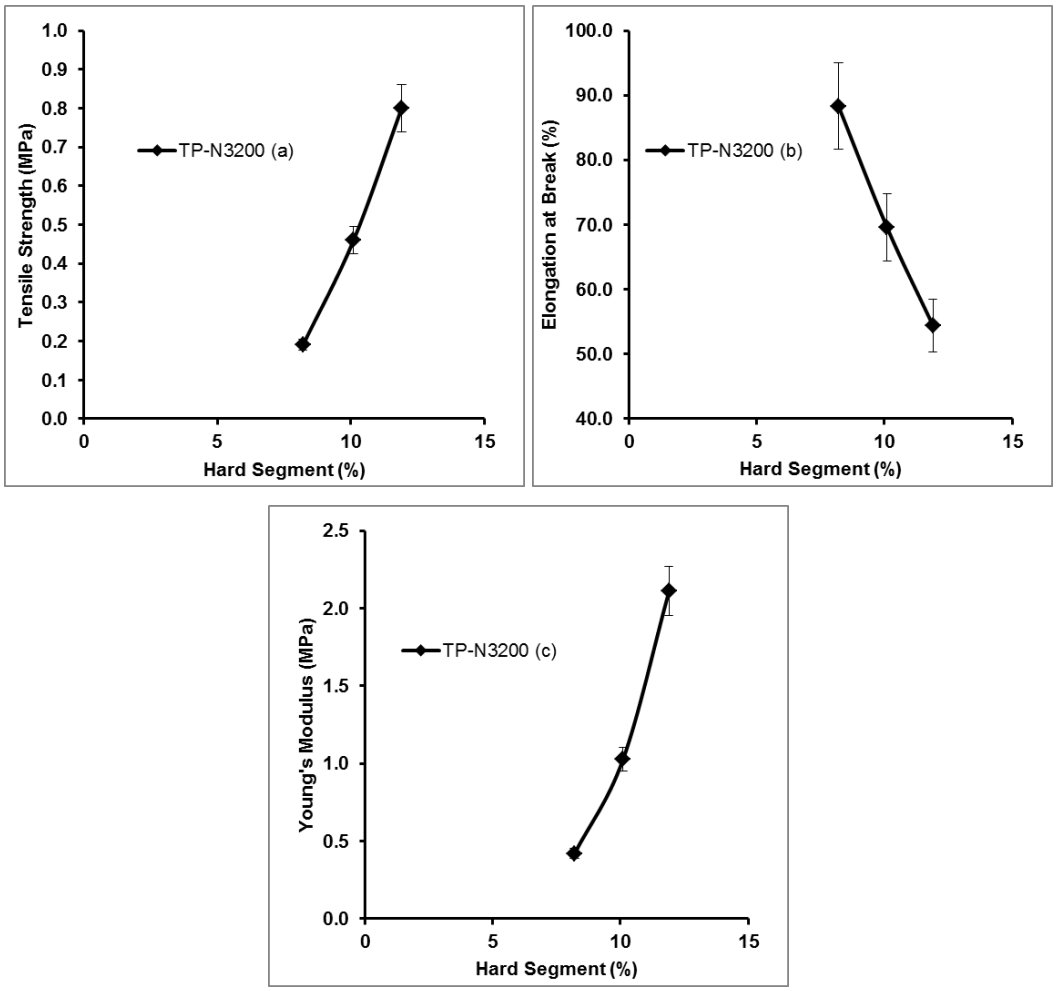

Figure 52 The effects of hard segment content (%) on the (a) Tensile strength (MPa), (b) Elongation at break (%), (c) Young's modulus of TP-N3200 samples

The stress-strain behavior of TP-N3200 polyurethane structures is shown in Figure 53. The matrix structures became harder and more rigid with an increase in NCO/OH ratio similar to TP-N100 samples. The higher NCO/OH ratio yielded an increase in stress property while strain values decreased.

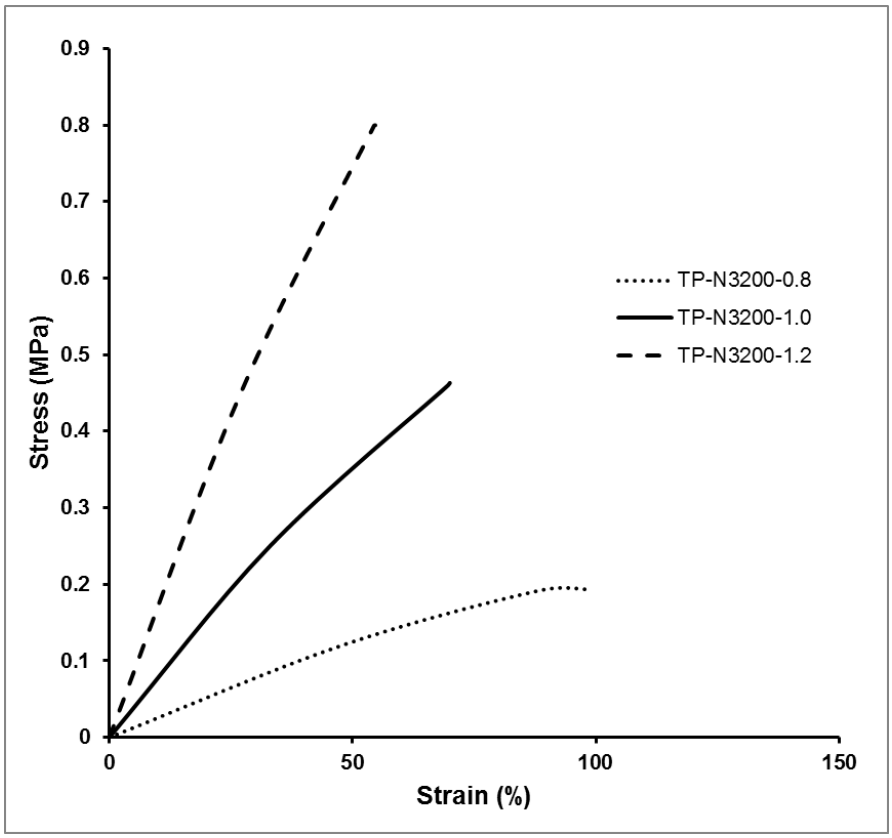

Figure 53 The stress-strain curves of TP-N3200 samples

TP-N3200 IPDI(2:1)-R1.0 sample contains IPDI as the co-isocyanate together with N3200. NCO/OH ratio was kept constant as 1.0. The mechanical test results which are shown in Appendix A, of TP-N3200 IPDI(2:1)-R1.0 is compared with TP-N3200-R1.0, and it is seen that ultimate tensile strength increased from 0.46 MPa to 0.59 MPa. Percent elongation at break showed a very high increase from 70% to 1171%. In addition, Young's modulus showed a small increase from 1.03 MPa to 1.05 MPa. These results might be due to the fact that low molecular weight of IPDI decreased the weight average molecular weight of the system. The number of urethane bonds increases with decreasing molecular weight of the isocyanate. High number of urethane bonds improves both the stress and strain properties and better elastomeric properties were obtained.

The effects of chain extender on the mechanical properties were analyzed by using BDO and TMP as diol and triol, respectively. The equivalent weight of the chain extender was changed in each TP-N3200-BDO sample where NCO/OH ratio was

kept constant as 1.0. The effects of variation of the HS content on the mechanical properties of TP-N3200-BDO samples are shown in Figure 54.

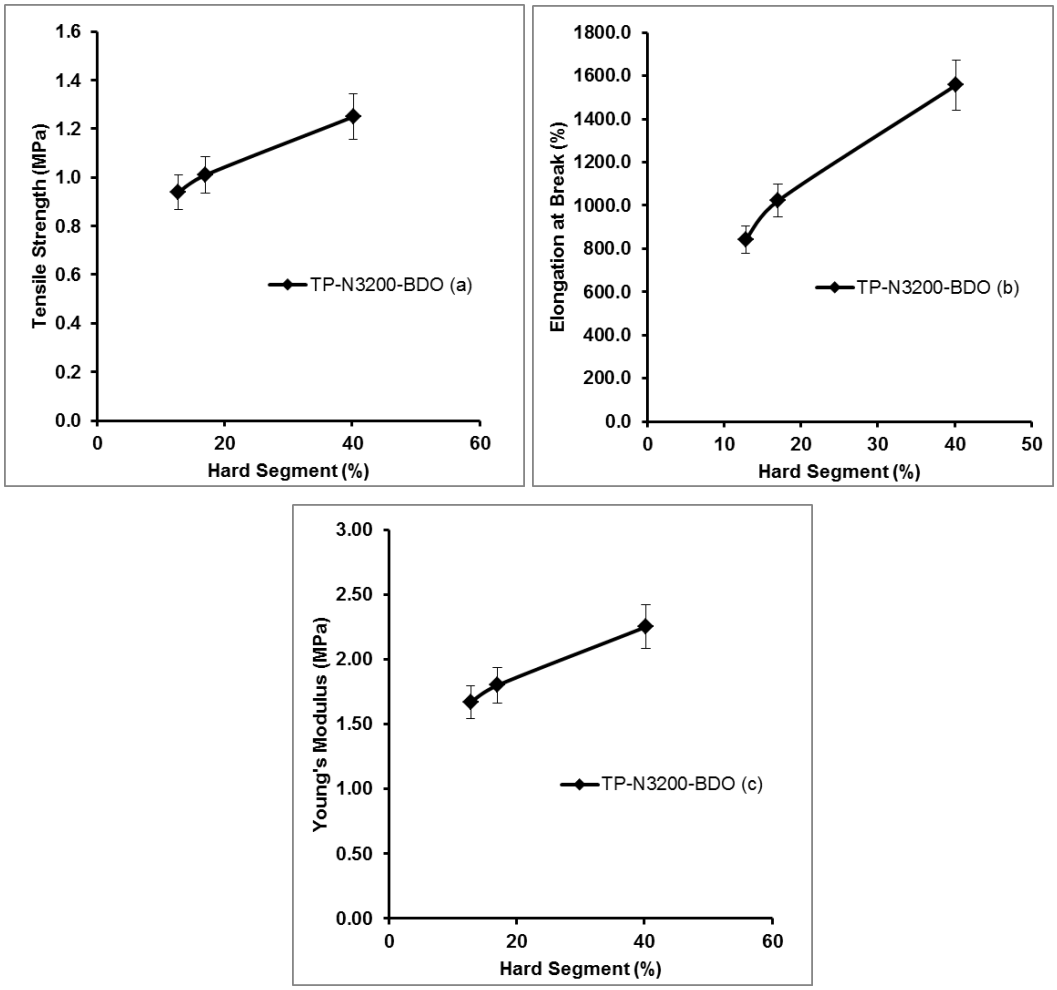

Figure 54 The effects of hard segment content (%) on the (a) Tensile strength (MPa), (b) Elongation at break (%), (c) Young's modulus of TP-N3200-BDO samples

Results which are given in Appendix A show that BDO increased the HS content of TP-N3200 sample structures even higher than TP-N3200-R1.2 sample in which N3200 was used as excess amount. The increase in BDO% led to approximately 3-fold increase in HS content from 12.0% to 40.0%. The mechanical characterization of TP-N3200-BDO samples showed that ultimate tensile strength, elongation at break and Young's modulus properties were all enhanced with respect to the TP-N3200 samples. These improvements were facilitated by the increase in BDO%. These changes can also be observed from the stress-strain property changes shown in Figure 55.

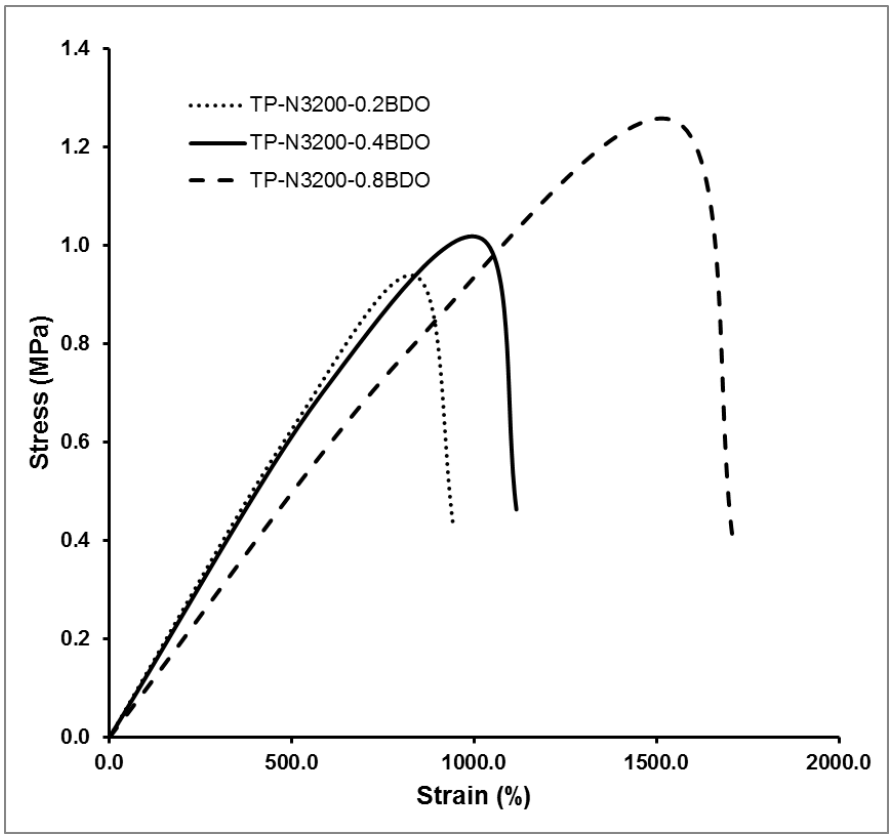

Figure 55 The stress-strain curves of TP-N3200-BDO samples

The increase in HS content increases the degree of interaction between HS. In addition to that, the chain extender increases the number of urethane bonds. This increases the interchain forces due to higher amount of hydrogen bonds between the polymer chains. This gives rise to improved mechanical properties such as increase in strength value. It is known that the use of excess chain extender reduces the polyurethane number average molecular weight by forming shorter polymer chains. The short polymer chains are less entangled. They slip more easily since the total forces acting on them decreases. This brings about increase in the strain properties of the polymer network as in the case studied.

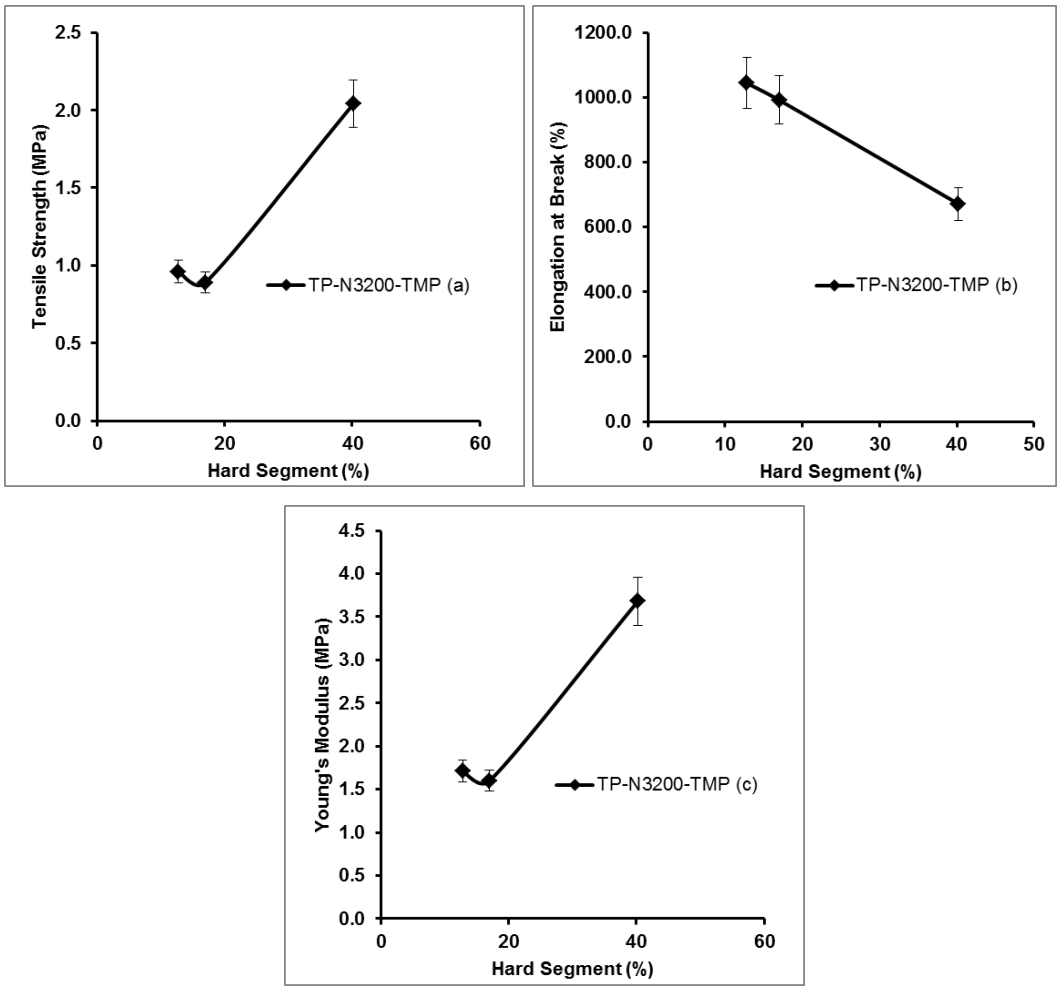

Figure 56 The effects of hard segment content (%) on the (a) Tensile strength (MPa), (b) Elongation at break (%), (c) Young's modulus of TP-N3200-TMP samples

When the mechanical test results, which are shown in Appendix A, of TP-N3200-TMP samples are compared with the ones obtained with BDO, it can be stated that the increase in TMP content led to increase in the HS content. The increase in HS content gave rise to increase in both the ultimate tensile strength and Young modulus, whereas the elongation values tended to decrease due to increase in crosslink density. When the stress-strain plots are analyzed from Figure 57, it is recognized that the increase in TMP content brought about a structural change from a soft and tough matrix to a hard and brittle structure. It is notable that there was no significant change in the mechanical properties observed with respect to BDO at 0.2 and 0.4 equivalent weights. However, TMP resulted in high tensile strength and Young's modulus while low elongation values were obtained with 0.8 equivalent weight.

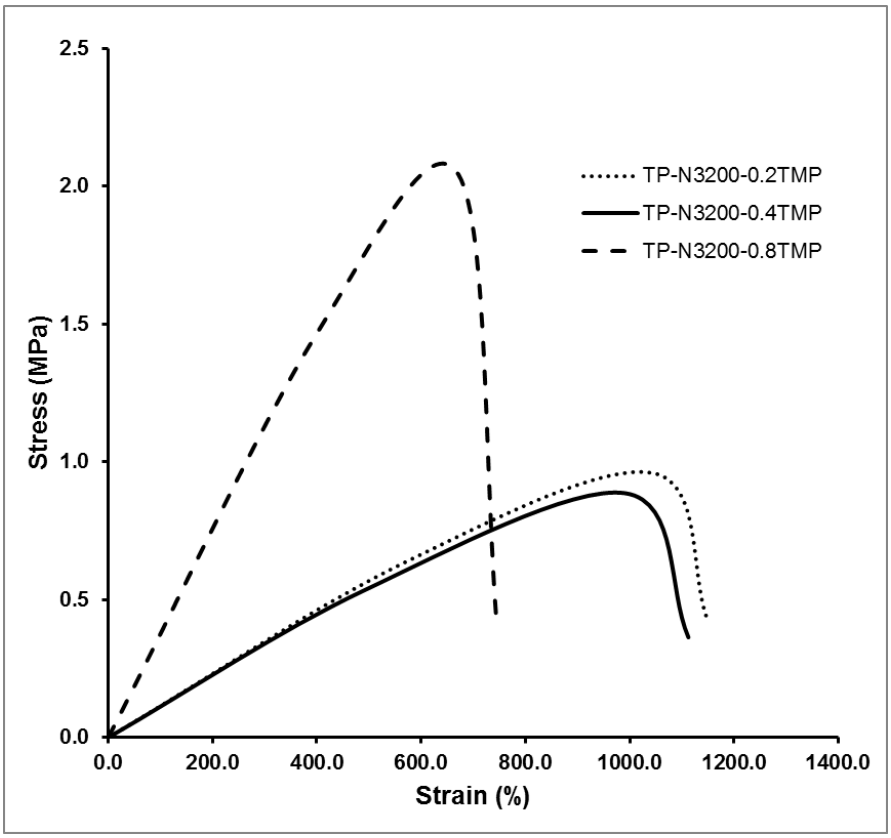

Figure 57 The stress-strain curves of TP-N3200-TMP samples

Results showed that there are no significant changes in ultimate tensile strength and Young's modulus when the chain extender type changed from BDO to TMP as diol and triol. It means that the similar results are obtained with the chain extenders of different functionalities of two or three. The increase in chain extender content enhanced the formation of urethane bonds which increased the hydrogen bonding between polymer chains. This provided the increase in interchain forces which resulted in the increase in crystallinity and rigidity of the hard segments. Also, the molecular slippage have decreased. This affected the mechanical properties and gave rise to high tensile strength and Young's modulus. However, elongation at break values displayed an opposite tendency with the increase in the amount of chain extender amount. The increase in BDO content increased the strain properties, on the other hand, TMP lead to decrease in elongation values. This might have resulted from the BDO uncrosslinked and TMP crosslinked structure.

The effects of curing catalyst on the mechanical properties of polymeric network were explored by using TPB, FeAA and DBTDL. Table 40 shows the samples, in

which only five of them were successfully cured. The curing catalyst type and amount were changed in which TP-N3200-BDO sample was used as the base formulation.

The catalytic activities of previously mentioned curing catalysts for polyurethane forming reaction are well-known. However, there were no studies related to the reactions with TPEG polyol in which an activity comparison was made. Catalysis in the reaction of urethane formation is often complicated by the fact that urethane formation is subject to multiple side reactions, and for this reason, the choice of catalyst may have considerable influence on the ultimate properties of the resulting polymer [109].

Results showed that TPB was relatively low in catalytic activity, whereas FeAA and DBTDL gave very fast reactions and the increase in the catalyst amount resulted in erratic cures, resulting in grains with tacky surfaces that caused unacceptable gassing [110]. Polyurethanes are formed with the isocyanate–hydroxyl reaction. The isocyanate–water reaction is the competing reaction which is thought to be the reason of gas formation. The urethane formation reaction mechanisms are different for these catalysts. For example, DBTDL forms a complex both with the isocyanate and hydroxyl and catalyze the urethane reactions via the formation of a ternary complex. However, TPB associates only with hydroxyl and activates the reaction through the isocyanate-hydroxyl complex which increases as reactions proceed [111]. Thus, a complete cure with relatively little gassing was obtained with TPB.

High tensile strength and Young modulus were obtained with FeAA and DBTDL as compared to TPB. They show higher catalytic activity to urethane reactions in comparison to TPB. An increase in the TPB content causes no changes in tensile strength and modulus, however, lower strain at break values were obtained. This can be explained by the increase in polyurethane molecular weight by forming longer polymer chains with higher catalytic activity by increasing the catalyst content. This gives rise to higher possibility of polymer entanglements which prevent the mobility and flexibility of polymer chains.

4.1.1.2 Tensile Test Results of the Propellant Developed

Uniaxial tensile tests were performed at three different temperatures of -40 ^{o}C, 25^{o}C and 60^{o}C with 50 mm/min. crosshead speed using the microtensile test specimen. The average stress-strain properties of three specimens are shown in Figure 58.

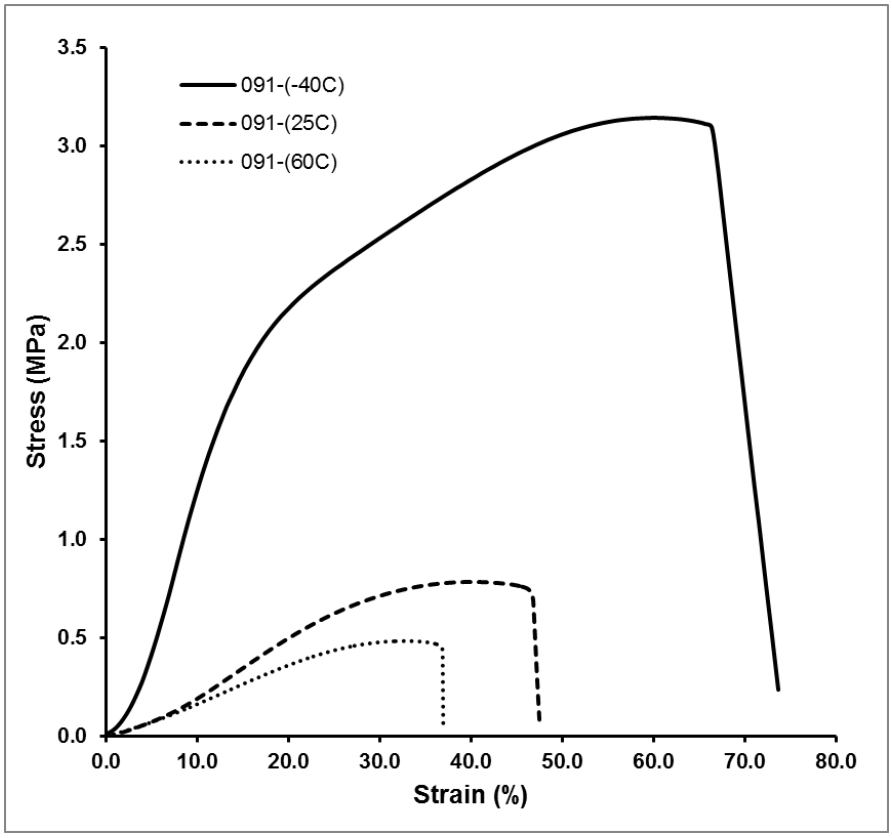

Figure 58 The stress-strain curves of propellant 091 at three different temperatures

Two different types of stress-strain behavior can be stated. The homogeneous (neckless) streching in which slightly linear stress-strain relationships were established and kept up to the point of ultimate tensile strength, and sample fracture was observed at 60^{o}C and 25^{o}C. As cooling from 60^{o}C and 25^{o}C to -40^{o}C took place, the stress-strain curves showed a transition from a neckless stretching into an inhomogeneous stretching with a characteristic necking at low elongations and pronounced brittle behavior, actually resulting in an increased overall elongation at break at -40^{o}C when compared to the stress-strain curves at 60^{o}C and 25^{o}C. There exist an increase in elongation at -40 ^{o}C after neck point up to break that can be linked to strain induced crystallization. It is known that the tensile deformation of

polymers can vary substantially according to both polymer type and temperature. The tensile behavior undergoes a transition from a homogeneous and neckless stretching at higher temperatures into an inhomogeneous stretching with necking at lower temperatures [112]. Thus, the highly polar TPEG-N3200 binder system which exists in the propellant composite exhibited semicrystalline behavior at low temperatures. This brought about necking, cold drawing and subsequently an increased elongation at break as strongly interacting polymer chains align themselves during cold drawing. The tendency of the propellant to strain induced crystallization increased this effect [113].

The variation of mechanical properties that are interpreted from the stress-strain curves of various temperatures are shown in Figure 59 through 61. All of the mechanical properties, tensile strength, elongation at break and Young's modulus showed a tendency to decrease with an increasing temperatures. However, the propellant seemed to have high tensile strength and strain at break capability. This shows that the isocyanate to polyol content ratio is well adapted for this formulation. In addition, the low cohesive bonding of the energetic particles to binder matrix which results in the dewetting of the particles brought about high strain at break properties.

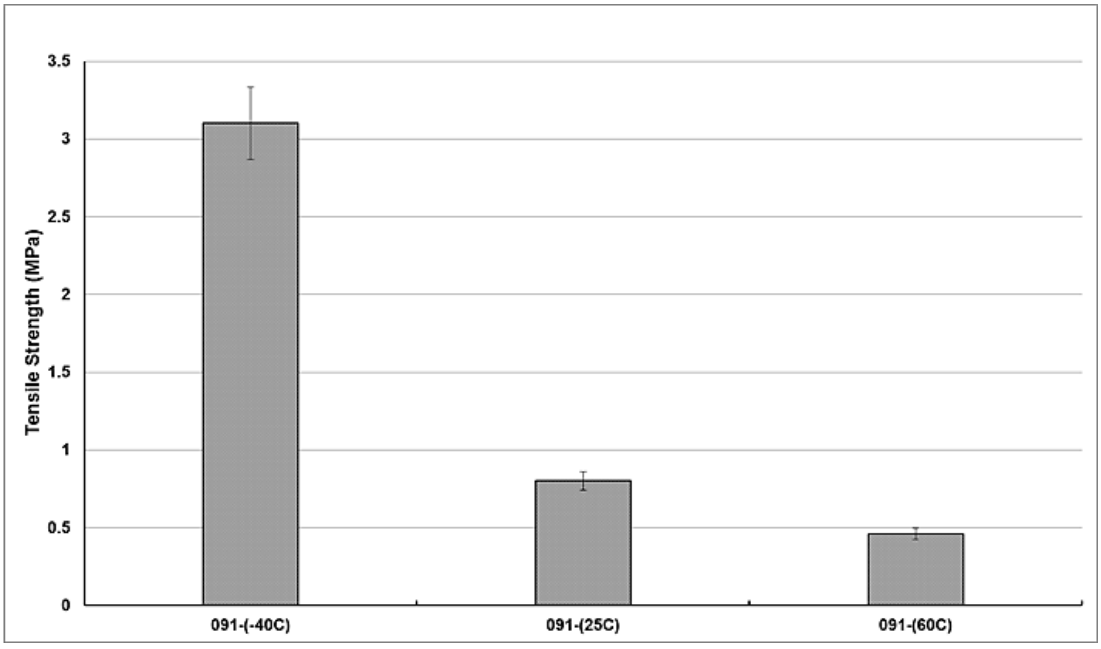

Figure 59 The ultimate tensile strength of propellant 091 as a function of temperature

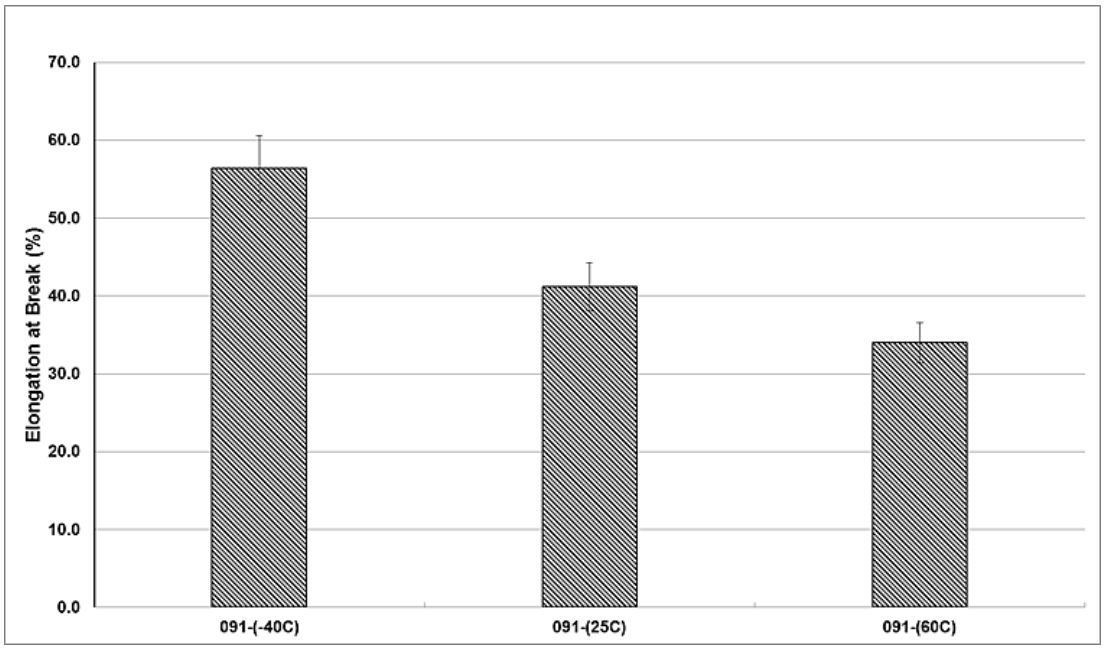

Figure 60 The elongation at break of propellant 091 as a function of temperature

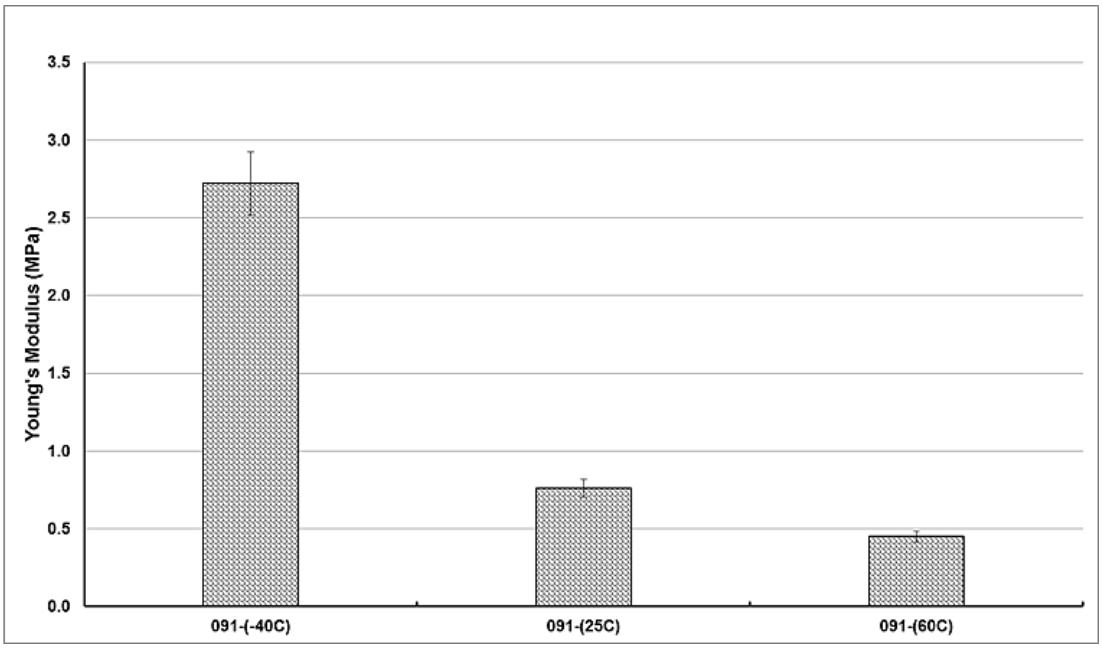

Figure 61 The Young's modulus of propellant 091 as a function of temperature

4.1.2 Hardness Tests

Hardness is a property of a material that enables it to resist plastic deformation. The durometer of Model A was used to measure the indentation hardness of the polymeric networks and the propellant. The operation is so simple, such that the corresponding material was subjected to a definite pressure applied by a calibrated

spring to an indenter that was a cone in our case, the depth of the indentation was measured. Hardness test results of polymeric networks and propellant are tabulated in Appendix A.

4.1.2.1 Hardness Test Results of Polymeric Networks

The results of hardness tests are shown in Figure 62. As we compare the trend with the tensile strength and modulus data, it can be noticed that there is close relationship between the strength and modulus properties and hardness values. The corresponding figures resemble each other supporting the fact that the increase in strength and modulus and the decrease in strain at break are related to the hardness of the material. This phenomenon can be linked to high degree of crystallinity in networks that have also high strength and high modulus. On the other hand, the low hardness and modulus values are caused by the low regularity and crystallinity in these polymeric network structures.

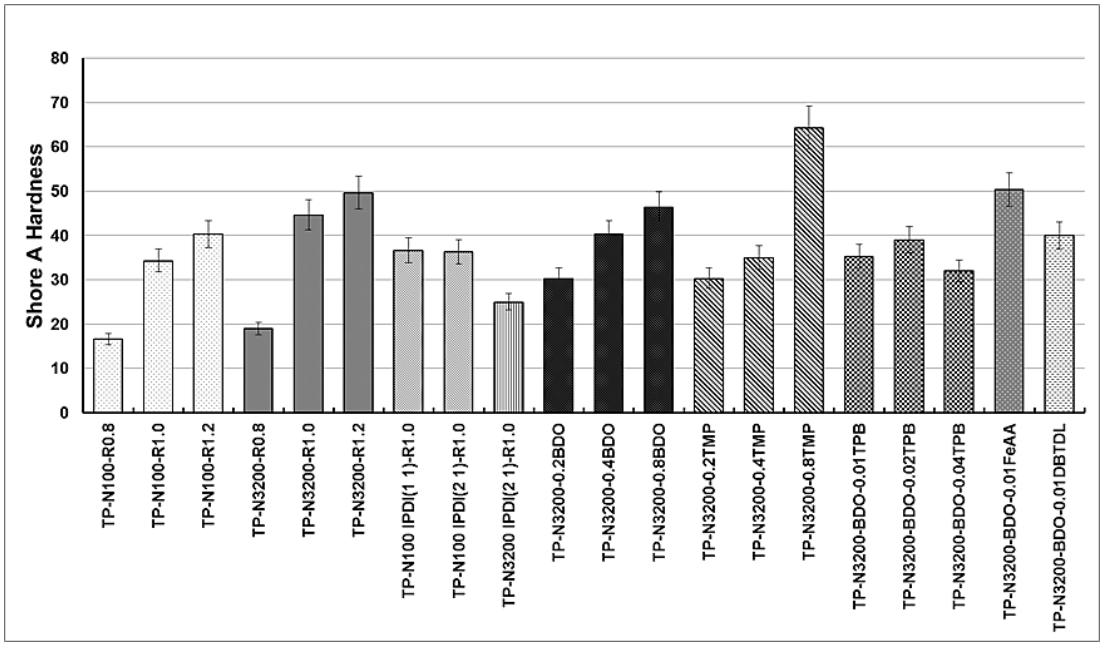

Figure 62 Hardness data of non-energetic polyurethane network structures

4.1.2.2 Hardness Test Results of the Propellant Developed

The hardness of the propellant 091 measures as Shore A 66 which is a bit higher than the hardness of the network structures. The results are shown in Appendix A. This is

mainly due to the presence of energetic solid ingredients like AP and Fe_2O_3. However, this value is acceptable when it is compared with conventional HTPB-AP propellants whose hardness values are in the range of Shore A 60-70 for tactical rocket motor requirements.

4.2 Structural Analysis

The behavior of polyurethane elastomers strongly depends on their chemical structure and morphology. The morphology is mainly determined by the compatibility of the various components constituting the elastomers. The degree of segregation of hard and soft segments, the ability to form domain structures, and the properties of each phase are among the important factors determining the polyurethane behavior [114]. In this thesis, the structural analysis was only applied to polymeric networks by conducting swelling tests and XRD analysis.

4.2.1 Swelling Tests

Crosslink density, ν_e, which can be defined as the concentration of elastically effective chains, is an important characteristic property of elastomeric polymer networks. The mechanical and viscoelastic properties of the elastomers are strongly dependent on the ν_e. The properties of elastomers, such as modulus, tensile strength, maximum extensibility, dynamic mechanical properties and degree of swelling critically depend on the degree of ν_e [75]. One of the methods for determination of ν_e is the measurement of the degree of swelling in a good solvent [115]. In this thesis, The Flory-Rhener relationship was applied to calculate ν_e from swelling data. The values experimentally obtained represent the combination of the true chemical crosslinks and physical chain entanglements which fall into two categories such as permanently trapped chain entanglements and temporarily trapped chain entanglements. It is extremely hard to differentiate one from the other. On the other hand, α-model theoretical approach may deliver exclusively the chemically manifested true chemical ν_e [116].

Table 41 shows the results of crosslink density and molecular weight between crosslinks, M_c, calculated for the compositions shown in the table. Following discussions can be made regarding the results.

Desmodur N-100 has a higher equivalent weight (191 g/eqv.) and lower % NCO content (%22) than Desmodur N-3200 (183 and %23, respectively). For the TP-N100-R1.0 sample, Desmodur N-100 gave a higher crosslink density and lower chain length between crosslinks with the same NCO/OH ratio that may be due to higher equivalent weight and lower % NCO content compared to TP-N3200-R1.0 sample in which Desmodur N-3200 were used. This may also be explained by the high HS content of TP-N100-R1.0 that induces the formation of more physical crosslinks.

Results showed that increase in concentration of crosslinker or increase in NCO/OH ratio gave rise to decrease in extent of swelling for the samples prepared with Desmodur N-3200 namely TP-N3200-R0.8, TP-N3200-R1.0, TP-N3200-R1.2. In other words, as the hard segment percent of polyurethane increased, swelling ratio decreased and crosslinking increased. ν_e and M_c were strongly affected by NCO/OH ratios. Similar trends have been obtained for both aniline and THF, although the extent of diffusion through polyurethane film was different due to their different molecular structure and polarity. It is known that the solubility of a polymer in any solvent strongly depends on the square of the difference between their solubility parameter values. This should be as small as possible for good solubility of a polymer in any solvent. The smaller the difference, the closer to the theoretical crosslink density obtained by corresponding solvent. Solubility parameter of HTPE based networks, aniline and THF can be taken as 10.5, 10.3 and 9.1 $(cal.cm^3)^{1/2}$, respectively [117]. This fact shows that the results obtained by aniline can be declared as closer to the theoretical ones. Variation of ν_e and M_c with HS content can be plotted as in Figure 63 for both solvents.

Table 41 Swelling test results for crosslink density and chain length between crosslinks

Composition	Solvent	Swelling Ratio	v_e (mol/m^3)	M_c (g/mol)	HS (%)
TP-N100-R1.0	Aniline	6.55	80.35	13069	10.5
	THF	4.70	42.54	24684	
TP-N3200-R0.8	Aniline	7.7	61.1	17193	8.2
	THF	7.1	16.6	63163	
TP-N3200-R1.0	Aniline	7.3	66.7	15740	10.1
	THF	5.4	30.4	34490	
TP-N3200-R1.2	Aniline	4.1	187.1	5612	11.9
	THF	3.3	96.5	10880	
TP-N100 IPDI(2 1)-R1.0	Aniline	9.08	45.3	23185	8.6
	THF	5.53	29.3	35845	
TP-N3200 IPDI(2 1)-R1.0	Aniline	10.1	37.6	27941	8.4
	THF	9.7	8.2	127686	
TP-N3200-0.2BDO	Aniline	7.8	58.7	17883	12.8
	THF	5.8	26.7	39341	
TP-N3200-0.2TMP	Aniline	6.51	85.2	12935	12.8
	THF	4.6	45.1	23317	
TP-N3200-BDO-0.01FeAA	Aniline	3.6	229.7	4570	17.0
	THF	2.9	129.5	8105	
TP-N3200-BDO-0.01DBTDL	Aniline	3.0	316.4	3319	17.0
	THF	2.2	222.9	4709	

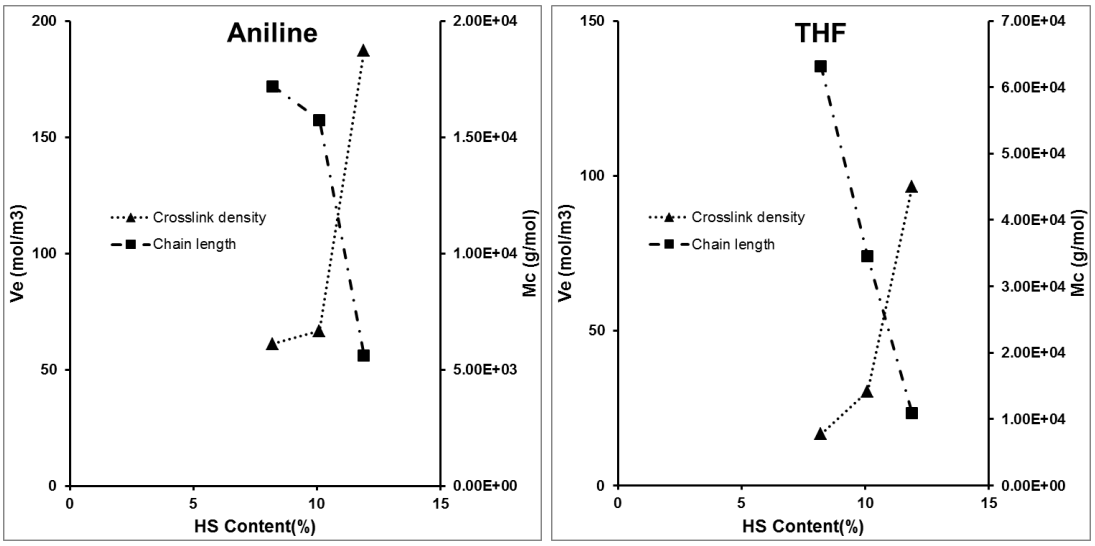

Figure 63 Variation of crosslink density and chain length with HS content (%) for TP-N3200 samples

The structure of molecular chains such as the polarity, crystallizability, and crosslink density mainly affect the solvent resistance of polymer networks. Highly polar molecular chains with crystalline structure and high crosslink density show more resistance to solvent intake. In both aniline and THF, swelling ratio decreases with an increase in crosslink density which tends to increase with R value. This may be ascribed to an increase in the concentrations of the polar groups which act as pseudocrosslinks with an increase in urethane bond concentration. The number of chemical crosslinks is almost negligible when NCO/OH ratio is less than 1.0. In such case, physical crosslinks are dominated through hydrogen bonding possibly by ether-urethane and urethane-urethane linkages. On the other hand, chemical crosslinks are effective because of allophanate reactions as the NCO/OH ratio is greater than 1.0. It can be seen from the figures that chemical crosslinks dominated the number of effective crosslinking in the polymeric networks since the crosslink density shows a sharp increase beyond NCO/OH ratio of 1.0 which corresponds to about 10% HS content.

As we compare the results of samples TP-N100-R1.0 and TP-N100 IPDI(2:1)-R1.0 in which IPDI was used as co-isocyanate in TPEG-Desmodur N-100 system, it can be said that decrease in crosslink density and increase in chain length between crosslinks were obtained. Similar results were obtained for TPEG-Desmodur N-3200 systems of TP-N3200-R1.0 and TP-N3200 IPDI(2:1)-R1.0. This observation may

have resulted from the fact that IPDI has a lower equivalent weight than Desmodur type isocyanates. This fact led to decrease in HS content of the system with respect to SS content. In addition, possible incompatibility with TPEG prepolymer and lower reactivity of IPDI due to strained molecular structure resulted in decrease in the number of urethane bonds. The urethane bonds are physically retained together through hydrogen bonding when NCO/OH ratio is less than or equal to 1.0 as in our case.

BDO and TMP were used as chain extenders at the same equivalent weight in TP-N3200-0.2BDO and TP-N3200-0.2TMP samples, respectively. As we compare the results with the ones obtained for TP-N3200-R1.0, it is observed that BDO, being a diol increased the molecular weight between crosslinks, on the other hand, lower crosslink density was obtained as opposed to TMP which has a triol structure containing three hydroxy functional groups. TMP increased the crosslink density of TP-N3200-R1.0 polyurethane matrix. The different molecular structure and functionality of BDO and TMP produced different results with the same hard segment content. As it is previously mentioned, the physical crosslinks, in which hydrogen bonding is the effective force dominates rather than chemical ones when NCO/OH ratio is less than 1.0. Hydrogen bonding may be enhanced more by TMP due to its triol structure. High degree of crosslinking and smaller effective chain length were obtained for higher levels of hydrogen bonding.

FeAA and DBTDL were used as catalysts for polyurethane reaction as an alternative to TPB in TP-N3200-BDO-0.01FeAA and TP-N3200-BDO-0.01DBTDL, respectively. It was realized that both catalysts enhanced the crosslink density while lower average molecular weight between crosslinks values were obtained as we compare these formulations with TP-N3200-0.2BDO. This can be explained in terms of the inherent nature of the reactions. It is known that the reactions catalyzed by FeAA and DBTDL proceed through different reaction mechanisms in polyurethane systems formed by HTPB, PPG and PEG. They show a higher catalytic activity to urethane reactions in comparison to TPB. The high catalytic activity of these catalyts might have led to formation of highly crosslinked polymer chains. This gave rise to higher possibility of polymer entanglements which prevented the mobility and flexibility of polymer chains.

4.2.2 X-Ray Diffraction Analysis

Polymer crystallinity is one of the important properties of all polymers. Polymers exist both in amorphous and crystalline forms. The degree of crystallinity can be expressed as the ratio of the crystalline region to both amorphous and crystalline regions. There are many methods to measure the polymer crystallinity which are DSC, dilatometry, FTIR, NMR and XRD. XRD was the choice of method in this thesis, although DSC is simpler, because the heat of fusion of %100 crystalline HTPE based polyurethane was unknown. X-ray diffraction profiles obtained for the polymeric structures are shown in Appendix C. The degree of crystallinity determined by the Hermans and Weidinger method and the crystallite size regarding the diffraction peak at about 20^o determined by Scherrer equation are tabulated in Table 42.

Table 42 The degree of crystallinity of HTPE based polyurethane network structures determined by XRD

Composition	HS (%)	Crystallinity (C_r) (%)	L_c (nm)
TP-N100-R1.0	10.5	39.4	1.44
TP-N3200-R0.8	8.2	46.7	1.50
TP-N3200-R1.0	10.1	10.0	1.42
TP-N3200-R1.2	11.9	9.8	1.84
TP-N100 IPDI(2 1)-R1.0	8.6	33.8	1.47
TP-N3200 IPDI(2 1)-R1.0	8.4	46.7	1.55
TP-N3200-0.2BDO	12.8	43.4	1.57
TP-N3200-0.2TMP	12.8	34.0	1.43
TP-N3200-BDO-0.01FeAA	17.0	28.4	1.47
TP-N3200-BDO-0.01DBTDL	17.0	43.0	1.55

The diffraction patterns of HTPE containing polyurethane elastomers do not exist in literature, however, it is apparent that results resemble to the X-ray profiles of HTPB-containing elastomers [118]. In general, polymeric networks showed mainly

three diffraction peaks which were resulted from the crystallization of the soft-segment phase at about 11º, 20.5º and 43º degrees with varying intensities. It is likely that some soft segment-hard segment phase mixing could occur in the system disturbing the soft segment [119]. This may result in broad diffractions which are indicative of very small crystals. It is clear that there does not exist any remarkable difference between crystallite sizes, which are between 1.4-1.8 nm, determined by Scherrer equation. There is no correlation between the crystallinity and crystallite size. The same situation is valid in the case of HS content and crystallite size. It is hard to make any consistent evaluation relating to the effects of the use of different isocyanates, co-isocyanate, curing catalyst or addition of chain extender on the degree of crystallinity. However, as the crosslink density results are assessed, it appears that with an increase in the degree of crosslinking, crystal perfection decreases and the intensity of diffraction peak in X-Ray diagrams tends to decrease.

Figure 64 shows the XRD patterns of the TPEG-N3200 based polymeric networks with different NCO/OH molar ratios. It shows that as the NCO/OH ratio increases or the hard segment content increases, the intensity of the diffraction peak decreases. It is clear that the excess hard segment content does not provide any ordered structure and possibly disrupts the likely ordered structure of TPEG by hydrogen bonding interaction of the urethane structures with the TPEG groups.

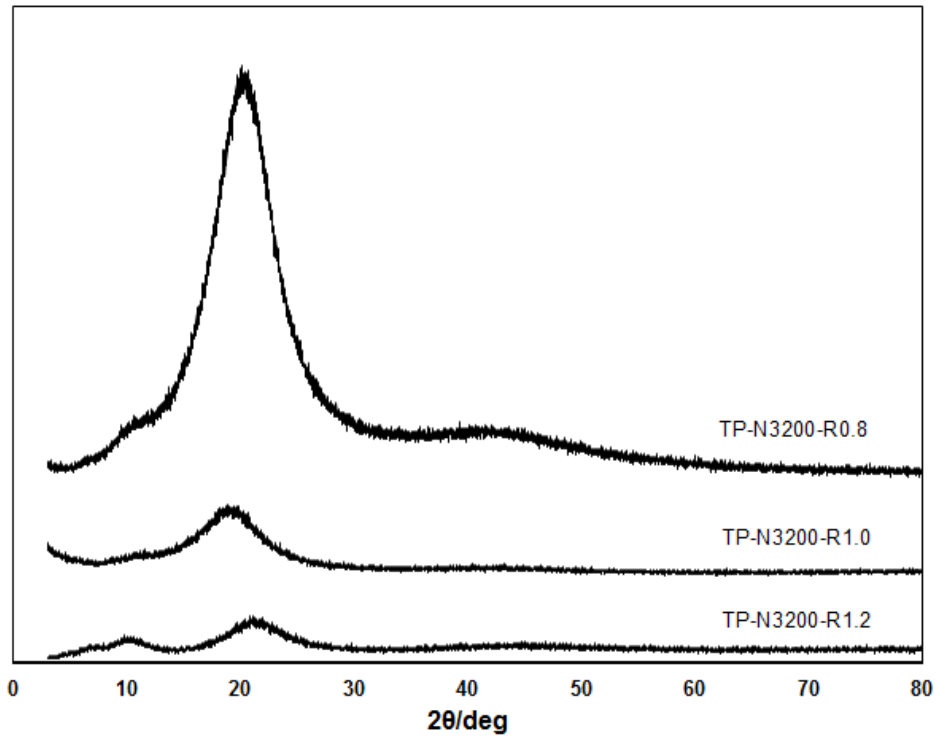

Figure 64 The diffraction patterns of TPEG-N3200 samples with different NCO/OH ratios

4.3 Thermal Analysis

Thermal analysis was performed on polymeric network systems as well as propellant samples. Thermograms show several thermal transitions related to the characteristics of structure of elastomers and propellants.

4.3.1 DSC Analysis

4.3.1.1 Polymeric Network Structures

DSC allows the determination of glass-rubber transition temperature, melting – recrystallization temperature and their corresponding heat transitions which give information about the characteristics of microphase separation or phase mixing of polymeric structures. DSC thermograms of TPEG polymeric networks are presented in Appendix D. Table 43 shows the results of DSC analysis of polymeric networks.

Table 43 The results of DSC analysis of polymeric networks

Composition	T_g (°C)	T_{cryst1} (°C)	T_{cryst2} (°C)	E_{cryst} (J/g)	T_{melt} (°C)	E_{melt} (J/g)	T_{melt2} (°C)
TP-N100-R1.0	-73.6	-	-29.9	-30.4	5.7	24.6	-
TP-N3200-R0.8	-73.3	-	-28.5	-30.3	10.1	27.4	250-450
TP-N3200-R1.0	-74.3	-	-27.7	-27.9	1.8	25.0	275-450
TP-N3200-R1.2	-73.5	-	-	-	-	-	250-450
TP-N100 IPDI(2:1)-R1.0	-74.3	-45.2	-24.7	-12.1	-0.1	15.4	250-450
TP-N3200 IPDI(2:1)-R1.0	-74.6	-45.0	-28.5	-22.3	1.9	33.9	250-450
TP-N3200-0.2BDO	-74.1	-	-30.7	-27.2	5.4	29.5	225-450
TP-N3200-0.2TMP	-73.9	-	-32.0	-30.6	7.5	27.0	250-450
TP-N3200-BDO-0.01FeAA	-74.1	-	-	-	-	-	250-450
TP-N3200-BDO-0.01DBTDL	-71.4	-	-	-	-	-	250-450

Three endotherms and one exotherm were mainly observed in the DSC thermograms. The lowest temperature endotherm can be attributed to the glass transition temperature which was determined as about -73°C. It is known that TPEG has a glass transition temperature of about -80°C [120]. As can be seen from the results, the glass transition of the soft segments is higher than that of TPEG reflecting the differences in the extent of phase mixing of the soft segments and the hard segments, and the degree of interaction between the phases. There are two main factors which may influence the T_g of the TPEG segments: the crystallization of TPEG segments and the hard segments in the molecules [121]. Both have the effect of shifting the T_g of the TPEG segments to higher temperatures. However, there is no correlation between the T_g of the soft segments and the HS content, since the HS contents of the polymeric networks are nearly similar. Identical T_g values reveal that identical molecular mobility was attained. The next endotherm was between the temperatures of 0-10°C which is the crystalline melting point. It involves a change from the crystalline solid state of the soft segment into the melt form. The small change between the melting transition temperatures can be related to the differences in the cohesive energy density associated with the density of sites for intermolecular

bonding. That means the increase in intermolecular bonding ranging from weak van der Waals forces through the much stronger hydrogen bonds led to higher melting point. The last broad endotherm can be seen between the temperature range of 200-450^{o}C. This high temperature endotherm can be ascribed to the melting of microcrystalline regions within hard microdomains [122]. The low temperature intense exotherm at around -30^{o}C can be linked to soft segment crystallization of ordered regions. It is interesting to note that samples containing IPDI as co-isocyanate showed a small shoulder like exotherm peak before this exotherm at -45^{o}C. This shows the presence of additional ordered regions in soft segment.

4.3.1.2 Propellant Samples

Thermal characteristics of propellant samples were investigated by DSC in order to evaluate phase transitions, decomposition temperatures and corresponding heat transfers. Results are shown in Table 44.

Table 44 The results of DSC analysis of propellant samples and propellant 091

Composition	T_g (^{o}C)	Peak Temperatures (^{o}C)	Decomposition Enthalpy ΔH(J/g)
TPAP-1	-65.9	192.7^{o}C (exotherm) 247.6^{o}C (exotherm) 341.6^{o}C (exotherm)	91.7 J/g 457.6 J/g 3036.0 J/g
TPAP-2	-65.4	250.2^{o}C (exotherm) 342.1^{o}C (exotherm)	792.0 J/g 1959.0 J/g
TPAP-3	-64.2	240.3^{o}C (exotherm) 329.9^{o}C (exotherm)	953.4 J/g 1219.0 J/g
TPAP-4	-64.8	233.1^{o}C (exotherm) 250.2^{o}C (exotherm) 336.5^{o}C (exotherm)	396.4 J/g 158.6 J/g 1156.0 J/g
TPAP-5	-65.4	230.9^{o}C (exotherm) 243.7^{o}C (exotherm) 350.8^{o}C (exotherm)	283.3 J/g 141.7 J/g 996.6 J/g
TPAP-6	-65.0	232.0^{o}C (exotherm) 245.2^{o}C (exotherm) 354.3^{o}C (exotherm)	295.5 J/g 147.7 J/g 1187.0 J/g
TPAP-7	-55.0	237.3^{o}C (exotherm) 245.0^{o}C (exotherm) 359.9^{o}C (exotherm)	293.4 J/g 54.5 J/g 1323.0 J/g
TPAP-8	-51.3	243.2^{o}C (exotherm)	63.0 J/g

		248.1°C (exotherm) 355.7°C (exotherm)	402.5 J/g 1318.0 J/g
TPAP-9	-64.9	243.8°C (endotherm) 312.5°C (exotherm) 400.4°C (exotherm)	54.9 J/g 362.9 J/g 219.2 J/g
TPAP-10	-66.3	245.4°C (endotherm) 314.0°C (exotherm) 406.5°C (exotherm)	57.0 J/g 371.2 J/g 66.4 J/g
TPAP-11	-70.2	241.2°C (exotherm) 246.4°C (exotherm) 361.2°C (exotherm)	198.5 J/g 132.3 J/g 1196.0 J/g
TPAP-12	-69.2	240.5°C (exotherm) 245.5°C (exotherm) 352.2°C (exotherm)	116.1 J/g 232.2 J/g 1120.0 J/g
TPAP-13	-69.6	241.8°C (exotherm) 246.6°C (exotherm) 354.1°C (exotherm)	97.9 J/g 293.6 J/g 1004.0 J/g
TPAPX-1	-66.7	245.0°C (endotherm) 250.7°C (exotherm) 255.2°C (exotherm) 353.7°C (exotherm)	52.5 J/g 319.0 J/g 321.5 J/g 698.1 J/g
TPAPX-2	-65.7	277.2°C (exotherm)	1256.0 J/g
TPAPXL-1	-65.9	244.0°C (endotherm) 263.1°C (exotherm) 275.0°C (exotherm) 341.3°C (exotherm)	53.4 J/g 578.7 J/g 64.3 J/g 413.5 J/g
TPAPXL-2	-66.5	244.3°C (endotherm) 250.4°C (exotherm) 275.4°C (exotherm) 334.2°C (exotherm)	46.5 J/g 480.0 J/g 68.6 J/g 488.7 J/g
TPAPXL-3	-65.9	247.5°C (exotherm) 250.3°C (exotherm) 277.2°C (exotherm) 340.2°C (exotherm)	156.6 J/g 234.9 J/g 78.3 J/g 768.9 J/g
TPAPSN-1	-66.2	119.8°C (endotherm) 129.1°C (endotherm) 155.9°C (endotherm) 190.5°C (exotherm) 240.7°C (exotherm) 246.1°C(exotherm) 345.5°C(exotherm)	4.7 J/g 4.6 J/g 13.4 J/g 258.4 J/g 135.2 J/g 97.8 J/g 826.8 J/g
Propellant 091	-61.2	238.5°C (exotherm) 323.2°C (exotherm)	252.4 J/g 831.2 J/g

As we examine the DSC traces of TPAP-1, TPAP-2 and TPAP-3 propellant samples in which the effect of AP particle size on the T_g and decomposition pattern was investigated, the following discussion can be made. The decrease in AP particle size

did not affect the T_g that was determined at about -65.0°C for all the three samples. It shows that the molecular mobility of the TPEG segments and its crystallization were not sensitive to change in oxidizer particle size due to relatively large particles. Three distinct exotherms exist in the TPAP-1 thermogram. The exotherm around 190°C can be linked to decomposition of BuNENA [123]. The two other exotherms at peak temperatures between 240-250°C and 330-340°C may have resulted from incomplete and complete combustion of AP, respectively [124]. It is interesting that the exotherm due to BuNENA decomposition disappeared in the TPAP-2 and TPAP-3 thermograms as the AP particle size decreased from 400μ to lower values. This shows that BuNENA decomposition exotherm overlapped with the lower temperature combustion exotherm of AP.

The effect of different modality on thermal properties of propellant samples was examined in the TPAP-4, TPAP-5 and TPAP-6 samples. The modality of propellant did not affect the T_g of propellants and it was the same as before about -65.0°C. It was realized that one additional exothermic transition appeared at around AP lower temperature combustion peak. The incomplete AP decomposition occurred in two stages by giving transitions at 230°C and 245°C. The combustion of AP particles was completed at between 340-350°C.

The DSC thermograms of TPAP-7 and TPAP-8 show that T_g of the propellant samples increased by 10-15°C from -65.0°C to 50-55°C. It was possibly due to the use of different energetic plasticizers TMETN and BDNPA-F in TPAP-7 and TPAP-8, respectively as compared to TPAP-2. Although TMETN decomposes at its boiling point of 182°C [125], this exotherm could not be observed in the TPAP-7 thermogram. The same situation occurred in the TPAP-8 thermogram. BDNPA-F gives a decomposition at maximum peak temperature of 255°C, however, this could not be observed. Instead, two exotherms at 240°C and 245°C which corresponded to partial combustion of AP were observed. The exotherm at 355°C related to complete combustion of AP were recorded in both thermograms.

The DSC traces of TPAP-9 and TPAP-10 give information on the effects of different burning rate catalysts on the T_g and decomposition pattern. Results showed that T_g was not affected from this change and it was around -65.0°C. The DSC thermograms

showed that Cr_2O_3 and SiO_2 burning rate catalysts which are different from Fe_2O_3 led to appearance of an endotherm at 245°C which represents the transition from orthorhombic form to cubic form of AP. In addition, partial combustion and complete combustion exotherms of AP moved to higher temperatures, i.e. from 245°C and 355°C to 315°C and 405°C, respectively. Hence, a significant alteration in the decomposition characteristics of AP was observed by the use of Cr_2O_3 and SiO_2. The increase in decomposition temperatures was due to the uncatalytic effect of these burning modifiers. This proves that inefficient heat transfer within the propellant and lower heat generation was obtained as compared to propellant samples containing Fe_2O_3.

The effect of increase in BuNENA concentration and the use of different burning rate catalyst combinations were studied in the thermograms of TPAP-11, TPAP-12 and TPAP-13 propellant samples. The decomposition peak of BuNENA was not observed although its concentration was doubled. However, T_g of corresponding propellant samples was lowered from -65.0°C to about -70.0°C due to higher BuNENA concentration. The thermograms showed incomplete combustion peaks at 240°C and 245°C and a complete combustion peak at 355°C of AP particles. It indicates that the increase in the plasticizer concentration and the use of mixed burning rate catalysts did not change the decomposition pattern of TPEG-AP based propellants.

The DSC trace of the TPAPX-1 sample containing AP and HMX as solid oxidizers showed an endothermic orthorhombic to cubic transition of AP at 245°C. The exothermic peak at 250°C can be related to the first partial decomposition of AP. Another exothermic transition at 255°C might be the overlapped peaks of partial decomposition of AP and decomposition of HMX. The complete combustion of AP occurred at 355°C. The DSC thermogram of TPAPX-2 exhibited a strong exothermic peak at 277°C which was due to the decomposition of HMX.

The DSC traces of TPAPXL-1 and TPAPXL-2 samples containing AP-HMX-Al as energetic ingredients resembles the DSC trace of TPAPX-1. The endothermic transition was observed at about 245°C which is due to the AP phase transition from orthorhombic to cubic form. The exothermic peaks between 250°C-263°C can be

linked to the initial decomposition of AP, then it was followed by an exothermic transition at about 275°C due to HMX combustion. The complete combustion of AP was achieved at about 340°C. The T_g of the propellant samples remained the same as -65.0°C showing that the use of Al as the metallic fuel did not affect the crystalline structure and hard segment content of propellants. The DSC thermogram of TPAPXL-3 was mainly the same as those of TPAPXL-1 and TPAPXL-2. The only difference can be observed at about 245°C. The exothermic transition due to the partial combustion of AP occurred instead of the endothermic AP phase transition. This shows that the partial combustion of AP took place before the AP phase transition due to the increase in Al concentration.

The DSC thermogram of TPAPSN-1 showed three endothermic and four exothermic transitions. The endothermic peak at about 120°C correspond to the thermolysis of BuNENA. The endotherm at 130°C might be due to the II→I phase transition of PSAN which was followed by an endotherm at 156°C owing to the melting of PSAN. PSAN decomposed at 190°C exhibiting an exotherm. The exothermic peaks shown at 240°C and 246°C can be linked to the partial combustion of AP particles and complete combustion of AP was achieved at about 345°C.

The DSC analysis of propellant 091 showed thermal transitions similar to those of TPAP propellant samples such that there existed an exothermic peak at about 240°C due to AP partial combustion and one more exothermic peak at about 320°C due to complete combustion of AP particles.

4.3.2 TGA Analysis

4.3.2.1 Polymeric Network Structures

The quantification of thermal degradation of polymeric networks was investigated by TGA. The initiation of thermal degradation and the number of steps are important, since it gives information about the structure and thermal stability. TGA thermograms of TPEG polymeric networks are shown in Appendix E. Table 45 shows the results of thermal degradation of polymeric networks, the temperatures at 5%, 30% weight loss and the maximum peak of DTG curves.

Table 45 The results of TGA analysis of polymeric networks

Composition	T_5 (°C)	T_{30} (°C)	Max DTG(°C)
TP-N100-R1.0	290.5	369.9	396.1
TP-N3200-R0.8	304.2	362.1	397.7
TP-N3200-R1.0	293.8	374.3	401.8
TP-N3200-R1.2	288.0	369.1	400.3
TP-N100 IPDI(2 1)-R1.0	279.4	367.7	392.3
TP-N3200 IPDI(2 1)-R1.0	287.2	355.3	383.7
TP-N3200-0.2BDO	305.5	368.5	392.8
TP-N3200-0.2TMP	301.9	367.5	392.8
TP-N3200-BDO-0.01FeAA	289.8	371.0	395.5
TP-N3200-BDO-0.01DBTDL	298.7	367.8	392.3

Results show that two stage degradation processes can be proposed for all the polymeric networks. The first degradation occurred at the maximum temperature of about 300°C which can be related to decomposition of urethane links. The second degredation is observed at around 360°C which reaches a maximum temperature of about 400°C. This can be connected to destruction of ether groups in SS. It can be realized from the TGA thermograms that the first stage of degradation is slow, but its rate increases with increasing SS content. It is known that the thermal degradation is mainly initiated within the HS. The weakest bonds in the polymer are broken in the first stage decomposition. The main process which occurs during degradation is the polyurethane decomposition yielding the diisocyanate and polyols [126]. Results revealed that polymeric networks tested showed almost the same thermal stability.

4.3.2.2 Propellant Samples

The weight loss due to thermal degredation of the propellant samples was studied by TGA. The thermal transitions observed in the DSC thermograms can be supported by the percent weight losses at corresponding temperatures. Table 46 presents the results of TGA analysis in which the onset temperature of the weight loss of the stages were recorded.

Table 46 The results of TGA analysis of propellant samples and propellant 091

Composition	T_1(ºC)	T_2(ºC)	T_3(ºC)
TPAP-1	136.5	232.5	306.5
TPAP-2	129.3	234.1	298.0
TPAP-3	133.0	236.8	-
TPAP-4	128.7	231.9	298.8
TPAP-5	130.0	234.9	287.8
TPAP-6	132.5	235.2	295.1
TPAP-7	134.4	234.2	296.6
TPAP-8	181.3	246.3	-
TPAP-9	129.1	250.7	302.7
TPAP-10	139.4	251.3	302.1
TPAP-11	138.6	234.4	299.7
TPAP-12	130.1	235.8	299.6
TPAP-13	130.0	235.3	299.2
TPAPX-1	137.3	248.6	293.4
TPAPX-2	137.1	238.1	272.3
TPAPXL-1	139.4	250.3	-
TPAPXL-2	139.8	251.8	-
TPAPXL-3	126.4	237.6	300.2
TPAPSN-1	146.1	249.1	322.6
Propellant 091	131.8	244.3	254.9

Observing the TGA results, the weight loss of TPEG-AP based TPAP propellant samples can be roughly divided into three stages. The weight loss during the first stage (100 ºC to 200ºC) resulted from decomposition of BuNENA apart from TPAP-7 and TPAP-8 in which TMETN and BDNPA-F were used as the energetic plasticizer. This accounts for %10 weight loss. The second stage (200 ºC to 275ºC) of weight loss can be related to the partial combustion of AP particles. This loss amounts to cumulative %30 weight change. The third stage (275 ºC to 350ºC) of weight loss was due to the complete combustion of AP. The third stage was absent in

the case of TPAP-3 and TPAP-8 in which AP combustion reaction was completed at lower temperature of about 240^{o}C.

The weight loss of TPEG-AP-HMX based TPAPX propellant samples can be described again in a three stage decomposition pattern. The first stage (125 ^{o}C to 190^{o}C) of the weight loss can be explained by the decomposition of BuNENA. This is responsible for about 10% weight loss as expected. The second stage of weight loss resulted from the partial combustion of AP and complete decomposition of HMX between 200 ^{o}C and 275^{o}C. This change accounts for 85% weight loss in the case of TPAPX-1 in which HMX Class I (average particle size is 150μ) was used. Cumulative 30% weight loss was recorded after the second stage in the case of TPAPX-2 in which HMX Class III (average particle size is 460μ) was used. This shows that the % weight loss was increased in the second stage of decomposition than TPAP propellant samples with the effect of HMX. The complete decomposition of AP led to the third stage of weight loss occurring between 275^{o}C and 325^{o}C.

For the TPEG-AP-HMX-Al based TPAPXL propellants, the weight losses observed were somewhat different than the others. Al provided a two stage decomposition pattern. Again, the BuNENA decomposition was responsible for the first stage (100 ^{o}C to 175^{o}C) of the weight loss which amounts to about 10%. The second stage (225^{o}C to 275^{o}C) of the weight loss was caused by both AP and HMX complete combustion. In this case, almost complete combustion was achieved for TPAPXL-1 and TPAPXL-2. In spite of this, a third stage (275^{o}C to 325^{o}C) weight loss was recorded for the TPAPXL-3 up to complete combustion by giving a high amount of residue (%25 residue). It indicates to incomplete combustion by producing Al_2O_3 as the possible residue. The weight loss pattern of TPEG-AP-PSAN based TPAPSN-1 propellant can be described by three stages of decomposition. The first stage (125^{o}C to 225^{o}C) of decomposition resulted from thermolysis of BuNENA and PSAN decomposition. This corresponds to about 35% weight loss. The second stage (225^{o}C to 275^{o}C) of the weight loss was caused by partial combustion of AP, and complete AP combustion was recorded between 275^{o}C and 375^{o}C by giving a third stage weight loss.

The weight loss trend of propellant 091 showed again three stage decomposition patterns. The first weight loss (100^{o}C to 200^{o}C) resulted from the decomposition of BuNENA which amounts to about 10% weight loss. The second stage (200^{o}C to 250^{o}C) of decomposition corresponding to 20% cumulative weight loss that can be explained by partial combustion of AP. The third stage of decomposition resulted from the complete combustion AP particles between 250^{o}C and 300^{o}C.

4.3.3 Vacuum Stability Analysis

Thermal stability of polymeric network samples were not measured. On the other hand, propellant samples were tested for their thermal stability behaviour under vacuum conditions. The criteria stated in the corresponding standard document declares that the gas evolved must not exceed 5 mL at standard temperature and pressure. Then, the propellant is said to be thermally stable under specified test conditions [127]. Vacuum stability test results are shown in Table 47.

Results showed that TPEG-AP based propellant samples between TPAP-1 to TPAP-10 seemed to be thermally stable under vacuum, whereas TPAP-11 to TPAP-13 samples decomposed under test conditions. The reason for that observation could be the relatively high amount of BuNENA concentration used in these propellant samples. BuNENA has a two step decomposition pattern giving exotherms at 120^{o}C and 200^{o}C [123]. The energy evolved near the first decomposition might lead to initiation of propellant degredation and then autocatalytically proceed to decomposition. TPEG-AP-HMX (TPAPX) and TPEG-AP-HMX-Al (TPAPXL) propellant samples were thermally stable under vacuum. However, in the case of TPEG-AP-PSAN (TPAPSN-1), there existed a thermal instability that proceeded to decomposition. The reason for the instability of TPAPSN-1 could be the incompatibility between the phase stabilizing agent KNO_3 used as an additive in PSAN and BuNENA. In addition, propellant 091 seemed to be thermally stable under vacuum by giving a gas evolution of 2.7 mL which was less than 5.0 mL.

Table 47 Vacuum stability test results of propellant samples and propellant 091

Composition	Gas Evolution (mL)
TPAP-1	0.23
TPAP-2	0.40
TPAP-3	0.21
TPAP-4	0.20
TPAP-5	0.19
TPAP-6	0.23
TPAP-7	0.26
TPAP-8	0.10
TPAP-9	0.19
TPAP-10	0.35
TPAP-11	Decomposition
TPAP-12	Decomposition
TPAP-13	Decomposition
TPAPX-1	0.39
TPAPX-2	0.23
TPAPXL-1	0.34
TPAPXL-2	0.58
TPAPXL-3	0.79
TPAPSN-1	Decomposition
Propellant 091	2.7

4.4 Ballistic Analysis

The knowledge of thermodynamic properties of propellant is significant because it affects the success of rocket motor design and development phase. Burning rate and related burning rate pressure exponent are the critical ballistic results that can be experimentally determined. They are functions of the propellant composition and can be changed by changing the propellant characteristics by manipulating the type and weight of propellant ingredients.

4.4.1 Thermochemical Calculations

The thermodynamic properties of the propellants in Table 48 were theoretically calculated by ICT Thermodynamic Code program. The calculations were made by assuming that the expansion ratio which is the ratio of combustion chamber pressure to expanded medium pressure was 70:1 in bar.

Table 48 Calculated thermodynamical properties of propellant samples

Composition	**Thermodynamical properties**					
	I_{sp} (sec)	**c^* (m/sec)**	**ρ (g/cm^3)**	**T_c (K)**	**M_{ave} (g/mol)**	**OB (%)**
TPAP-1	251.8	1470	1.621	2478.3	22.139	-31.21
TPAP-2	251.8	1470	1.621	2478.3	22.139	-31.21
TPAP-3	251.8	1470	1.621	2478.3	22.139	-31.21
TPAP-4	251.8	1470	1.621	2478.3	22.139	-31.21
TPAP-5	251.8	1470	1.621	2478.3	22.139	-31.21
TPAP-6	251.8	1470	1.621	2478.3	22.139	-31.21
TPAP-7	258.2	1497	1.661	2695.1	23.365	-24.23
TPAP-8	254.5	1479	1.648	2597.1	23.011	-26.55
TPAP-9	251.9	1470	1.621	2479.6	22.029	-31.26
TPAP-10	252.0	1469	1.618	2477.4	22.029	-31.26
TPAP-11	238.7	1409	1.545	2113.2	20.272	-45.04
TPAP-12	238.6	1409	1.545	2111.0	20.239	-45.07
TPAP-13	238.8	1409	1.543	2113.0	20.221	-45.07
TPAPX-1	236.7	1396	1.616	2140.3	20.959	-41.84
TPAPX-2	236.7	1396	1.616	2140.3	20.959	-41.84
TPAPXL-1	261.0	1465	1.653	2516.1	17.918	-54.30
TPAPXL-2	263.1	1420	1.693	2717.8	16.820	-66.60
TPAPXL-3	263.6	1431	1.696	2724.8	17.395	-61.03
TPAPSN-1	232.5	1365	1.586	2058.2	21.198	-33.68

Following discussions can be made regarding the results tabulated in Table 48. There was no change in the thermodynamical properties of TPAP-1 through TPAP-6

propellant samples, since they had the same weight percent of propellant ingredients. The only difference is the distribution of AP particle size which can not be taken into account theoretically. TMETN, as the energetic plasticizer that was used in TPAP-7, gave the best specific impulse in comparison to BUNENA and BDNPA-F. It shows that the high energy content of TMETN increased the performance of propellant in comparison to TPAP-2, TPAP-7 and TPAP-8. There were no dramatic changes in the performances by the use of Fe_2O_3, Cr_2O_3 and SiO_2 as the burning rate catalyts. The corresponding properties can be compared for the TPAP-2, TPAP-9 and TPAP-10. The BuNENA content was doubled while the AP content was decreased in TPAP-11 propellant sample. It was realized that this change resulted in significant decrease in propellant performance, although it increased the ease of propellant processing. The burning rate couples of Fe_2O_3-Cr_2O_3 and Fe_2O_3-SiO_2 were used in the propellant samples of TPAP-12 and TPAP-13 in 1/1 weight fraction for investigation of possible synergetic effects on the performance. It was seen that the use of mixed catalysts did not affect the thermodynamic properties. In general, when the AP content was lowered, lower oxygen balance was obtained. Due to lower oxygen balance, the average molecular weight of the gaseous combustion products were reduced from TPAP-1-10 to that of TPAP-11-13. This indicates the fact that combustion efficiencies in the latter propellant sets were low. Lower combustion efficiencies decreased the adiabatic flame temperature and specific impulse significantly.

Furthermore, replacement of AP with HMX in equal amount decreased the specific impulse and characteristic velocity compared to TPAP propellant samples. HMX increased the oxygen demand for the resulting mixture and decreased the mean molecular weight of the reaction products. This is predictable due to the fact that nitramines such as RDX or HMX contain relatively few oxidizing radicals, and the binder surrounding the nitramine crystals cannot be fully oxidized. The binder is decomposed at the combustion temperature, and it forms gases rich in hydrogen and carbon monoxide which reduces the molecular weight, and cools the gases to a lower combustion temperature [128]. On the other hand, addition of Al as metallic fuel significantly increased the specific impulse and adiabatic flame temperature which should be as high as possible for high performance. As opposed to Al, the use of PSAN decreased the specific impulse. It is known that PSAN is a mixture of

inorganic nitrate, and it is the form of ammonium nitrate (AN) with small amounts of stabilizer such as NiO or KNO_3 that change the phase transition temperature of AN from 32°C to above 60°C [41]. It is generally used for low performance rocket and gas generator applications. The lowest propellant density have been gathered by PSAN which is critical for volume specific impulse. It is required that a more chamber volume for a given performance was needed in this case.

4.4.2 Strand Burner Tests

The burning rate and pressure exponent of propellant samples and propellant 091 were determined by strand burner measurements for the pressure range of 6.9 – 13.8 MPa at constant temperature of 20°C according to MIL-STD-286C. Table 49 shows the results.

In general, the burning rate of a composite solid propellant depends on the pressure, initial temperature, and particle size of energetic solid components, the presence or absence of a metal in the composition of the propellant, the oxidizer to fuel ratio, and the chemical nature of the propellant [129].

As the tabulated results are examined, it can be stated that almost all of the pressure exponents lie between the range of 0.3-0.5 which is desirable for simple grain configurations except for TPAPX-1, TPAPX-2, TPAPXL-3 and TPAPSN-1. The use of different energetic plasticizers like TMETN and BDNPA-F decreased the pressure exponent from 0.4 to 0.3 in comparison to BUNENA. SiO_2 used as the burning rate catalyst increased the burning rate and decreased the burning rate exponent compared to Fe_2O_3 (TPAP-2 and TPAP-10).

The decrease in the AP particle size (TPAP-1, 2, 3) increased the burning rate, but no changes in burning rate exponent were observed. The smaller the particle size of AP, the closer is the flame and the higher the heat flux to the surface and therefore the higher burning rate of the propellant. The burning rate is directly proportional to the heat flux from the propellant surface. The heat flux is due to the flame composed of O_2 from the AP and small hydrocarbons from the pyrolysis of the binder. The high

interaction between O_2 and hydrocarbons enhances the rate of AP decomposition and pyrolysis of the binder [129].

Table 49 Burning rate and pressure exponent results of the propellant samples

Composition	Burning Rate (mm/s)			Pressure Exponent
	6.9 (MPa)	10.3 (MPa)	13.8 (MPa)	
TPAP-1	8.5±0.2	10.3±0.3	11.4±0.1	0.43
TPAP-2	9.4±0.4	11.1±0.3	12.6±0.1	0.42
TPAP-3	10.3±0.1	12.9±0.3	14.1±0.5	0.46
TPAP-4	10.7±0.4	13.1±0.3	14.5±0.2	0.44
TPAP-5	10.0±0.7	12.0±0.5	13.5±0.5	0.43
TPAP-6	9.2±0.4	11.1±0.3	12.9±0.3	0.41
TPAP-7	8.3±0.4	9.5±0.6	10.3±0.4	0.31
TPAP-8	7.3±0.4	8.6±0.5	9.1±0.4	0.32
TPAP-9	8.7±0.1	10.4±0.3	11.8±0.1	0.44
TPAP-10	12.7±0.4	13.9±0.3	15.6±0.4	0.30
TPAP-11	8.6±0.4	10.2±0.3	11.5±0.1	0.42
TPAP-12	8.1±0.4	9.7±0.2	10.7±0.3	0.40
TPAP-13	10.0±0.1	11.4±0.2	12.8±0.4	0.35
TPAPX-1	7.7±0.1	9.6±0.2	11.9±0.1	0.62
TPAPX-2	8.0±0.2	9.7±0.3	11.8±0.1	0.56
TPAPXL-1	7.0±0.2	8.7±0.2	9.7±0.1	0.48
TPAPXL-2	6.9±0.3	7.8±0.2	9.1±0.3	0.39
TPAPXL-3	6.9±0.2	8.7±0.1	10.5±0.2	0.61
TPAPSN-1	5.2±0.3	6.4±0.2	7.5±0.2	0.53

Cr_2O_3 decreased the burning rate compared to Fe_2O_3 (TPAP-2 and TPAP-9) and almost no change in burning rate exponent was obtained. The burning rate and pressure exponent values obtained by dual burning rate catalysts lied in the range obtained from individual catalysts. The increase in energetic plasticizer content and

equal decrease in the AP content resulted in lower burning rate, however the burning rate exponent did not change.

It is interesting to note that the partial replacement of AP with HMX, Al and PSAN reduced the burning rate. In addition, higher pressure exponent values were obtained which were greater than 0.5. These values are higher than the ones obtained for TPAP propellant samples.

The use of HMX in different particle sizes (TPAPX-1 and TPAPX-2) did not affect the regression rate of propellants, since the combustion wave structure of HMX composite propellants are different than that of AP composite propellants, although they are both considered to be heterogeneous. The luminous flame produced above the burning surface is almost attached to the burning surface of the AP propellant. On the other hand, the luminous flame front in the case of HMX propellants is far from the burning surface of HMX which is similar to the dark zone of double-base propellants [130]. This flame standoff distance decreases as the pressure and temperature increases which resulted in increase in the burning rate of the propellant.

In spite of this, the use of Al (TPAPXL-1, TPAPXL-2) reduced the pressure exponent and burning rates compared to TPEG-AP and TPEG-AP-HMX (TPAPX-1, TPAPX-2) based propellants. It is clear that Al increases the adiabatic flame temperature, and it is expected to increase the burning rate, but its combustion is so far from the surface that it does not influence much the regression rate of the propellant [131].

In the case of PSAN (TPAPSN-1), results showed that temperature near the surface temperature which has a strong effect on the burning rate of propellant of PSAN is low. This leads to an increase in the dark zone and decreases the burning rate [132]. Also, the sensitivities of the burning rate to pressure is increased as in the case studied.

4.4.3 Static Test Firings

Rocket test motor firings were performed to verify the calculated specific impulse and to determine the pressure exponent and the burning rates at different pressures. Results showed that the propellant had a burning rate of approximately 15 mm/s at 6.89 MPa with a pressure exponent that is below 0.5. There existed 15% deviation from the theoretical specific impulse. In practice, it has been found that the experimental values are, in general, 3 to 12% lower than those calculated, because the nozzle inefficiencies must be considered, and only a portion of this correction (perhaps 1 to 4%) is due to combustion inefficiencies. It is also depends on the propellant types and whether the engine is solid or liquid [133]. The variations of combustion pressure and thrust with time are shown in Figures 65 and 66, respectively. It is clear that the maximum thrust level tends to increase with an increase in combustion pressure. Results of the ballistic analysis are tabulated in Table 50.

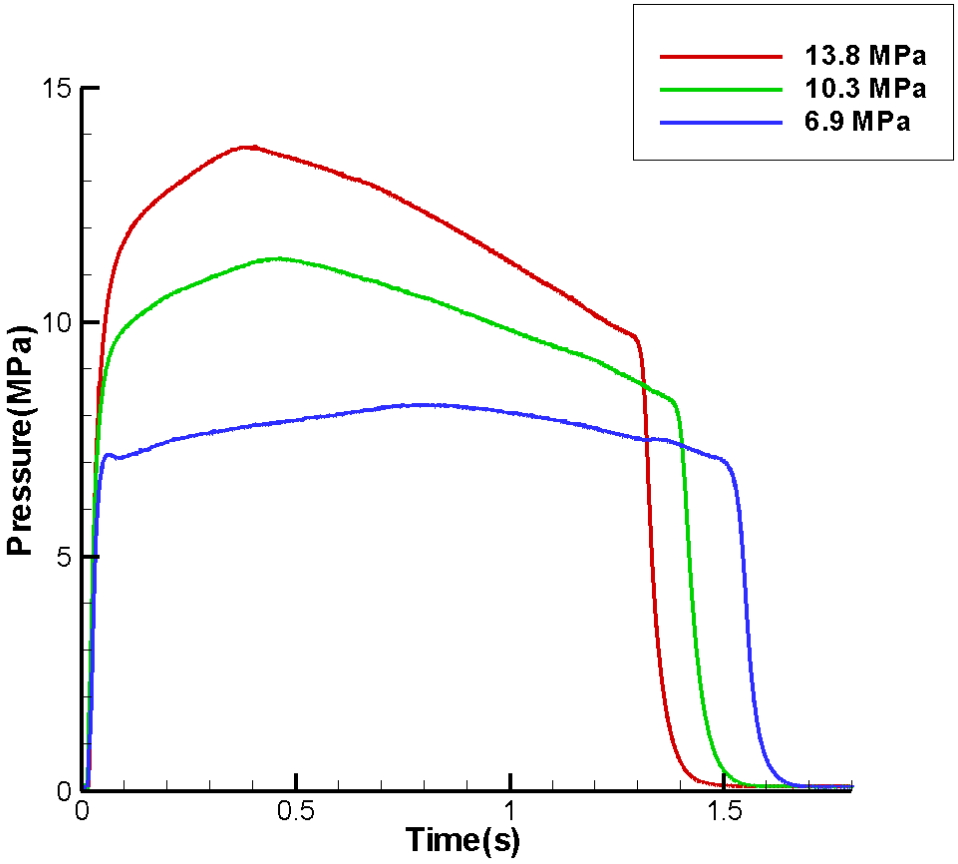

Figure 65 The variation of combustion pressure with time during test firings at three different pressures

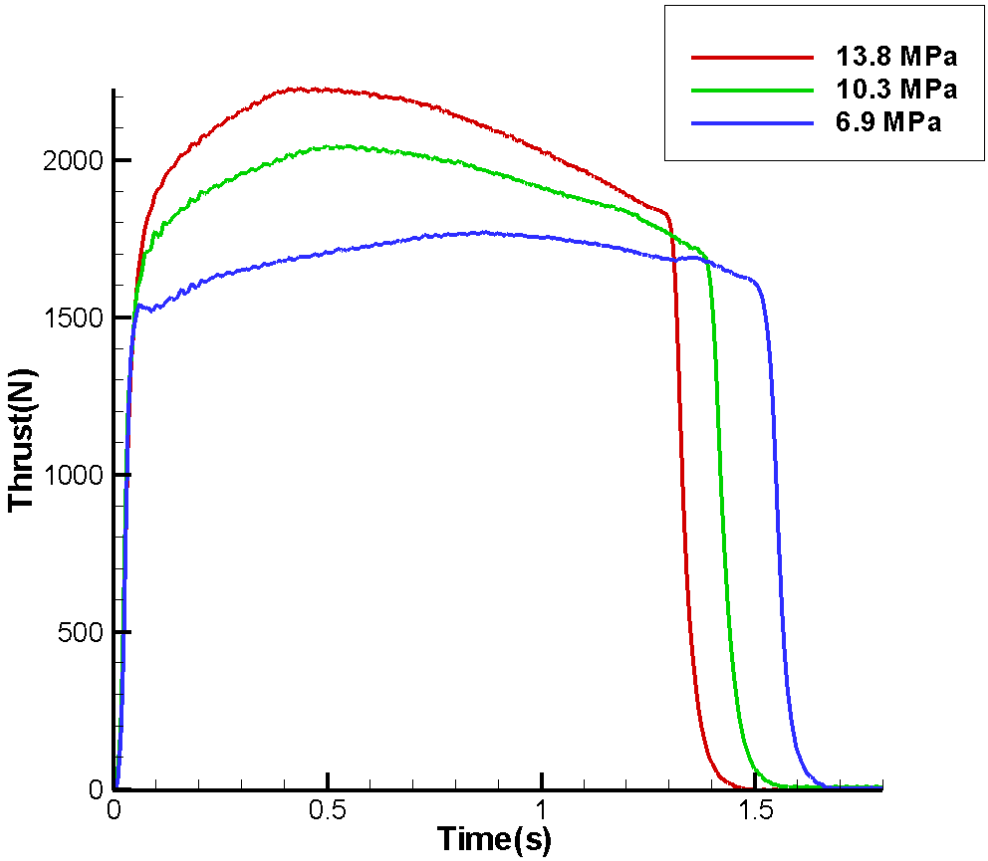

Figure 66 The variation of thrust with time during test firings at three different pressures

Table 50 Ballistic analysis results of propellant 091

Property	**Value**
Burning rate (mm/s) (@6.9 MPa, 20°C)	15.1
Burning rate (mm/s) (@10.3 MPa , 20°C)	17.3
Burning rate (mm/s) (@13.8 MPa, 20°C)	19.3
Pressure Exponent(n) (between 6.9-13.8 MPa)	0.35
Theoretical specific impulse (Pressure ratio 70/1, s)	254
Delivered specific impulse (Pressure ratio 70/1, s)	216

4.5 Safety and Signature Analysis

The hazard data of propellant samples and propellant 091 were interpreted by the impact and friction tests which are the generally accepted procedures in order to assess the hazard properties of a given explosive. Furthermore, signature classification is one of the important propellant design characteristics, since it represents the smoke classification of exhaust plume that should be preferably with reduced signature. The calculations were done according to STANAG 6016 standard. Impact and friction test results and signature classification of propellant samples and propellant 091 are shown in Table 51.

The propellants seemed to be friction sensitive compared to HTPB-AP based composite propellants whose friction sensitivities are generally greater than 170 N. It is known that double base or nitramine propellants have an impact sensitivity generally smaller than 4 J [134]. Almost all propellants had an impact sensitivity greater than that value except for TPAP-1. It is hard to discuss the effects of different formulations on the friction sensitivity, however, for impact sensitivities the following conclusions can be made. As the particle size of AP increased, the propellant became more sensitive to impact. In addition, the increase in modality or particle size distribution gave rise to the decrease in impact sensitivity. There was no significant effect of the use of different kinds of materials mixed in these propellant sets. The signature analysis of exhaust plume was theoretically done according to STANAG 6016 standard. It is seen that all the TPAP propellants can be classified as AC corresponding to a reduced smoke propellant. In addition, the AP-HMX based propellants, TPAPX-1 and TPAPX-2, seemed to be more friction sensitive than AP-HMX-Al and AP-PSAN type propellants. Furthermore, Al containing propellants like TPAPXL-1, TPAPXL-2, TPAPXL-3 can be classified as CC corresponding to a smokey propellant. Propellant 091 had impact and friction sensitivities of 6 J and 168 N, respectively, similar to the values obtained in HTPB-AP based propellants.

Table 51 The hazard data and signature classification of propellants

Sample No	Safety Data		Signature Classification	
	Impact Sensitivity (J)	**Friction Sensitivity (N)**	**Primary AGARDP**	**Secondary AGARDS**
TPAP-1	4	112	A	C
TPAP-2	6	80	A	C
TPAP-3	8	120	A	C
TPAP-4	14	112	A	C
TPAP-5	10	72	A	C
TPAP-6	10	96	A	C
TPAP-7	6	112	A	C
TPAP-8	12	112	A	C
TPAP-9	12	80	A	C
TPAP-10	8	112	A	C
TPAP-11	10	80	A	C
TPAP-12	8	96	A	C
TPAP-13	8	96	A	C
TPAPX-1	10	80	A	C
TPAPX-2	8	96	A	C
TPAPXL-1	8	168	C	C
TPAPXL-2	12	168	C	C
TPAPXL-3	8	144	C	C
TPAPSN-1	10	192	A	C
Propellant 091	6	168	A	C

4.6 Accelerated Aging Analysis

Isothermal microcalorimetry measurements were performed on three different types of propellants. One of them was the HTPE-AP based propellant (Propellant 091) developed in the thesis study. The others were the HTPB-AP (Propellant A) and HTPB-AP-Al (Propellant B) based propellants which were used as references. The sum of the heat flows which were produced during the aging of a propellant by chemical and physical reactions, was measured through two channels at a constant

temperature of 80°C for 10.6 days which is the time considered to be equivalent to at least 10 years of storage at 25°C. The maximum permissible heat flow limit was calculated as 114 μW/g which was derived from Arrhenius equation by assuming an activation energy of 120 kJ/mol. The details of calculations are given in a NATO standard [135].

STANAG 4582 describes a method for establishing the chemical stability of propellants for a minimum of 10 years when stored at 25 °C. Quantitative estimation of chemical stability of propellants is based on the calculation of the critical conditions of the time and temperature for thermal explosion. The main reactions during the aging of the propellants containing nitrate ester plasticizers are nitration and nitrosation of stabilizers used in the formulation. The temperature dependence of these reactions varies only in a small range, because they are controlled by the slower decomposition of nitro containing compound like BuNENA. For that reason, only one temperature heat flow method is sufficient to detect propellants if the following conditions are realized. First, the extrapolation of test duration to ambient temperature needs to be established in order to calculate a test duration that is at least equivalent to a thermal stress of 10 years of isothermal storage at 25°C. Second, the temperature of a propellant may rise considerably above the ambient temperature for short periods in the service lifetime. A heat flow limit that keeps the system nearly isothermal should be estimated by assuming the highest expected stress. The temperature depence of heat flow of single base propellant is shown in Figure 67. It was clear that there is a slope change around 60°C in Arrhenius plot. It is reasonable, therefore, setting the activation energy to 80 kJ/mole for temperatures below 60°C and to 120 kJ/mole above this temperature. It was assumed that the reactions were identical above and below 60 °C [136].

The heat flow curves of the three propellants are shown in Figure 68. It is clear that the HTPE based propellant behaved differently than the typical HTPB based propellants. The behavior of HTPE propellant resembles to that of a double base propellant which includes nitrate ester type energetic plasticizer. In our case, the nitrate ester energetic plasticizer was BuNENA. The heat flow curve of HTPE propellant can be described as follows. The sharp increase (1st maximum, A) in the heat flow at the beginning can be explained by the primary reaction of the propellant

with oxygen. Another contribution was probably due to the equilibration processes when the sample temperature was raised from ambient to 80°C. It was followed by constant decomposition (1st minimum, B) of the propellant accompanied by consumption of MNA which is a stabilizer used in the formulation. After the consumption of MNA stabilizer was completed, possibly the next stabilizer product N-NO-MNA was slowly decreasing which is shown as a second maximum, C. The constant decomposition rate of N-NO-MNA and the formation of N-NO-NO_2-MNA is shown as point D in the Figure. After point D, the autocatalytic reaction began to proceed and reached a maximum heat flow at point E [137]. For comparison, propellant A and propellant B were also tested and the heat flow curves are shown in Figure 68. They have both a negligible heat production which indicates a very high stability at 80°C. It is apparent that the heat flow behavior of HTPE propellant resembles to the one of double based propellant. Energetic plasticizers are used in these two types of propellants. This fact could be stated as the possible reason of higher heat flows.

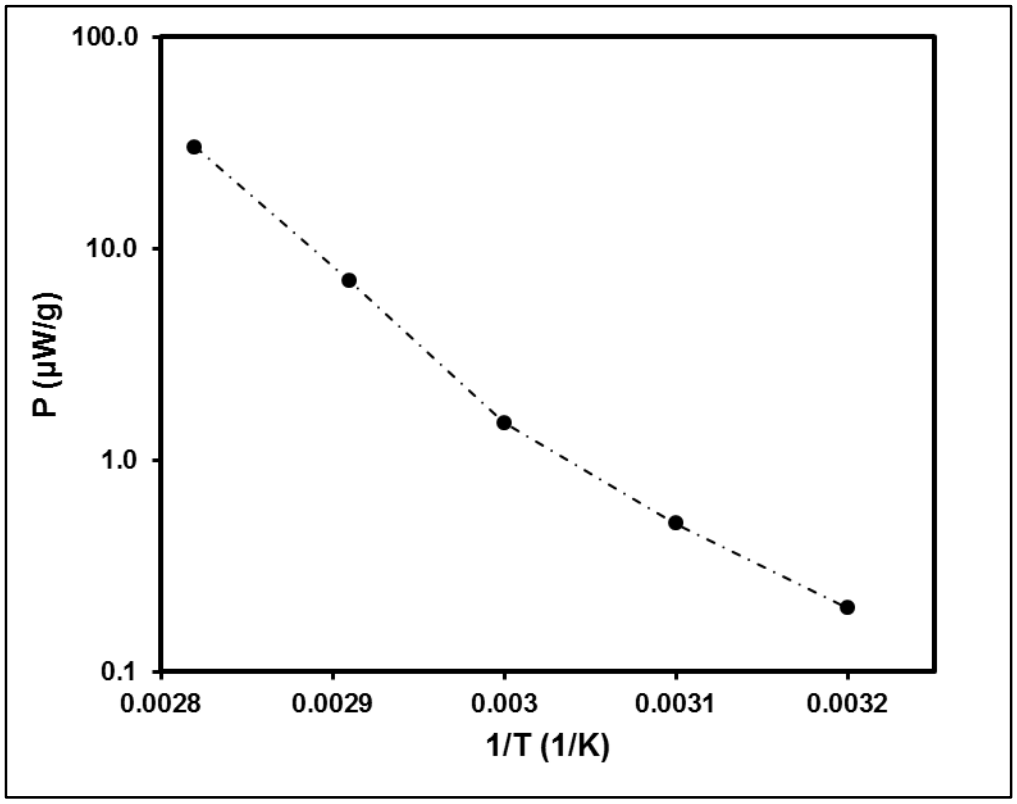

Figure 67 Temperature dependence of heat flow of a single base propellant [136].

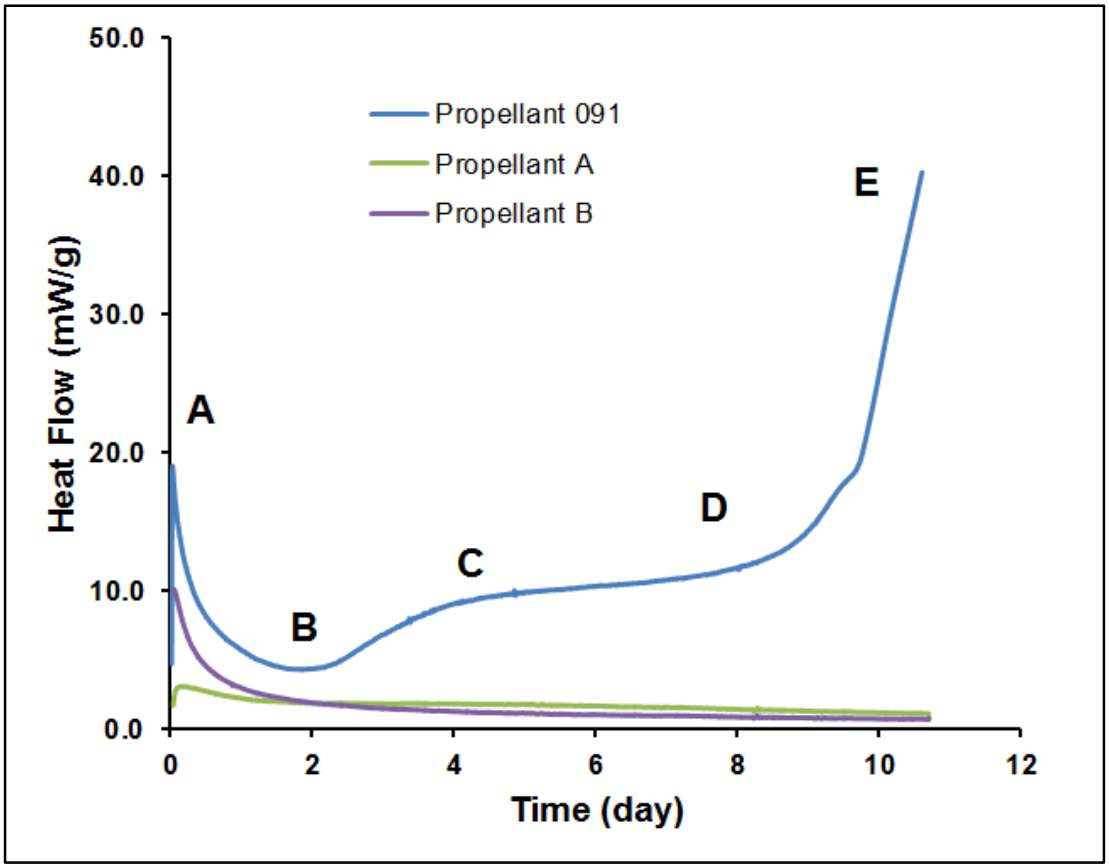

Figure 68 Heat flow measurement of propellants at 80°C for 10.6 days

The test duration of 10.6 days at 80°C can be determined as 114 µW/g of heat flow limit for 10 years of lifetime [135]. Figure 69 illustrates the heat flow curve of three different propellants with heat flow limit for 10 years of chemical stability. It is seen that the HTPE based propellant as well as propellants A and B were all below that limit. Therefore, HTPE based propellant 091 is said to be chemically stable for 10 years at 25°C storage condition.

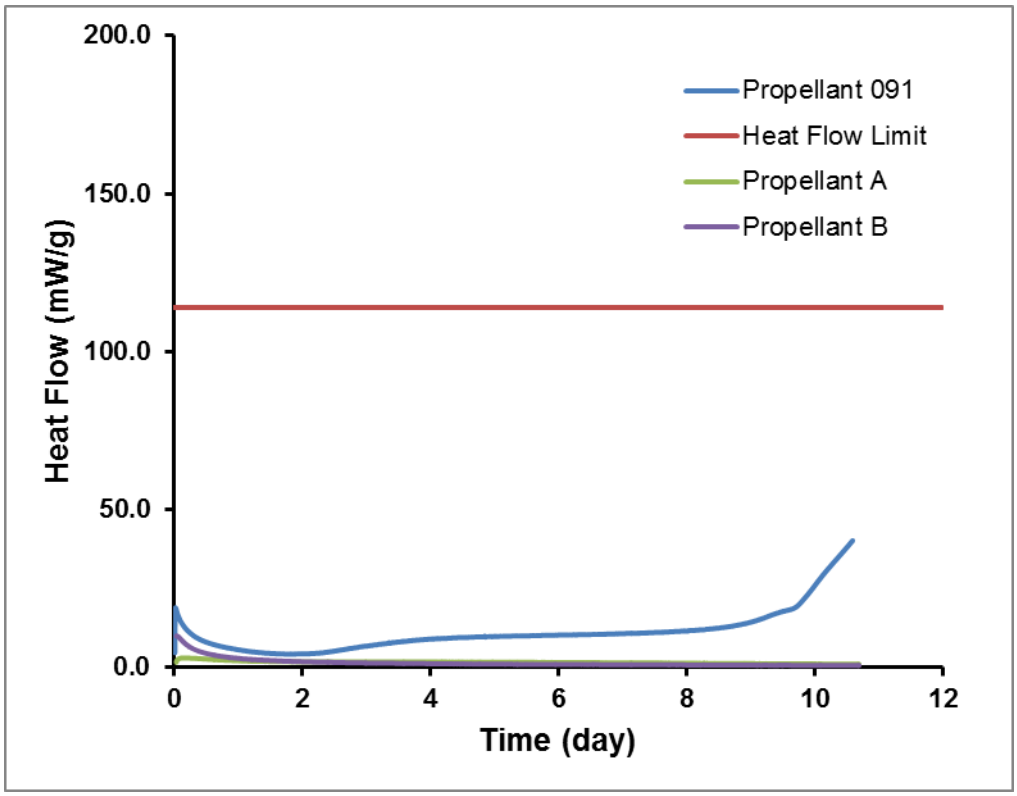

Figure 69 Heat flow measurement of propellants compared with heat flow limit at 80ºC for a storage of 10 years at 25ºC

CHAPTER 5

CONCLUSIONS

The study presented herein described the development of a new generation HTPE based composite propellant in order to meet the challenging insensitive munition requirement of solid rocket motors. This study consists of mainly three parts which can be noted as synthesis and characterization of polymeric network structures, synthesis and characterization of propellant samples, and then manufacturing of candidate HTPE based propellant and its characterization.

In the first part of this study, HTPE based networks were synthesized to investigate the structure-property relationships in segmented polyurethane structures. The best mechanical strengths were obtained with Desmodur type of isocyanates like Desmodur N-100 and Desmodur N-3200. They enabled the formation of organized structures leading to phase segregation which resulted from high intermolecular interactions between urethane linkages due to high hydrogen bonding through the nitrogen atoms on isocyanate and amide functionalities with TPEG and other polar urethane groups. The use of chain extenders BDO and TMP as diol and triol, respectively, also upgraded the mechanical properties such that tensile strength and Young's modulus increased. However, elongation at break values showed different tendencies with the increase in the chain extender content. The increase in BDO content also increased the elongation values, on the other hand, TMP decreased the elongation values. FeAA and DBTDL showed higher catalytic activities to urethane reactions in comparison to TPB and this resulted in higher tensile strength and Young's modulus. Structural analysis of polymeric network structures showed that the increase in NCO/OH ratio increased the hard segment content which led to lower extent of swelling and higher crosslinking for the samples prepared with Desmodur N-3200 in both aniline and THF. Polyurethane samples showed mainly three diffraction peaks which were resulted from the crystallization of the soft-segment phase at about 11^{o}, 20.5^{o} and 43^{o} degrees. The broad diffraction profiles may be resulted from the soft segment-hard segment phase mixing which could also led to

formation of small crystals ranging between 1.4-1.8 nm. It was realized that as the degree of crosslinking increased, crystal perfection decreased and the intensity of diffraction peak in X-Ray diagrams tended to decrease. Thermal characterization of polymeric network structures showed that identical intensity of molecular mobility was attained since identical T_g values were obtained in the DSC analysis. Based on the TGA analysis, two stage degradation processes at the temperatures of about 300^{o}C and 400^{o}C can be proposed for all the polymeric networks.

In the second part of this study, propellant samples were prepared by adding some energetic compounds into the HTPE-Desmodur N-3200 based elastomeric structure. The thermal analysis showed that the T_g of the propellant samples was only influenced by the type of energetic plasticizer. The particle size of AP, the modality of AP, the type of burning rate catalyst, the use of HMX, PSAN and Al as secondary energetic oxidizers and metallic fuel, respectively, did not affect the molecular mobility and crystallization nature of the propellants. In fact, the different energetic ingredients possessed different decomposition patterns. DSC analysis showed that propellant samples were completely decomposed between 350^{o}C and 400^{o}C by giving the highest exothermic response. The weight loss patterns depicted from TGA analysis mainly illustrated three stages of decomposition. The onset temperature of weight loss of stages were recorded approximately as 130^{o}C, 230^{o}C and 300^{o}C. Ballistic characterization of propellant samples were made by strand burner tests. They showed that the decrease in average particle size of AP led to increase in the burning rate. Further, the partial use of HMX, Al and PSAN instead of AP resulted in lower burning rates and pressure exponent values higher than 0.5 which is the value in the case of TPAP propellant samples. Fe_2O_3 seemed to be the best efficient burning rate enhancer giving high burning rate values. The propellant samples had friction sensitivities less than 170 N, the typical value for HTPB-AP based propellants. The impact sensitivities were determined generally to be greater than 4 J. It can be noted that as the particle size of AP increased, the propellant became more sensitive to impact. Further, the increase in modality or particle size distribution gave rise to lower impact sensitivity. Signature analysis was conducted theoretically and the propellants containing AP, HMX and PSAN were classified as AC corresponding to reduced smoke propellant. However, Al containing propellants were classified as CC corresponding to smokey propellant.

Last but not least, the third part of this study was focused on the manufacturing and characterization of candidate HTPE based propellant, namely propellant 091. The mechanical properties like ultimate tensile strength, elongation at break and Young's modulus decreased with increasing temperature. However, propellant 091 seemed to have good tensile strength and strain capability which proves the fact that the isocyanate to polyol content ratio was well adapted and the cohesive bonding of the energetic particles to binder matrix brought about high strain properties. The T_g of the propellant was determined approximately as -61.0^{o}C which is similar to the T_g of other propellant samples. Again, the DSC analysis showed that propellant 091 had thermal transitions similar to the TPAP propellant samples. Two exothermic transitions at 240^{o}C and 320^{o}C were recorded due to partial and complete combustion of AP, respectively. A three stage decomposition pattern can be proposed based on the weight loss measurement by TGA. The onset temperatures of decompositions can be stated approximately as 130^{o}C, 245^{o}C and 255^{o}C which are due to the thermolysis of BuNENA, and partial and complete decomposition of AP particles. The ballistic properties of propellant 091 were determined by static test firings conducted at room temperature. The burning rate was calculated as 15 mm/s at 6.89 MPa with a pressure exponent below 0.5 between the 6.9-13.8 MPa pressure range. The impact and friction sensitivities of propellant 091 were determined as 6 J and 168 N, respectively. Signature analysis showed that propellant 091 can be classified as AC reduced smoke propellant according to STANAG 6016. The accelerated aging study was conducted with heat flow calorimetry method. Results showed that propellant 091 was chemically stable for 10 years at 25^{o}C.

REFERENCES

[1] Oberth, A.E., Principles of Solid Propellant Development, CPIA, Publication 469, Chemical Propulsion Information Agency (CPIA), Johns Hopkins University, Laurel, Md., 1987

[2] Boyars, C., Klager, K., Proceedings of Symposium on Propellants Manufacture, Hazards and Testing, American Chemical Society, Washington, D.C., 1969

[3] Ciaremitari, D.A, Chan, M.L., High Performance Reduced-Smoke Propellant Formulations, CPIA Publication 580, Vol. 2, CPIA, Johns Hopkins University, 1992

[4] Wilson, T.D, New Solid Propellant Processing Techniques, CPTR 191-47, CPIA Publications, Johns Hopkins University, Laurel, Md., 1991

[5] STANAG 4439 JAIS (Edition 2)-Policy for Introduction and Assessment of Insensitive Munitions (IM), NATO Standardization Agency, 2009

[6] Military Standard, Hazard Assessment Tests for Non-Nuclear Ordnance, MIL-STD-2105B, 1994

[7] Tenden, S., Fossumstuen, K., IM Improvement of Rocket Motor by Composite Motor Case, RTO-MP-091, 2002

[8] NIMIC NEWSLETTER, Solid Rocket Propellant for Improved IM Response-Part 2 IM Propellant Examples, p: 2-4, 2003

[9] STANAG 4439, Policy for Introduction, Assessment and Testing for Insensitive Munitions (MURAT), Edition 1, North Atlantic Treaty Organization, 1998

[10] Comfort, T., Shanholtz, C. and Fletcher, G., Progress in HTPE Propellants, NDIA 39th Annual Gun & Ammunition/Missiles & Rocket Conference, Baltimore, MD, USA, 2004

[11] Davenas, A., Development of Modern Solid Propellants, J. Propul. Power, Vol 19 No: 6, p: 1108-1128, 2003

[12] Sutton, K.K., Summerfield, M., Fundamentals of Solid Propellant Combustion, Vol 90, Progress in Astronautics and Aeronautics, American Institute of Aeronautics and Astronautics Inc, New York, 1984

[13] Cardarelli, F., A Concise Desktop Reference Materials Handbook, 2nd Edition, Springer-Verlag, p: 1011-1013, 2008

[14] Klein, N., Liquid Propellants for Use in Guns, Gun Propulsion Technology, Vol. 109, Progress in Astronautics and Aeronautics, AIAA, Washington DC, Chapter 14, p: 473-497, 1988

[15] Volk, F., Thermodynamic Performance Data and Selection Criteria for Hypergolic Bipropellants and Monopropellants, Fraunhofer-Institut für Chemische Technologie, Rept. B5.02, Pfinzhal-Berghausen, Germany, 1983

[16] Turner, M. J. L., Rocket and Spacecraft Propulsion Principles, Practice and New Developments, 3rd Edition, Springer-Berlin, p: 62, 2009

[17] Turner, M. J. L., Rocket and Spacecraft Propulsion Principles, Practice and New Developments, 3rd Edition, Springer-Berlin, p: 109-111, 2009

[18] Agrawal, J.P., High Energy Materials, Propellants Explosives and Pyrotechnics, 1st Edition, Wiley-VCH Verlag, Weinheim, p: 213-215, 2010

[19] Gerard, A.B., Neidert J.B., Pledger K.L., High Performance Propellant Development and Demonstration, 41st AIAA/ASME/SAE/ASEE Joint Propulsion Conference&Exhibit, 2005

[20] Klager, K., Zimmerman, G.A., Steady Burning Rate and Affecting Factors: Experimental Results, Vol 143, Chapter 3, Progress in Astronautics and Aeronautics, AIAA, USA, 1992

[21] Sutton, G.P., Biblarz, O., Rocket Propulsion Elements, Wiley, New York, NY, USA, 7th edition, 2001

[22] Barrère, M., Jaumotte, A., Fraeijs De Veubeke, B., Vandenkerckhove, J., Rocket Propulsion, Elsevier Publishing Company, Amsterdam, Netherlands, 1960

[23] Crawford, B.L.Jr., Huggett, C., Daniels, F., Wilfong, R.E., Direct Determination of Burning Rates of Propellant Powders. Anal. Chem. , 19(9): p: 630-633, 1947

[24] Hessler, R.O., An Analysis of Burning Rate Round-Robin Data, Technical Report, JANNAF Combustion Meeting, West Palm Beach, FL, 27-31 October, 1997

[25] Timnat,Y.M., Advanced Chemical Rocket Propulsion, Academic Press, London, UK, 1987

[26] Kubota, N., Survey of Rocket Propellants and Their Combustion Characteristics, Chapter 1, Vol 90, Progress in Astronautics and Aeronautics, AIAA, USA, 1984

[27] Cruise, D.R., Theoretical Computations of Equilibrium Compositions, Thermodynamic Properties and Performance Characteristics of Propellant Systems, Technical Publ. 6037, Naval Weapons Center, China Lake, CA, 1979

[28] Chan, M.L., Reed Jr., R., Ciaramitaro, D.A., Advances in Solid Propellant Formulations, Vol 185, Chapter 1.7, Progress in Astronautics and Aeronautics, AIAA, USA, 2000

[29] Sarner, S.P., Propellant Chemistry, Reinholt, New York, 1966

[30] Siegel, B., Schieler, L., Energetics of Propellant Chemistry, Wiley, New York, 1964

[31] Turner, M. J. L., Rocket and Spacecraft Propulsion Principles, Practice and New Developments, 3rd Edition, Springer-Berlin, p: 57, 2009

[32] Gordon, S., McBride, B.J., Computer Program for Calculation of Complex Chemical Equilibirum Compositions, Rocket Performance, NASA Lewis Research Center, SP-273, 1971

[33] Volk, F., Bathelt, H., Computational Program in Basic Fortran IV for Performing Calculation of Rocket Propellants, ICT-Report 9/1970

[34] Volk, F., Bathelt, H., Application of the Virial Equation of State in Calculating Interior Ballistic Quantities, Propellants and Explosives 1, 1976

[35] Rossi, M.J., Bottaro, J.C., McMillen, D.F. Thermal Decomposition of the New Material Ammonium Dinitramide in Relation to Nitramide and Ammonium Nitrate, J. Chem. Kinetics, 25, p: 549-570, 1993

[36] Brill, T.B., Brush, P.J., Patil, D.G., Thermal Decomposition of Energetic Materials 58. Chemistry of Ammonium Nitrate and Ammonium Dinitramide Near the Burning Surface Temperature, Combust. Flame, 91, p: 178-186, 1992

[37] Akhavan, J., Explosives and Propellants, Kirk Othmer Encyclopedia of Chemical Technology, John Wiley&Sons, Vol 10, p: 719-744, 2004

[38] Boileau, J., Fauquignon, C., Hueber, B., Meyer, H.H., Explosives, Ullman's Encyclopedia of Industrial Chemistry, Wiley –VCH, Vol 13, p: 621-654, 2012

[39] Kirk Othmer Encyclopedia of Chemical Technology, Vol 2, 4th Ed. John Wiley&Sons, p: 698-705, 1992

[40] Zapp, K.H., Wostbrock, K.H., Schafer, M., Sato, K., Seiter, H., Zwick, W., Creutziger, R., Leiter, H., Ammonium Compounds, Ullmann's Encyclopedia of Industrial Chemistry, Vol A2, 5th Edn., VCH, Germany, p: 243-252, 1989

[41] Oommen, C., Jain, S.R., Ammonium Nitrate: A Promising Rocket Propellant Oxidizer, J. Hazard. Mater., A67, p: 253-281, 1999

[42] Hendricks, S.B., Posnjak, E., Kracek, F.C., The Variation of the Crystal Structure of Ammonium Nitrate with Temperature, J. Am. Chem. Soc., Vol 54, p: 2766-2786, 1932

[43] Müller, W., Über Die Anderung des Umwandlungspunktes von Ammonium Nitrat bei 32^{o}C durch Zusatz von Kaliumnitrat, Z. Phys. Chem., 31, p: 354-359, 1962

[44] Campbell, A.N., Campbell J.R., The Effect of a Foreign Substance on the Transition NH_4NO_3 IV - NH_4NO_3 III, Can. J. Res., Vol 24, p: 93-108, 1946

[45] Engel, W., Eisenreich, N., Thermal Analysis of the System $NH_4NO_3/CsNO_3$ by Means of X-ray Diffraction, Thermochim. Acta, 85, p 35-38, 1985

[46] Engel, W. Beitrang zur Phasenstabilisierung von Ammoniumnitrat, Explosivstoffe, Vol 21, p: 9-13, 1973

[47] Klager, K. Polyurethanes, the Most Versatile Binder for Solid Composite Propellants, 20th AIAA/SAE/ASME Joint Propulsion Conference, AIAA-84-1239, 1984

[48] Jain, S.R., Sekkar, V., Krishnamurthy, V.N., Mechanical and Swelling Properties of HTPB-based Copolyurethane Networks, J. Appl. Polym. Sci. 48, p: 1515-1523, 1993

[49] Fischer, M., Sharp, M. Advances in Rocket Performance Life and Disposal, conference held in Aalborg, Denmark, RTO-MP-091, 2002

[50] Goleniewsky, J.R., Roberts, J.A., Solid Propellant with Non-Crystalline Polyether/Energetic Plasticizer Binder, US Patent 5,783,769, 1998

[51] Jain, S.R., Solid Propellant Binders, J. Sci. Ind. Res., Vol 6, p: 899-911, 2002

[52] Borman, S., Advanced Energetic Materials for Military and Space Applications, Chem. Eng. News., p: 18-21, 1994

[53] Sahu, S.K., Chavan, M.Y., Thakur J.V., Kulkarni, S.G., Panda, S.P., Performance Evaluation of Glycidyl Azide Polymers as Integrated Ram Rocket Propellants, Proc. Second Int. High Ener. Mater. Conf. Exhibit, p: 126-130, 1998

[54] Derr, R.L., Bulletin of the 13th JANNAF Meeting, CPIA Publication 281, Vol. 1, CPIA, Johns Hopkins University, Laurel, Md., p: 225, 1976

[55] Kuentzmann, P., Specific Impulse Losses of Metallized Solid Propellants, FTD-NC-23-2717-74, Air Force Foreign Technology Division, Wright Patterson Air Force Base, Dayton, Ohio, 1974

[56] Rhein, R.A. Energetic Polymers and Plasticizers, Naval Weapons Center, China Lake , NWC TP 6410, 1983

[57] Hori, K., Iwama, A., Fukuda, T., Enhancement of Matrix - Filler in HMX/AP/HTPB Composite Propellant, Proc.18th Intl Ann. Conf. ICT, Karlsruhe, Germany, p: 1-13, 1987

[58] Wallace, I.A., Ambient Temperature Mix, Cast, and Cure Composite Propellant Formulations, US Patent 5,472,532, 1995

[59] Agrawal, J.P., Chhabra, J.S., Athar, J., Singh, H., Comparative Study of Various Antioxidants for HTPB Prepolymer, Plast. Rub. Compos. Process. Appl., 20, p: 305-310, 1993

[60] Yang, Y., Yu, X., Wang, J., Wang, Y., Effect of the Dispersibility of Nano-CuO Catalyst on Heat Releasing of AP/HTPB Propellant, J. Nanomater., p: 1-5, 2011

[61] Vuga, S.M., Effects of Liquid Burn Rate Catalysts on Rheological Properties of High Energy Composite Propellants, Prop. Explos. Pyrotech., 16, p: 293–298, 1991

[62] Saunders, J.H., Fritsch, K.C., Polyurethane, Chemistry and Technology, Interscience Publishers, Part 11, p: 772, 1962

[63] Adam, N., Avar, G., Blankenheim, H., Polyurethanes, Ullmanns Encyclopedia of Industrial Chemistry, Vol 29, p: 545-604, 2012

[64] Blomshield, F.S., Crump, J.E., Mathes, H.B., Beckstead, M.W., Stability Testing of Full Scale Tactical Motors, 27th AIAA/ASME/SAE/ASEE Joint Propulsion Conference&Exhibit, AIAA-91-1954, 1991

[65] Blomshield, F.S., Stalnaker, R.A., Beckstead, M.W., Combustion Instability Additive Investigation, 35th AIAA/ASME/SAE/ASEE Joint Propulsion Conference&Exhibit, AIAA-99-2226, 1999

[66] Thiele, L., Isocyanatreaktionen und Katalyse in der Polyurethanchemie Fortschrittsbericht, Acta Polym. 30, 323, 1979

[67] Dobbins, T.O., Thermodynamics of Rocket Propulsion and Theoretical Evaluation of Some Prototype Propellant Combinations Report, WADS-TR-59-757, WADC, Air Research and Development Command, 1959

[68] Gordon, L.J., et.al, Calculation, Measurement, Extrapolation and Correlation of Solid Propellant Specific Impulse, Proceedings of the Fifth Meeting of the JANAF-NASA Thermochemical Panel, 51, 1967

[69] Brown, R.S., Anderson, R., Shannon, L.J., Ignition and Combustion of Solid Propellants, Advances in Chemical Engineering, Vol 7, Academic Press, 1968

[70] Kelley, F.N., Solid Propellant Mechanical Property Testing, Failure Criteria and Aging, Propellant Manufacture Hazards and Testing, Advances in Chemistry Series 88, American Chemical Society, Washington, DC, 1969

[71] Thrasher, D.I., State of the Art of Solid Propellant Rocket Motor Grain Design in the United States, Design Methods in Solid Propellant Rocket Motors, AGARD Lecture Series 150, Revised Version, 1988

[72] ICRPG Solid Propellant Mechanical Behavior Manual Sec. 4.3.2. Constant Strain Rate Uniaxial Tensile Test Standart, CPIA Publication 21, 1967

[73] Jain, S.R., Sekkar, V., Krishnamurthy, V.N., Mechanical and Swelling Properties HTPB-Based Copolyurethane Networks, J. Appl. Polym. Sci., Vol. 48, p: 1515-1523, 1993

[74] Judge, M.D., An Investigation of Composite Propellant Accelerated Ageing Mechanisms and Kinetics, Prop. Explos. Pyrotech., 28, No. 3, 2003

[75] Mark, J. E., Experimental Determination of Crosslink Densities, Rubber Chem. Technol., 55, p: 762-768, 1982

[76] Eisele, U. Introduction to Polymer Physics; Springer-Verlag: Berlin, 1990

[77] Lobillard, C.L., Dowler, W.L., Shafer, J.I., Udlock, D.E., Heat Sterilizable Solid Propellant Technical Report, 32-1187, JPL-CalTech, 1967

[78] Ticmanis, U., Wilker, S., Pantel, G., Guillaume, P., Balès, C., Van der Meer, N., Principles of a STANAG for the Estimation of the Chemical Stability of Propellants by Heat Flow Calorimetry, Proc. Int Annu. Conf. ICT 31, 2, 2000

[79] Anon.: ICRPG Solid Propellant Mechanical Behavior Manual, CPIA Publ. 21, 1963

[80] Joint Technical Bulletin, Department of Defense Ammunition and Explosives Hazard Classification Procedures, TB 700-2 NAVSEAINST 8020.8B TO 11A-1-47 DLAR 8220.1, US Army, 1998

[81] Groenewoud, W.M., Characterisation of Polymers by Thermal Analysis, Elsevier, 2001

[82] Pask, J.A., Warner, M.F., Differential Thermal Analysis Methods and Techniques, Techical Report, Series No: 18, Issue No: 5, 1953

[83] Wunderlich, B., Thermal Analysis, Academic Press Inc., New York, 1990

[84] Mathot, V.B.F., Calorimetry and Thermal Analysis of Polymers, Hanser Publishers, Munich, 1994

[85] Rocco, J.A.F.F., Lima, J.E.S., Frutuoso, A.G., Iha, K., Ionashiro, M., Matos, J.R., Suarez-Iha, M.E.V., Thermal Degredation of a Composite Solid Propellant Examined by DSC, J. Therm. Anal. Calorim., Vol. 75, p: 551–557, 2004

[86] Department of Defense, MIL-STD-650, Impact Sensitivity Test, U.S. Bureau of Mines (BoM) Impact Apparatus Method T 505.1, Department of Defense, USA. 1962

[87] Kohler, J., Meyer, R., Explosives, 4th edn. Wiley-VCH Verlag GmbH, Weinheim, Germany, 1993

[88] Poschl, H., Seidel, H., Chem. Tech., 18 (9), 565, 1967

[89] MIL-STD-650, Explosive Sampling, Inspection and Testing, Friction Sensitivity Test Method T 510.1 Department of Defense, 1987

[90] Trumman, H., Krueger, G., Pfeil, N., Safety Characteristic Data and Thermochemistry of Ternary Pyrotechnic Systems, Proc. 13th Intl Pyrotechnics Seminar, USA, p: 785-804, 1988

[91] NATO Standardization Agency, STANAG 4487, Explosives, Friction Sensitivity Tests, Edition 2, 2009

[92] NATO Standardization Agency, STANAG 6016, Solid Propellant Smoke Classification, Edition 1, 1994

[93] Greer, C.L., Jr, Thorn, L.B., Wharton, W.W., Signature Suppression and Evaluation in Static Motors, JANNAF Propulsion Meeting, San Diego, California, 1985

[94] Oliver, R.C., Smokeless Solid Propellants: an Overview, Institute for Defense Analysis Alexandria, Virginia, Research Paper, p: 46-47, 1979

[95] Boggs, T., Propellants to Meet Insensitive Munitions Requirements; Naval Air Warfare Center Weapons Division, China Lake, CA, USA; AIAA Solid Rocket Technical Committee Lecture Series, Reno, Nevada, USA, 1994

[96] Miller, R., Research on New Energetic Materials; Department of the Navy (USA), ONR; International Defense & Technologie, 1994

[97] Stokes, B., Operational Hazards and Solution Trade-Offs; NIMIC, Brussels, Belgium; Presented in Session 1 (Insensitive/Low Hazard Rocket Propellants) of the AIAA Solid Rocket Technical Committee Lecture Series, Reno, Nevada, USA, 1994

[98] NIMIC NEWSLETTER, Solid Rocket Propellant for Improved IM Response-Part 2 IM Propellant Examples, p: 2-4, 2003

[99] Hartman, K.O., Insensitive Munitions Technology for Small Rocket Motors, Small Rockets Motors and Gas Generator for Land, Sea and Air Launched Weapons, RTO Meeting Proceedings 23, RTA, Neully sur Seine, France, 2000

[100] Fossumstuen, K., Raudsandmoen G., IM Evaluation of the Evolved Sea Sparrow Missile Propulsion Section; NAMMO Raufoss AS, Raufoss, Norway; K.

Hartman & T. Comfort, Alliant Techsystems, Allegany Ballistics Laboratory, Rocket Center, WV, USA, 1999

[101] Hartman, K., Insensitive Munitions Technology for Small Rocket Motors; Alliant Techsystems, Allegany Ballistics Laboratory, Rocket Center, WV, USA; RTO Symposium on Small Rocket Motors and Gas Generators for Land, Sea and Air Launched Weapons, Corfu, Greece, 1999

[102] Flory, P.J., Rehner, J., Statistical Mechanics of Crosslinked Polymer Networks II. Swelling, J. Chem. Phys., 11, 521, 1943

[103] Herman P. H., Weidinger A., On the Determination of the Crystalline Fraction of Polyethylenes from X-ray Diffraction, Makromol. Chem, 24, 44, 1961

[104]MIL-STD-286C, Military Standard, Propellants, Solid: Sampling, Examination, and Testing, 1991

[105] Prisacariu, C., Polyurethane Elastomers from Morphology to Mechanical Aspects, Springer Verlag, 2011

[106] Fedors. R.F., A Method for Estimating Both the Solubility Parameters and Molar Volumes of Liquids, Polym. Eng. Sci. 147. M(2), 1974

[107] Haponiuk, J. T., Strankowski, M., Lazarewicz, T., DSC Study of Polyurethanes Obtained from 4, 4'-Bis (10-Hydroxydecaoxy) biphenyl, J. Therm. Anal. Cal. 74, 609, 2003

[108] Hepburn, C., Polyurethane Elastomer, Applied Science Publishers, London, p: 4, 1982

[109] Luo, S. G., Tan, H. M., Zhang J. G., Wu, Y. J., Pei, F. K., Meng, X. H., Catalytic Mechanisms of Triphenyl Bismuth, Dibutyltin Dilaurate, and Their Combination in Polyurethane-Forming Reaction, J. Appl. Polym. Sci., p: 1217-1225, 1997

[110] Reed, R.Jr., Chan, M.L., Propellant Binders Cure Catalyst, U.S. Pat. 4,379,903, 1983

[111] Belgacem, M.N., Quillerou, J., Gandini, A. Rivero, J., Roux, G., Urethanes and Polyurethanes Bearing Furan moieties 2. Comparative Kinetics and Mechanism of the Formation of Furanic and Other Monourethanes, Eur. Polym. J., 25, p: 1125, 1989

[112] Lazurkin, J.S., Cold-Drawing of Glass-Like and Crystalline Polymers, J. Polym. Sci. 30, p: 595-604, 1958

[113] Landsem, E., Jensen, T.L., Hansen, F.K., Unneberg, E., Kristensen, T.E., Neutral Polymeric Bonding Agents (NPBA) and Their Use in Smokeless Composite Rocket Propellants Based On HMX-GAP-Bunena, Prop. Explos. Pyrotech. 37, p: 581-591, 2012

[114] Siegmann, A., Cohen, D., Narkis, M., Polyurethane Elastomers Containing Polybutadiene and Aliphatic Diols: Structure-Property Relationships, Polym. Eng. Sci., Vol 27, p: 1187-1194, 1987

[115] Oikawa, H., Murakami, K., Some Comments on the Swelling Mechanism of Rubber Vulcanizates, Rubber Chem. Technol., 60, p: 579-591, 1987

[116] Marsh, H.E. NASA Report No. NASA-CR-158788; Jet Propulsion Laboratory, California Institute of Technology: Pasadena, California, 1979

[117] Chang, K.K., Soo, B.B., Jae, R.A., In, J.C., Structure Property Relationships of Hydroxyterminated Polyether Based Polyurethane Network, Polym. Bull. , 61, p: 225-233, 2008

[118] Y. Minoura, S. Yamashita, H. Okamoto, T. Matsuo, M. Igawa, and S. I. Kohmoto, Crosslinking and Mechanical Property of Liquid Rubber I. Curative Effect of Aliphatic Diols, J. Appl. Polym. Sci., 22, p: 1817, 1978

[119] Kim, B.K., Lee, S.Y., Xu, M., Polyurethanes Having Shape Memory Effects, Polymer, 37, 5781-5793, 1996

[120] Bednarek, M., Kubisa, P., Cationic Copolymerization of Tetrahydrofuran with Ethylene Oxide in the Presence of Diol: Composition, Microstructure, and Properties of Copolymers, J. Polym. Sci., Part A: Polym. Chem, Vol. 37, p: 3455-3463, 1999

[121] Li, F., Hou, J., Zhu, W., Zhang, X., Xu, M., Luo, X., Ma, D., Kim, B. K., Crystallinity and Morphology of Segmented Polyurethanes with Different Soft-Segment Length, J. Appl. Polym. Sci., 62, p: 631-638, 1996

[122] Koberstein, J.T., Galambos, A.F., Leung, L.M., Compression-Molded Polyurethane Block Copolymers. 1. Microdomain Morphology and Thermomechanical Properties, Macromol. 25(23), p: 6195-6204, 1992

[123] Abdullah, M., Gholamian, F., Zarei, A.R., Noncrystalline Binder Based Composite Propellant, ISRN Aerospace Engineering, p: 1-6, 2013

[124] Patil, P.R., Krishnamurthy, V.N., Joshi, S.S., Differential Scanning Calorimetric Study of HTPB Based Composite Propellants in Presence of Nano Ferric Oxide, Prop. Explos. Pyrotech. 31, p: 442-446, 2006

[125] Fedoroff, B.T., Sheffield, O.E., Kaye, S.M., Encyclopedia of Explosives and Related Items Picatinny Arsenal, Dover, New Jersey, Vol 2, 1962

[126] Krol, P., Synthesis Methods, Chemical Structures and Phase Structures of Linear Polyurethanes: Properties and Applications of Linear Polyurethanes in Polyurethane Elastomers, Copolymers and Ionomers, Progress in Materials Science 52(6), p: 915, 2007

[127] STANAG 4556 Explosives: Vacuum Stability Test

[128] Boggs, T.L., The Thermal Behavior of Cyclotrimethylenetrinitramine(RDX) and Cyclotetramethylenetetranitramine(HMX), Fundamentals of Solid Propellant

Combustion, edited by Kuo, K.K., and Summerfield, M., Progress in Astronautics and Aeronautics, Vol 90, Chapter 3, AIAA, Newyork, 1984

[129] Komarov, F., Catalysis and Inhibition of the Combustion of Ammonium Perchlorate Based Solid Propellants, Combust. Explos., Shock Waves, Vol. 35, No. 6, 1999

[130] Kubota, N., Combustion Mechanisms of Nitramine Composite Propellants, 18th Symposium on Combustion, The Combustion Institute, Pittsburgh, p 187-194, 1981

[131] Price, E.W., Sigman, R.K., Sambamurthi, J.K., Park, C.J., Behavior of Aluminum in Solid Propellant Combustion, School of Aerospace Engineering, Georgia Inst. of Technology, Atlanta, 1982

[132] Dong, C.S., Wang, Y., Study of the Combustion Wave Structure of Solid Propellants with W-Re Microthermocouple Measuring Temperature Technique, Explos. Prop., No. 2, p: 22-26, 1995

[133] NASA-SP 8064-Space Vehicle Design Criteria, Solid Propellant Selection and Characterization, p: 20-25, 1971

[134] Menke, K., Eisele, S., Rocket Propellants with Reduced Smoke and High Burning Rates, Prop. Explos. Pyrotech. 22, p: 112-119, 1997

[135] STANAG 4582, Explosives, Nitrocellulose Based Propellants, Stability test Procedure and Requirements Using Heat Flow Calorimeter, Edition 1, 2004

[136] Guillaume, P., Rat, M., Wilker, S., Pantel, G., Microcalorimetric and Chemical Studies of Propellants, Proc. Int Annu. Conf. ICT 29, 133, 1998

[137] Fletcher, W.G., Comfort, T.F., Updates on HTPE Propellant Service Life, IMEMTS Bristol Conference, 2006

APPENDIX A

MECHANICAL TEST RESULTS

Table A.1 Tensile strength data of non-energetic polyurethane network structures

Composition	Ultimate tensile strength (MPa)	Std. Dev.
TP-N100-R0.8	0.17	0.01
TP-N100-R1.0	0.39	0.04
TP-N100-R1.2	0.56	0.06
TP-N3200-R0.8	0.19	0.02
TP-N3200-R1.0	0.46	0.05
TP-N3200-R1.2	0.80	0.03
TP-N100 IPDI(1:1)-R1.0	0.70	0.06
TP-N100 IPDI(2:1)-R1.0	0.65	0.04
TP-N3200 IPDI(2:1)-R1.0	0.59	0.02
TP-N3200-0.2BDO	0.94	0.06
TP-N3200-0.2TMP	0.96	0.03
TP-N3200-0.4BDO	1.01	0.07
TP-N3200-0.4TMP	0.89	0.09
TP-N3200-0.8BDO	1.25	0.07
TP-N3200-0.8TMP	2.04	0.18
TP-N3200-BDO-0.01TPB	0.63	0.10
TP-N3200-BDO-0.02TPB	0.66	0.02
TP-N3200-BDO-0.04TPB	0.54	0.05
TP-N3200-BDO-0.01FeAA	1.17	0.08
TP-N3200-BDO-0.01DBTDL	0.84	0.03

Table A.2 Percent elongation at break data of non-energetic polyurethane network structures

Composition	Elongation at break (%)	Std. Dev.
TP-N100-R0.8	74.28	6.69
TP-N100-R1.0	53.36	8.78
TP-N100-R1.2	51.09	9.54
TP-N3200-R0.8	88.34	8.76
TP-N3200-R1.0	69.59	4.56
TP-N3200-R1.2	54.40	3.68
TP-N100 IPDI(1:1)-R1.0	1180.00	91.00
TP-N100 IPDI(2:1)-R1.0	796.23	82.00
TP-N3200 IPDI(2:1)-R1.0	1171.10	218.17
TP-N3200-0.2BDO	842.00	23.66
TP-N3200-0.2TMP	1044.10	54.49
TP-N3200-0.4BDO	1021.50	111.08
TP-N3200-0.4TMP	991.30	238.47
TP-N3200-0.8BDO	1557.33	78.82
TP-N3200-0.8TMP	671.53	48.26
TP-N3200-BDO-0.01TPB	107.48	21.70
TP-N3200-BDO-0.02TPB	91.31	4.64
TP-N3200-BDO-0.04TPB	73.39	21.27
TP-N3200-BDO-0.01FeAA	64.89	5.19
TP-N3200-BDO-0.01DBTDL	69.90	2.15

Table A.3 Young's modulus data of non-energetic polyurethane network structures

Composition	Young's modulus (MPa)	Std. Dev.
TP-N100-R0.8	0.40	0.06
TP-N100-R1.0	1.03	0.16
TP-N100-R1.2	1.60	0.20
TP-N3200-R0.8	0.42	0.00
TP-N3200-R1.0	1.03	0.12
TP-N3200-R1.2	2.11	0.15
TP-N100 IPDI(1:1)-R1.0	1.25	0.11
TP-N100 IPDI(2:1)-R1.0	1.15	0.07
TP-N3200 IPDI(2:1)-R1.0	1.05	0.04
TP-N3200-0.2BDO	1.67	0.11
TP-N3200-0.2TMP	1.71	0.06
TP-N3200-0.4BDO	1.80	0.12
TP-N3200-0.4TMP	1.60	0.16
TP-N3200-0.8BDO	2.25	0.13
TP-N3200-0.8TMP	3.68	0.33
TP-N3200-BDO-0.01TPB	1.14	0.18
TP-N3200-BDO-0.02TPB	1.19	0.03
TP-N3200-BDO-0.04TPB	0.97	0.08
TP-N3200-BDO-0.01FeAA	2.10	0.05
TP-N3200-BDO-0.01DBTDL	1.50	0.01

Table A.4 Mechanical properties test results of propellant 091 at three different temperatures

Property	-40°C	Std. Dev.	25°C	Std. Dev.	60°C	Std. Dev.
Ultimate Tensile Strength (MPa)	3.10	0.06	0.80	0.01	0.46	0.01
Elongation at Break (%)	56.40	1.84	41.20	0.58	34.00	0.90
Young's Modulus (MPa)	2.72	0.06	0.76	0.01	0.45	0.01

Table A.5 Hardness test results of polymeric networks and propellant

Composition	Shore A Hardness	Std. Dev.
TP-N100-R0.8	17	1.5
TP-N100-R1.0	34	2.1
TP-N100-R1.2	40	1.5
TP-N3200-R0.8	19	1.0
TP-N3200-R1.0	45	1.5
TP-N3200-R1.2	50	0.6
TP-N100 IPDI(1:1)-R1.0	37	2.1
TP-N100 IPDI(2:1)-R1.0	36	2.5
TP-N3200 IPDI(2:1)-R1.0	25	1.0
TP-N3200-0.2BDO	30	1.5
TP-N3200-0.2TMP	40	1.5
TP-N3200-0.4BDO	46	1.5
TP-N3200-0.4TMP	30	1.5
TP-N3200-0.8BDO	35	1.0
TP-N3200-0.8TMP	64	2.1
TP-N3200-BDO-0.01TPB	35	1.5
TP-N3200-BDO-0.02TPB	39	1.0
TP-N3200-BDO-0.04TPB	32	1.0
TP-N3200-BDO-0.01FeAA	50	0.6
TP-N3200-BDO-0.01DBTDL	40	1.0
Propellant 091	66	1.0

APPENDIX B

STRESS-STRAIN CURVES

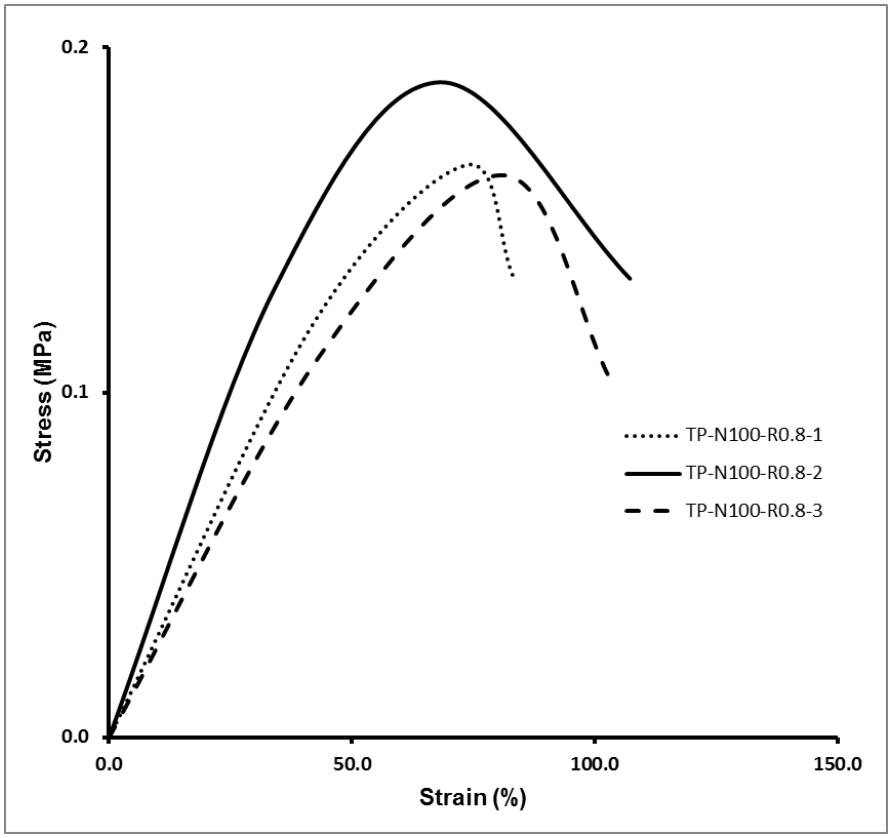

Figure B.1 The stress-strain curves of TP-N100-R0.8 samples

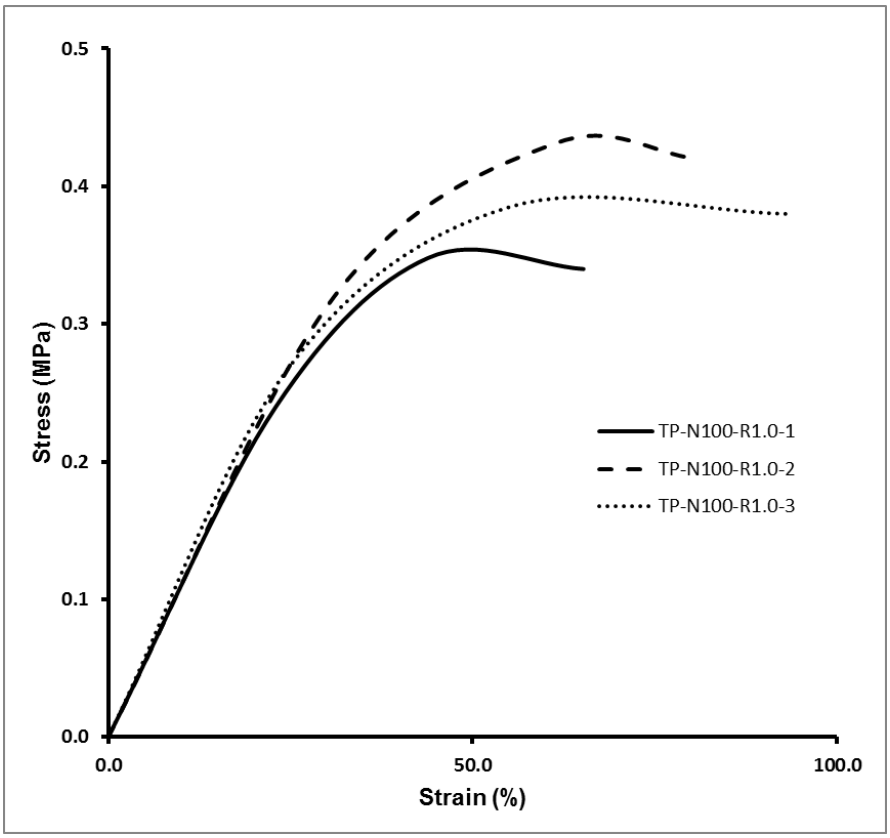

Figure B.2 The stress-strain curves of TP-N100-R1.0 samples

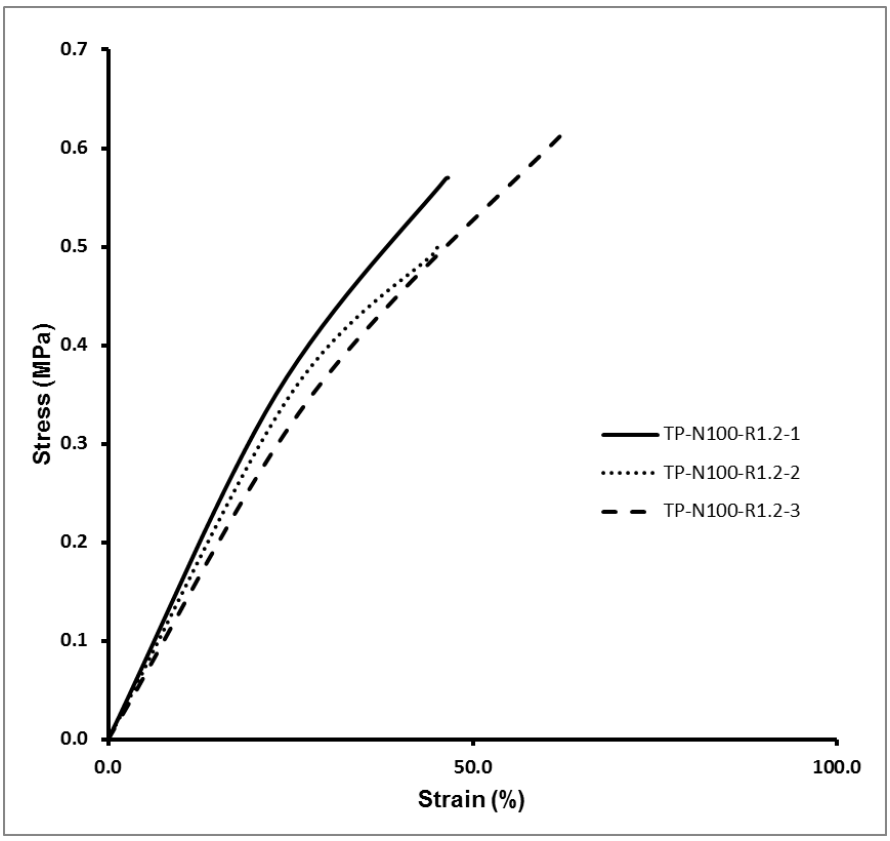

Figure B.3 The stress-strain curves of TP-N100-R1.2 samples

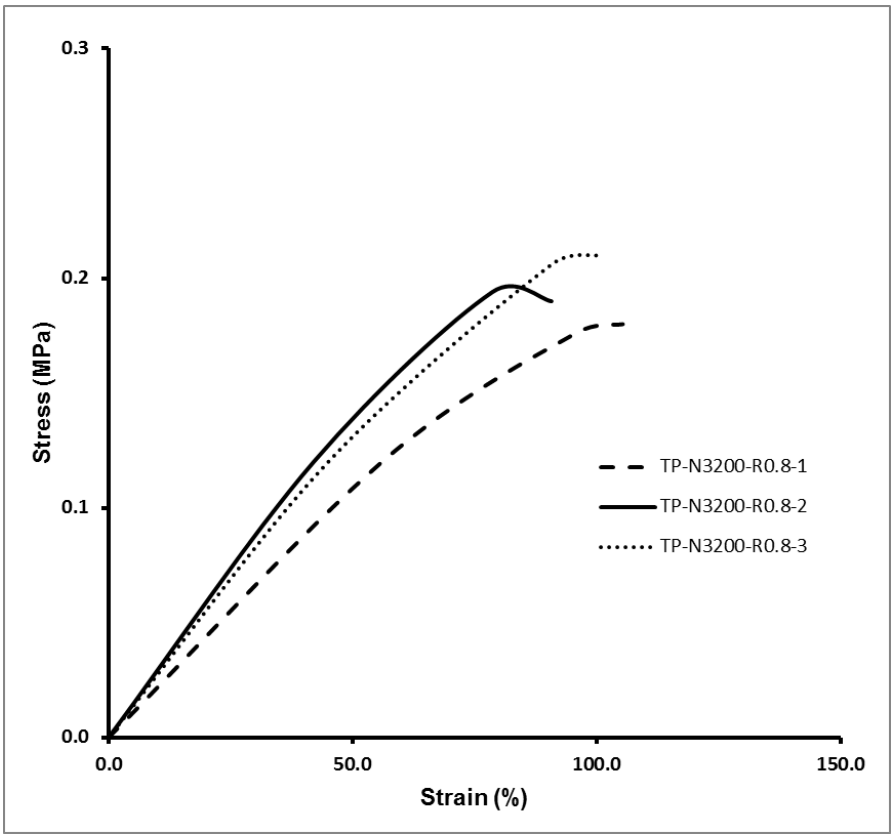

Figure B.4 The stress-strain curves of TP-N3200-R0.8 samples

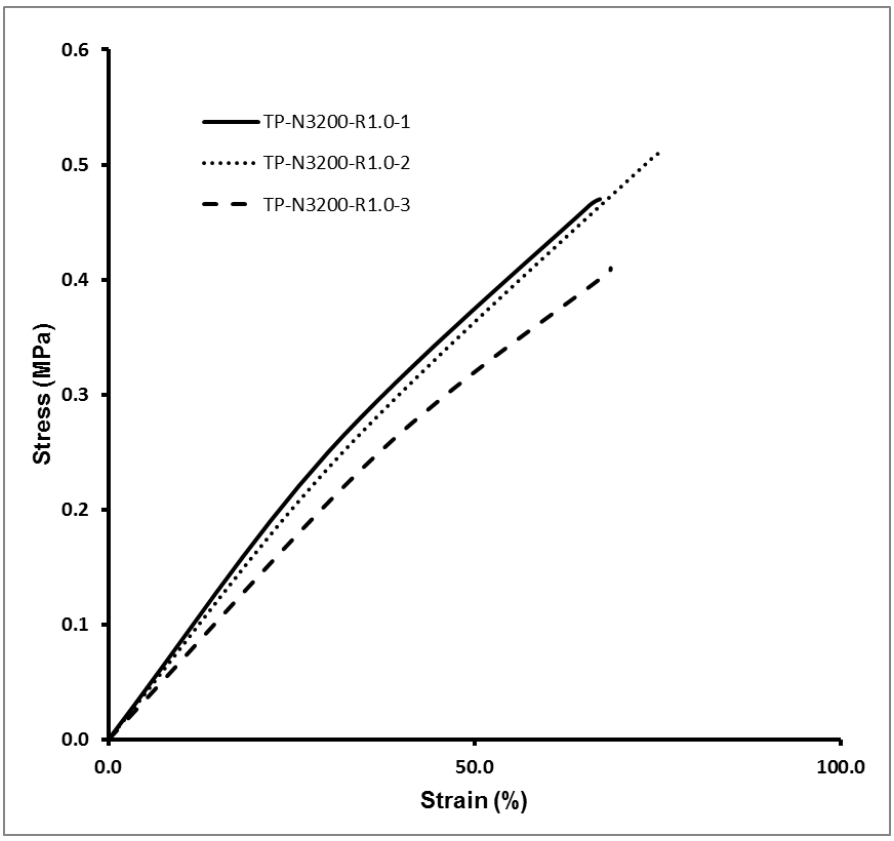

Figure B.5 The stress-strain curves of TP-N3200-R1.0 samples

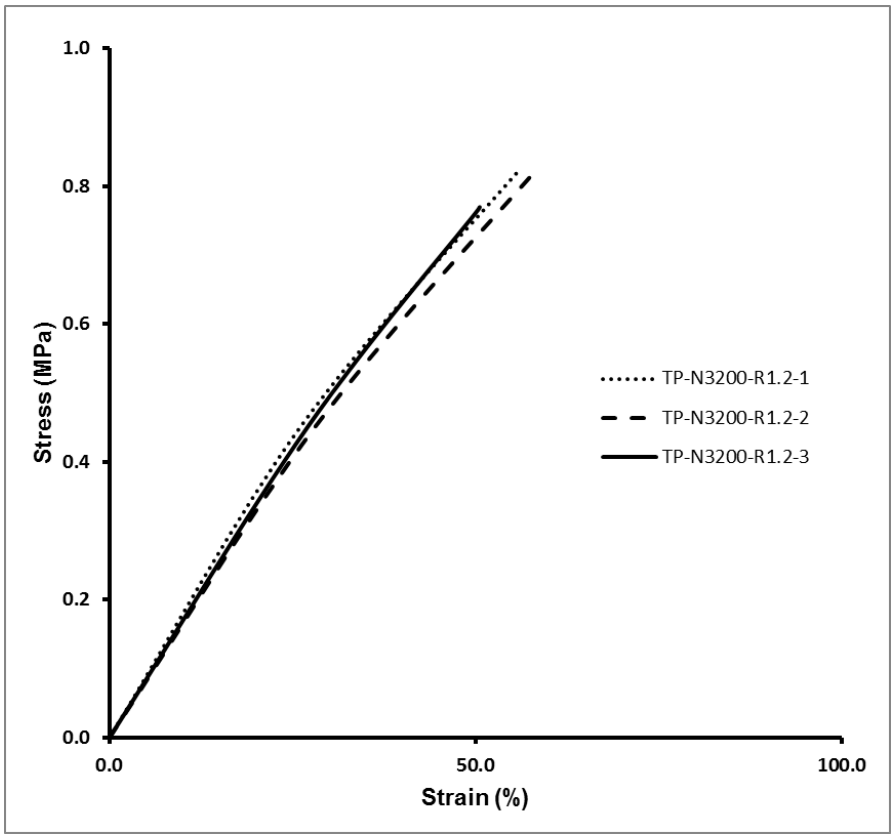

Figure B.6 The stress-strain curves of TP-N3200-R1.2 samples

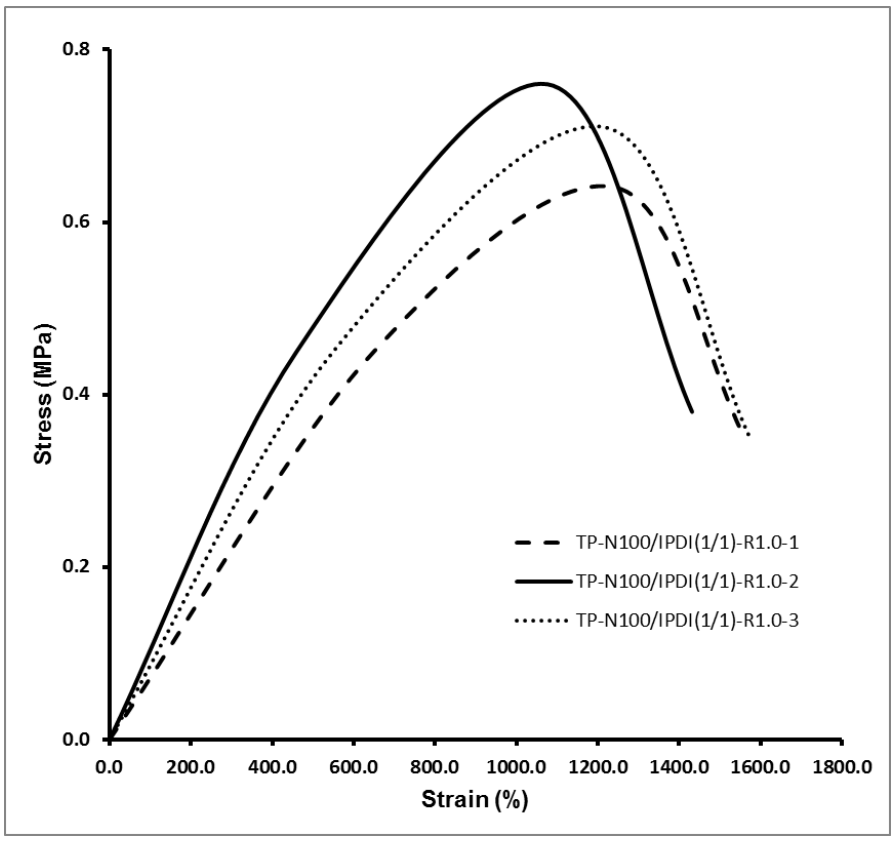

Figure B.7 The stress-strain curves of TP-N100/IPDI(1:1)-R1.0 samples

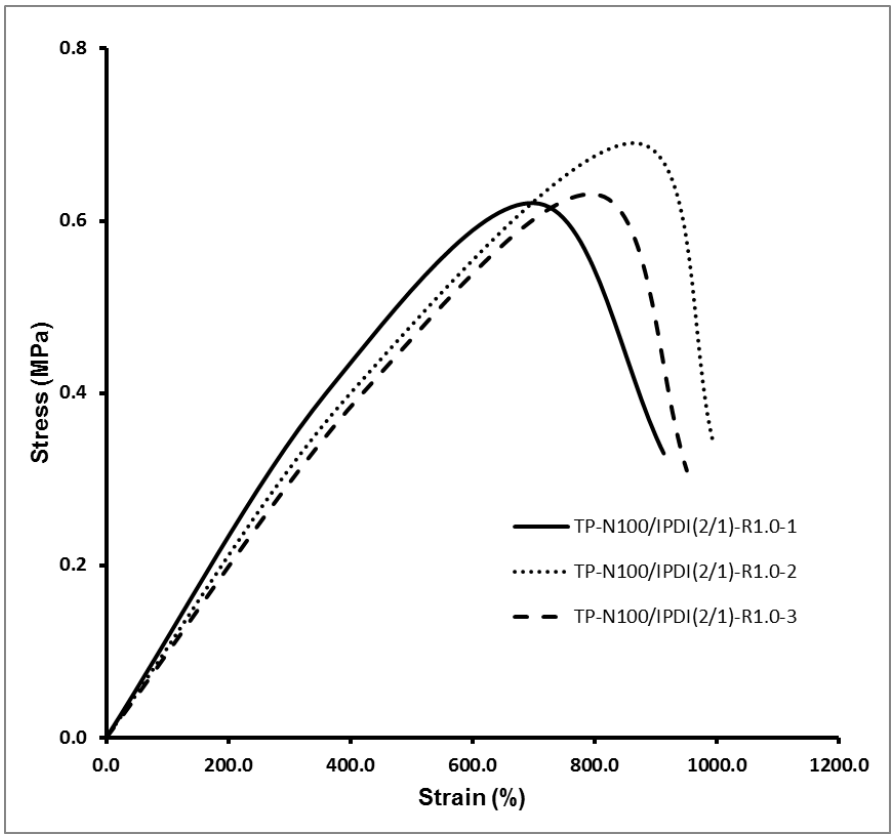

Figure B.8 The stress-strain curves of TP-N100/IPDI(2:1)-R1.0 samples

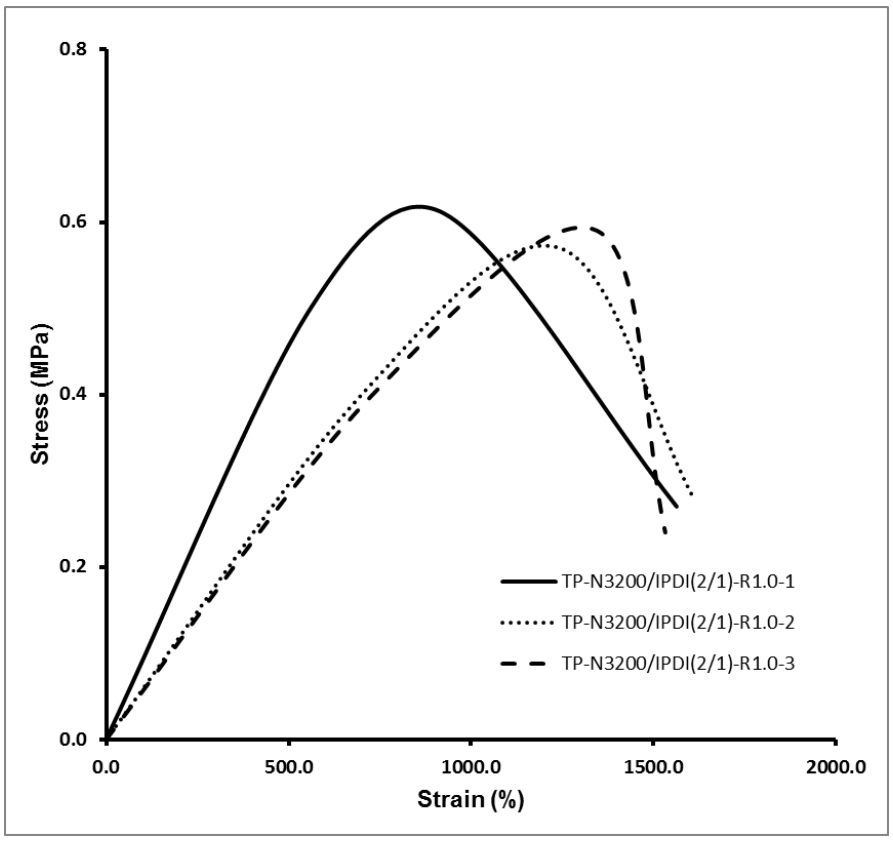

Figure B.9 The stress-strain curves of TP-N3200/IPDI(2:1)-R1.0 samples

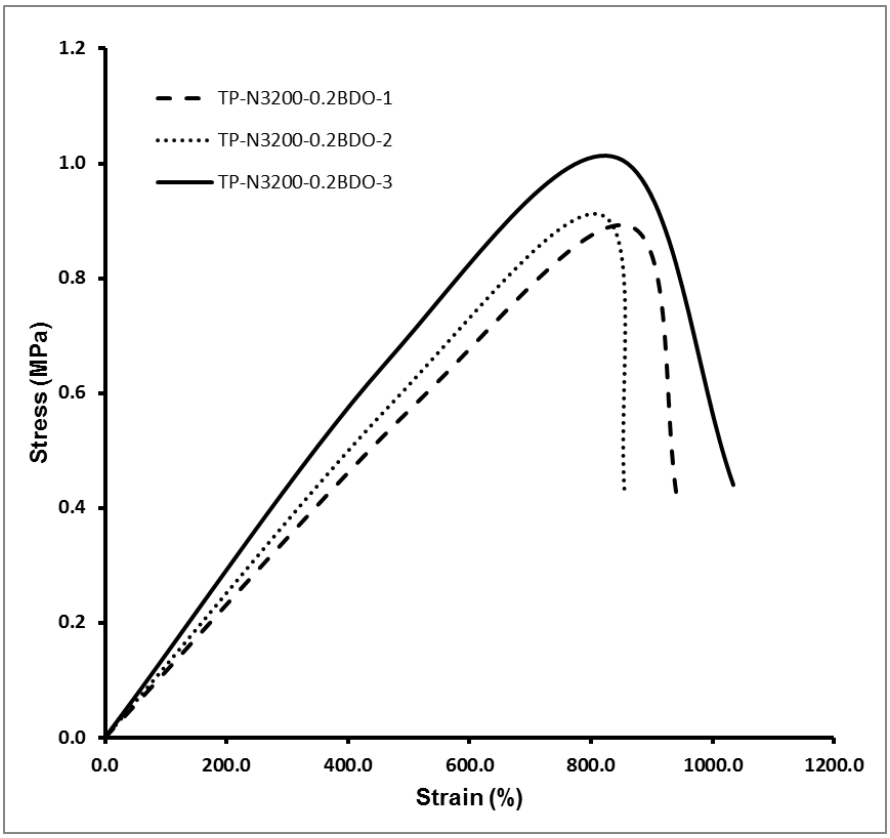

Figure B.10 The stress-strain curves of TP-N3200-0.2BDO samples

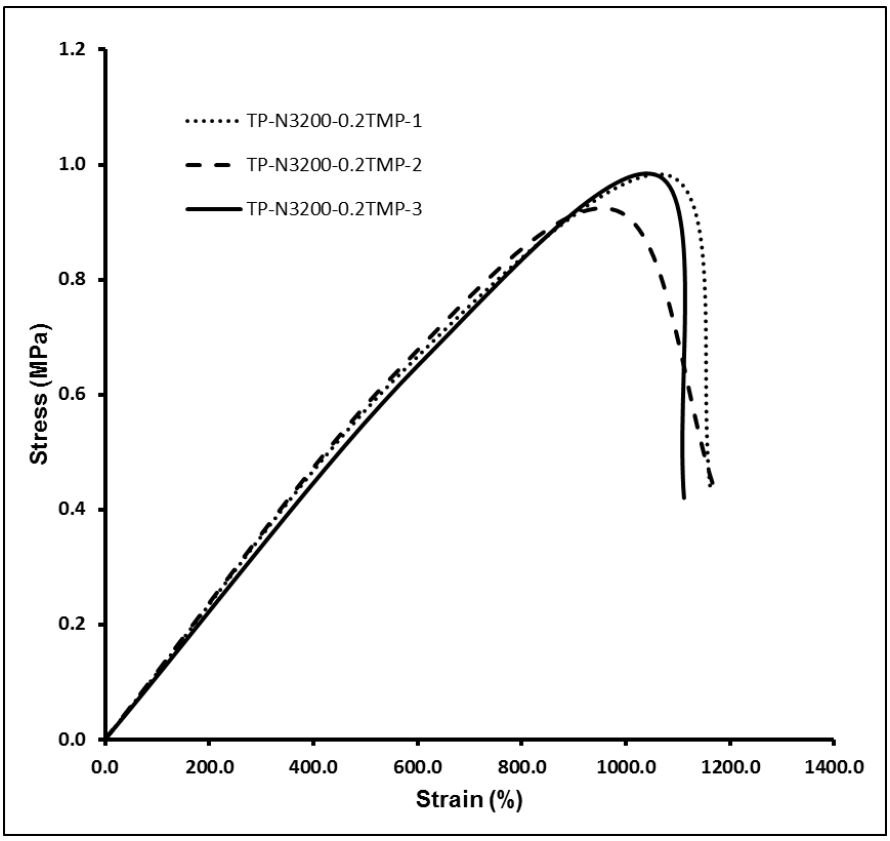

Figure B.11 The stress-strain curves of TP-N3200-0.2TMP samples

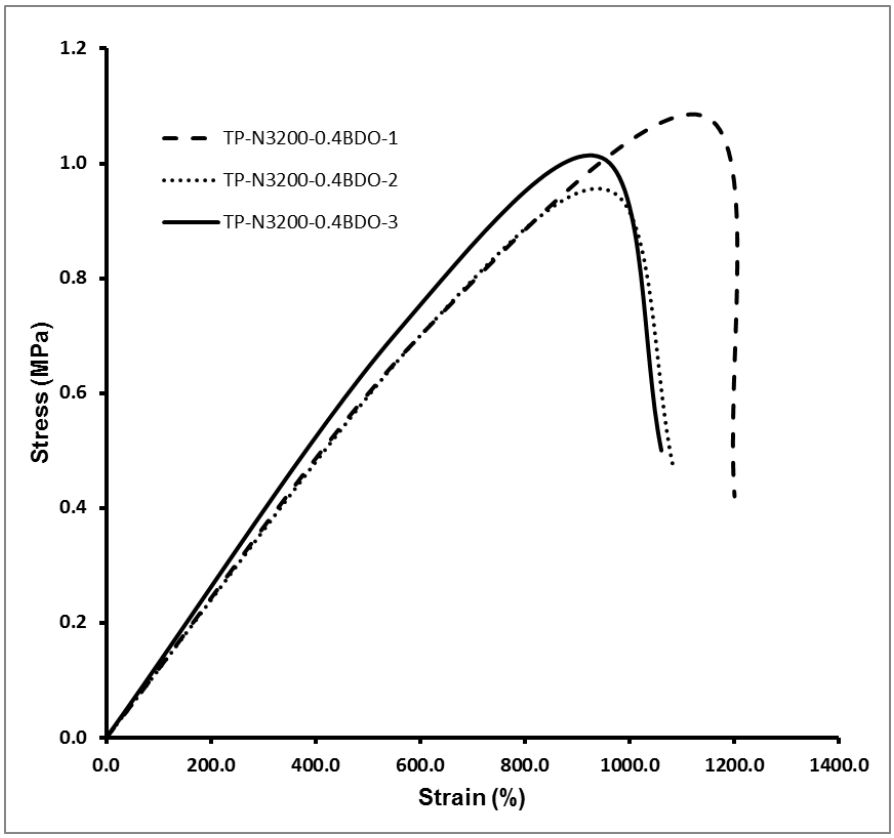

Figure B.12 The stress-strain curves of TP-N3200-0.4BDO samples

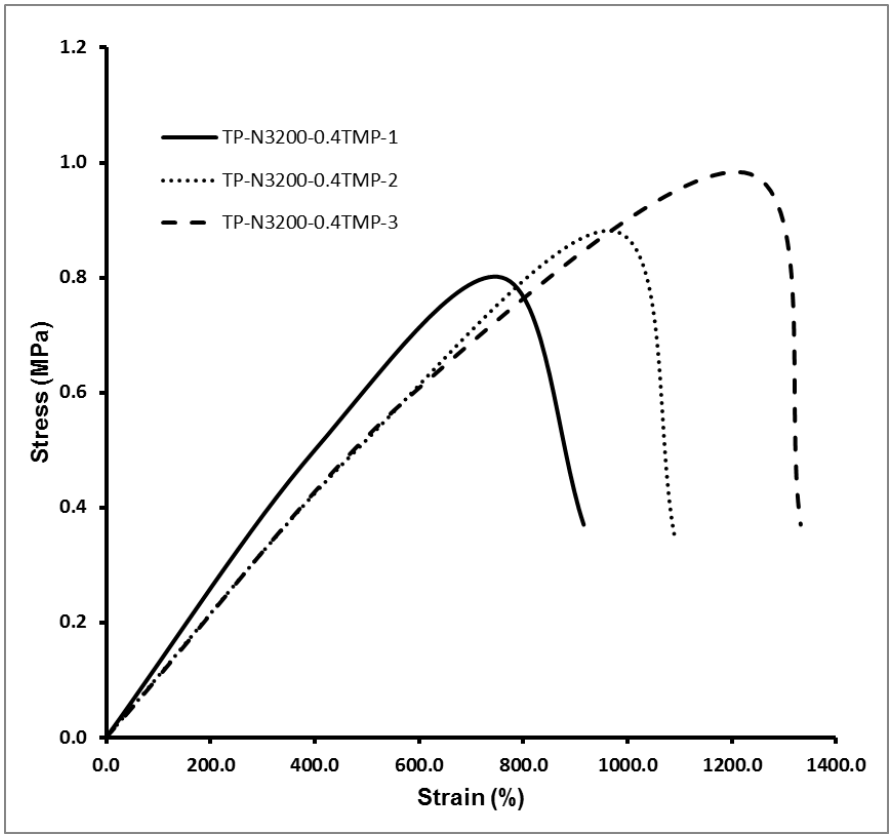

Figure B.13 The stress-strain curves of TP-N3200-0.4TMP samples

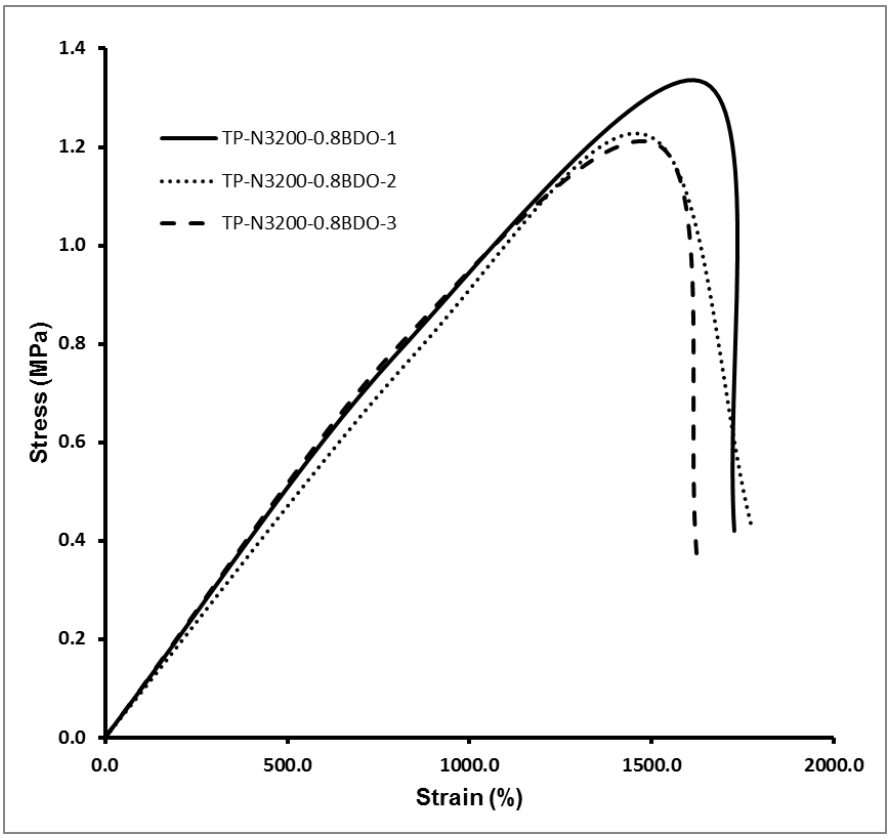

Figure B.14 The stress-strain curves of TP-N3200-0.8BDO samples

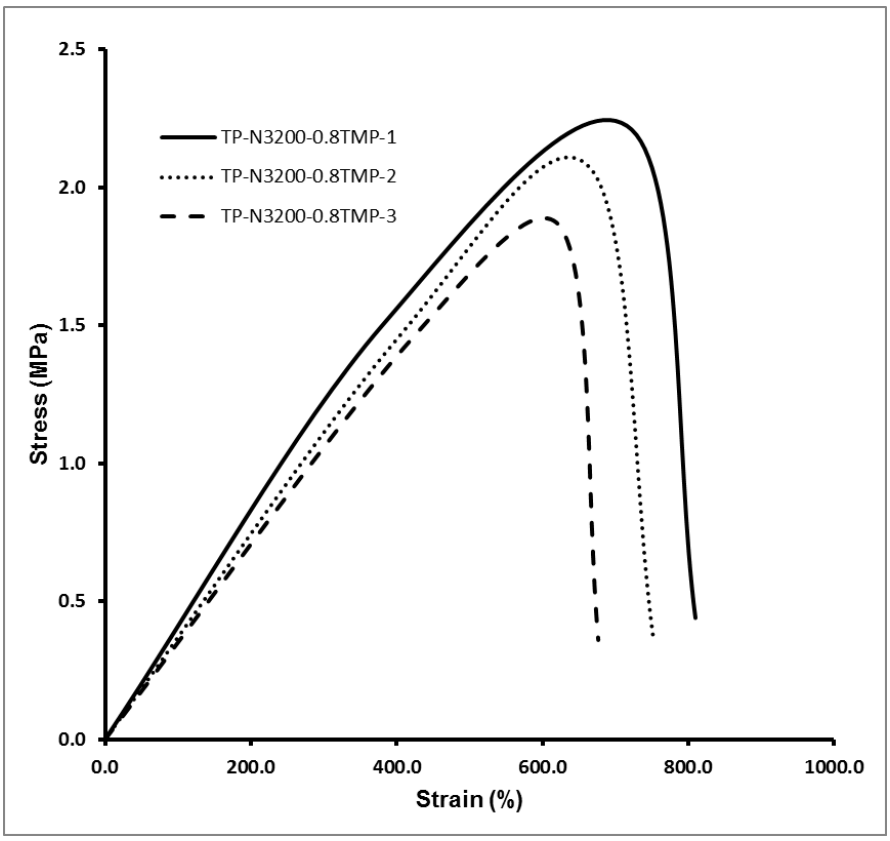

Figure B.15 The stress-strain curves of TP-N3200-0.8TMP samples

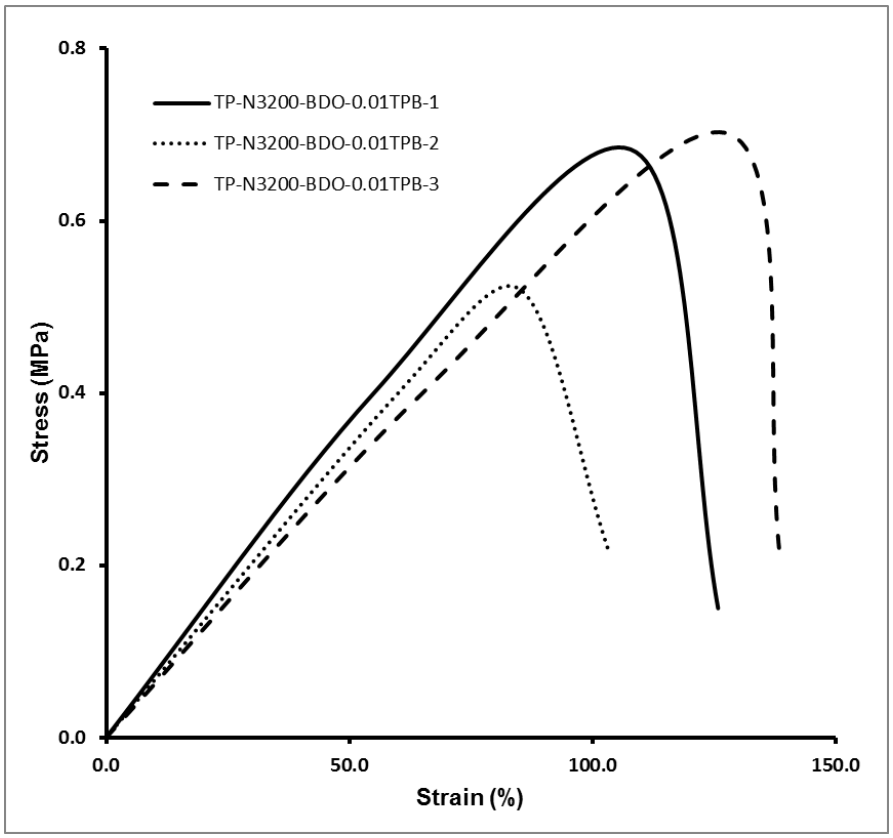

Figure B.16 The stress-strain curves of TP-N3200-BDO-0.01TPB samples

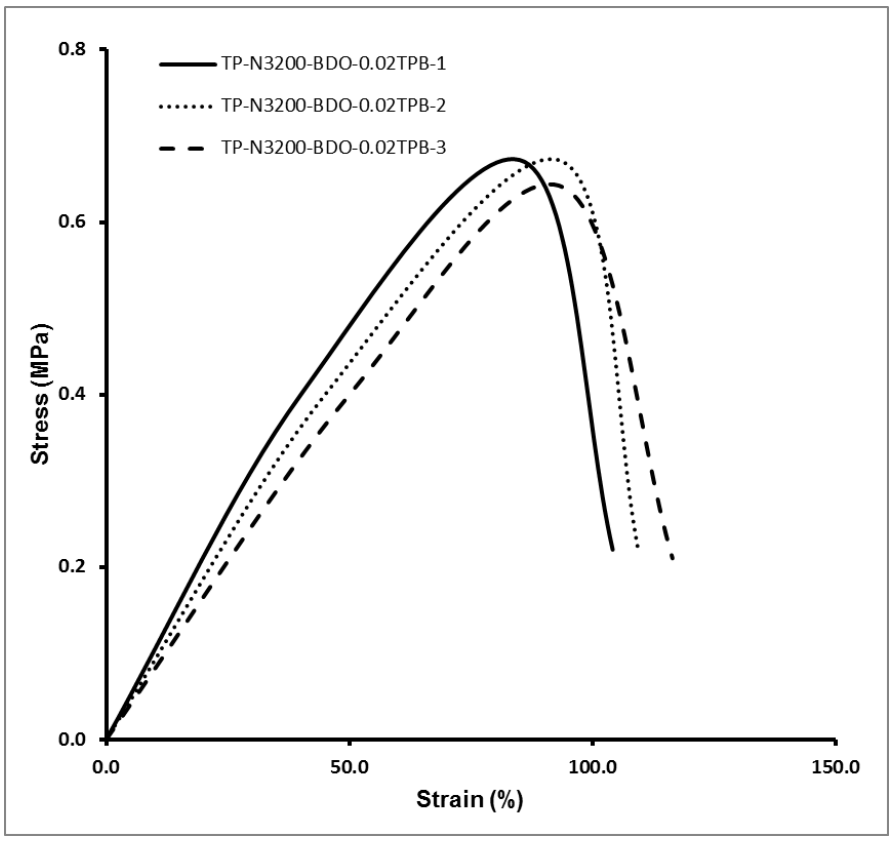

Figure B.17 The stress-strain curves of TP-N3200-BDO-0.02TPB samples

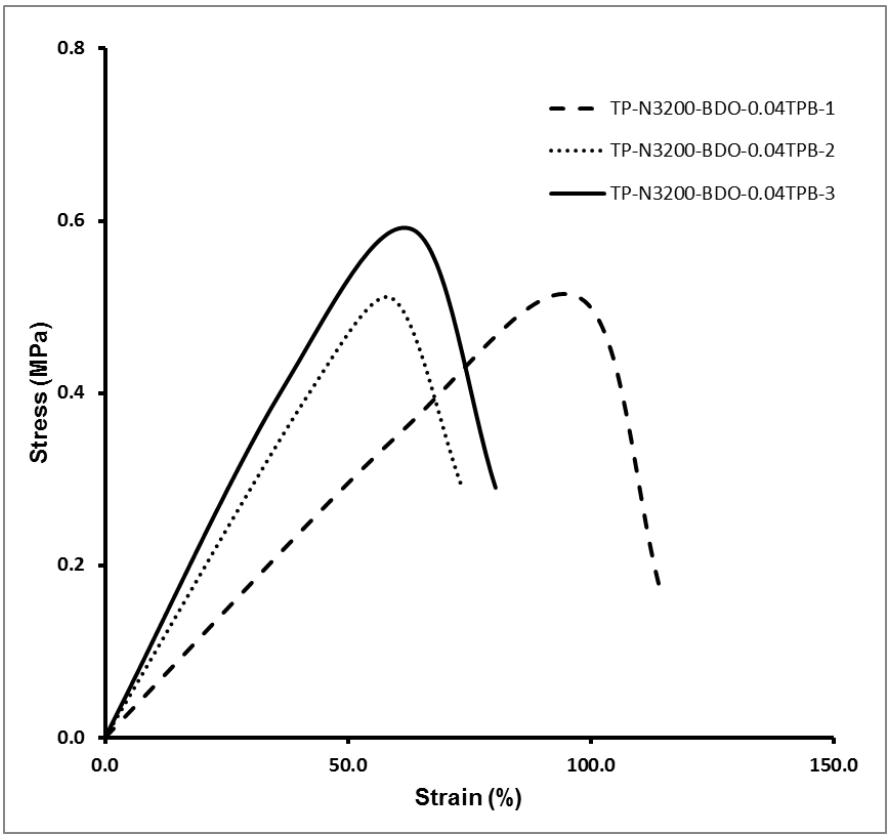

Figure B.18 The stress-strain curves of TP-N3200-BDO-0.04TPB samples

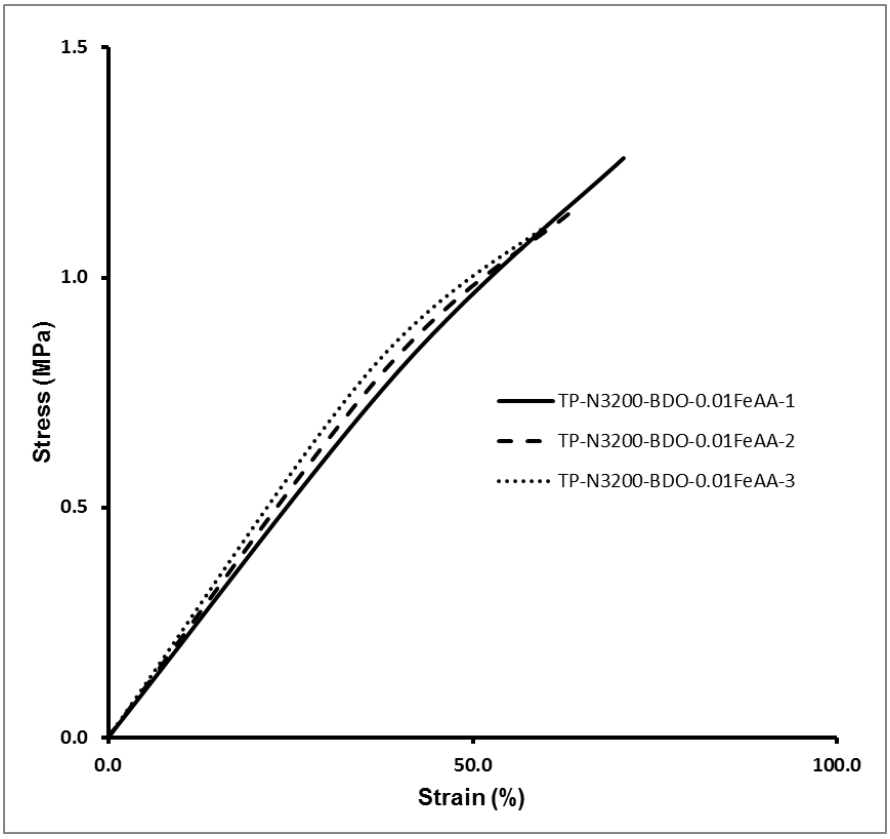

Figure B.19 The stress-strain curves of TP-N3200-BDO-0.01FeAA samples

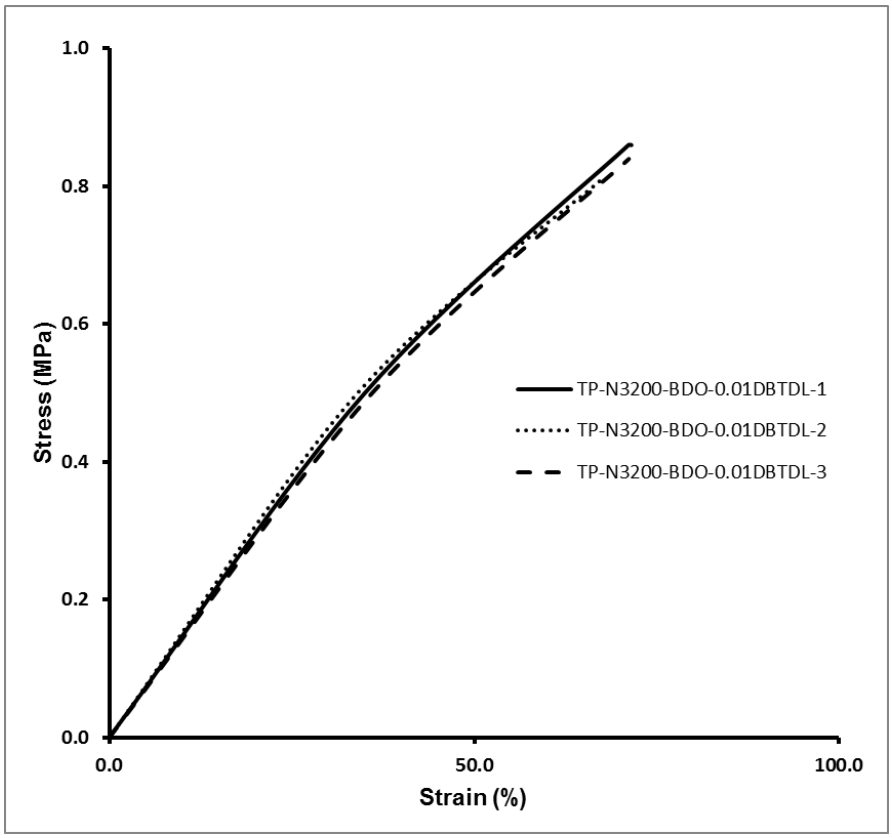

Figure B.20 The stress-strain curves of TP-N3200-BDO-0.01DBTDL samples

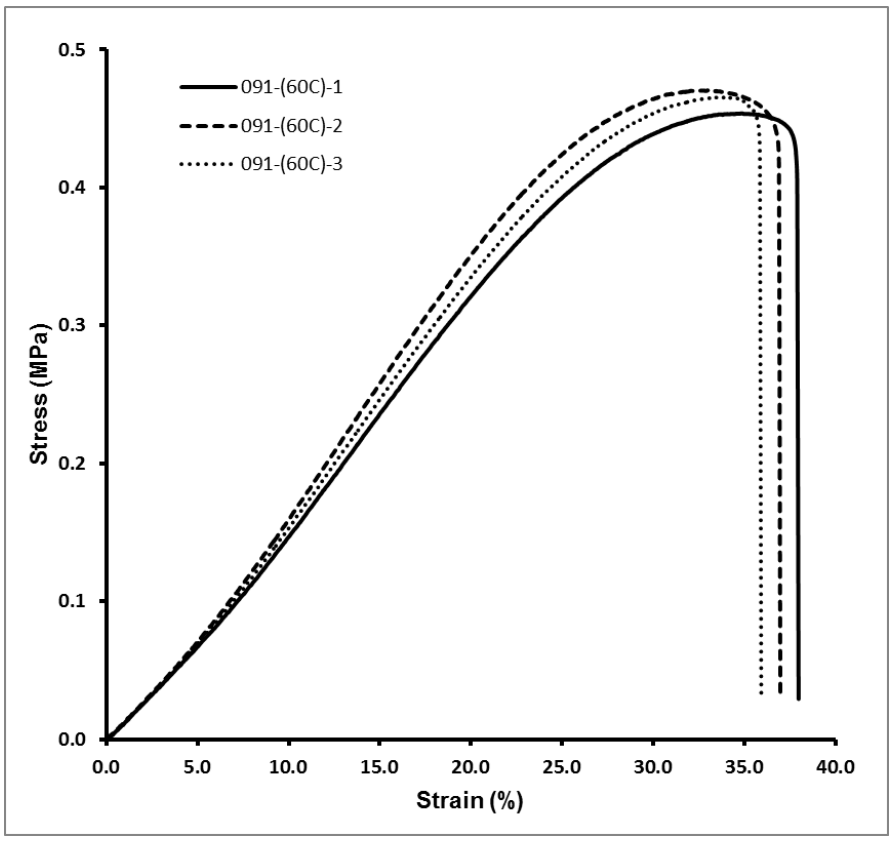

Figure B.21 The stress-strain curves of propellant 091 at 60^{o}C

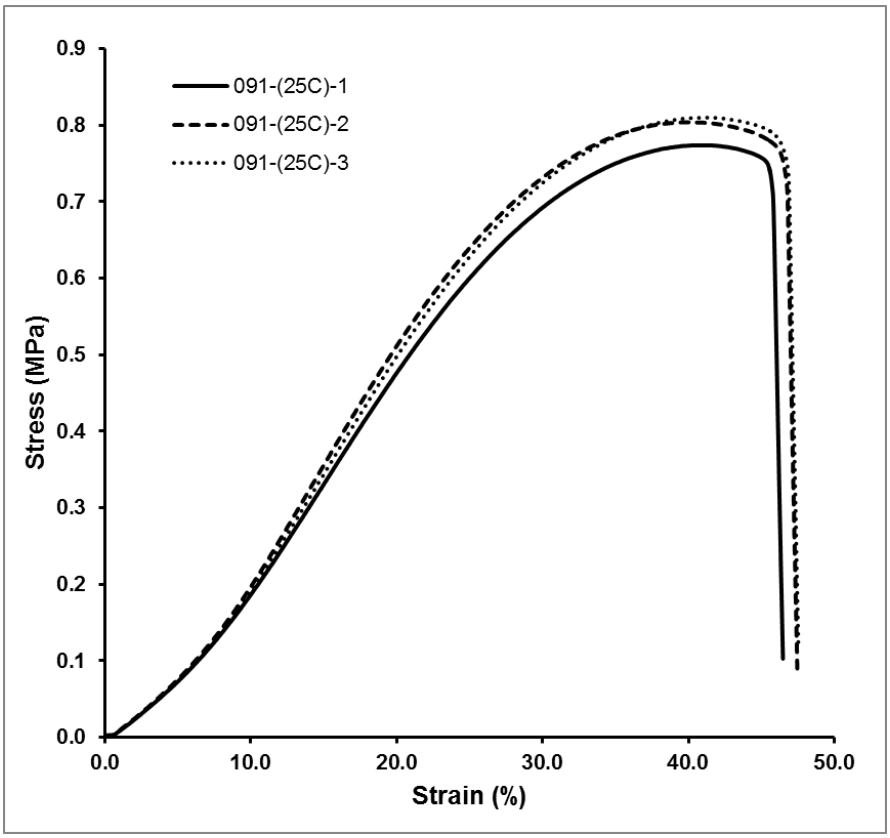

Figure B.22 The stress-strain curves of propellant 091 at 25^{o}C

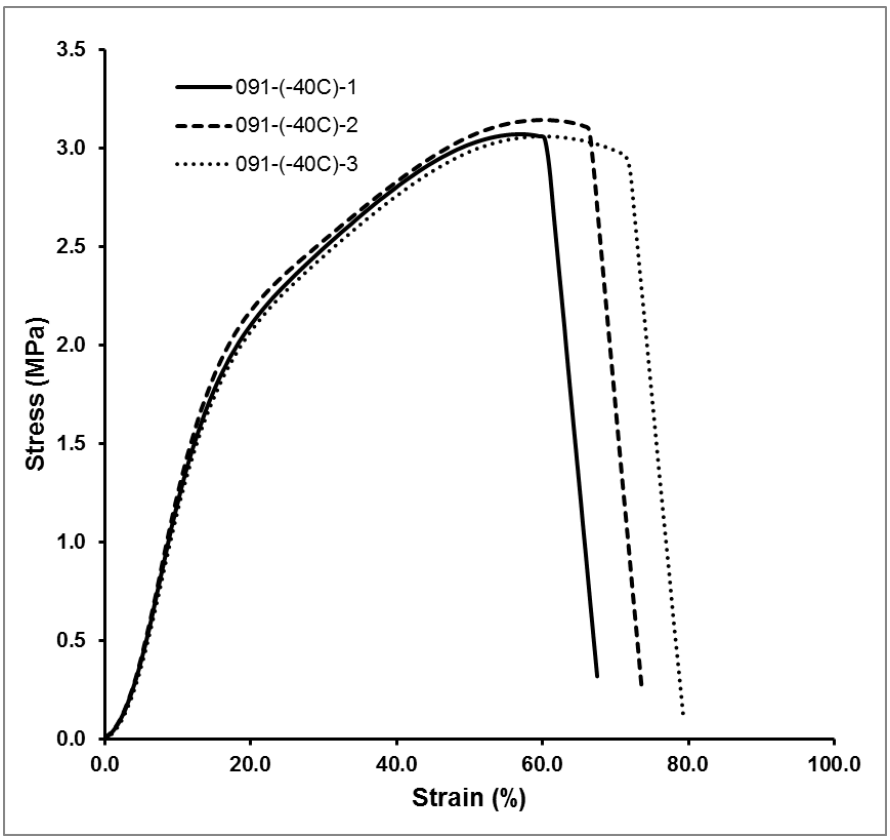

Figure B.23 The stress-strain curves of propellant 091 at -40^{o}C

APPENDIX C

X-RAY DIFFRACTION PATTERNS

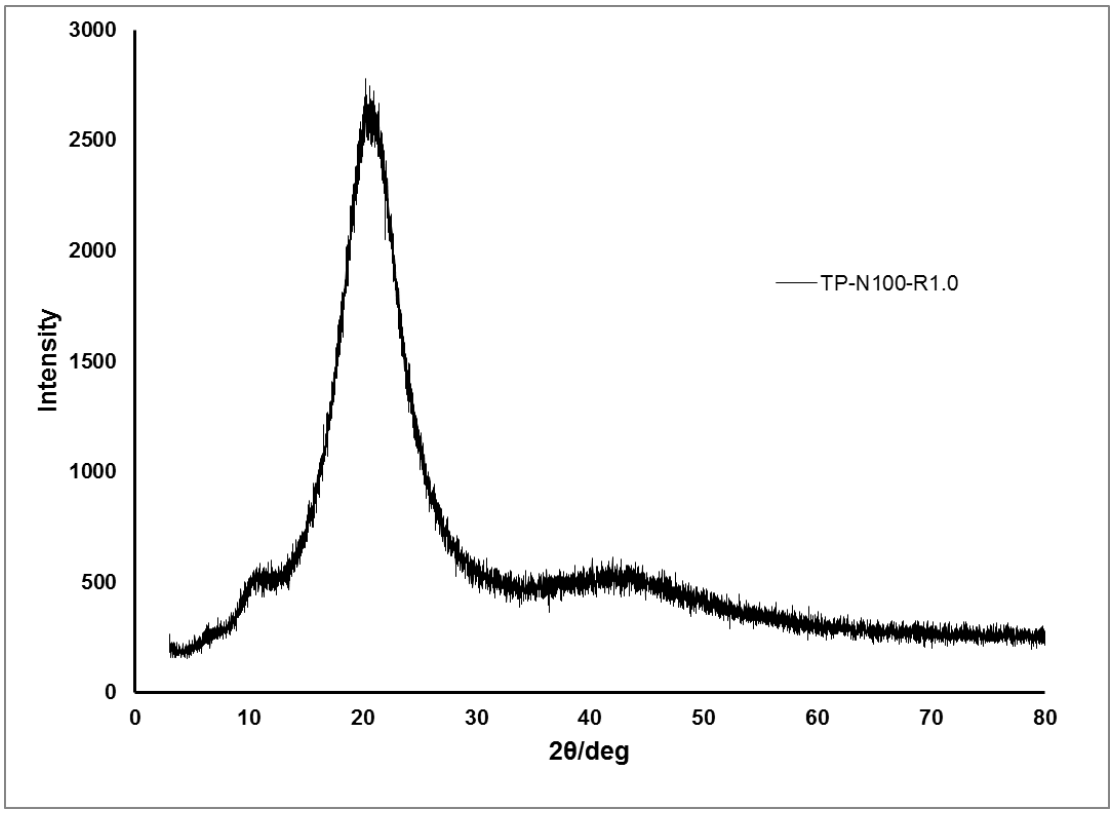

Figure C.1 XRD pattern of TP-N100-R1.0

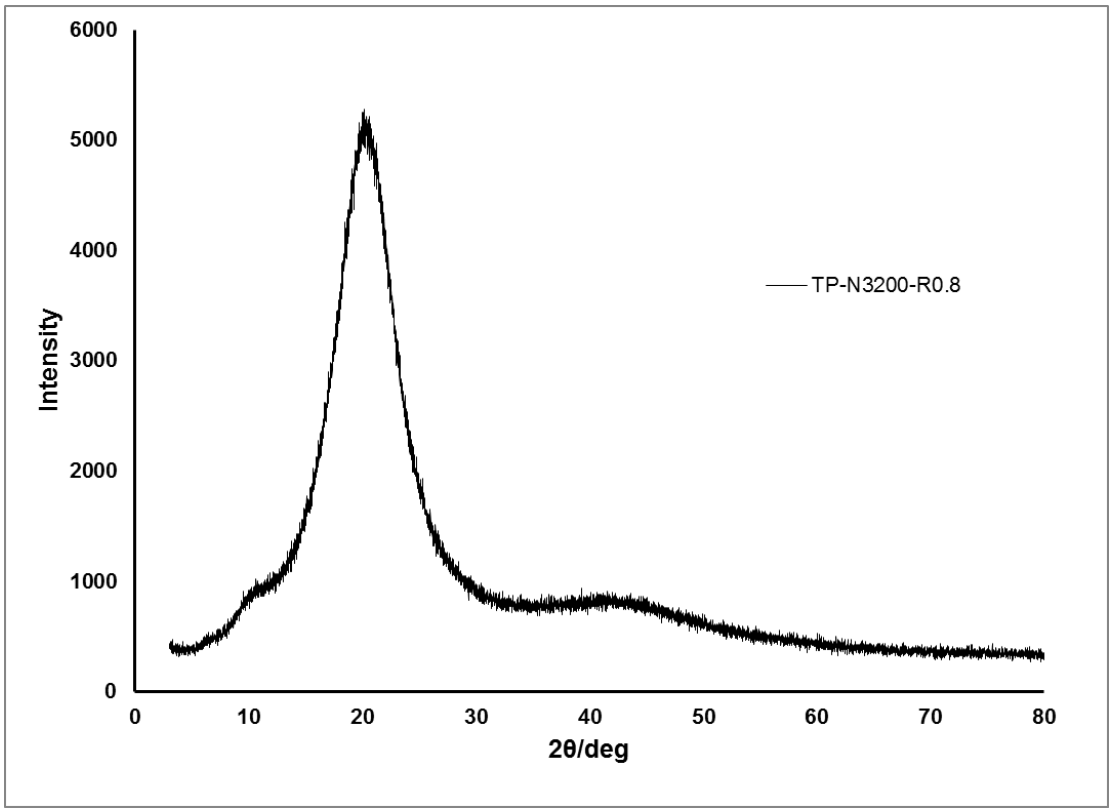

Figure C.2 XRD pattern of TP-N3200-R0.8

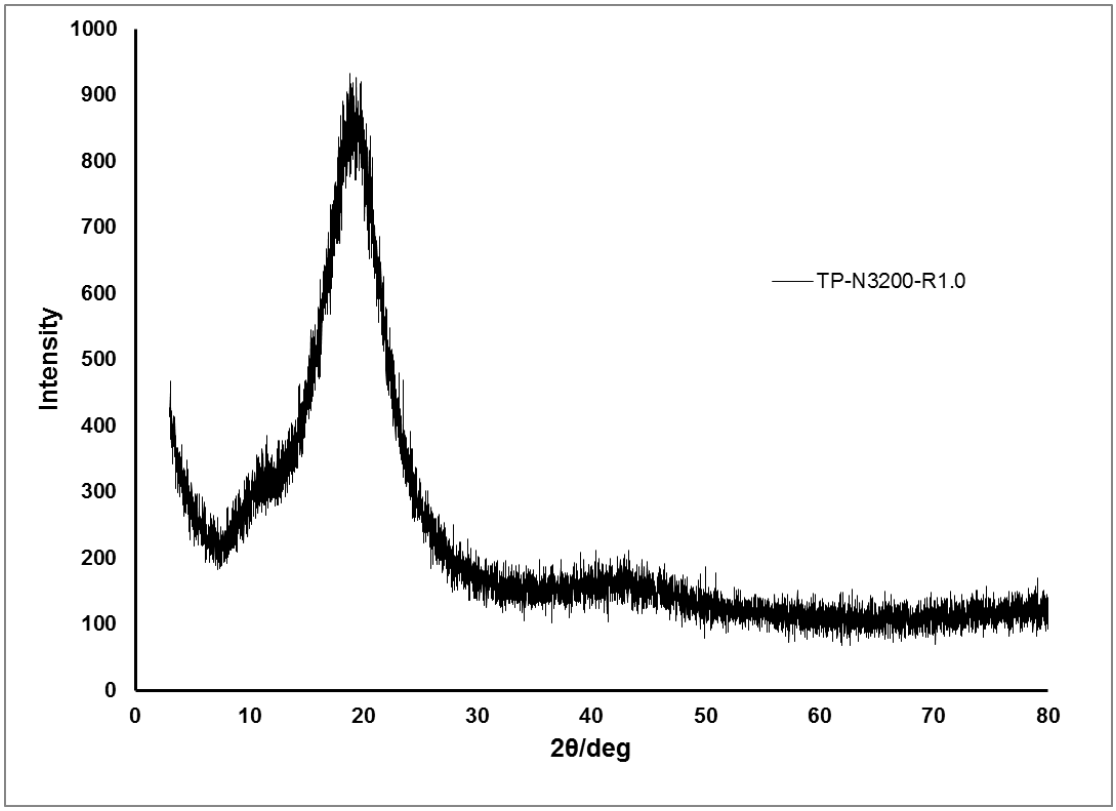

Figure C.3 XRD pattern of TP-N3200-R1.0

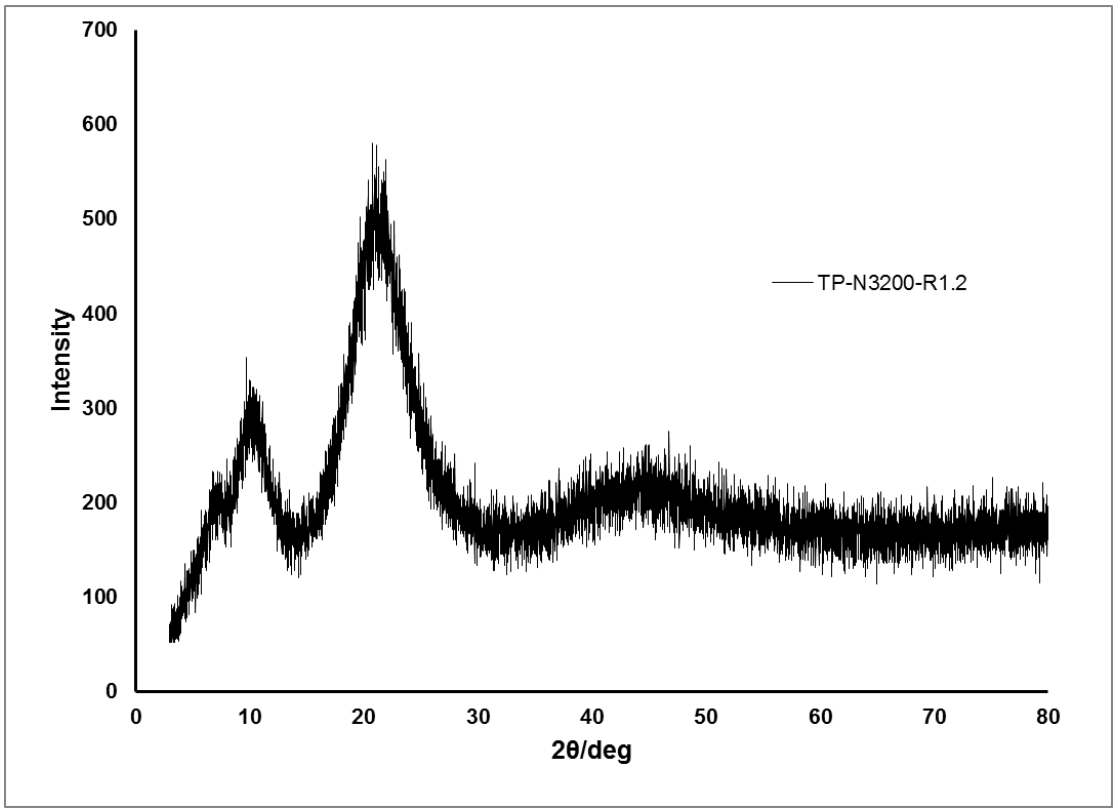

Figure C.4 XRD pattern of TP-N3200-R1.2

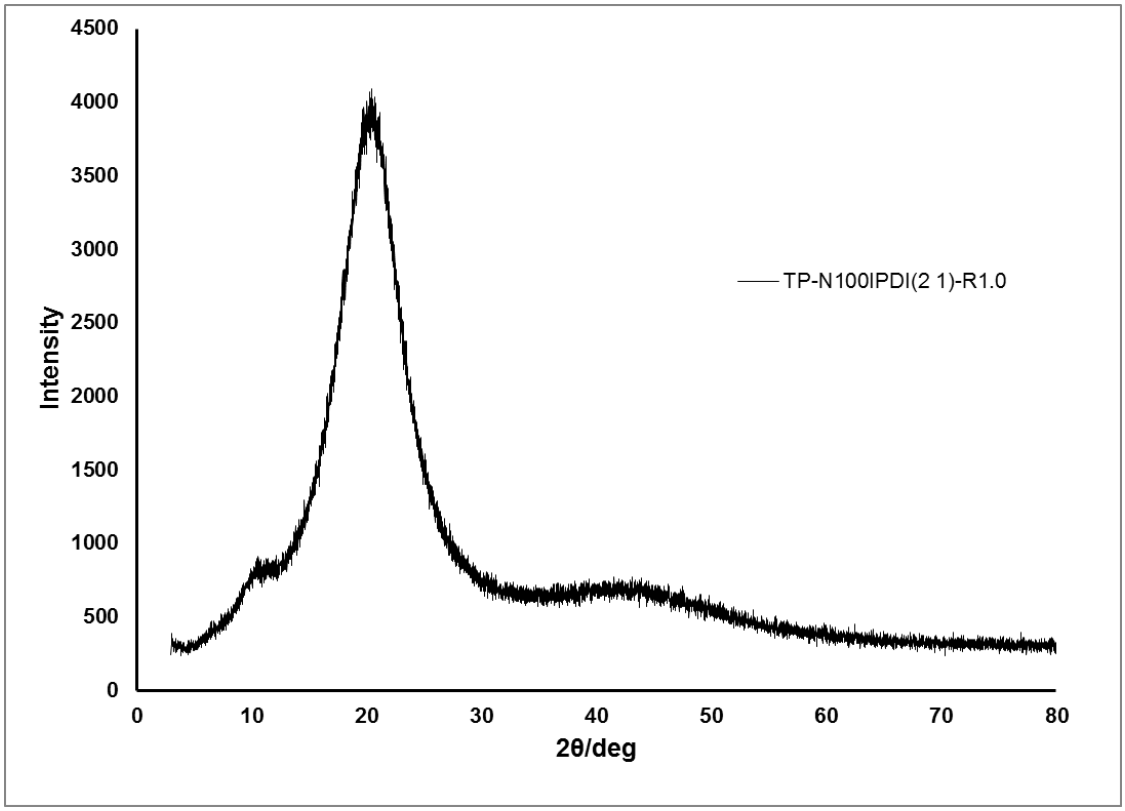

Figure C.5 XRD pattern of TP-N100 IPDI(2:1)-R1.0

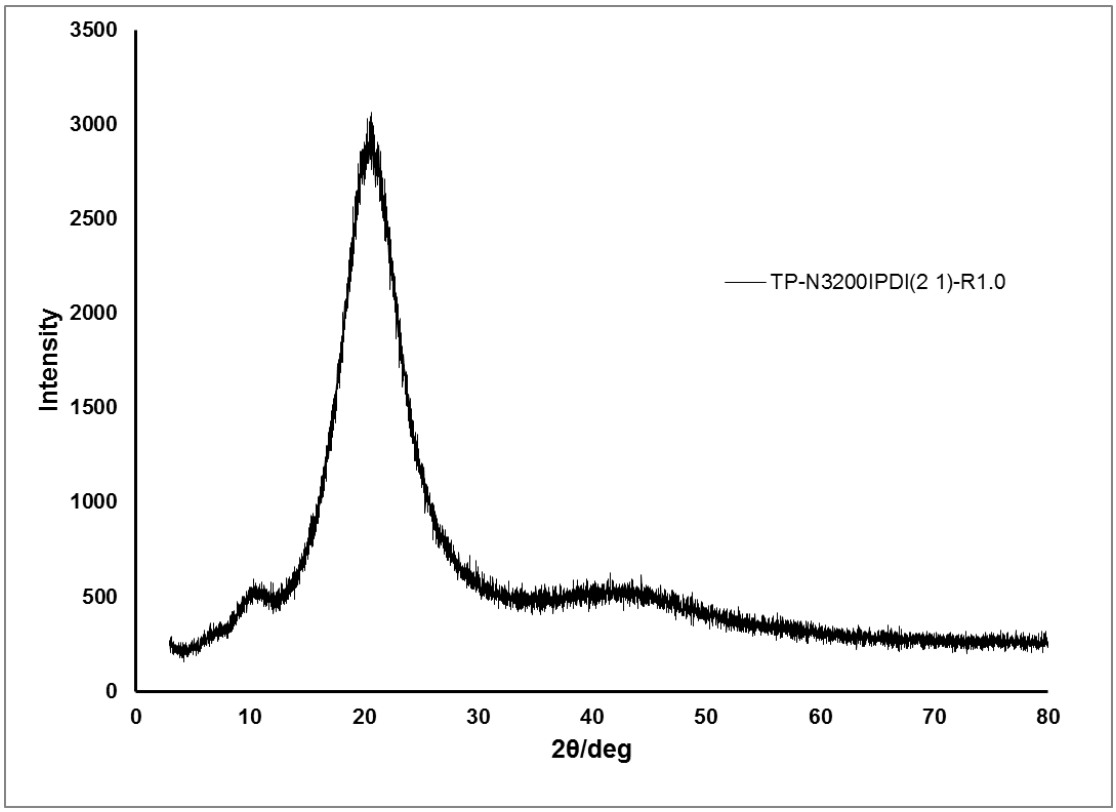

Figure C.6 XRD pattern of TP-N3200 IPDI(2:1)-R1.0

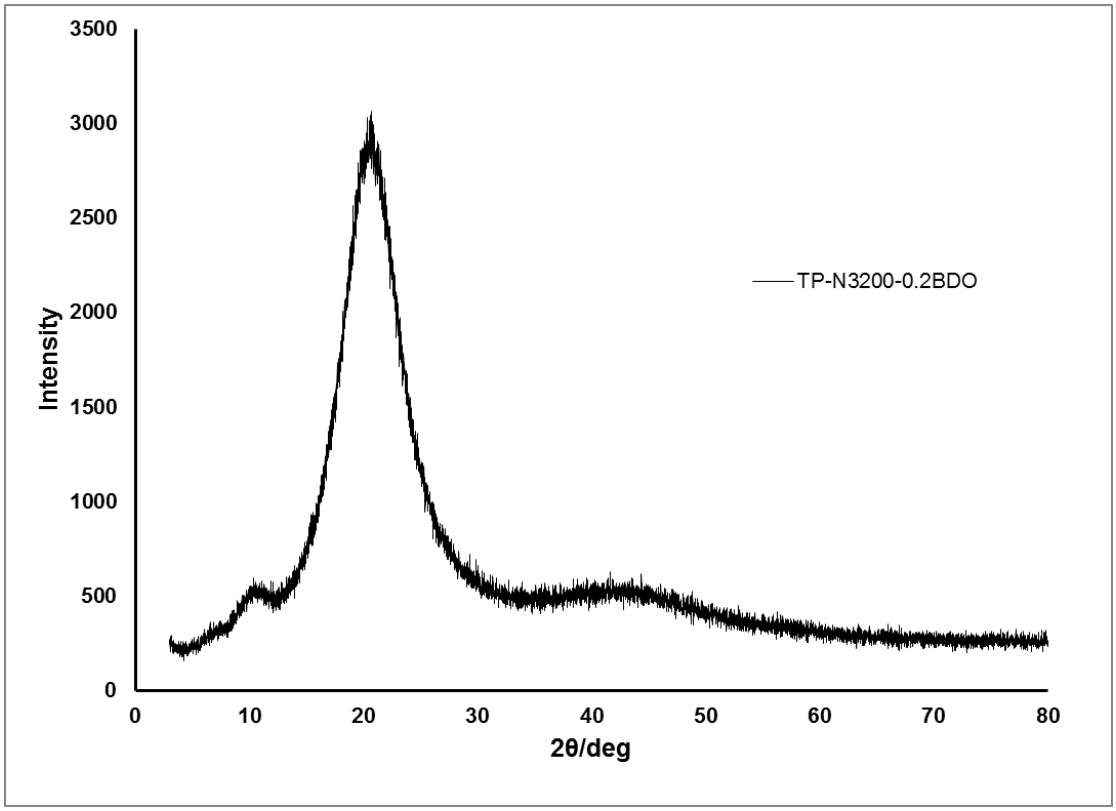

Figure C.7 XRD pattern of TP-N3200-0.2BDO

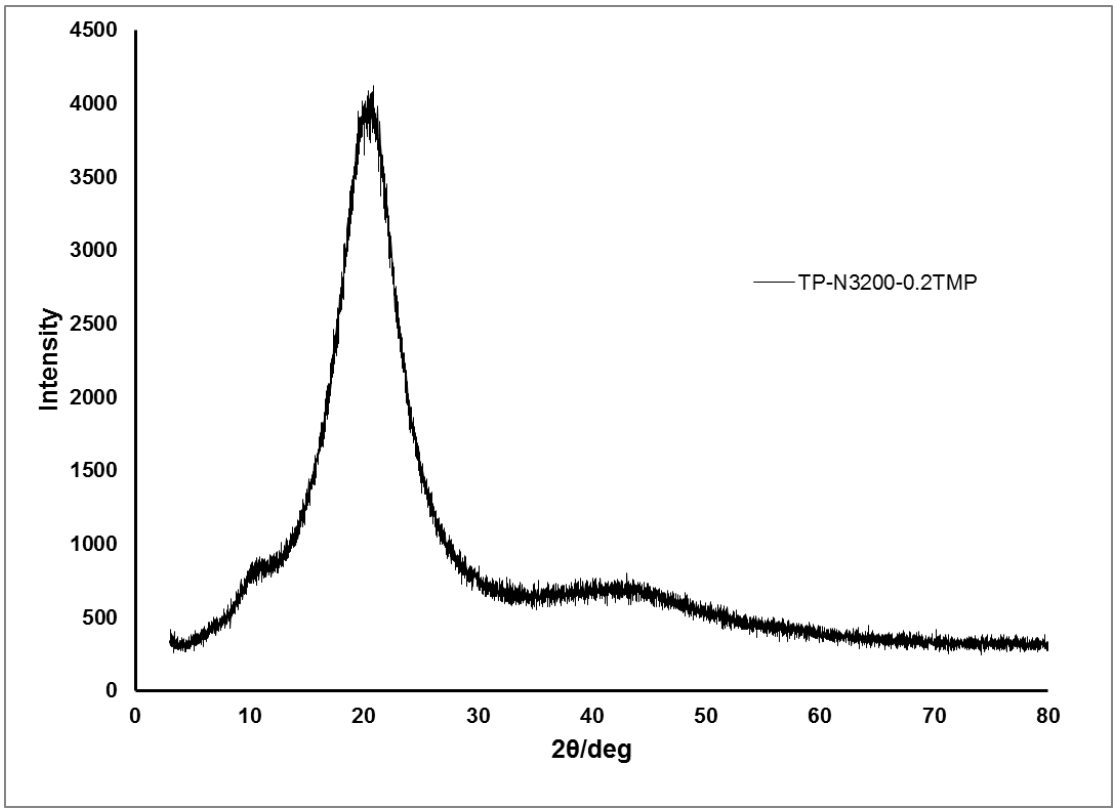

Figure C.8 XRD pattern of TP-N3200-0.2TMP

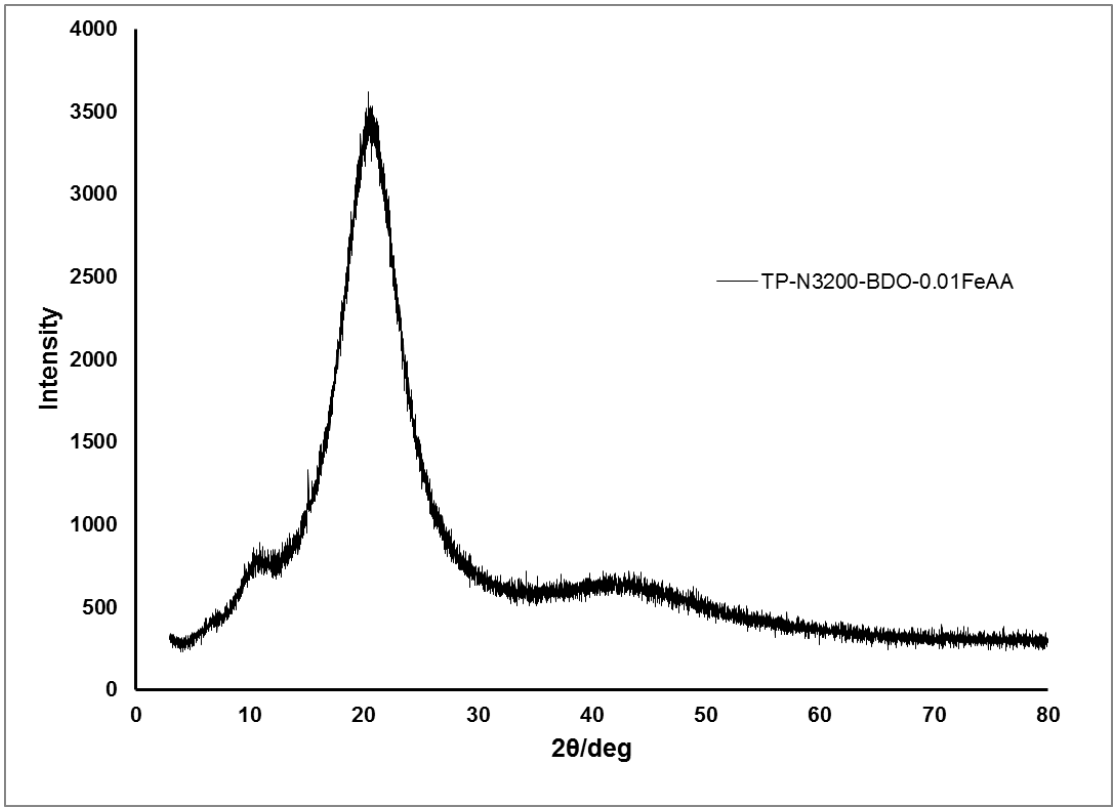

Figure C.9 XRD pattern of TP-N3200-BDO-0.01FeAA

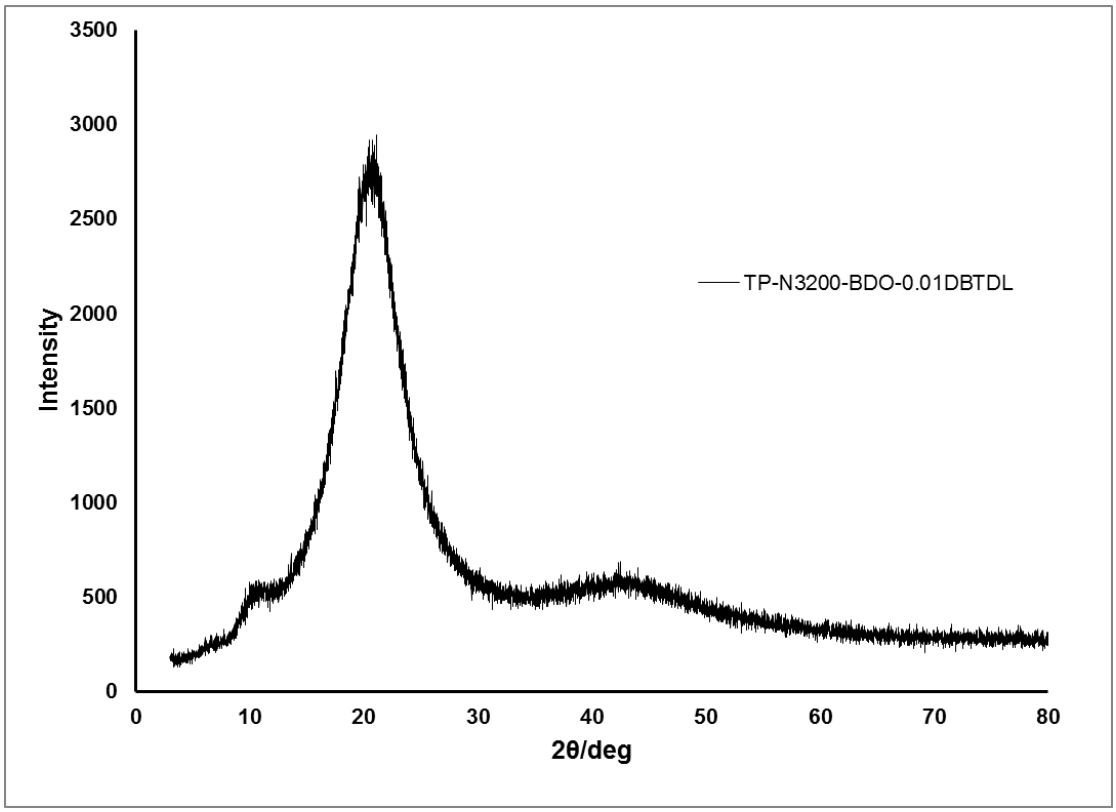

Figure C.10 XRD pattern of TP-N3200-BDO-0.01DBTDL

APPENDIX D

DSC THERMOGRAMS

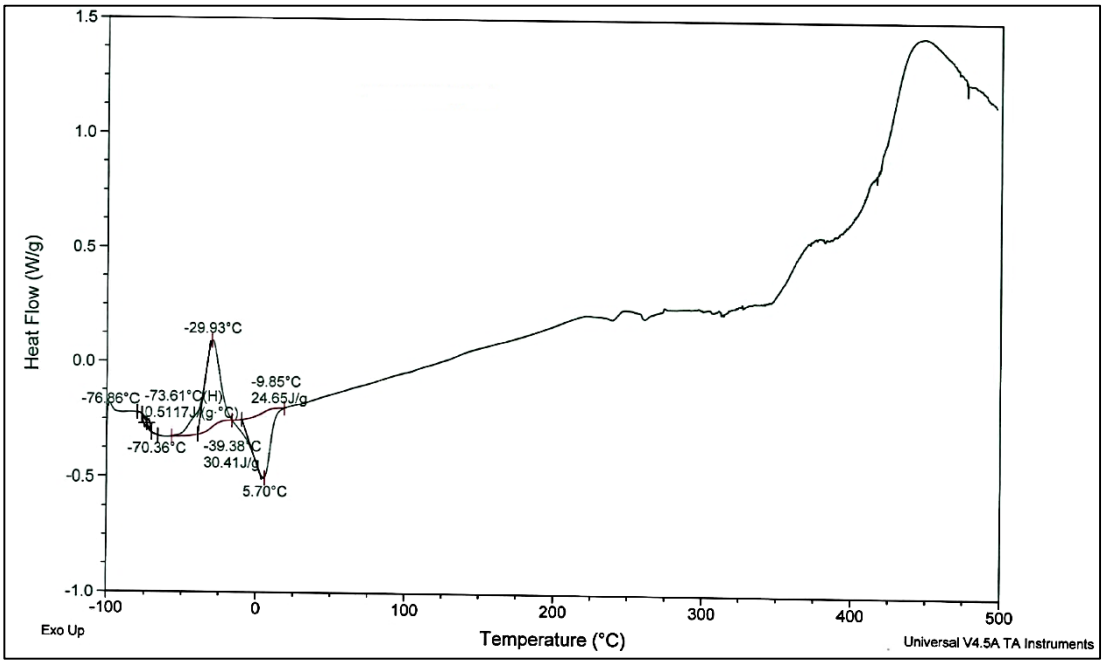

Figure D.1 DSC thermogram of TP-N100-R1.0

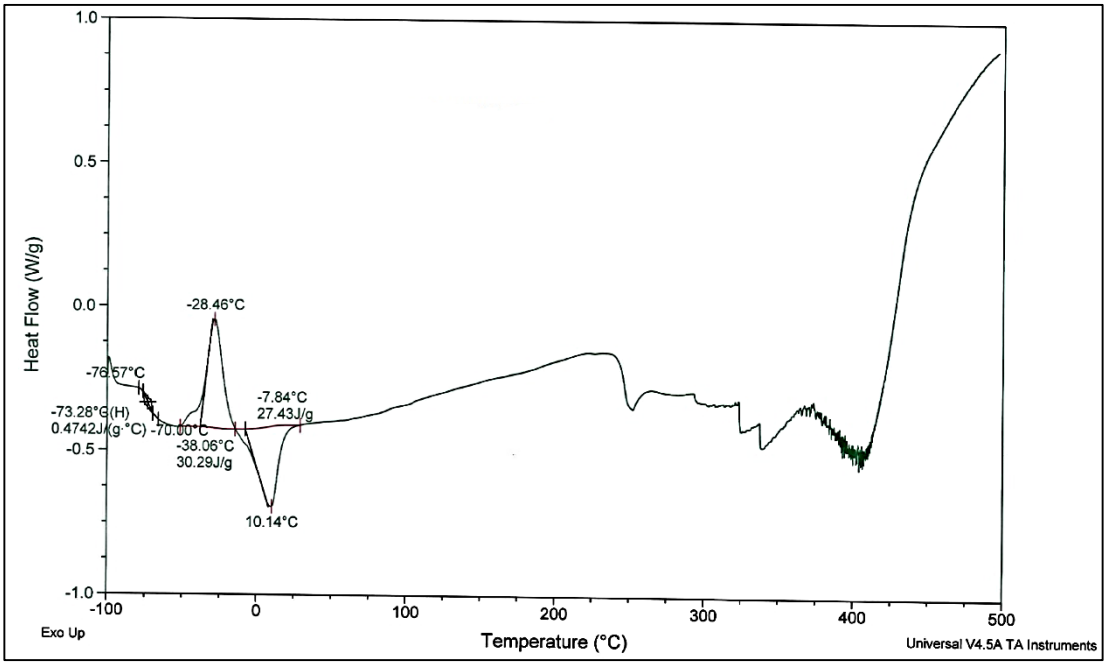

Figure D.2 DSC thermogram of TP-N3200-R0.8

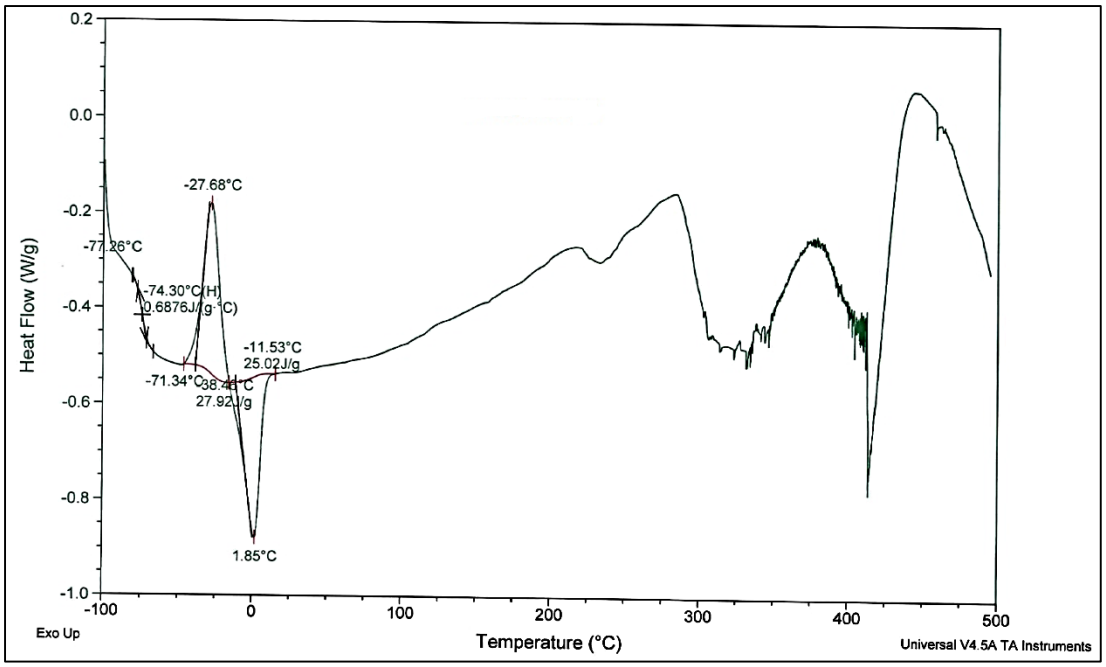

Figure D.3 DSC thermogram of TP-N3200-R1.0

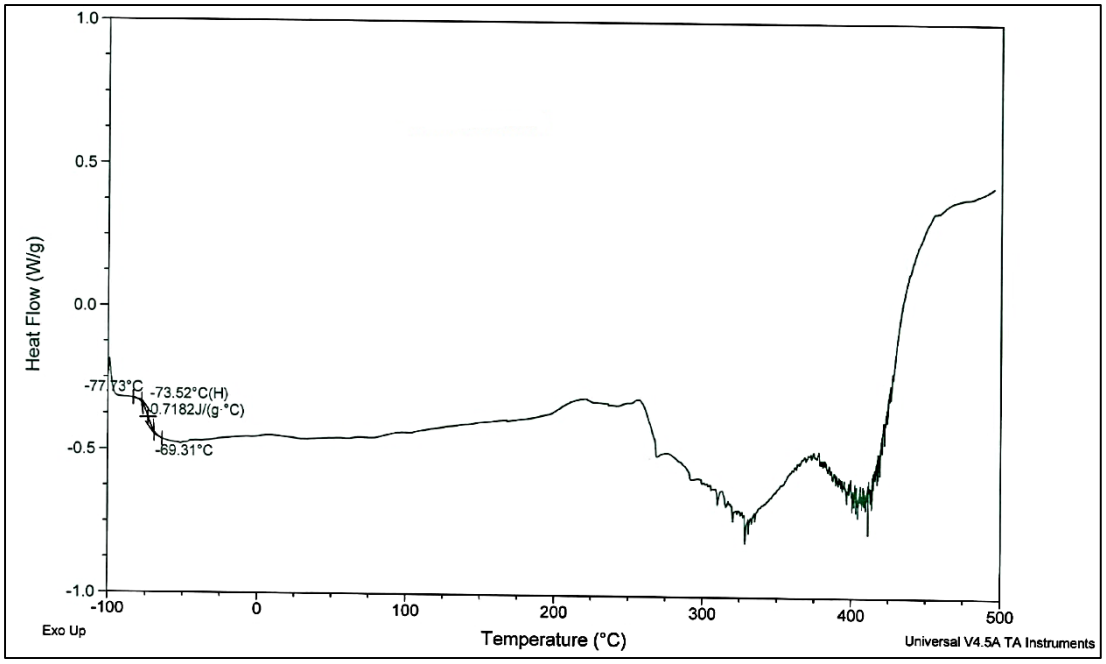

Figure D.4 DSC thermogram of TP-N3200-R1.2

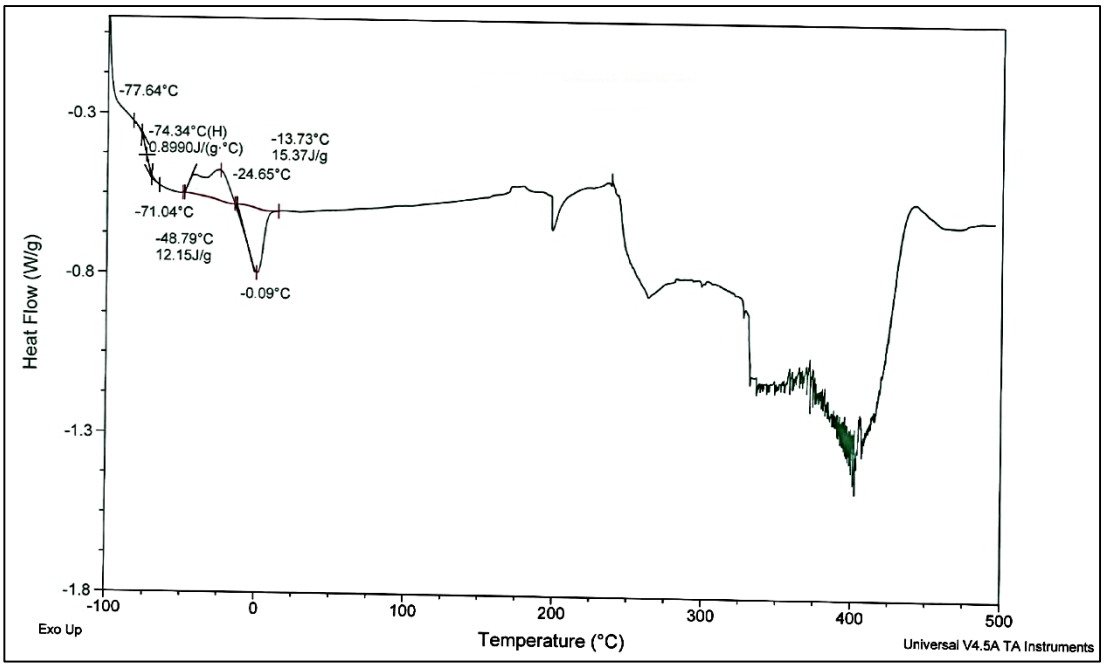

Figure D.5 DSC thermogram of TP-N100 IPDI(2:1)-R1.0

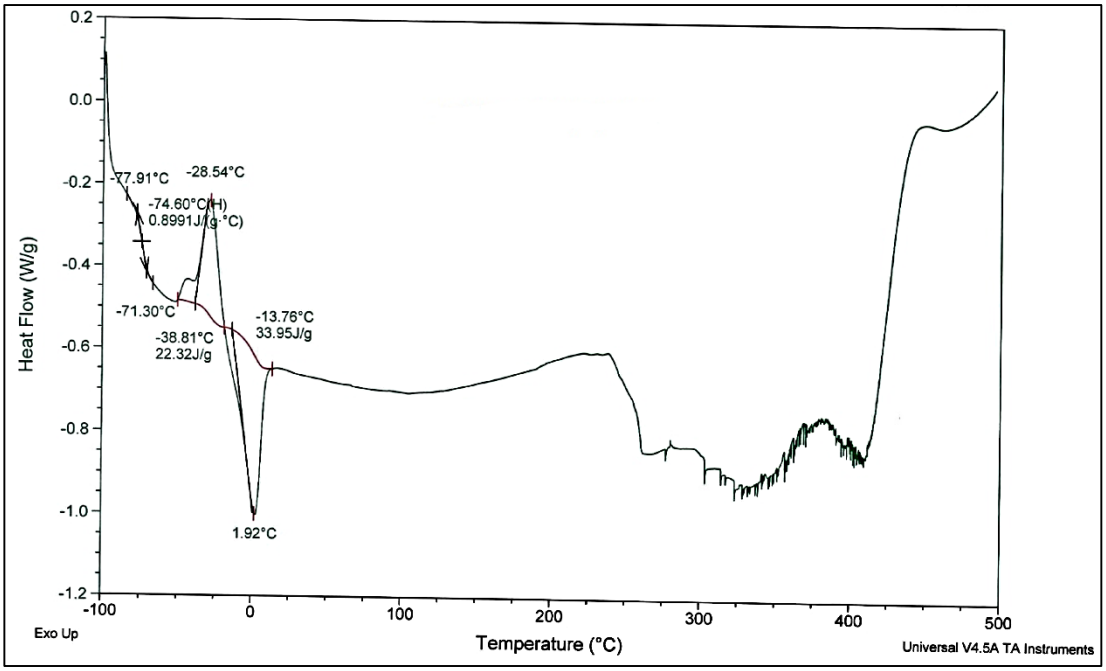

Figure D.6 DSC thermogram of TP-N3200 IPDI(2:1)-R1.0

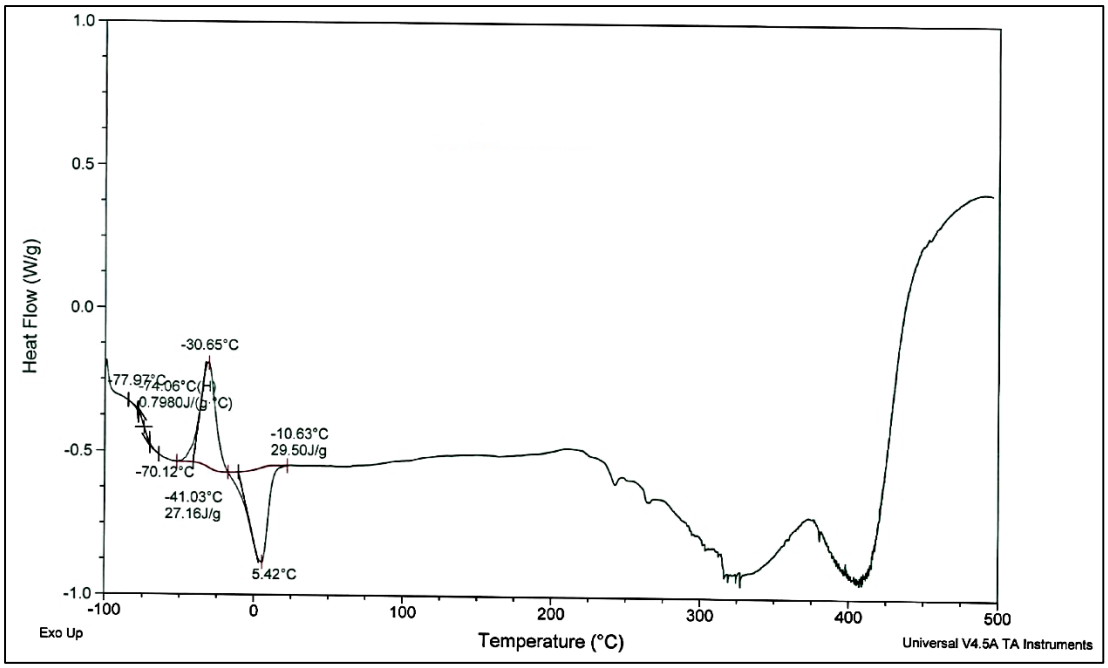

Figure D.7 DSC thermogram of TP-N3200-0.2BDO

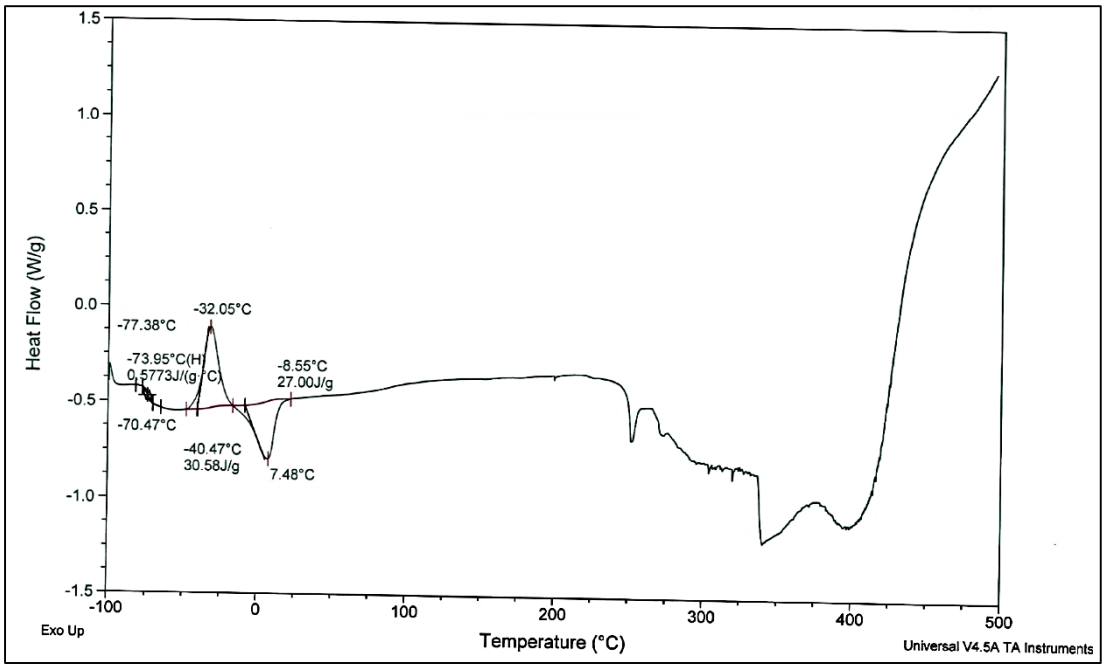

Figure D.8 DSC thermogram of TP-N3200-0.2TMP

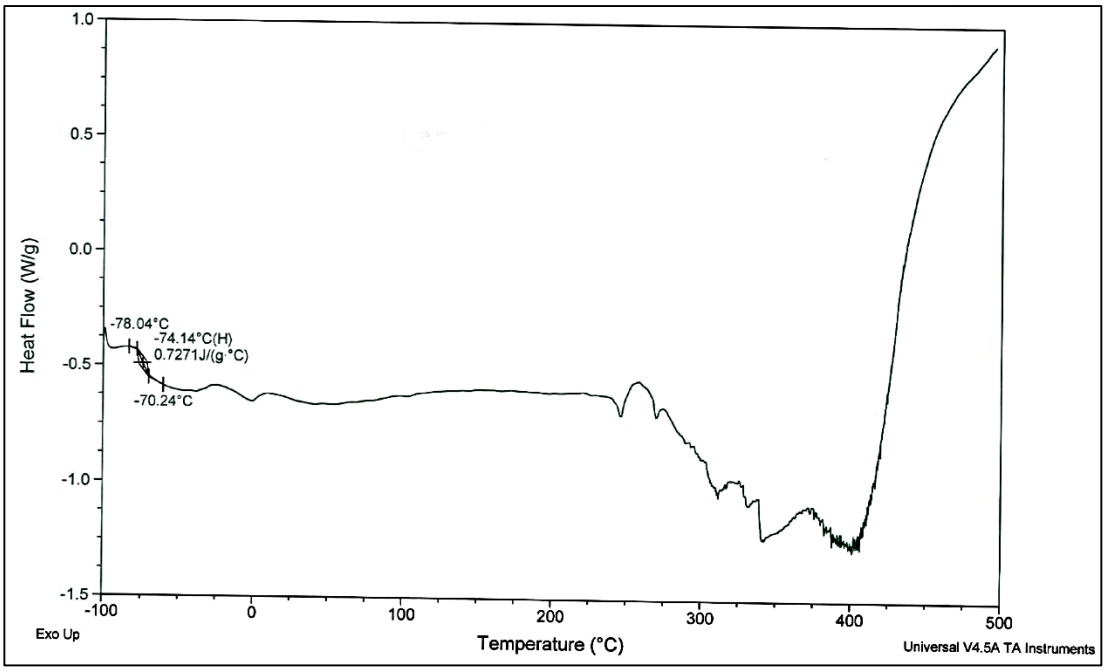

Figure D.9 DSC thermogram of TP-N3200-BDO-0.01FeAA

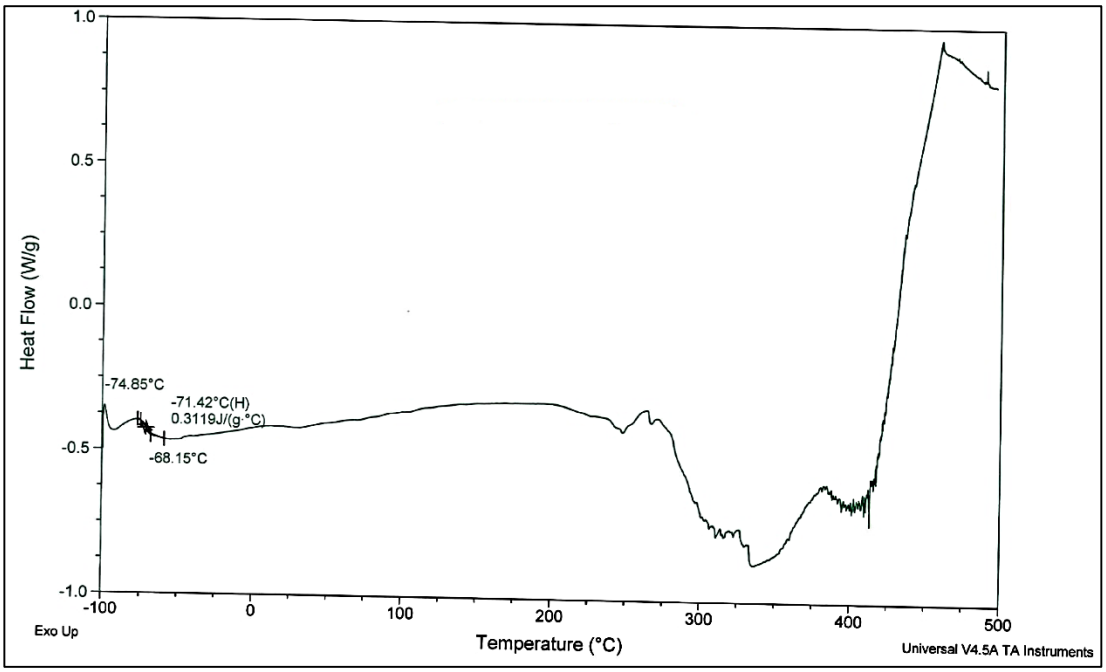

Figure D.10 DSC thermogram of TP-N3200-BDO-0.01DBTDL

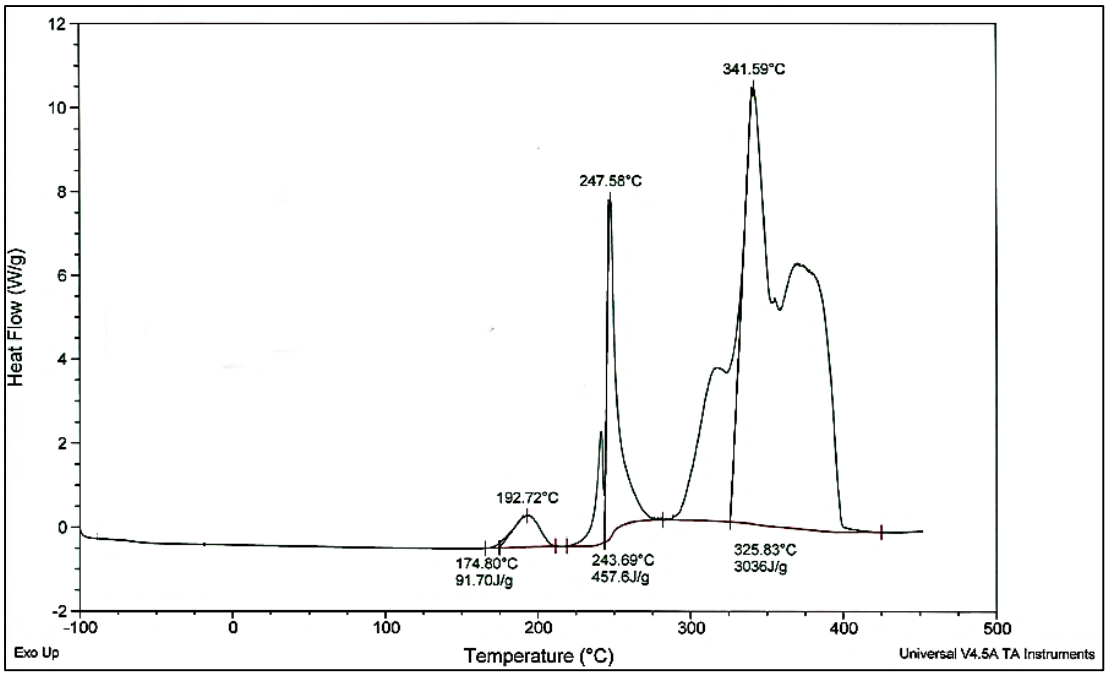

Figure D.11 DSC thermogram of TPAP-1

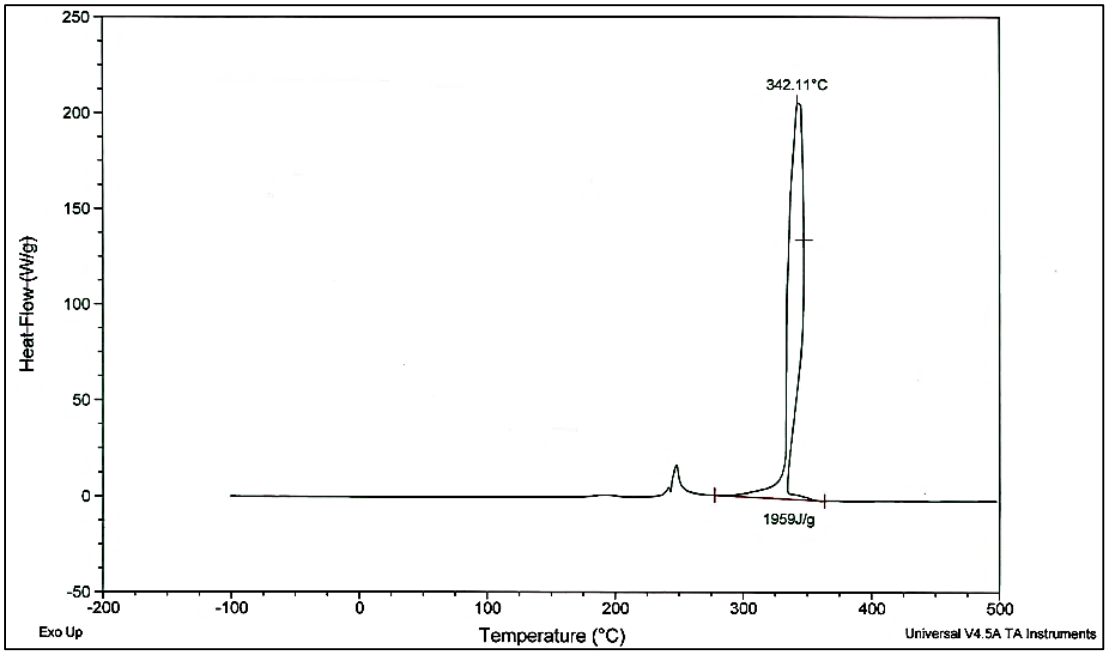

Figure D.12 DSC thermogram of TPAP-2

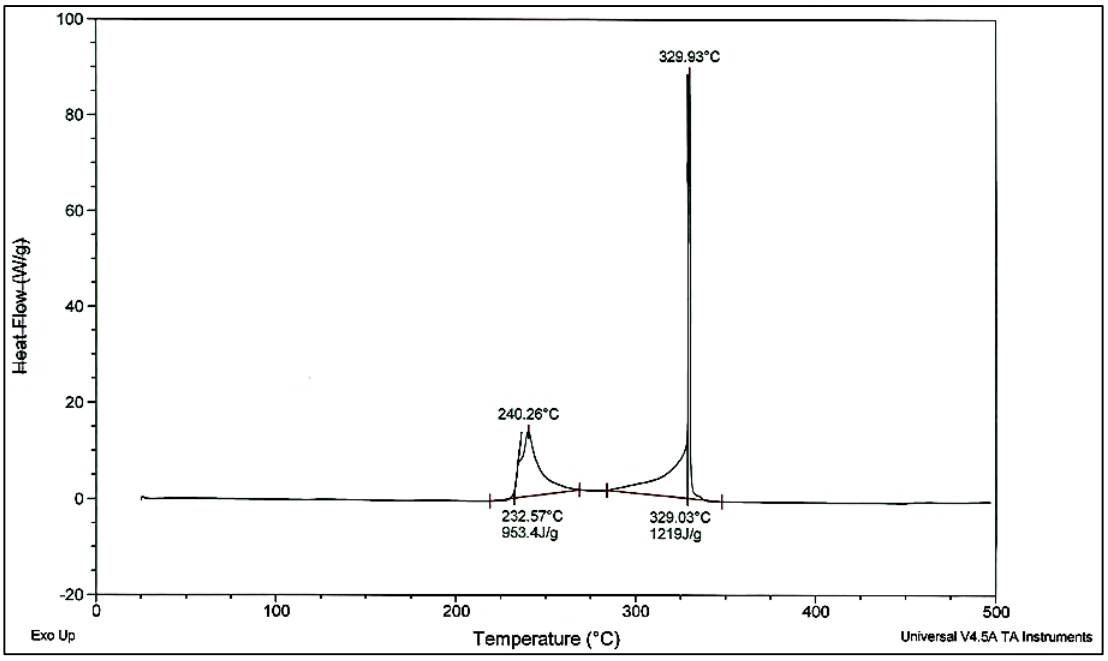

Figure D.13 DSC thermogram of TPAP-3

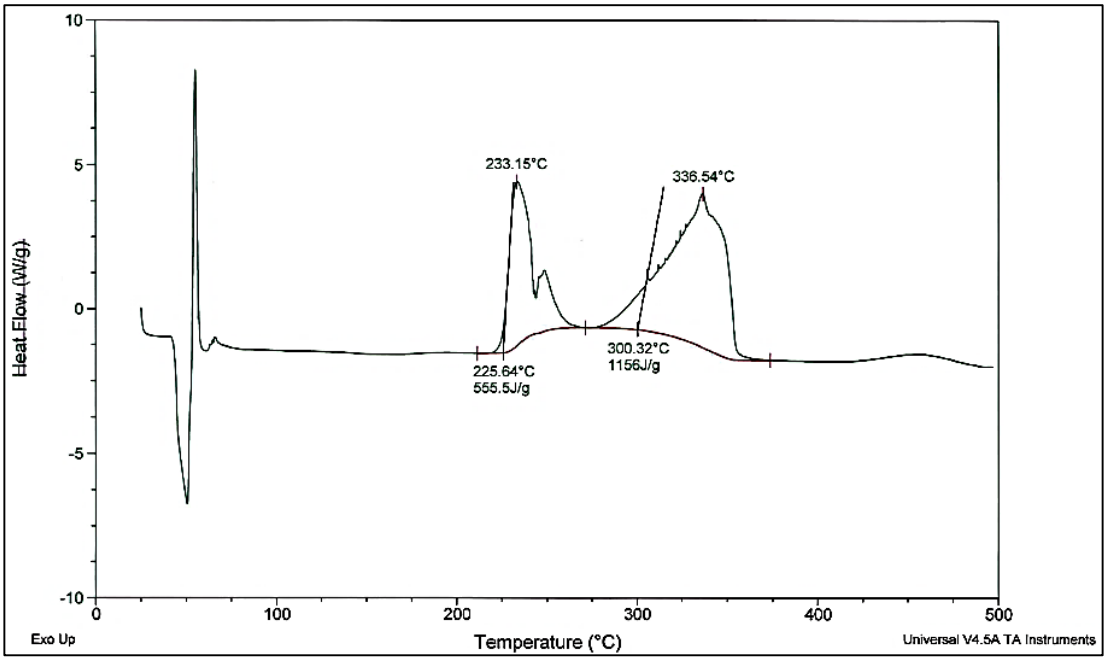

Figure D.14 DSC thermogram of TPAP-4

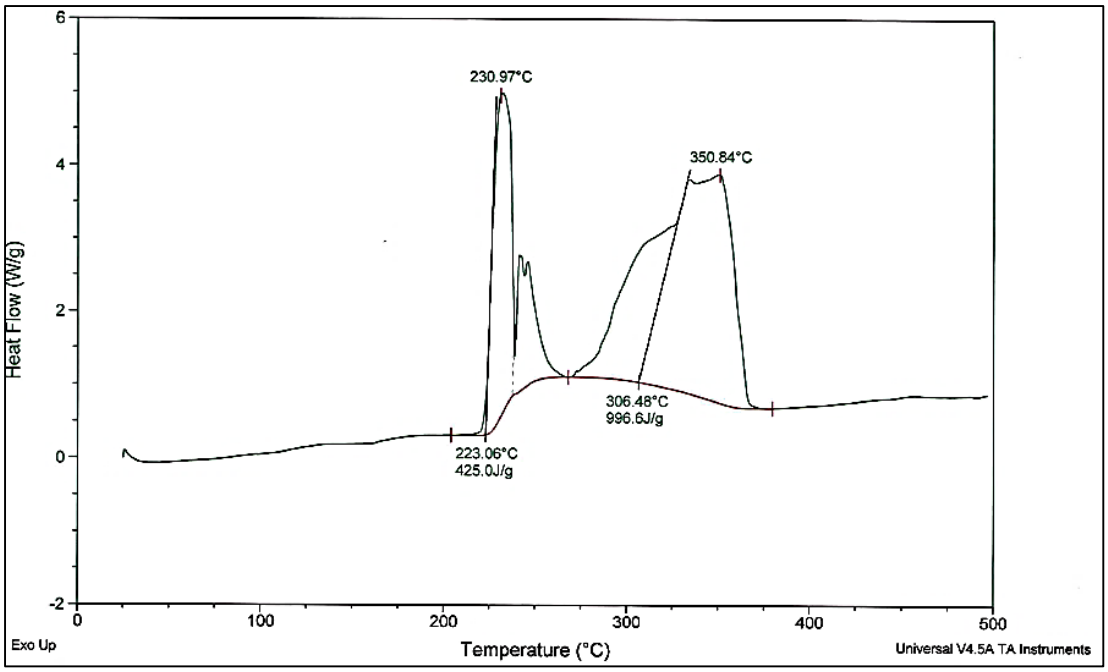

Figure D.15 DSC thermogram of TPAP-5

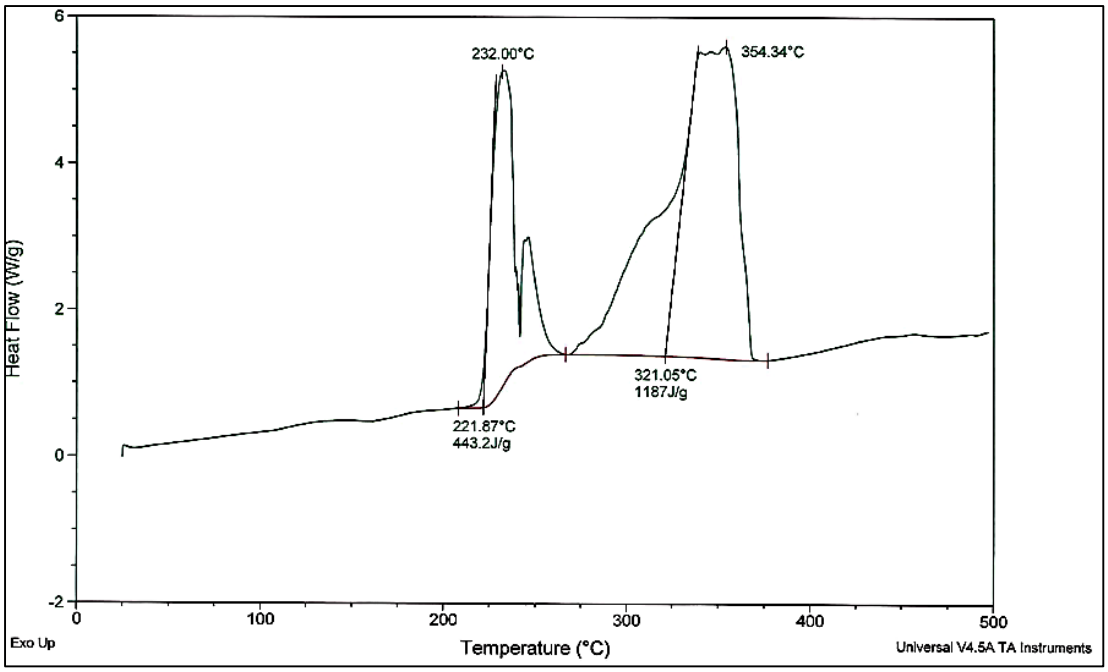

Figure D.16 DSC thermogram of TPAP-6

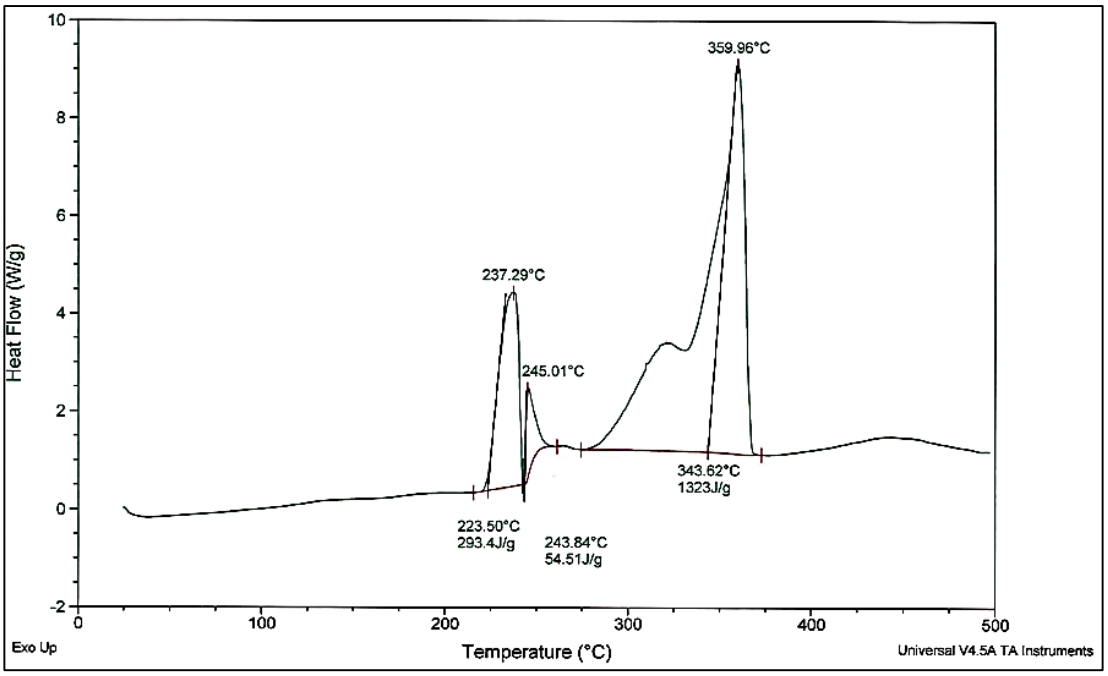

Figure D.17 DSC thermogram of TPAP-7

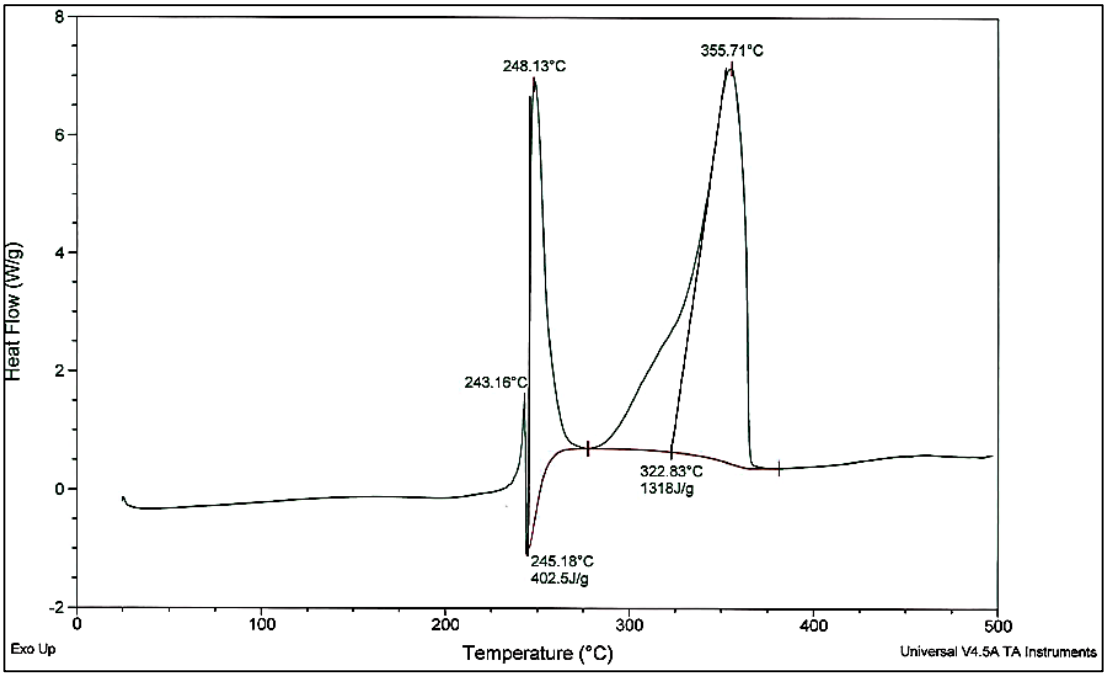

Figure D.18 DSC thermogram of TPAP-8

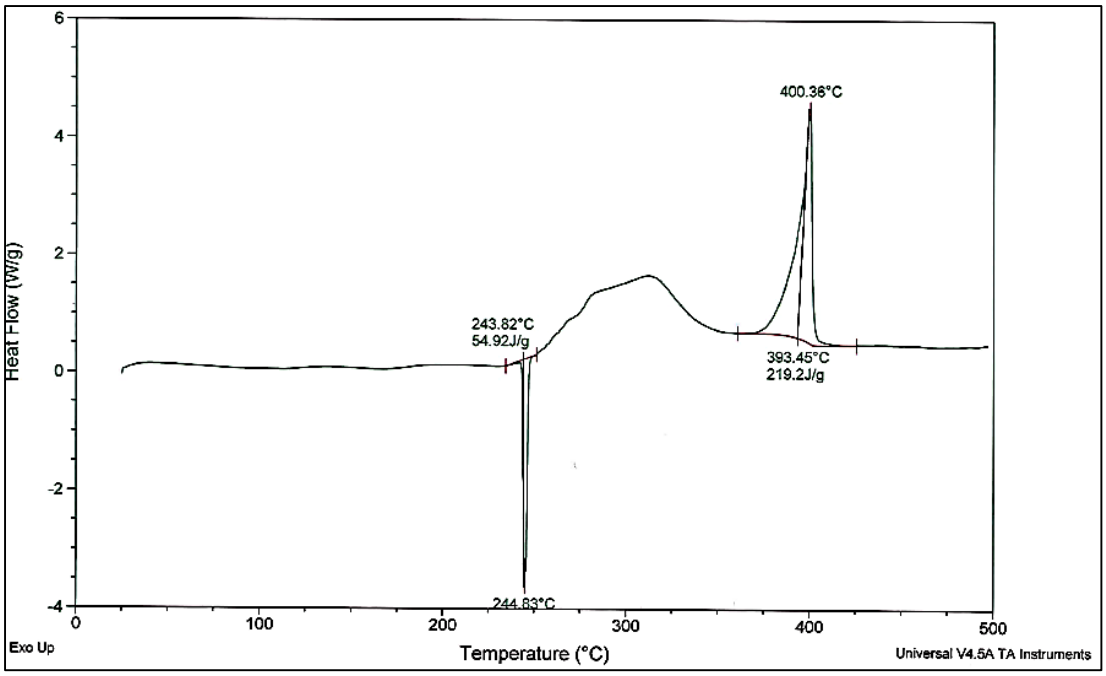

Figure D.19 DSC thermogram of TPAP-9

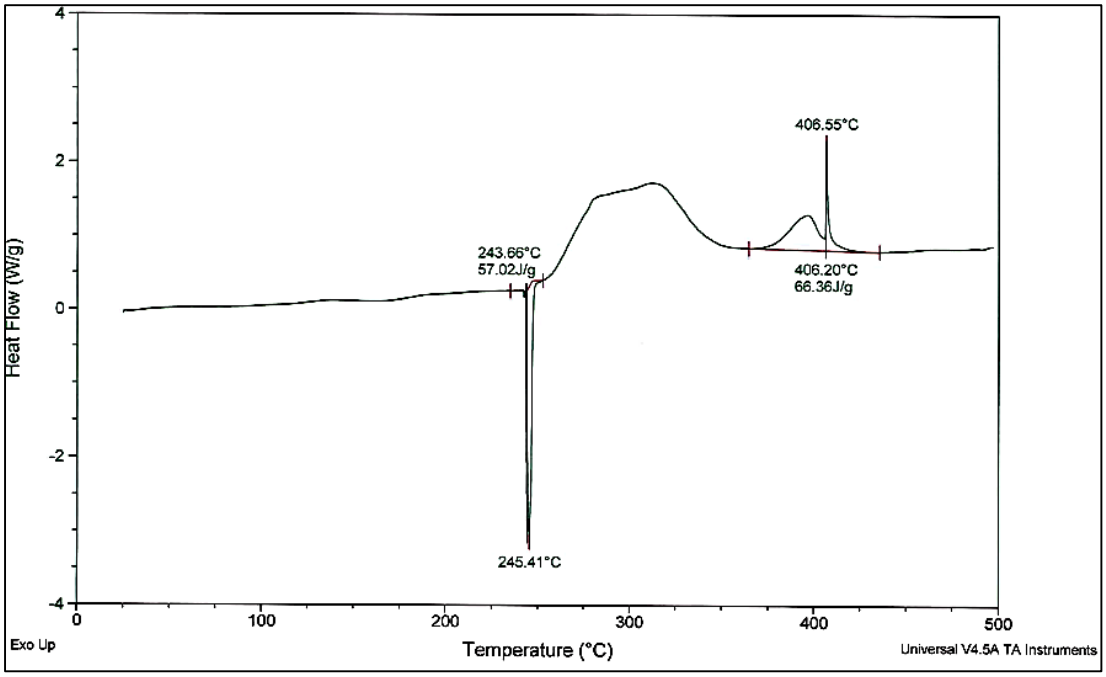

Figure D.20 DSC thermogram of TPAP-10

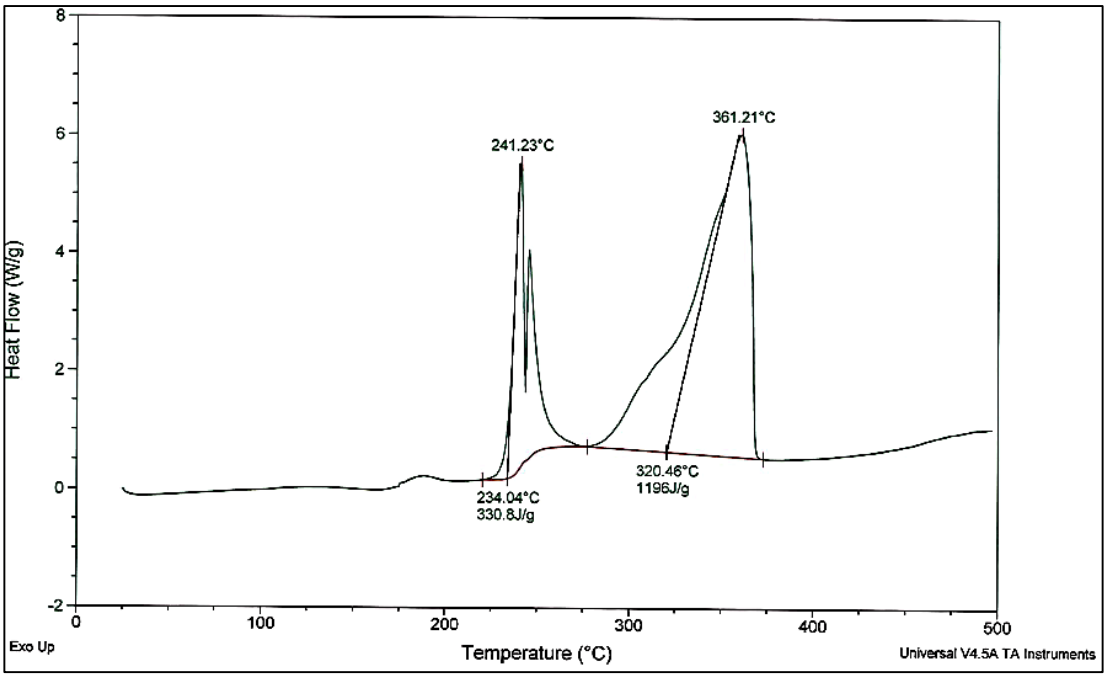

Figure D.21 DSC thermogram of TPAP-11

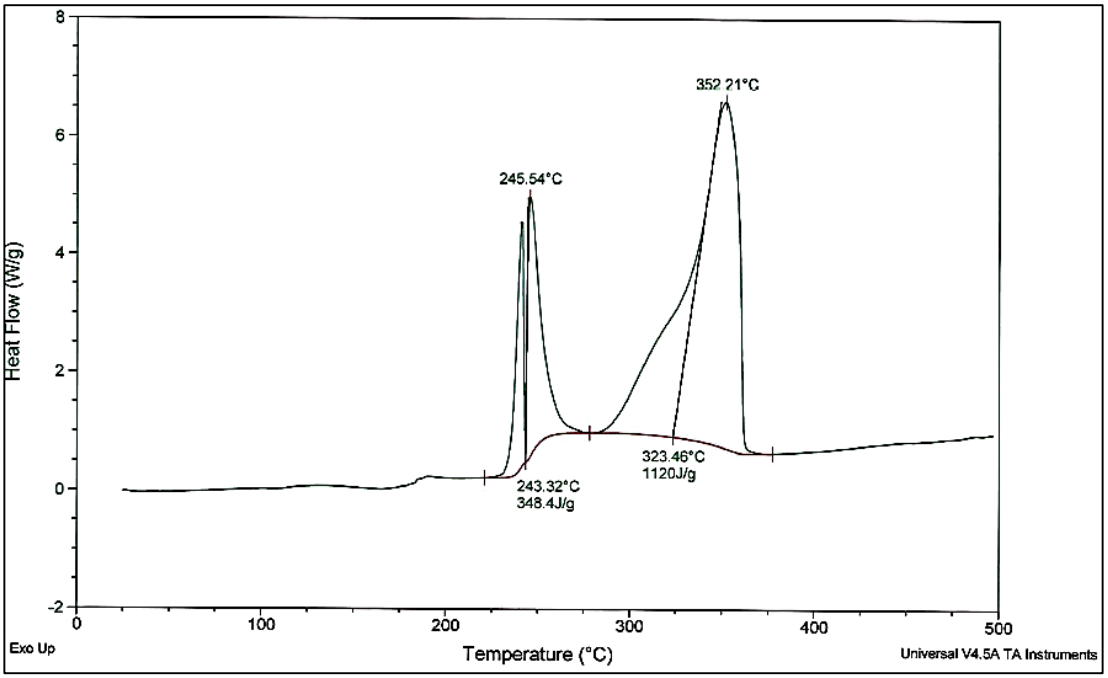

Figure D.22 DSC thermogram of TPAP-12

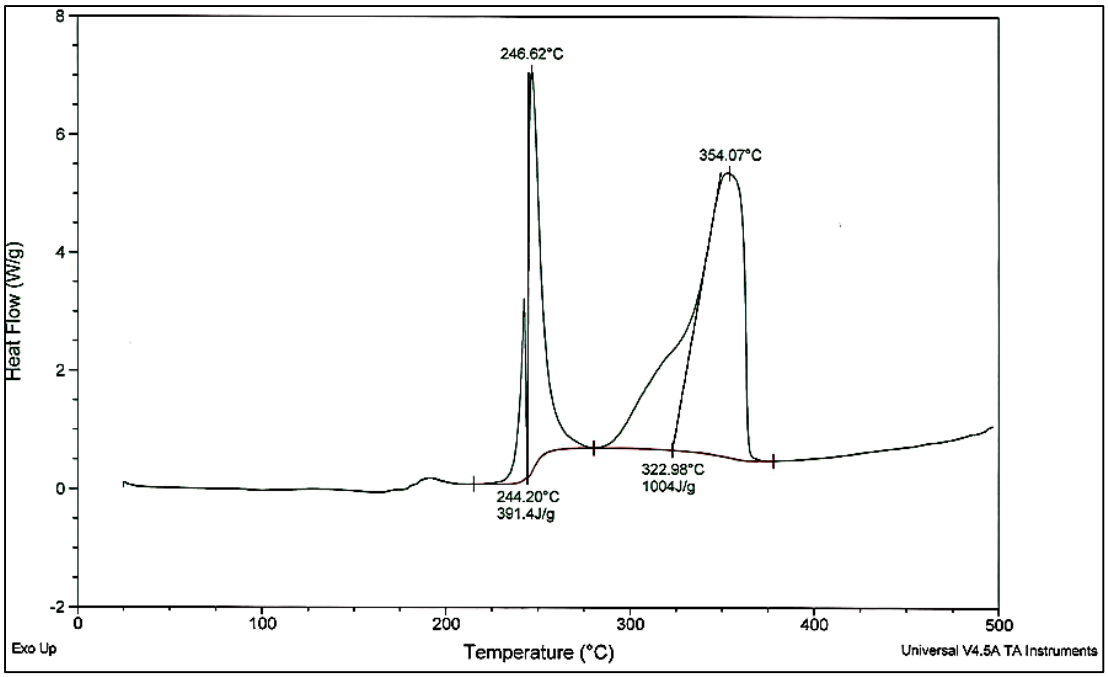

Figure D.23 DSC thermogram of TPAP-13

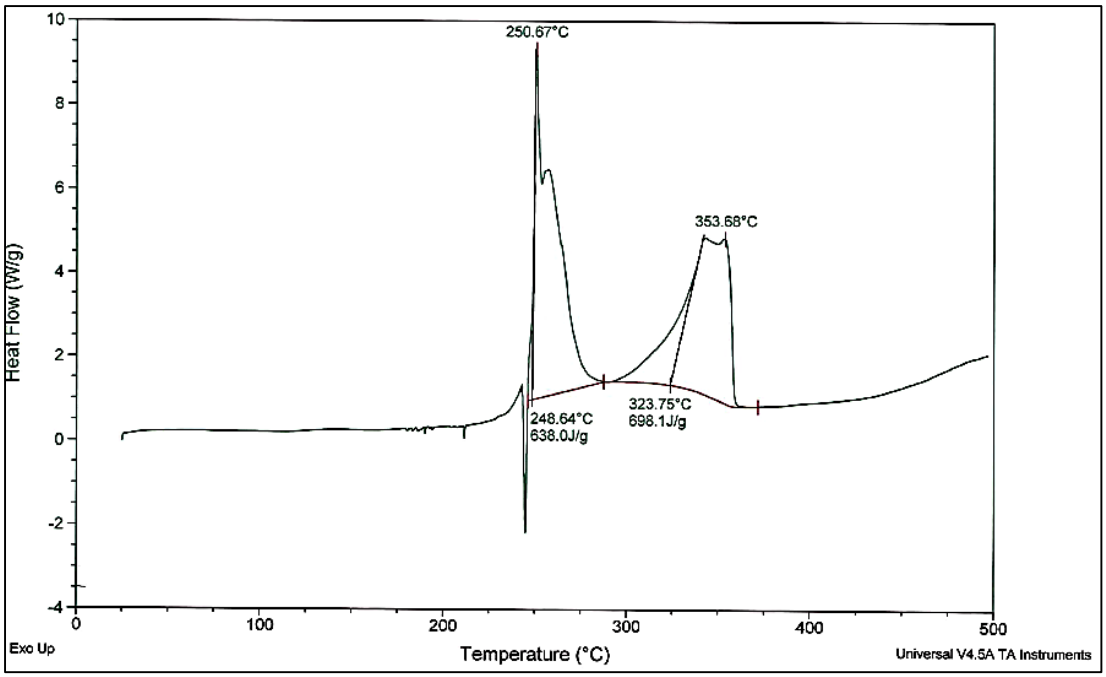

Figure D.24 DSC thermogram of TPAPX-1

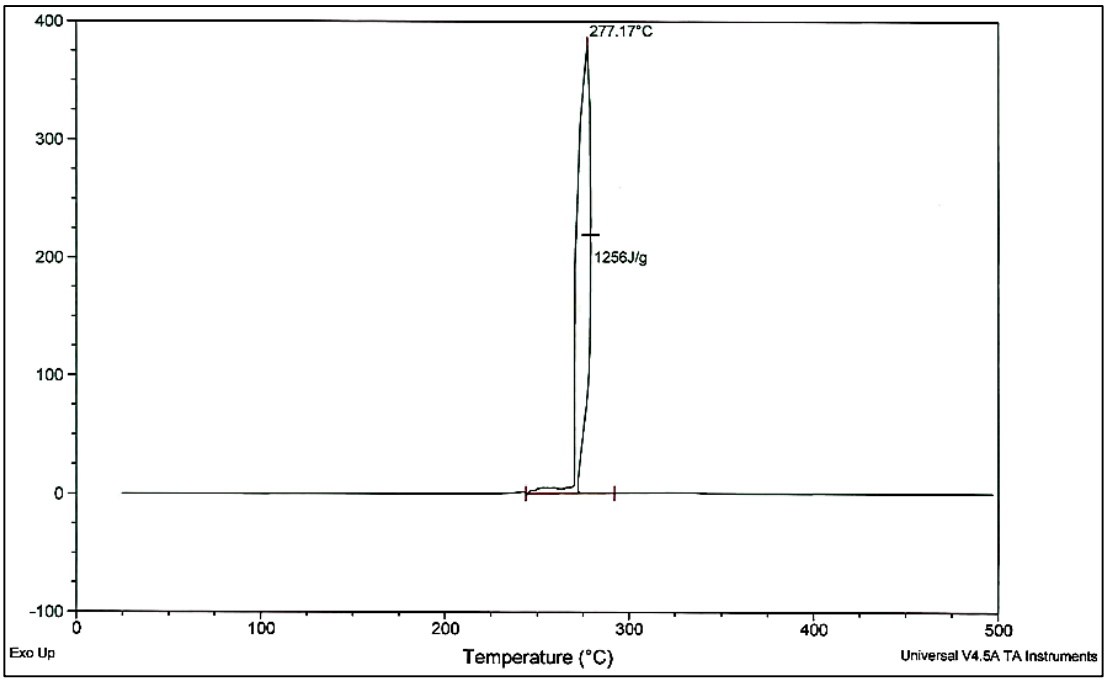

Figure D.25 DSC thermogram of TPAPX-2

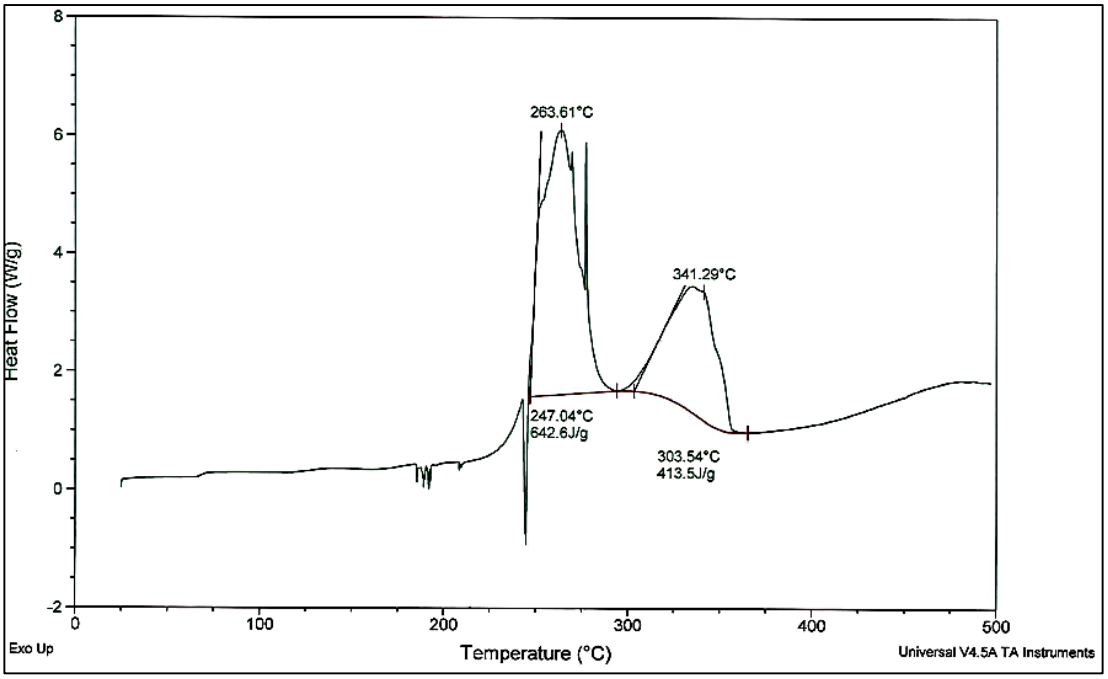

Figure D.26 DSC thermogram of TPAPXL-1

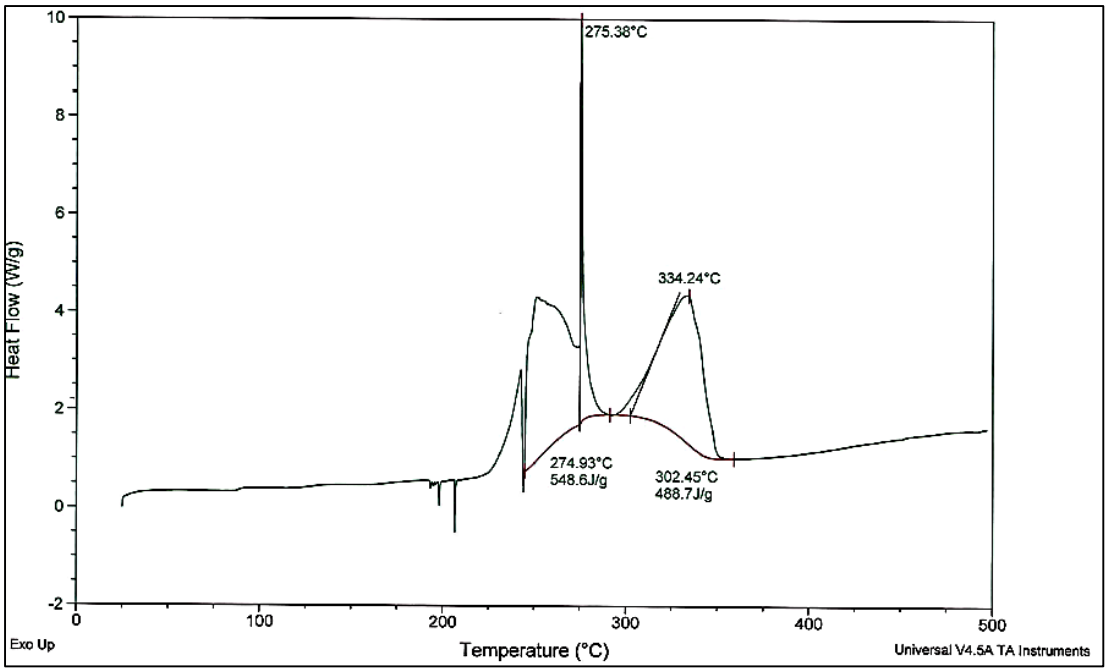

Figure D.27 DSC thermogram of TPAPXL-2

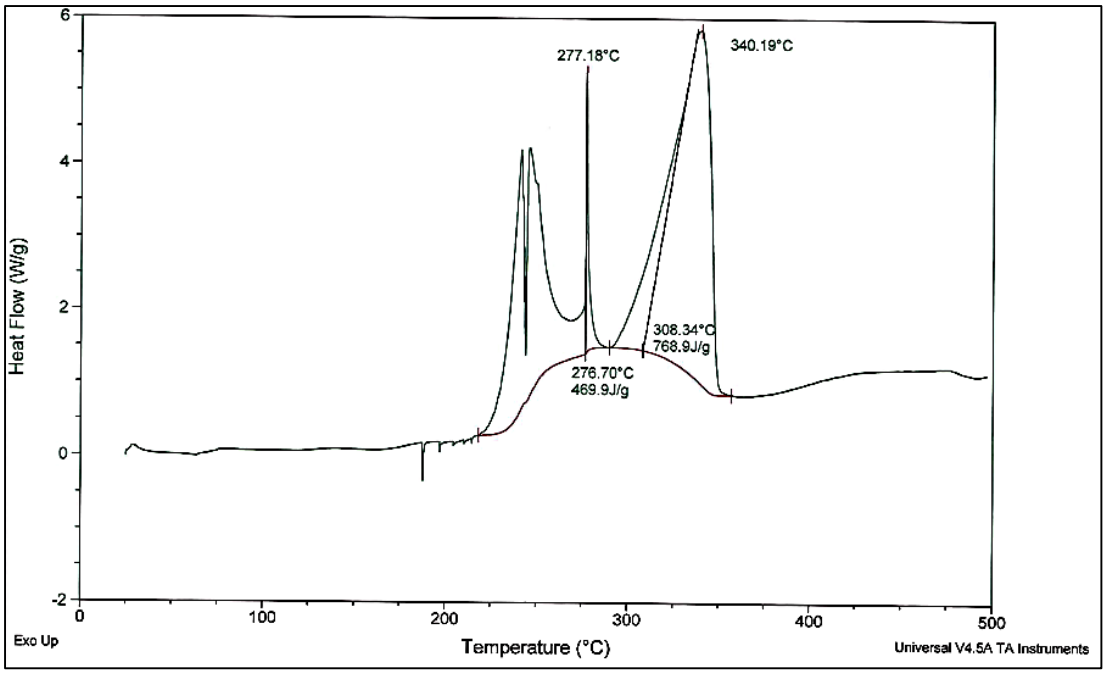

Figure D.28 DSC thermogram of TPAPXL-3

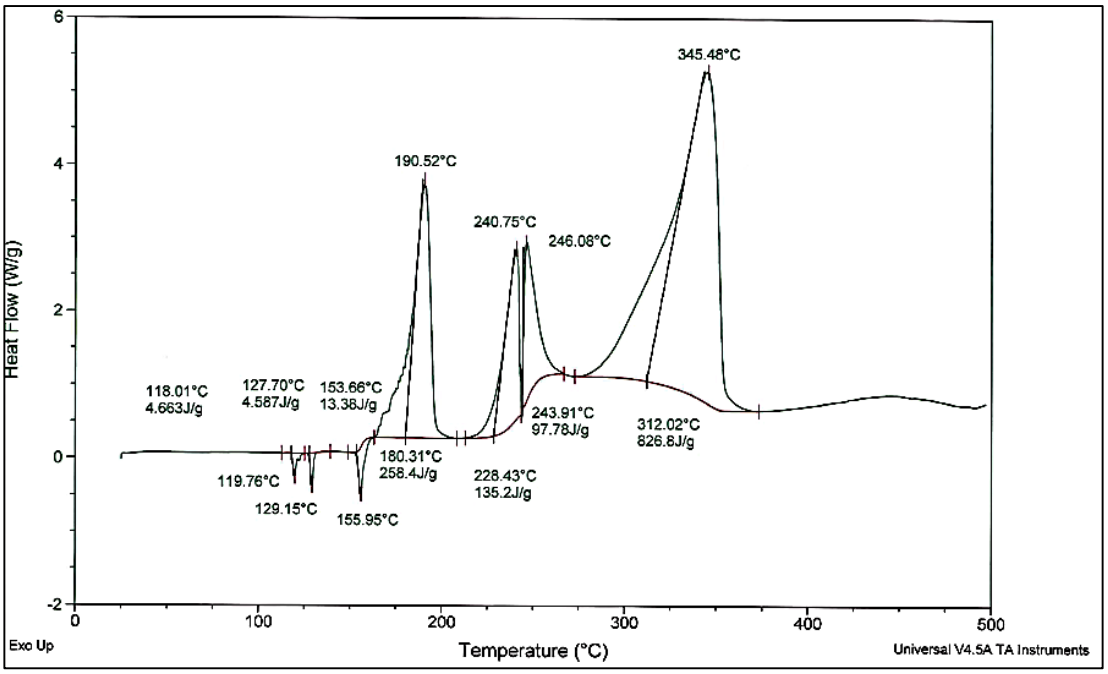

Figure D.29 DSC thermogram of TPAPSN-1

APPENDIX E

TGA THERMOGRAMS

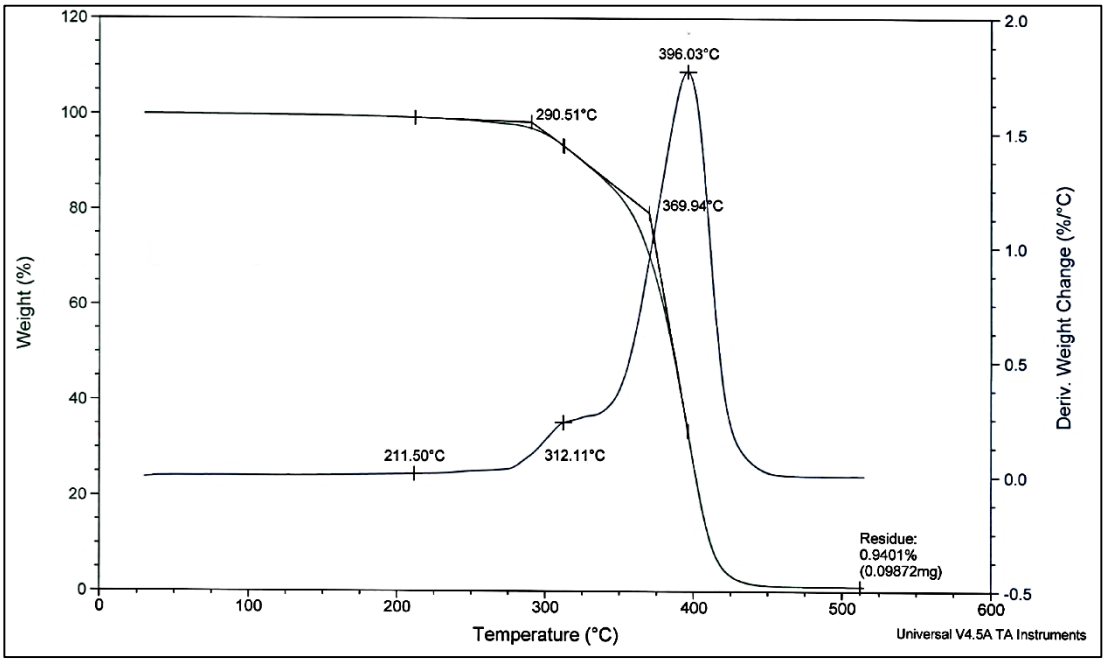

Figure E.1 TGA thermogram of TP-N100-R1.0

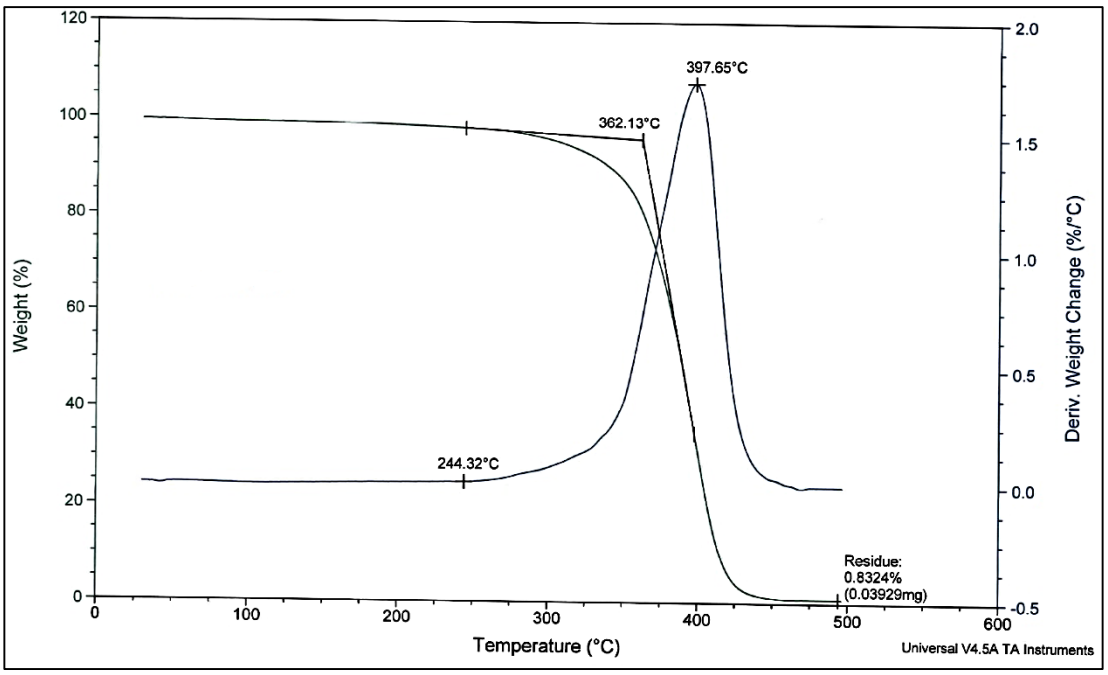

Figure E.2 TGA thermogram of TP-N3200-R0.8

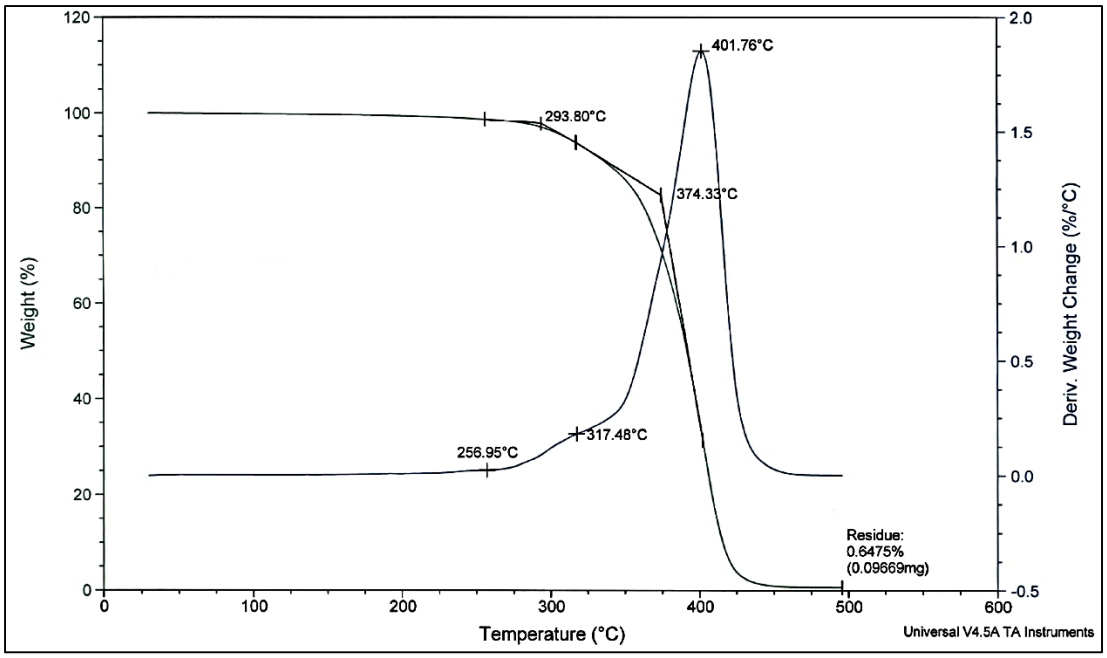

Figure E.3 TGA thermogram of TP-N3200-R1.0

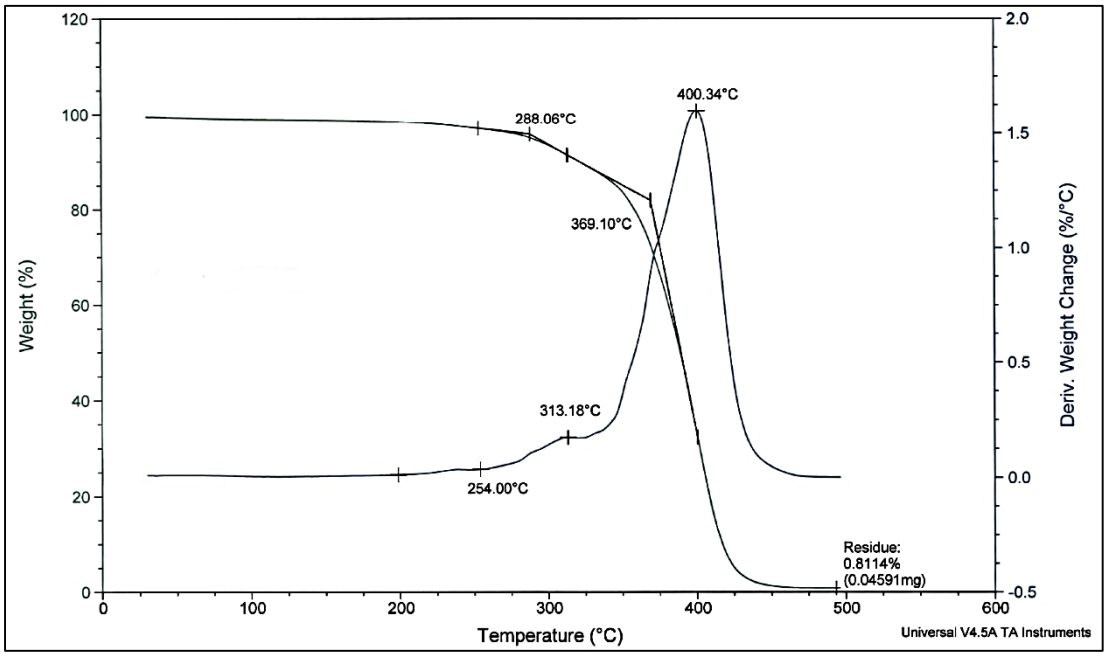

Figure E.4 TGA thermogram of TP-N3200-R1.2

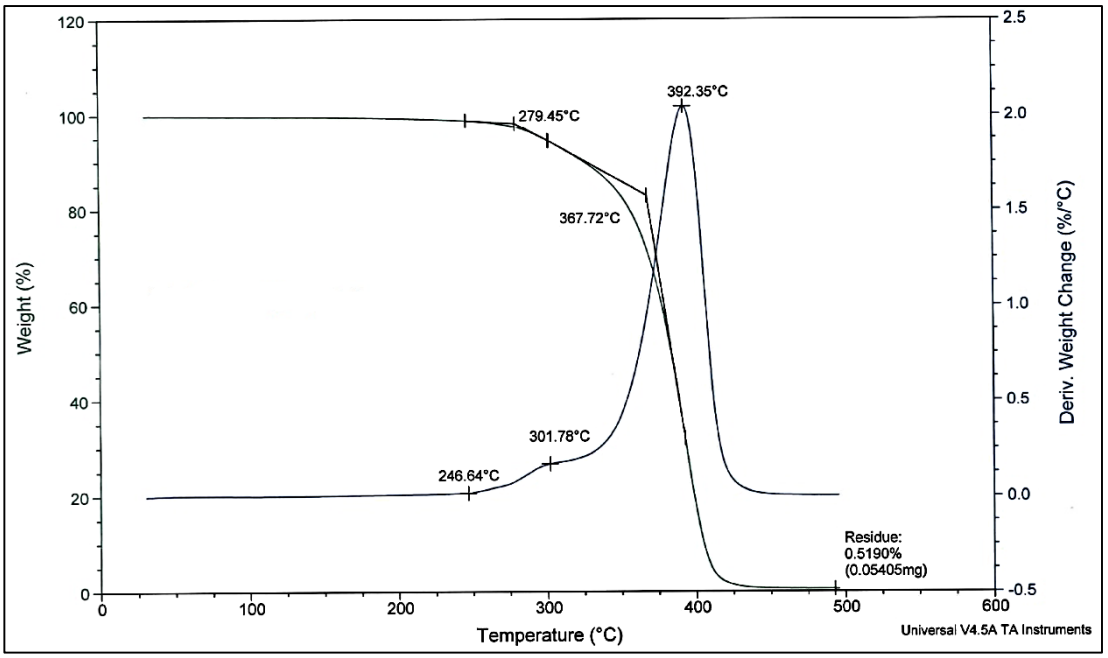

Figure E.5 TGA thermogram of TP-N100-IPDI(2:1)-R1.0

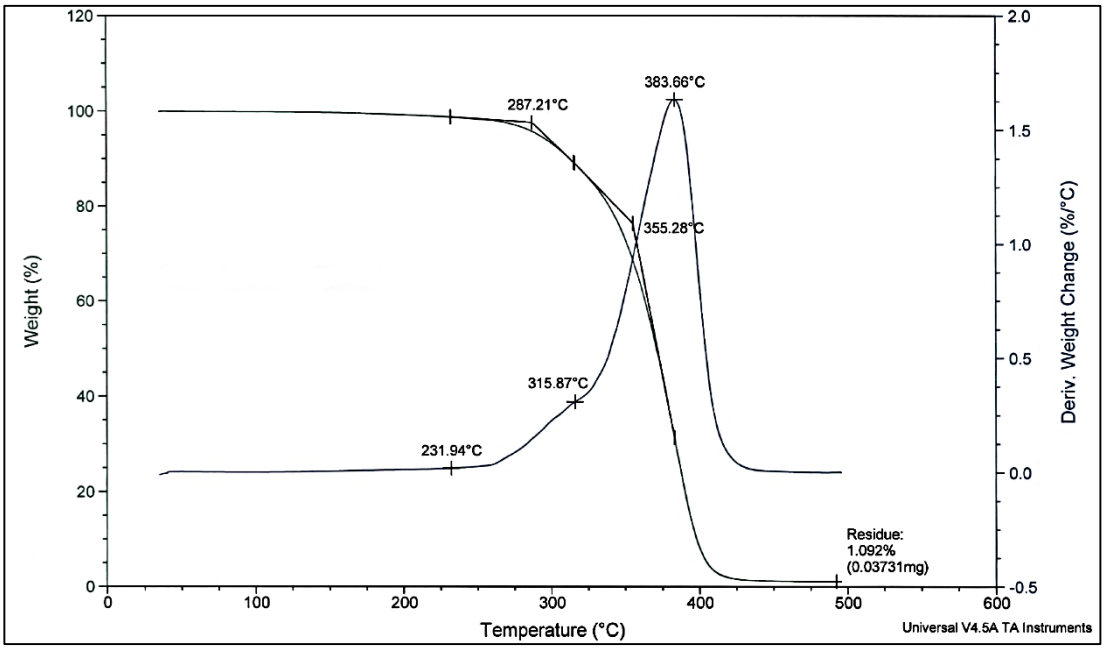

Figure E.6 TGA thermogram of TP-N3200-IPDI(2:1)-R1.0

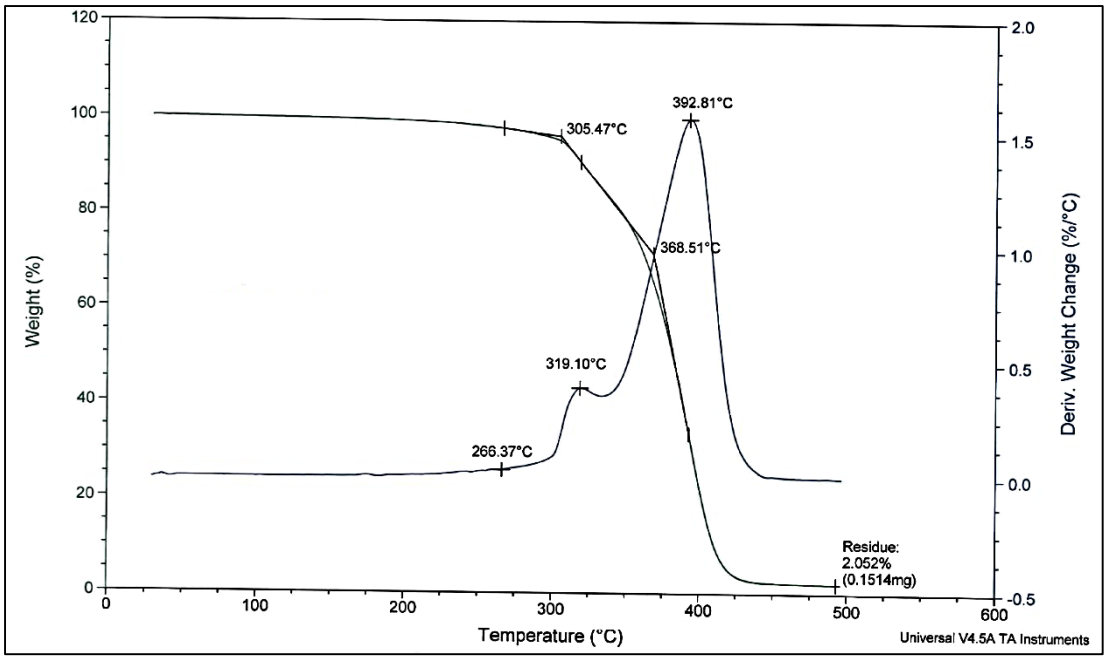

Figure E.7 TGA thermogram of TP-N3200-0.2BDO

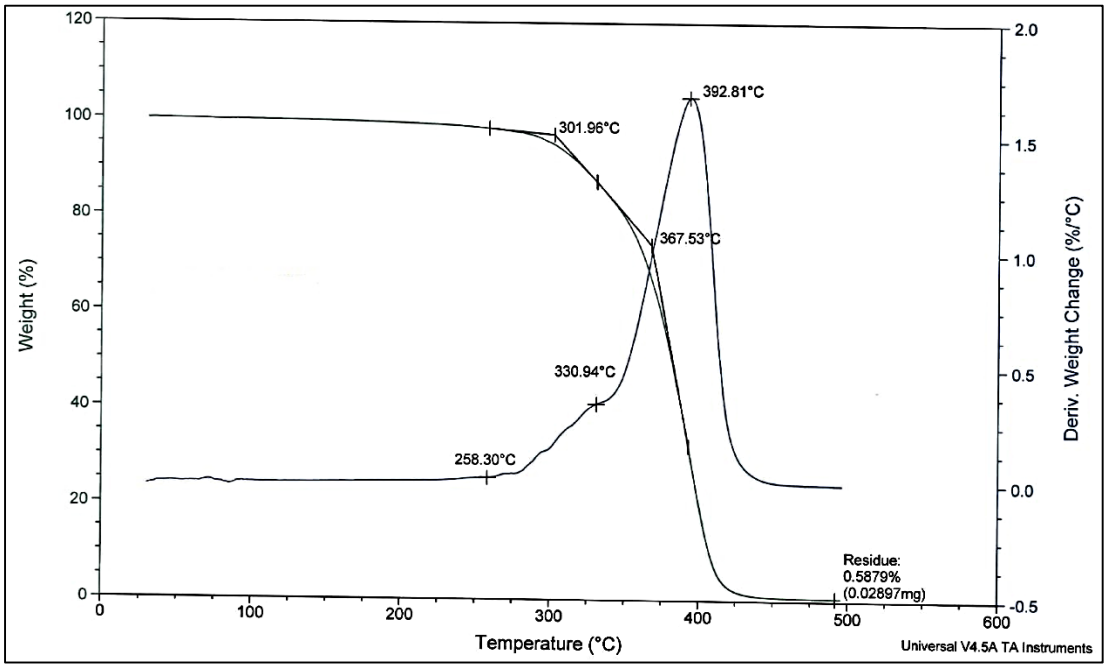

Figure E.8 TGA thermogram of TP-N3200-0.2TMP

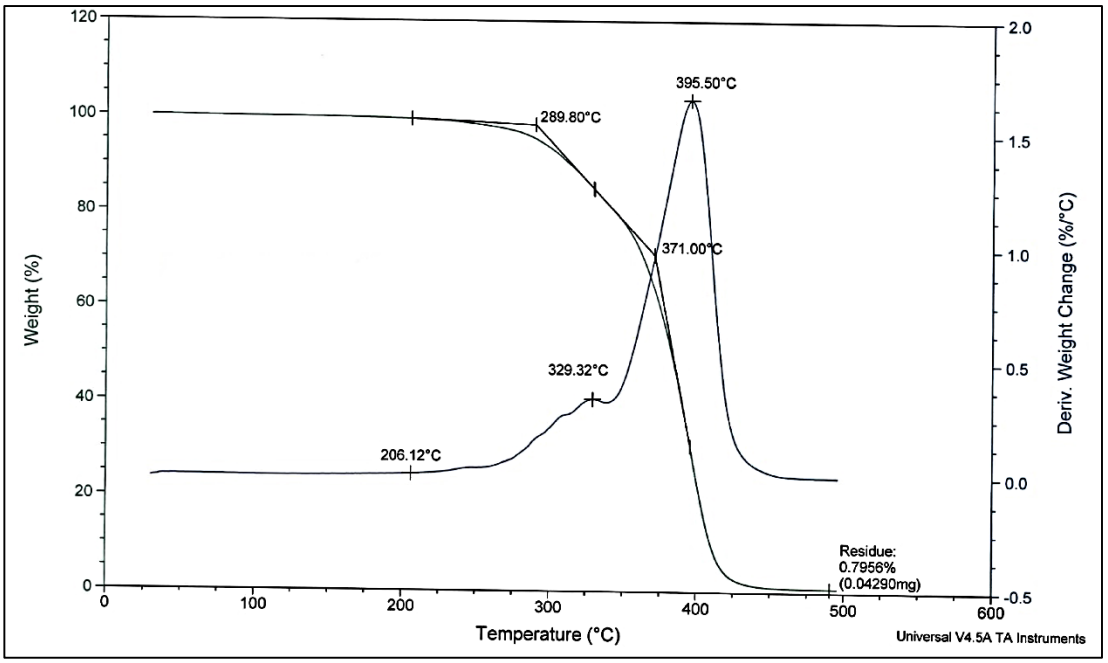

Figure E.9 TGA thermogram of TP-N3200-BDO-0.01FeAA

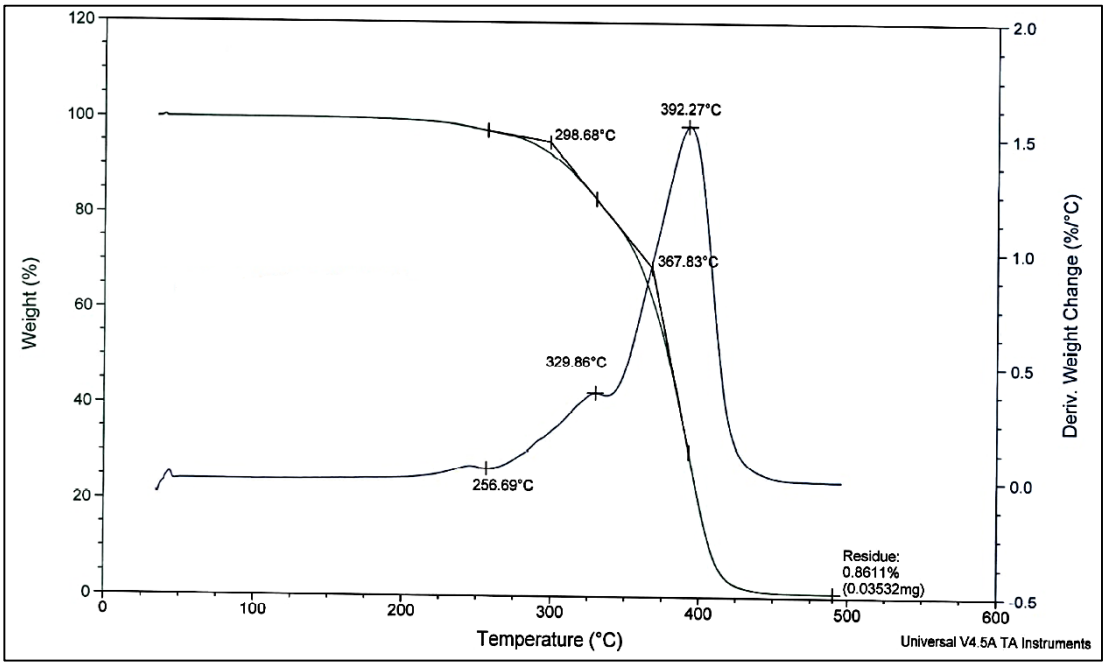

Figure E.10 TGA thermogram of TP-N3200-BDO-0.01DBTDL

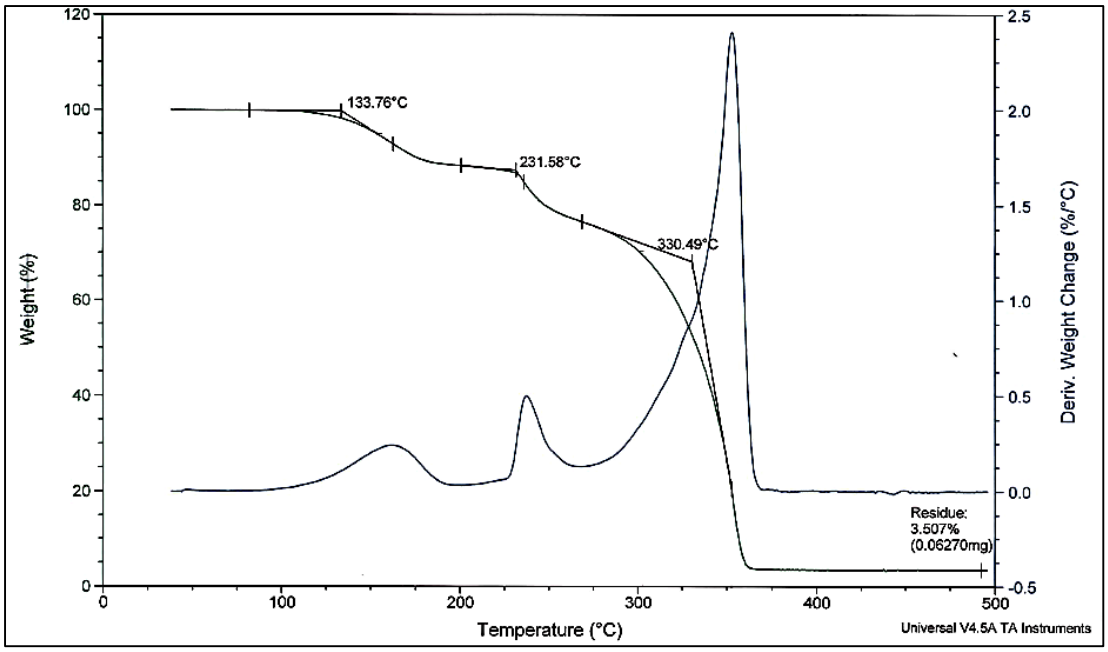

Figure E.11 TGA thermogram of TPAP-1

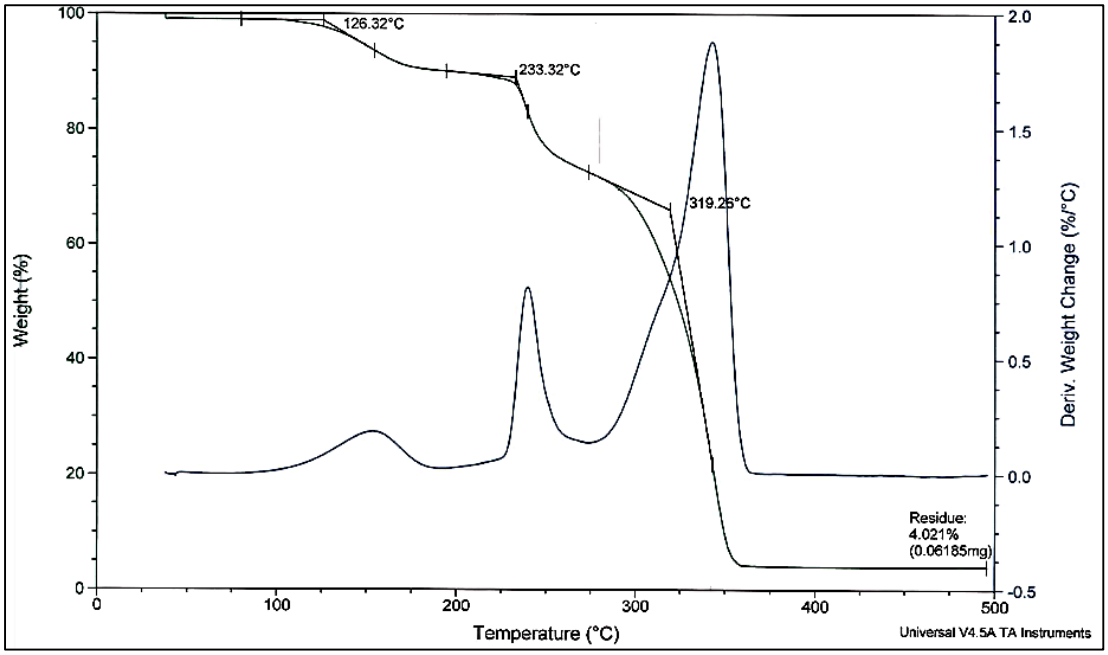

Figure E.12 TGA thermogram of TPAP-2

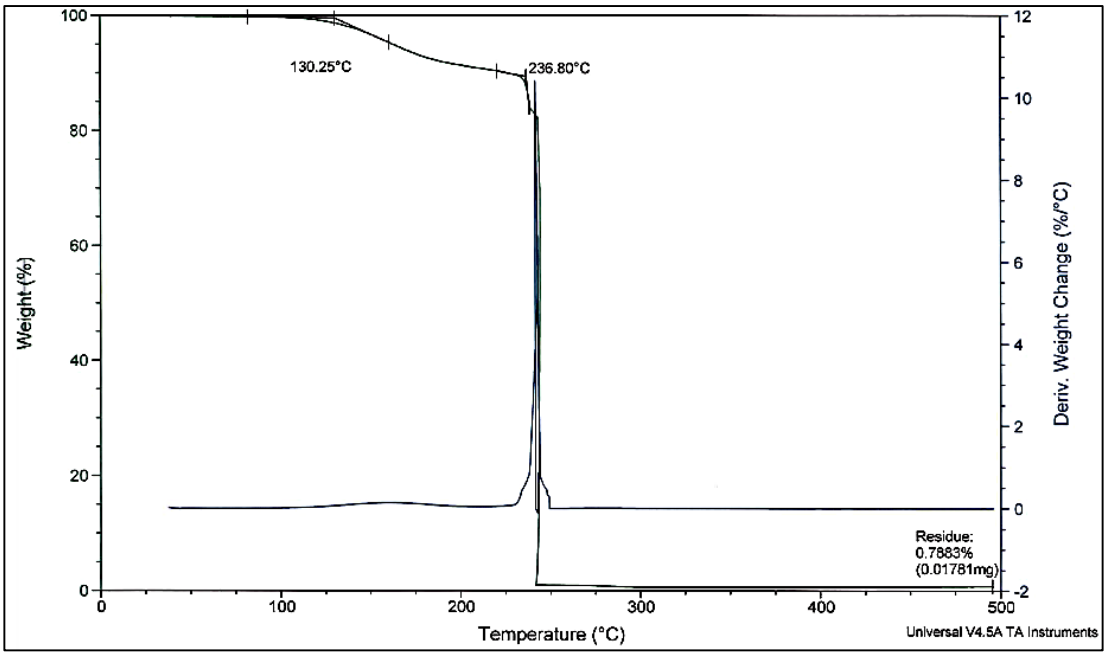

Figure E.13 TGA thermogram of TPAP-3

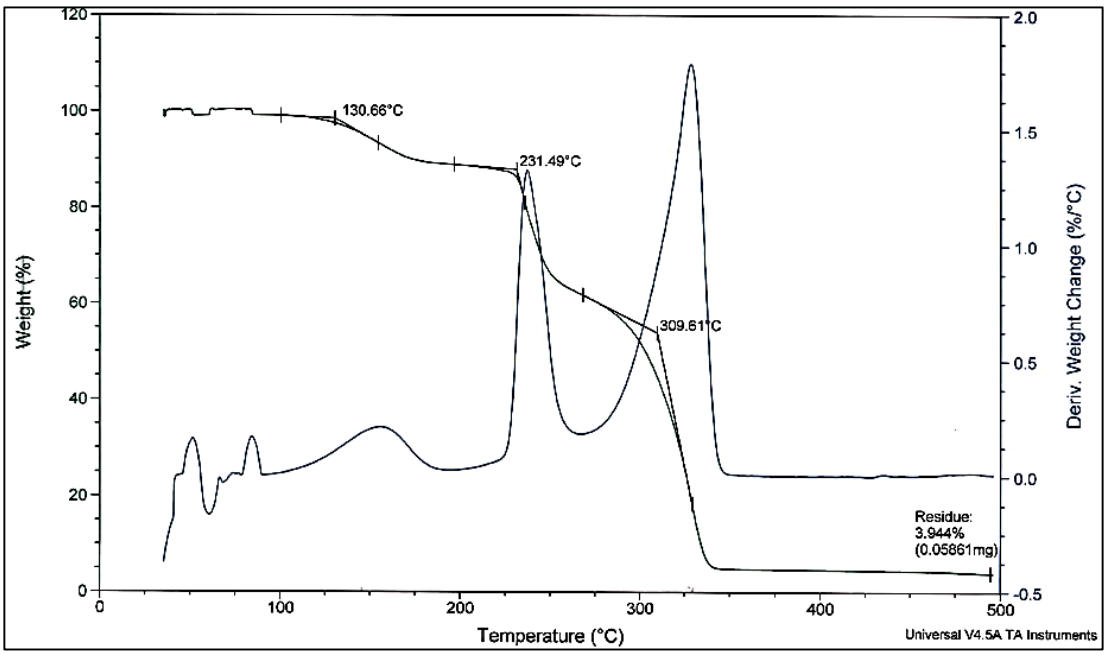

Figure E.14 TGA thermogram of TPAP-4

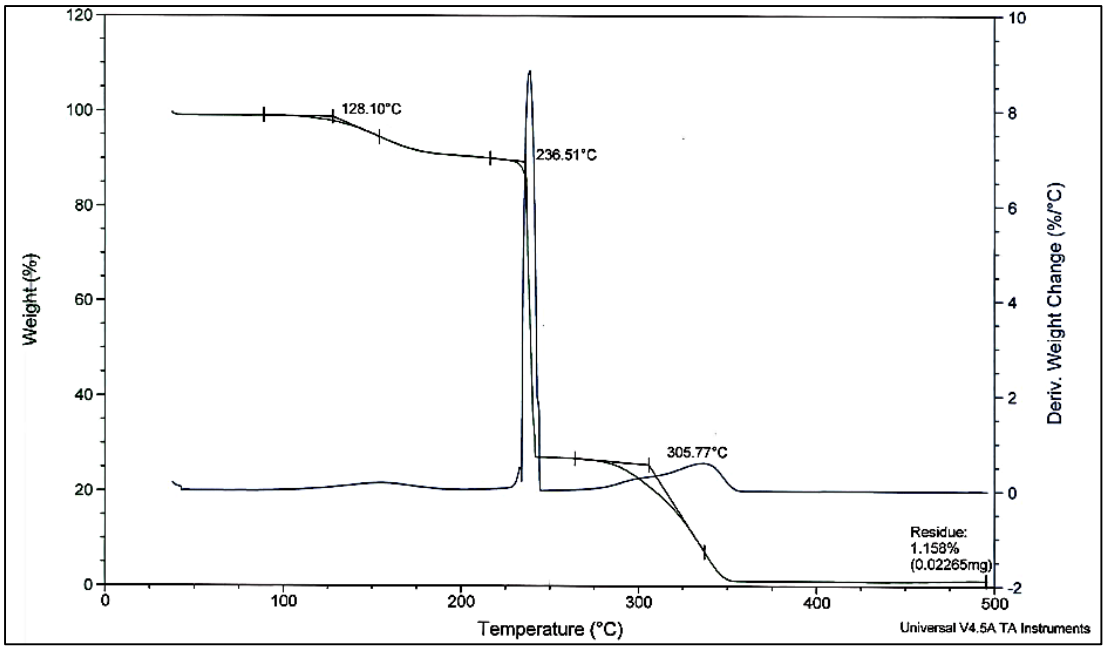

Figure E.15 TGA thermogram of TPAP-5

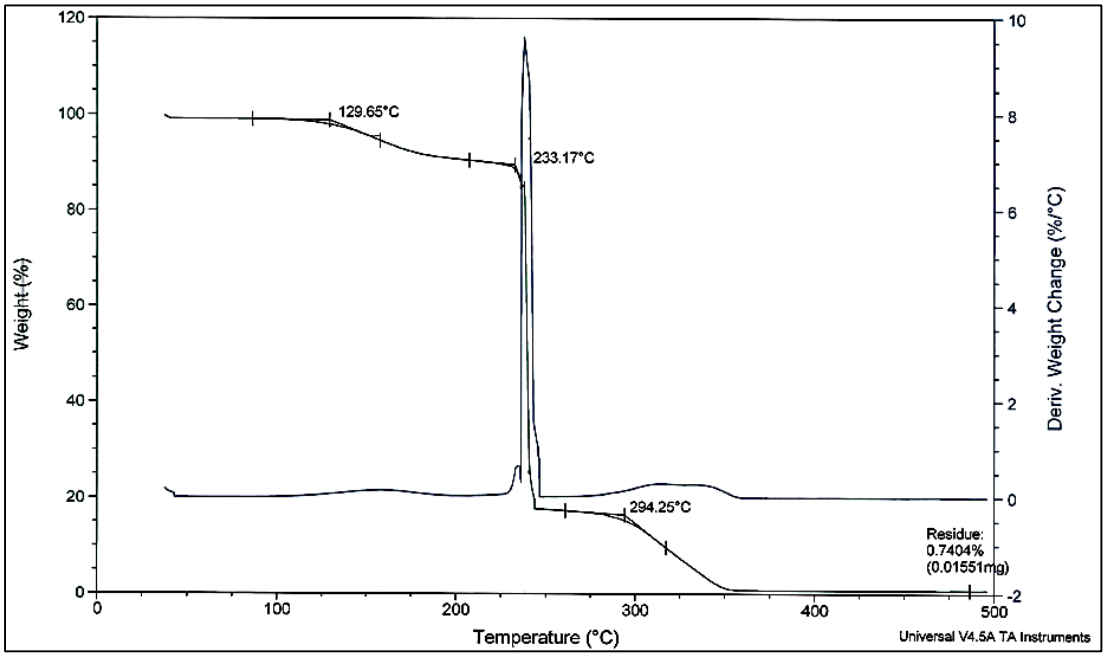

Figure E.16 TGA thermogram of TPAP-6

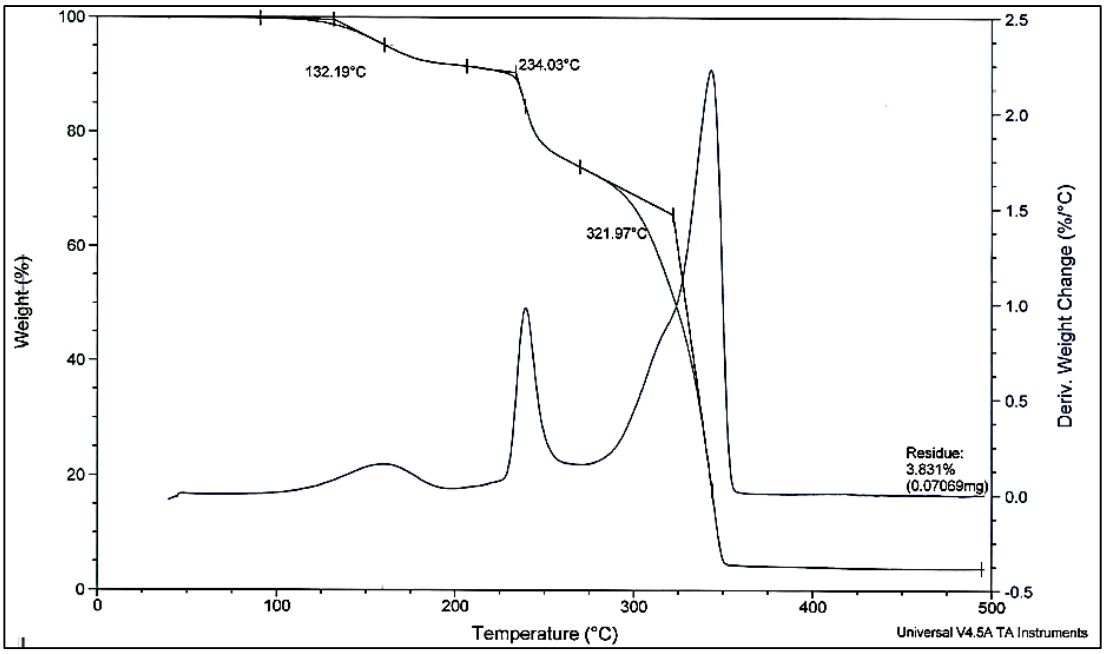

Figure E.17 TGA thermogram of TPAP-7

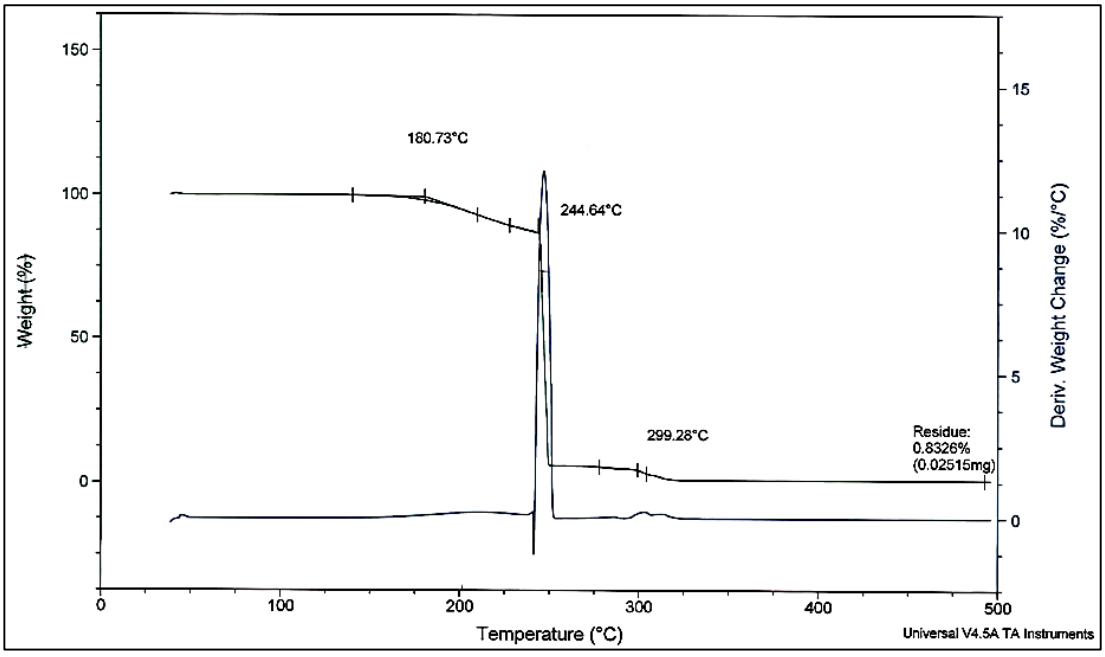

Figure E.18 TGA thermogram of TPAP-8

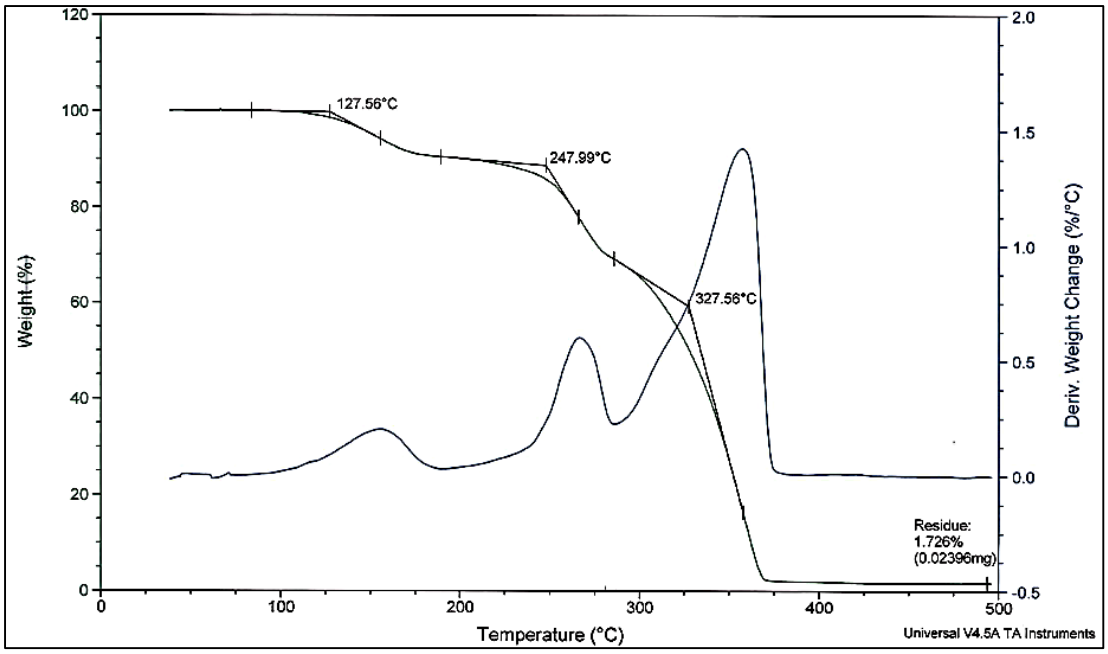

Figure E.19 TGA thermogram of TPAP-9

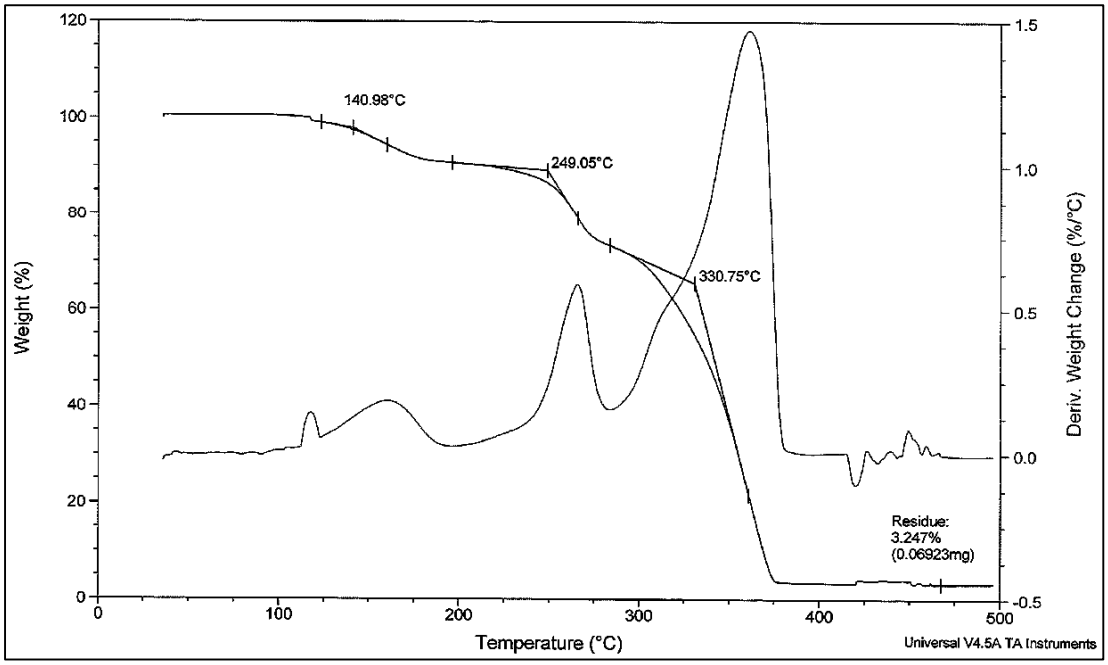

Figure E.20 TGA thermogram of TPAP-10

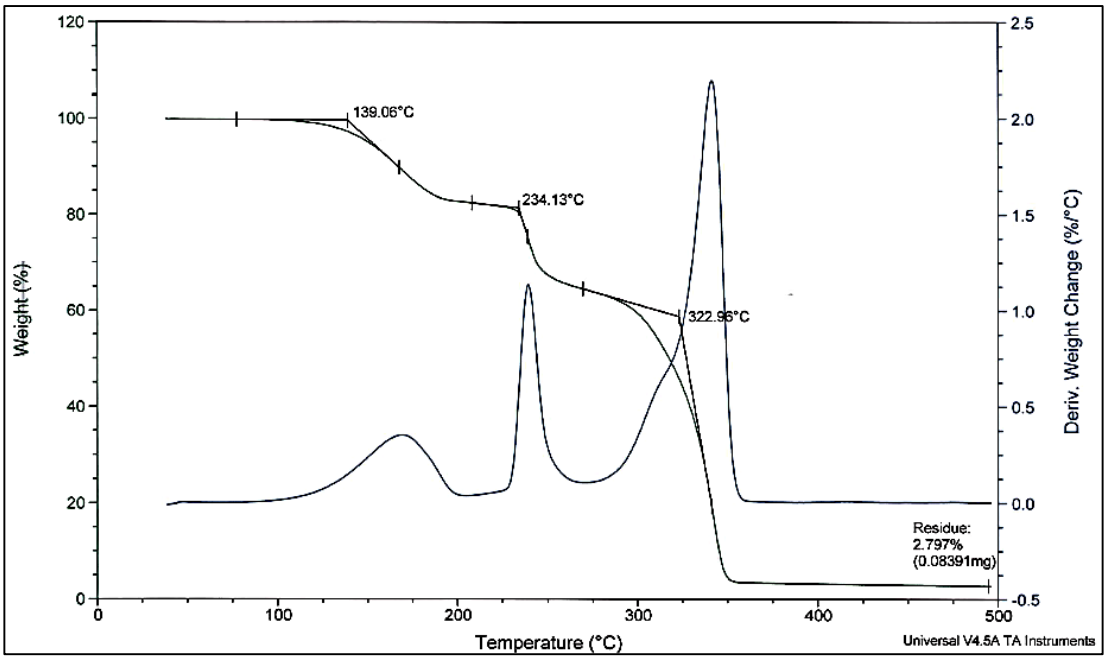

Figure E.21 TGA thermogram of TPAP-11

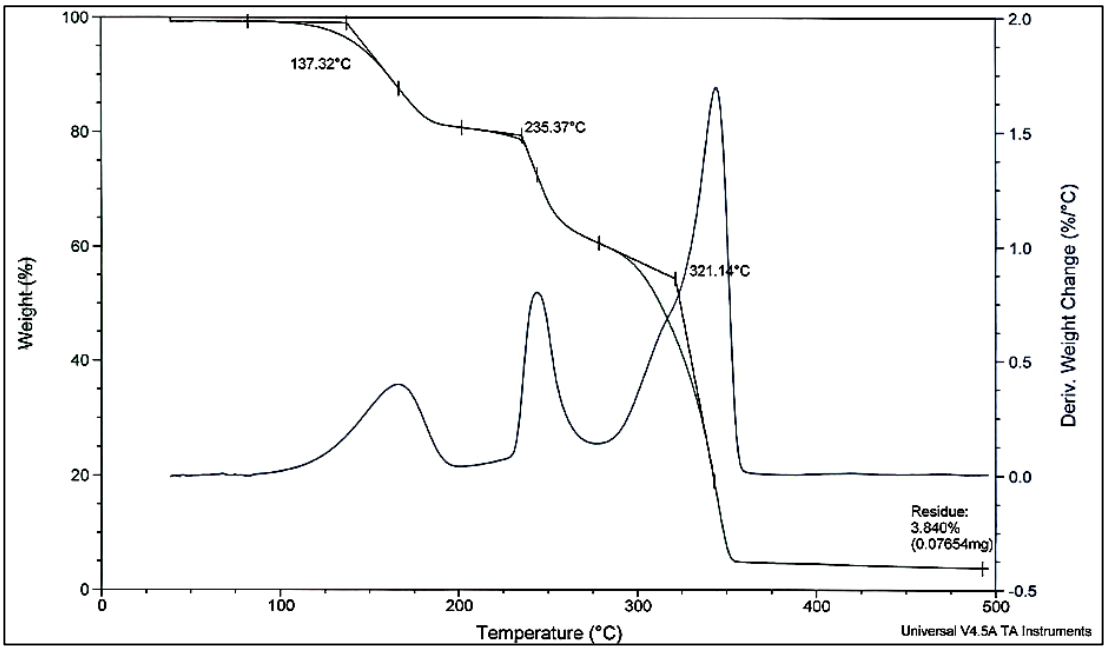

Figure E.22 TGA thermogram of TPAP-12

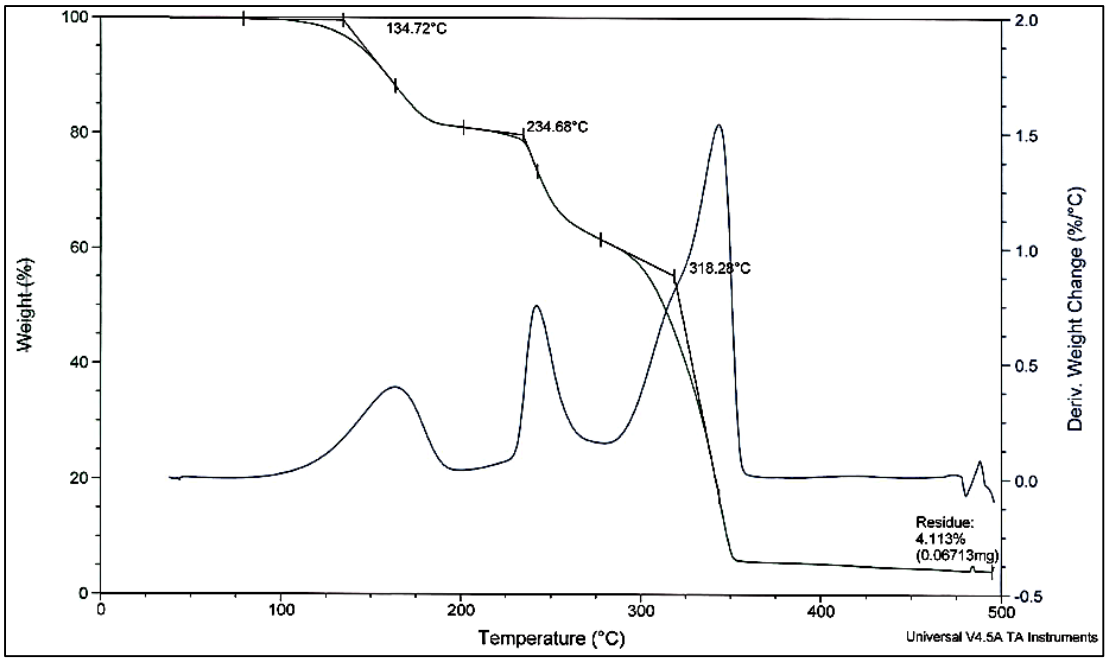

Figure E.23 TGA thermogram of TPAP-13

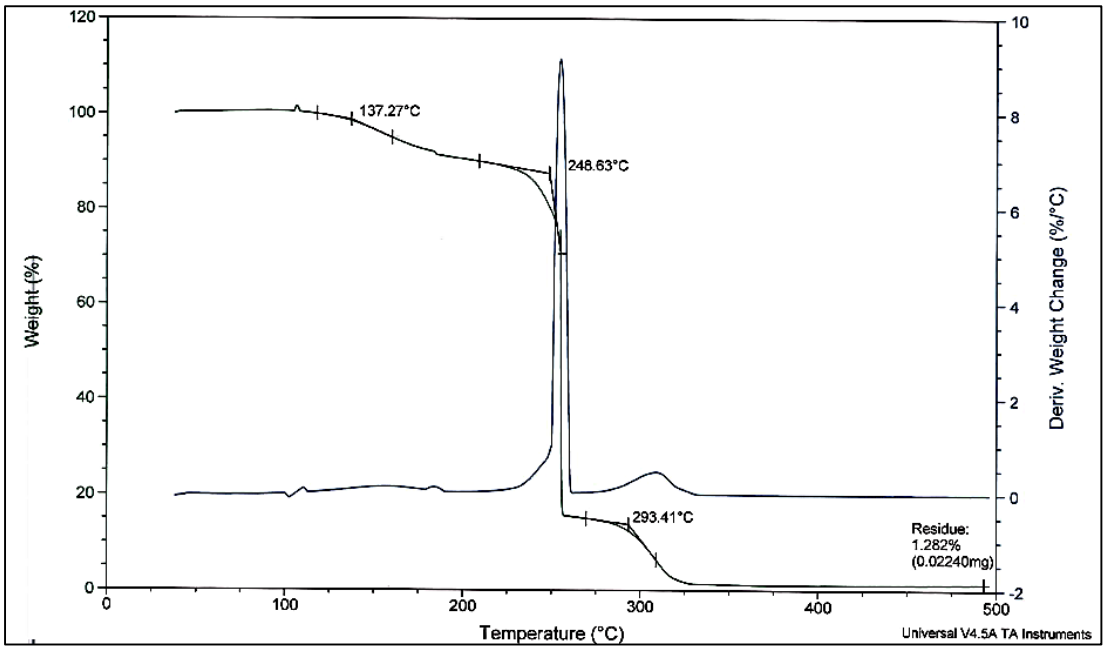

Figure E.24 TGA thermogram of TPAPX-1

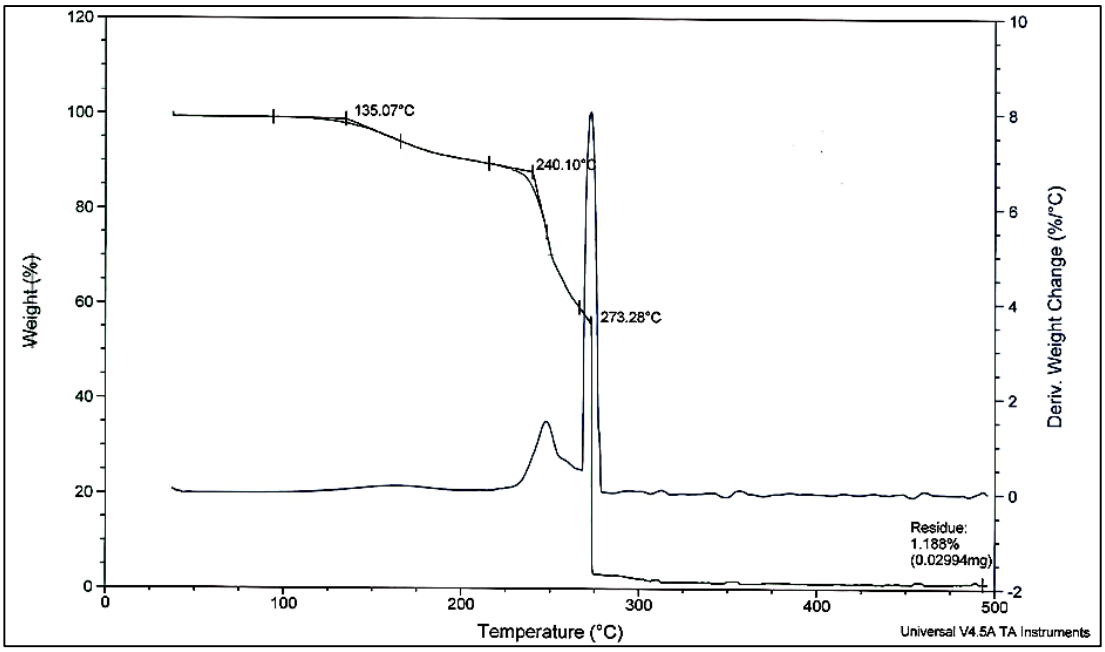

Figure E.25 TGA thermogram of TPAPX-2

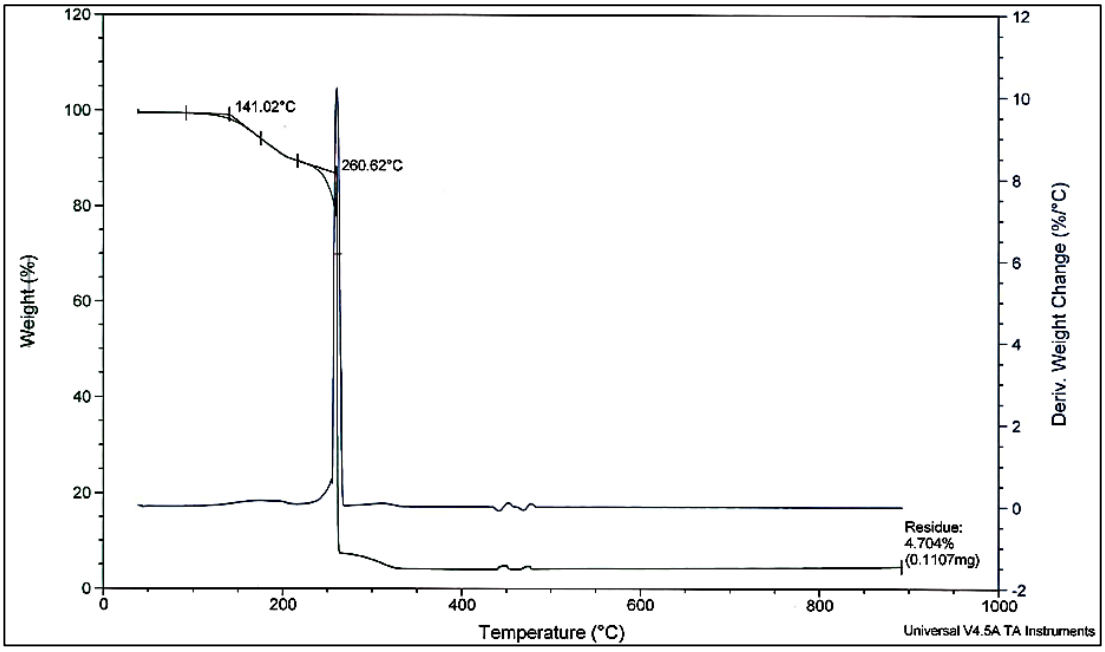

Figure E.26 TGA thermogram of TPAPXL-1

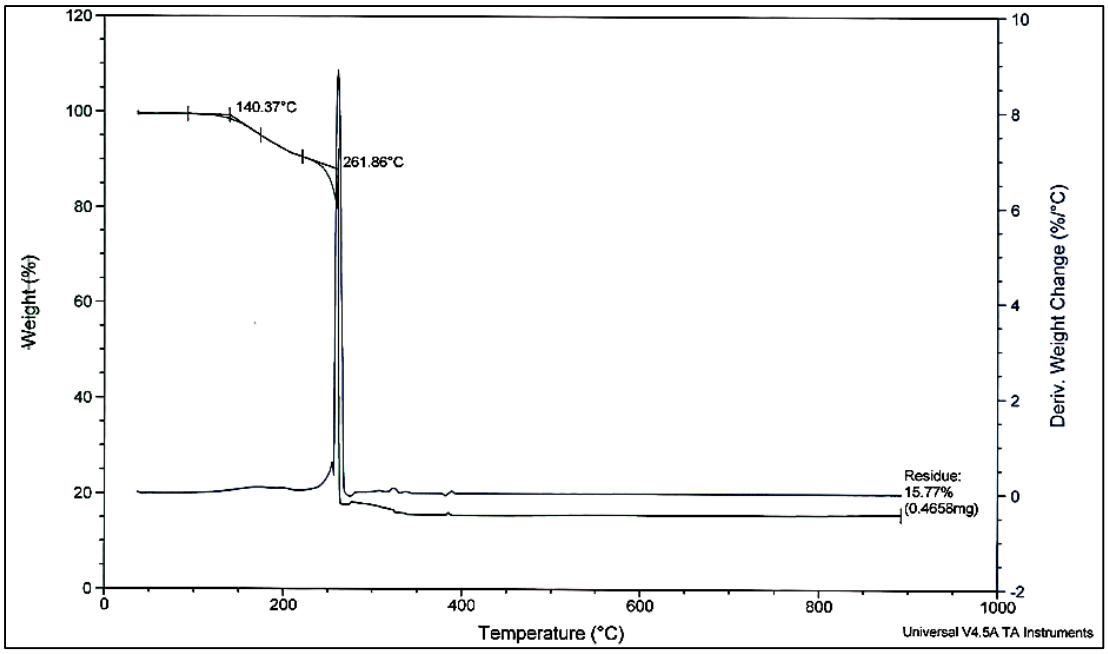

Figure E.27 TGA thermogram of TPAPXL-2

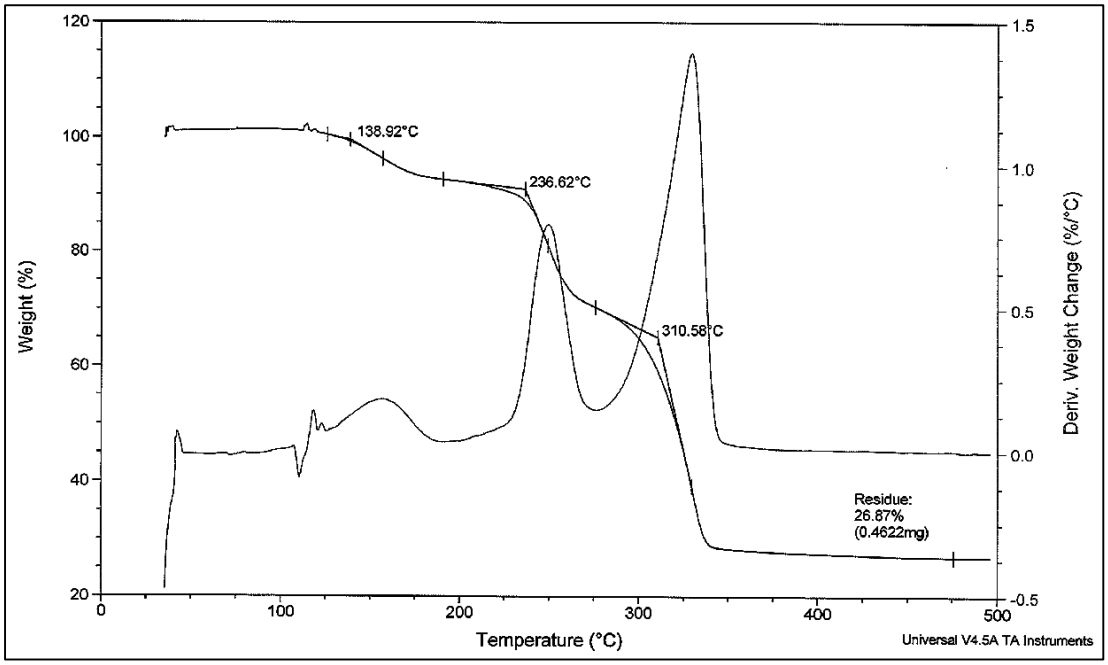

Figure E.28 TGA thermogram of TPAPXL-3

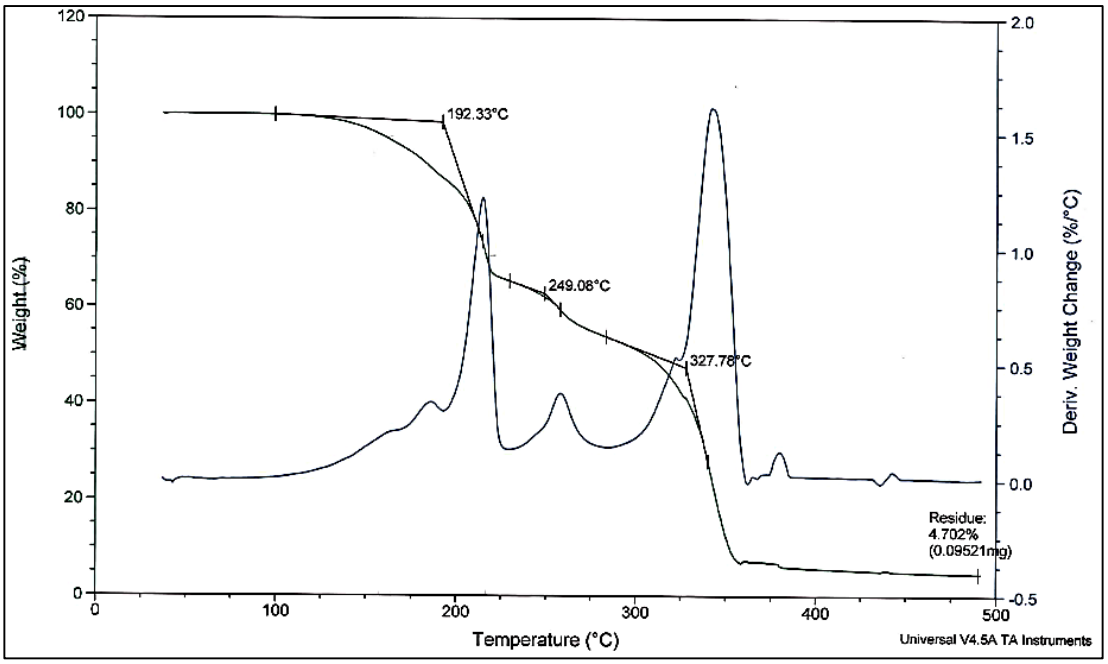

Figure E.29 TGA thermogram of TPAPSN-1

CURRICULUM VITAE

PERSONAL

Surname, Name: Eşiyok, Hacı
Date of birth: February 14, 1982
Place of birth: Ankara, Turkey
Address: Ümit Mah. Meksika Cad. Almina Apt. No: 57/17 06810 Ümitköy-ANKARA
Citizenship: Turkish
Marital Status: Married
E-mail: hesiyok@yahoo.com
Mobile: +90 545 664 07 99

EDUCATION

Middle East Technical University, Ankara, Turkey
Master of Science in Biotechnology. GPA: 3.64/4.00 January 2008
Thesis: Enantioselective Chemoenzymatic Synthesis of Oseltamivir Intermediates
Thesis advisors: Prof. Ayhan S. Demir and Prof. Ufuk Bakır

Middle East Technical University, Ankara, Turkey
Bachelor of Science in Chemical Engineering. GPA: 3.47/4.00 June 2006
Bachelor of Science in Chemistry. GPA: 3.46/4.00 June 2005

PROFESSIONAL EXPERIENCE

Roketsan Missile Industries, Ankara, Turkey
Senior Design Engineer, Propellant and Explosive Technologies Department

November 2009- To Date

Design and formulation of new generation solid and especially liquid propellants, their characterization and integration to rocket motors.

Toprak Ceramic Health Equipments Plant, Bozüyük, Turkey
Summer intern, Production Department Summer 2005

Monitored and controlled the production parameters in mud preparation, molding, glazing drying stages.

Novagenix Bio Analitical R&D Centre, Ankara, Turkey
Summer intern, Research &Development Summer 2004

Investigated and validated new methods for biologically active molecules.

GRANTS

TEV Undergraduate Scholarship	2000-2005
TÜBİTAK National Master Scholarship	2006-2008

PUBLICATIONS

Journal Publications

"Theoretical and Experimental Packing Density Study of Hydroxyl Terminated Polybutadiene Ammonium Perchlorate Based Propellant and Its Influence on Burning Rate", H. Eşiyok, M.E. Candarlı, International Journal of Energetic Materials and Chemical Propulsion, 13 (5): 455-469, 2014

Contributed Poster Presentations

"Synthesis of 4-hydroxy-3-oxocyclohex-1-ene carboxylate starting from Tamiflu precursor", H. Eşiyok, A.S. Demir, 21st National Chemistry Conference, Malatya, Turkey, August 23-27, 2007.

"Synthesis of 4-hydroxy-3-oxocyclohex-1-ene carboxylate starting from Oseltamivir precursor", H. Eşiyok, A.S. Demir, 15th National Biotechnology Conference, Antalya, Turkey, October 28-31, 2007.

"Study on Mechanical and Swelling Properties of HTPE-Based Polyurethane Networks", H. Eşiyok, U. Yilmazer, 45th International Annual Conference of the Fraunhofer ICT, Karlsruhe, Germany, June 24-27, 2014.

Contributed Oral Presentations

"HTPE Bazlı Poliüretan Bağlayıcı Yapının Deneysel ve Teorik Olarak İncelenmesi", H. Eşiyok, U. Yilmazer, 6th Savunma Teknolojileri Kongresi, Ankara, Turkey, June 20-22, 2012

"Theoretical and Experimental Packing Density Study of HTPB-AP Based Propellant and Its Influence on Burning Rate", H. Eşiyok, M.E. Candarlı, 10th International Symposium on Special Topics in Chemical Propulsion, Poitiers, France, June 02-06, 2014

"Investigation of Hypergolicity of Liquid Fuels with White Fuming Nitric Acid", H. Eşiyok, M.Bayramoglu, 5th Space Propulsion Conference, Roma, Italy, May 02-06, 2016

INTERESTS

Motor sports, bird, fish, photography, reading

LANGUAGES

- English (fluent), German (intermediate)